**Deanship of Graduate Studies**

**Al-Quds University**

# Brownian Dynamics Simulations for Complexation of DNA with Nano-Cationic Dendrimers

**Alaa Jawad Yaqoob Murrar**

**M.Sc. Thesis**

**Jerusalem – Palestine**

**1439 H. / 2018 A.D.**

# Brownian Dynamics Simulations for Complexation of DNA with Nano-Cationic Dendrimers

Prepared by:
**Alaa Jawad Yaqoob Murrar**

B.Sc. Physics / Science. Birzeit University - Palestine

Supervisor: **Dr. Khawla Qamhieh**

A Thesis Submitted in Partial Fulfillment of requirements for the degree of Master of Science of Physics, Al-Quds University.

**1439 H. / 2018 A.D.**

Al-Quds University

Deanship of Graduate Studies

Physics Program / Physics Department

Thesis Approval

# Brownian Dynamics Simulations for Complexation of DNA with Nano-Cationic Dendrimers

Prepared by: Alaa Jawad Yaqoob Murrar
Registration No.: 21512597

Supervisor: Dr. Khawla Qamhieh

Master thesis submitted and accepted, Date: 26 / شعبان / 1439 H.
12 / 05 / 2018 A.D.

The names and signatures of the examining committee members are as follows:

1- Head of Committee: Dr. Khawla Qamhieh Signature: .....
2- Internal Examiner: Dr. Husain Alsamamra Signature: .....
3- External Examiner: Dr. Jamal Ghabboun Signature: .....

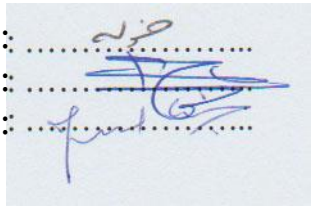

**Jerusalem - Palestine**

**1439 H. / 2018 A.D.**

# Dedication

I dedicate this humble work to the Islamic Ummah.

A grateful thanks to my lovely parents whose love, encouragement, support and day and night call Almighty Allah in their prayers to luck me and give me the highest levels of success.

**Alaa Jawad Yaqoob Murra**

## Declaration

I Certify that this thesis submitted for the degree of Master, is the result of my own research, except where otherwise acknowledged, and that this study (or any part of the same) has not been submitted for a higher degree to any other university or institution.

Signed: 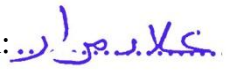

**Alaa Jawad Yaqoob Murrar**

Date: 26 / شعبان / 1439 H.
12 / 05 / 2018 A.D.

## Acknowledgment

First of all, I wish to express my gratitude to the Almighty Allah for providing me the grant to make this thesis possible.

My grateful thanks to my supervisor Dr. Khawla Qamhieh for her support, encouragement and for providing me this chance to achieve the knowledge and experience in the field of research. I would also like to thank Dr. Abdallah Sayyed Ahmad and the teacher Doa' Hawamdeh from Birzeit University for helping me, teaching me the basics of this subject and providing me with the required programs.

Thanks a lot, to Prof. Axel Kohlmeyer, Dr. Andrew I. Jewett, Dr. Stefan Paquay and Dr. Steve Plimpton from LAMMPS (The simulator used) mail list, Prof. Ronald G. Larson, Dr. Shi Yu and Dr. Dan Hinckley for helping me, guiding me and answering all my questions.

Thanks, and appreciation to my committee Dr. Jamal Ghabboun (external examiner) and Dr. Husain Alsamamra (internal examiner).

My gratitude also goes to the computer Eng. Sufyan Aqtam for his assistance in providing me an access to high computational servers at Al-Quds University IT center and also to the head of archiving and community service Hamdallah Rasmi Mari for providing me with all articles that I needed.

Very Thanks to Al-Quds University for everything it has given to me.

My grateful thanks to my family, friends, who stood beside me and encouraged me constantly.

**Alaa Jawad Yaqoob Murrar**

## Abstract

We employed Brownian Dynamics (BD) simulations to study the effect of salt concentration and pH on the interactions of the dsDNA chain with poly(amido amine) (PAMAM) dendrimer, determine the role of both the salt concentration and the dsDNA chain length (number of bps) in the formation of linker and tail/s in the dsDNA-two-dendrimer aggregate, and to know what are the morphologies that appear when different generations of the dendrimer form an aggregate with the dsDNA chain. To fit our computing capabilities and achieve simulation speed without going into some complicated details, we used the bead-spring model for the dsDNA chain and the charged hard sphere model for the dendrimer.

Our models predict that the dsDNA chain strongly wraps around the dendrimer at both low salt concentration (10 mM) and pH $\leq$ 7 and the dsDNA-dendrimer complex is formed, whereas no complex is formed in both of high salt concentration and high pH.

In the aggregate that consists of dsDNA chain and two dendrimers (G4 and G6), the linker and/or the tail/s clearly appear/s at a salt concentration $\geq$ 10 and $\leq$ 120 *mM* with dsDNA chain length $\geq$ 97 *nm* (number of bps $\geq$ 288). In addition to that, for longer dsDNA chains, we noticed the overcharge phenomenon for the dendrimers in the aggregate and we found that its degree depends on the dsDNA chain length (*i.e.*, the number of bps).

When a certain number of the lower generations of the dendrimer (G2 and G4) interact with the dsDNA chain to form aggregates at 10 *mM* salt concentration, a rod-like morphology appears, also we got a globular one for the G4 aggregate, whilst for a high generation (G6), we obtained almost rod-like morphologies.

## Table of Contents

## List of Tables

## List of Figures

## List of Appendices

## List of Abbreviations

| | |
|---|---|
| Deoxyribonucleic acid | (DNA) |
| National Institutes of Health | (NIH) |
| Polyelectrolyte | (PE) |
| Linear PE | (LPE) |
| Nanometer/s | (nm) |
| Poly(amido amine) | (PAMAM) |
| Generations | (G) |
| Molecular Weight | (MW) |
| CuI-catalysed azide-alkyne cycloaddition | (CuAAC) |
| Diels–Alder cycloaddition | (DA) |
| Thiol–ene coupling | (TEC) |
| Thiol–yne coupling | (TYC) |
| Base-catalyzed Michael addition | (MA) |
| Transmission electron microscopy | (TEM) |
| Ethylenediamine | (EDA) |
| Confocal Laser Scanning Microscopy | (CLSM) |
| Poly Ethoxy Ethyl Glycinamide | (PEE-G) |
| High-Performance Liquid Chromatography | (HPLC) |
| Potential of Hydrogen | (pH) |
| Atomic Force Microscopy | (AFM) |
| Ribonucleic acid | (RNA) |
| Double-strand/ed DNA | (dsDNA) |
| Base-pairs | (bp) |
| Ångström/s | ($Å$) |
| Millimeter/s | ($mm$) |
| The persistence length of the LPE chain (e.g., DNA) | ($l_p$) |
| Molecular dynamics | (MD) |
| Radius of gyration | ($R_g$) |
| Poly(propylene imine) | (PPI) |
| Millimolar | (mM) |
| Cryogenic-TEM | (Cryo-TEM) |
| Radius | (R) |
| Charge/s | ($q$) |
| Monte Carlo | (MC) |
| Length/s | ($L/l$) |
| The optimal wrapping length of chain around dendrimer | ($l_{opt}$) |
| Original radius | ($R_o$) |
| The maximum number of dendrimers needed to neutralize the charge of the DNA per DNA molecule | ($N_{max}$) |
| Bjerrum length | ($l_B$) |
| Dynamic Light Scattering | (DLS) |
| Charge ratio/s | ($r_{charge}$) |
| The experimental number of dendrimers | ($N_{exp}$) |
| Number of functional groups in the dendrimer | ($Z_{dend}$) |
| The total charge of the DNA chain | ($Z_{DNA}$) |
| Brownian Dynamics | (BD) |
| Number of the monomers on the chain | ($N_{ch}$) |
| Single-strand/ed DNA | (ssDNA) |

| | |
|---|---|
| Atomistic (All Atom) MD | (AAMD) |
| Coarse-Grained | (CG) |
| The translational diffusion coefficient of dsDNA chain | ($D_t$) |
| Large-scale Atomic/Molecular Massively Parallel Simulator | (LAMMPS) |
| Langevin Dynamics | (LD) |
| The distance between centers of masses | ($D_{coms}$) |
| Adsorption fraction of dsDNA chain (beads) into dendrimer surface | ($\omega$) |
| Order parameter (curvature) of the DNA-dendrimer complex | ($\gamma$) |
| Toroidal parameter | ($\tau$) |
| Visual Molecular Dynamics | (VMD) |
| The Mean-Squared Displacement | (MSD) |
| Center of Mass | (COM) |
| The Scientific Data Analysis and Visualization program | (SciDAVis) |
| The Open Visualization Tool program | (Ovito) |
| Brownian Dynamics step | (BDS) |

# Chapter One

## Introduction

# 1 Chapter One: Introduction

## 1.1 Gene Therapy

Nanoparticle drug-delivery systems are popular as they are able to increase the selectivity and stability of therapeutic agents and it is the most common form that carries the genetic material of gene therapy involves using Deoxyribonucleic acid (DNA) that controls all functions inside living cells. The unique material properties of DNA have made it an attractive molecule for material scientists and engineers whom interested in Micro- and Nanofabrication.

Gene therapy is one promising and rapidly developing medical approach, which means the therapeutic delivery of nucleic acid polymers into a patient's cells as a drug to treat disease **(Ermak, 2015)** (see Figure 1.21). Although important progress has been made in the area of gene therapy, there is a main problem in gene therapy which is the loss of efficient and safe vectors for gene delivery. In the 1980s, Scientists began to look into gene therapy and the first attempt at modifying human DNA was performed by Martin Cline. However, the first successful nuclear gene transfer in humans, approved by the National Institutes of Health (NIH), was performed in May 1989 **(Rosenberg, et al., 1990)**. The gene therapy is a hopeful treatment option for a number of diseases that have no other cures, (including inherited disorders, combined immunodeficiency syndromes, muscular dystrophy, hemophilia, certain viral infections and many cancers result from the presence of defective genes).

The challenge and main principle of developing successful gene therapy for any specific condition are to prepare the best delivery (vectors and methods) for the drug into the human cells to get the needy result in nanomedicine. There are many ways to deliver the gene inside the cell: viral (Viruses) and non-viral (*i.e.*, chemical). On one hand, non-viral vectors such as Liposome, Cationic polymers, and Cationic dendrimers, are attractive because of their lower immunogenicity, greater safety and ease of preparation. On the other hand, viral vectors have been used in ~70% of the clinical trials to date **(Edelstein, Abedi, Wixon, & Edelstein, 2004)**. There are certain types of virus used as carrier for genetic material such as Adenovirus and Retrovirus. Although viral systems have many benefits to carry and connect the gene into a specific target cell and have high transfection efficiency. Furthermore, there are many side defects which are related to the safety risk, at large-scale production, its toxicity for human body and highly immune response **(Itaka & Kataoka, 2009)**. Therefore, and because of this side effect, we need to replace the viral system and use the natural and chemically synthetic polymers such as dendrimers.

In a living organism, DNA is vital for its function and information storage **(Zinchenko & Chen, 2006)**. The practical application of DNA compaction is seen in gene therapy and antisense therapy, and this compaction is needed before transferring DNA to the interior of the cell nucleus. To transfer DNA to cells, scientists and nanoscience workers use systems contain Polyelectrolytes (PEs) such as DNA interacting with compact colloids like proteins **(Schiessel H. , 2003) (Arcesi, Penna, & Perico, 2007)**, surfactant micelles **(Lindman & Thalberg, 1993) (Dekker, 1998)**, cationic liposomes **(Wolfert, et al., 1996) (Lasic, Strey, Stuart, Podgornik, & Frederik, 1997) (Martin-Herranz, et al., 2004)** and dendrimers **(Tomalia, Naylor, & Goddard(III), 1990) (Bielinska, Chen, Johnson, & Baker, 1999)**. The interactions between charged Linear PE (LPE) and oppositely charged sphere form complexes which are a common pattern in chemistry, physics, and biology. A more or less

tightly wrapped polymers conformations are produced by the electrostatic attraction between the sphere and LPE chain, *e.g.*, in a cell, there is a positively charged protein known as histone, it interacts with DNA and forms the nucleosomes structure. These nucleosomes form higher order structures like beads on a string and produce the chromatin structure **(Schiessel H. , 2003)**.

The compaction of DNA using nanoscale objective can help us to understand some of the fundamental questions, namely, how the complex conformation depends on the various system parameters such as charge of the sphere and LPE chain, LPE chain length, sphere diameter and salt concentration of the surrounding medium **(Netz & Joanny, 1999)**. Numerous experimental and theoretical studies have been made on DNA compaction on various nanoscale objects such as dendrimers alongside with computer simulations for it **(Ainalem, et al., 2009) (Carnerup, Ainalem, Alfredssona, & Nylander, 2011) (Arcesi, Penna, & Perico, 2007) (Boroudjerdi, Naji, & Netz, 2011) (Tian & Ma, 2010) (Nandy & Maiti, 2011)**, the experimental and theoretical studies showed that when the length of LPE chain exceeds the length that is needed to neutralize the total charge of dendrimer, the overcharging phenomena of dendrimer appears and the degree of it depends on dendrimer generation (size and charge) and salt concentration, also they concluded that the morphology and binding model of dendrimer-LPE chain depends on the generation and this binding model is cooperative. While computer simulation studies reported that there is a penetration inside dendrimer by LPE chain and this degree of penetration increases with the dendrimer generation or with an increase in the charge ratio. Dendrimer can mimic biological macromolecules such as enzymes, viral protein, antibodies, histone, and polyamine like spermine and spermidine **(Tomalia, Naylor, & Goddard(III), 1990) (Bielinska, Chen, Johnson, & Baker, 1999)**, as a consequence, dendrimers form stable complexes with DNA and protect DNA against degradation **(Wang, et al., 2010) (Fant, et al., 2010)**, such properties make dendrimer excellent tools for gene delivery **(Lee, MacKay, Fréchet, & Szoka, 2005)**.

## 1.2 Dendrimers

### 1.2.1. The definition:

Dendrimers are highly branched, star-shaped polymers with nanometer (*nm*)-scale dimensions and monodisperse nature. The name come from the Greek words, dendron (which translates to “tree” or “branch”) and meros (which translates to “part”). The family of dendritic macromolecules comprises not only dendrimers, but also dendrons, hyperbranched polymers, dendrigrafts, dendritic-linear hybrids and dendritic-surface hybrids (see Figure 1.1) **(Tomalia, Christensen, & Boas, 2012) (Gao & Yan, 2004) (Teertstra & Gauthier, 2004) (Gitsov, 2008)**.

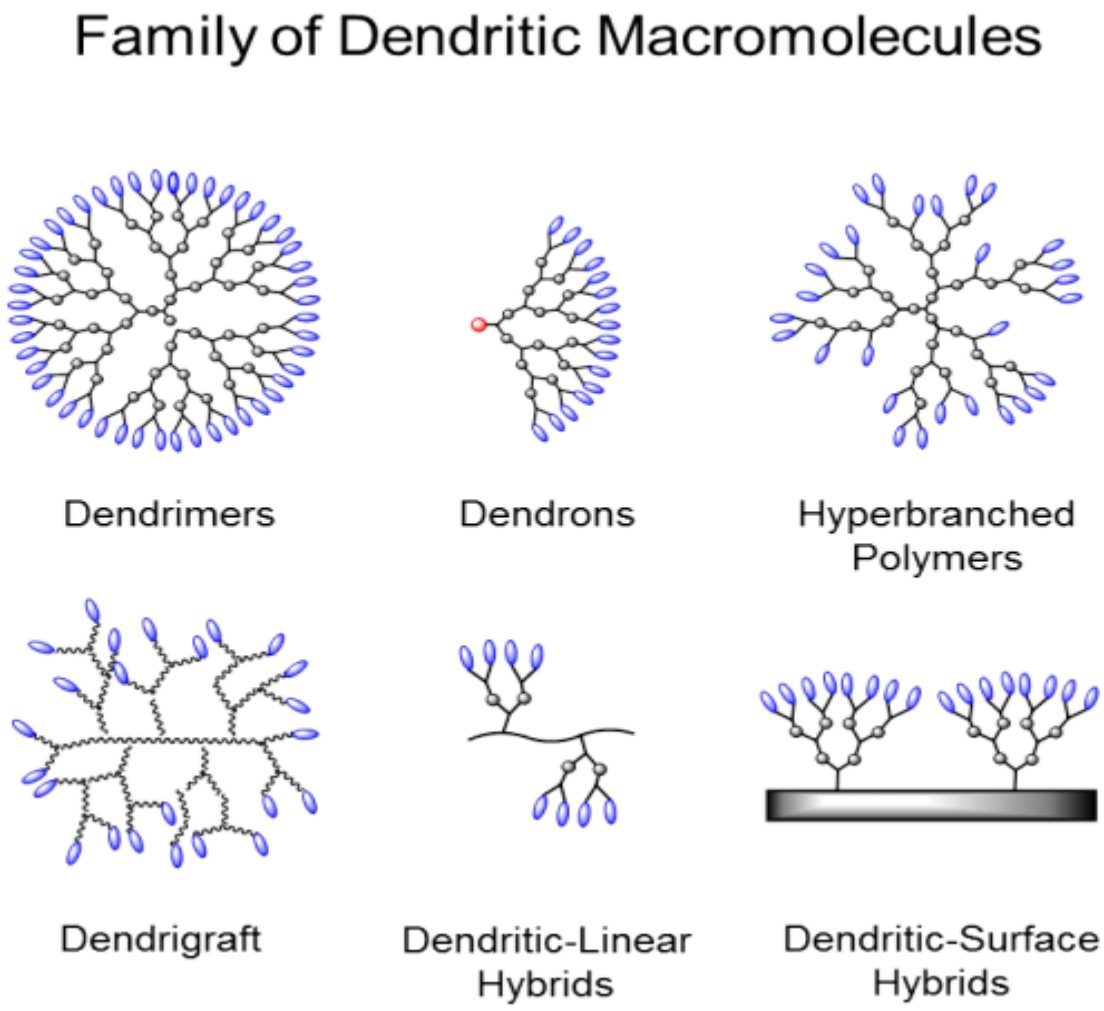


**Figure 1.1:** Dendritic family (a trifunctional core and bifunctional branches example for dendrons and dendrimers).

### 1.2.2. History of the dendrimer molecule:

Dendrimers have often been referred to as the "Polymers of the 21st century". In 1978 the first successful attempt to create and design dendrimer structures were carried out by Fritz Vögtle and co-workers **(Buhleier, Wehner, & Vögtle, 1978)** and they named the structure "cascade molecules". In the 1980s, dendrimers were made by R.G. Denkewalter, also Donald G. Tomalia and his co-workers had worked and synthesized the first family of "dendrimers" which is Poly(amido amine) (PAMAM) dendrimers -a special organization of polymer units-, they were the first ones who used the word "dendrimers" that comes from Greek words previously illustrated **(U.S. Patent No. US4289872 A, 1979) (U.S. Patent No. US4410688 A, 1981) (U.S. Patent No. US4507466 A, 1983) (Tomalia, et al., 1985) (Treelike molecules branch out., 1996)**. At the same time Prof. George R. Newkome's group independently reported the synthesis of similar macromolecules, they called it "arborols" from the Latin word "arbor" also meaning a tree **(Newkome, Yao, Baker, & Gupta, 1985)**. Until the end of the 1980s all work was made by divergent synthesis approaches, and in 1990 a convergent synthetic approach was introduced by Craig Hawker and Jean Fréchet **(Hawker & Frechet, 1990)**.

### 1.2.3. Dendrimers Structure:

Dendrimers are often called "artificial proteins" due to their spherical three-dimensional morphology. Typically, and as in Figure 1.2, the dendritic structure is characterized by a core (in dendrimers) or focal point (in dendrons), where all the branches arise; several branching units which determine the different Generations (G), sizes and shapes, and a highly functional periphery consisting of terminal groups that frequently determine the surface reactivity and chemical properties of the macromolecule **(Tomalia, Christensen, & Boas, 2012) (Gao & Yan, 2004) (Teertstra & Gauthier, 2004) (Gitsov, 2008)**.

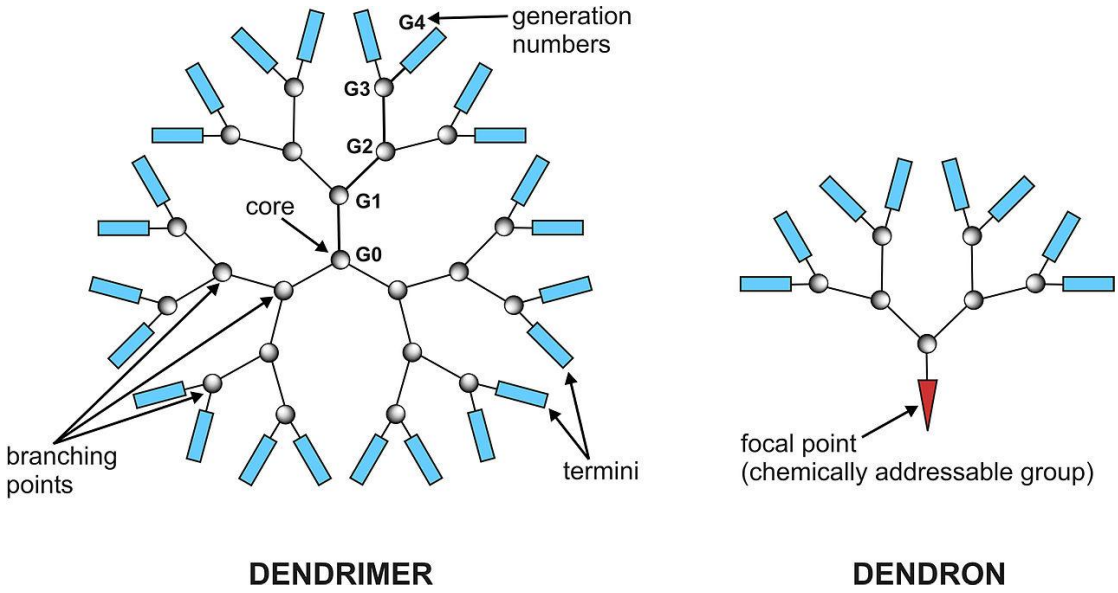


**Figure 1.2:** The structure of dendrimer and dendron (a trifunctional core and bifunctional branches example).

Unlike traditional linear polymer synthesis that produces a mixture of materials ranging in Molecular Weight (MW), dendrimers are the product of multistep organic synthesis. This difference makes dendrimers in theory, but not always in practice, be single chemical entities.

### 1.2.4. Dendrimers Synthesis:

As previously mentioned, dendrimers can be considered to have three major portions: a core, an inner shell, and an outer shell. Ideally, a dendrimer can be synthesized to have different functionality in each of these portions to control properties such as solubility, thermal stability, and attachment of compounds for particular applications. Synthetic processes can also precisely control the size and number of branches on the dendrimer. There are many methods of dendrimer synthesis, the most well-known are divergent synthesis and convergent synthesis, also recently the click chemistry approach is going to be familiar. However, because the actual reactions consist of many steps needed to protect the active site, it is difficult to synthesize dendrimers using either method. This makes dendrimers hard to make and very expensive to purchase. At this time, there are only a few companies that sell dendrimers; Polymer Factory Sweden AB and Dendritech Inc. are the only kilogram-scale producers of PAMAM dendrimers. Dendritech Inc., from Midland,

Michigan, USA produces PAMAM dendrimers and other proprietary dendrimers. Polymer Factory Sweden AB from Stockholm, Sweden commercializes dendritic materials.

### 1.2.4.1. Divergent methods:

In 1978, Vö gtle made the first successful divergent synthesis of dendrimers **(Buhleier, Wehner, & Vögtle, 1978)**. As shown in Figure 1.3, the dendrimer is assembled from a multifunctional core, which is extended outward by a series of reactions, commonly a Michael reaction **(Little, Masjedizadeh, Wallquist, & McLoughlin, 1995)**. Each step of the reaction must be driven to full completion to prevent mistakes in the dendrimer, which can cause trailing generations (some branches are shorter than the others). Such impurities can impact the functionality and symmetry of the dendrimer but are extremely difficult to purify out because the relative size difference between perfect and imperfect dendrimers is very small **(Holister, Vas, & Harper, 2003)**.

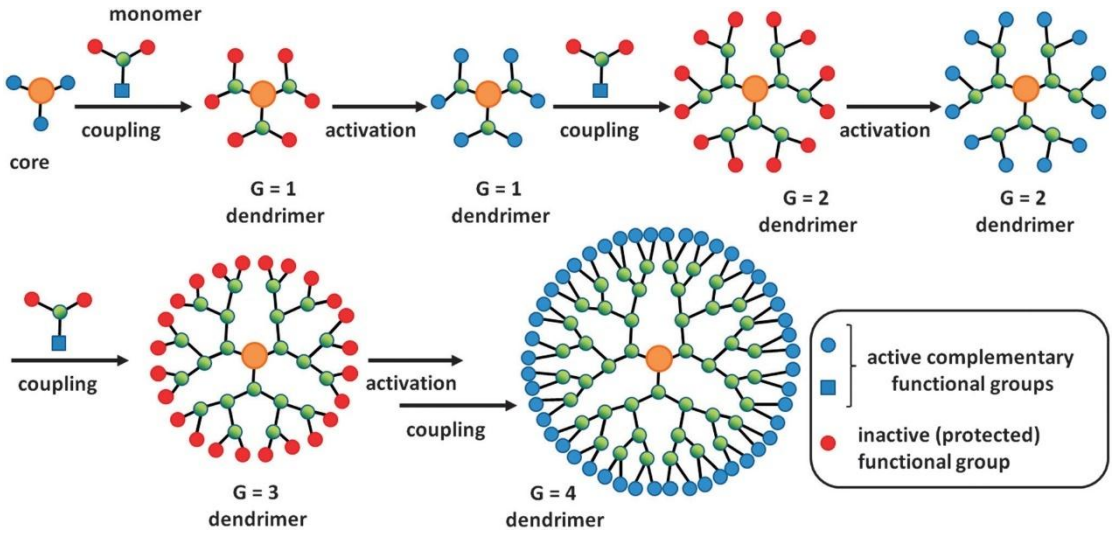


**Figure 1.3:** Schematic of divergent synthesis of dendrimers (a trifunctional core and bi-functional branches example) **(Sowinska & Urbanczyk-Lipkowska, 2014)**.

### 1.2.4.2. Convergent methods:

Dendrimers are built from small molecules that end up at the surface of the sphere, and reactions proceed inward building inward and are eventually attached to a core (see Figure 1.4). This method makes it much easier to remove impurities and shorter branches along the way so that the final dendrimer is more monodisperse. However, dendrimers made this way are not as large as those made by divergent methods because crowding due to steric effects along the core is limiting **(Holister, Vas, & Harper, 2003)**.

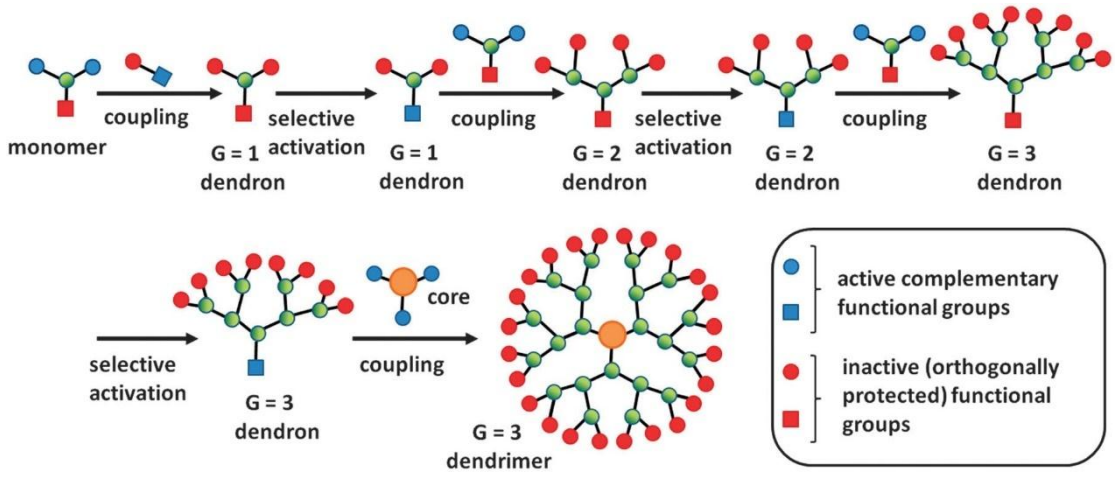


**Figure 1.4:** Schematic of convergent synthesis of dendrimers (a trifunctional core and bi-functional branches example) **(Sowinska & Urbanczyk-Lipkowska, 2014)**.

### 1.2.4.3. Click chemistry:

The click chemistry concept introduced by Sharpless *et al.* in 2001 **(Kolb, Finn, & Sharpless, 2001)** encompasses a number of versatile reactions that are highly stereo/regioselective, gives readily separable products, usually in excellent yield close to 100%. The click reactions are usually accompanied by the inoffensive byproducts (or none) and utilize readily available starting materials and reagents. Additionally, these reactions are tolerant to the presence of a wide range of functional groups and can be carried out using a broad set of reaction conditions (including water, air, biphasic systems, *etc.*). Therefore, in recent years the click chemistry methodology had found widespread applications in the synthesis of dendrimers. It has also provided an additional impetus for a "greener" approach in constructing dendrimers. To date, the click reactions that have been successfully adapted in the field of dendrimer chemistry may be classified as the $Cu^{I}$-catalysed azide-alkyne cycloaddition (CuAAC), the Diels-Alder cycloaddition (DA), especially those involving furan and maleimide moieties, and the thiol-based click reactions that can proceed *via* two routes, namely, the anti-Markovnikov radical addition [the thiol-ene coupling (TEC) or the thiol-yne coupling (TYC)] or base-catalyzed Michael addition (MA) **(Sowinska & Urbanczyk-Lipkowska, 2014)**. Figure 1.5 shows the click reactions widely utilized for the preparation of dendrimers and Figure 1.6 shows an example of this method.

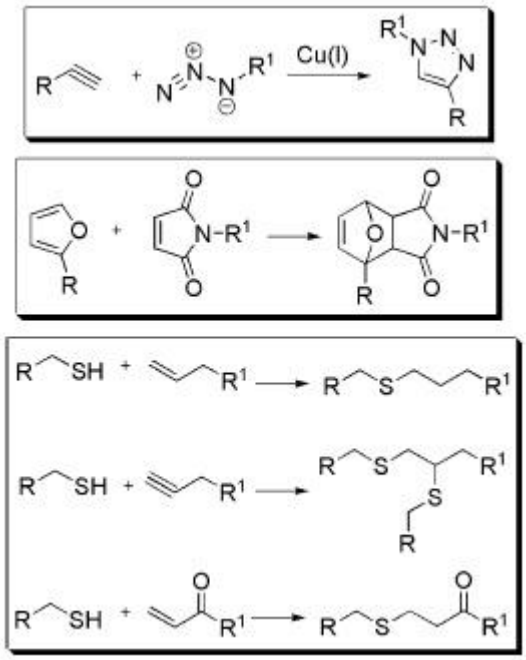


**Figure 1.5:** Schematic representation of the click reactions widely utilized for the preparation of dendrimers **(Sowinska & Urbanczyk-Lipkowska, 2014)**.

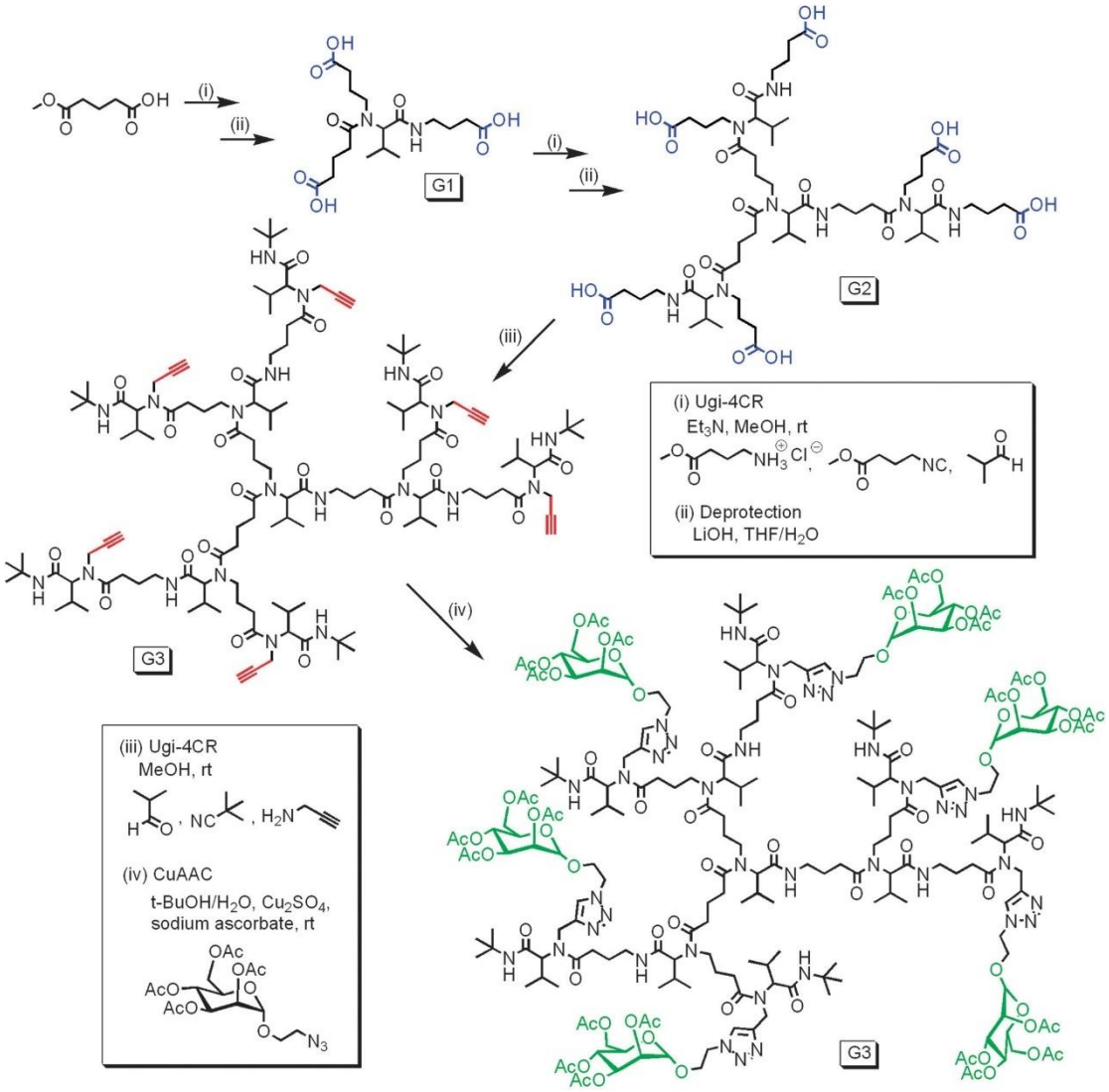


**Figure 1.6:** Synthesis of G3 acetylene-terminated dendrimers and their further functionalization with mannose functions via CuAAC click reactions **(Sowinska & Urbanczyk-Lipkowska, 2014)**.

There are ample avenues that can be opened by exploring this chemistry in dendrimer synthesis.

### 1.2.5. Dendrimer properties:

#### 1.2.5.1. Monodispersity and Polyvalency:

Dendrimers can be constructed with a well-defined molecular structure because they are dendritic polymers, *i.e.*, being monodisperse, unlike the linear polymers. Mass spectrometry, size-exclusion chromatography, Gel electrophoresis and transmission electron microscopy (TEM) have been extensively used to verify the monodispersity of dendrimers **(Jackson, et al., 1998)**. In general, convergent methods produce the most nearly monodisperse dendrimers as determined by mass spectrometry. This is because the convergent growth process permits the purification process at each step of the synthesis and eliminates cumulative effects due to failed couplings. For this reason, Tomalia said that convergently

produced dendrimers are probably the most precise synthetic macromolecules that exist today **(Tomalia D. A., 2005)**. Mass spectrometry has also shown that PAMAM dendrimers produced by the divergent method are remarkably monodisperse for the earlier generations (*i.e.*, G = 0-5) **(Tomalia D. A., 1994)**. Now, researchers have the possibility to work with well-defined scalable sizes due to monodispersity. This property is useful for applications such as the synthesis of container molecules.

As dendrimers coordinate to materials, many interactions are provided by the polyvalency of them. Polyvalency shows the outward presentation of reactive groups on the dendrimer nano-structure exterior, the functional groups that are attached to the tip of a dendrimer's branches determine the dendrimer's polyvalent, these functional groups can participate in multiple interactions with receptors on biological structures like cell membranes and viruses **(Halford, 2005)**. Also, these functional groups on the molecular surface are responsible for reactivity, high solubility, and miscibility. The solubility of dendrimers is strongly influenced by the nature of surface groups which can be hydrophilic groups that are soluble in polar solvents, and dendrimers having hydrophobic end groups which are soluble in nonpolar solvents **(Klajnert & Bryszewska, 2001)**. These safely improved physical and chemical properties are shown by the architecture of dendrimer molecular when they are compared to linear polymers.

#### 1.2.5.2. Nanoscale size and shape:

Dendrimers are highly symmetric and spherical polymer having nanoscale in diameter with unique structural whose properties are catching great interest from both scientists and technologists. Size, generation, and surface functional groups of the dendrimers are playing an important and fundamental role in the performance of these dendrimers. The shape of dendrimer is also very important, as it allows the defined placement of functions not only on dendrimer surface but also inside the dendritic scaffold, *e.g.*, within the PAMAM dendrimer family, the lower generation (G0-G3) with Ethylenediamine (EDA) core have ellipsoidal shapes, whereas the higher generation (G4-G10) have roughly spherical shapes, so the shape of dendrimer changes when generation changes. In addition, the diameter of the dendrimer increases as the generation of dendrimer increase, for instance, the diameter of the PAMAM dendrimer of the generation (G1- G10) with EDA core increases from 1.1-12.4 *nm* **(Cheng, Xu, Ma, & Xu, 2008)**.

#### 1.2.5.3. Comparison with linear polymers:

**Table 1.1:** Properties of dendrimer and linear polymers **(Mishra, 2011)**.

| Property | Dendrimers | Linear Polymers |
|---|---|---|
| Structure | Compact, Globular | Not compact |
| Synthesis | Careful & Stepwise growth | Single step polycondensation |
| Structural control | Very high | Low |
| Architecture | Regular | Irregular |
| Shape | Spherical | Random coil |
| Crystallinity | * Non-crystalline, amorphous materials<br>* lower glass temperatures | * Semi crystalline/crystalline materials<br>* Higher glass temperatures |
| Aqueous solubility | High | Low |
| Nonpolar solubility | High | Low |
| Viscosity | Nonlinear relationship with a molecular weight | Linear relation with molecular weight |
| Reactivity | High | Low |
| Compressibility | Low | High |
| Polydispersity | Mono | Poly |

An opportunity to control dendrimer size, shape, and surface reactivity has brought these molecules to the forefront of biomedicine and drug delivery in particular. Also, the interest in dendrimers is mainly based on their potential applications in various fields ranging from materials engineering to biomedicine and pharmacy. To name but a few, dendrimers have been used to deliver oligonucleotides to the cell **(Delong, et al., 1997) (Yoo, Sazani, & Juliano, 1999)**. They enhance cytosolic and nuclear availability as indicated by Confocal microscopy or Confocal Laser Scanning Microscopy (CLSM) as well as cell uptake and transfection efficiency of plasmid DNA **(Kukowska-Latallo, et al., 1996)**.

### 1.2.6. Dendrimer's Applications:

Applications of dendrimers typically involve conjugating other chemical species to the dendrimer surface that can function as detecting agents (such as a dye molecule), affinity ligands, targeting components, radioligands, imaging agents, or pharmaceutically active compounds. Dendrimers have very strong potential for these applications because their structure can lead to multivalent systems. In other words, one dendrimer molecule has hundreds of possible sites to couple to an active species. Researchers aimed to utilize the hydrophobic environments of the dendritic media to conduct photochemical reactions that generate the products that are synthetically challenged. Carboxylic acid and phenol-terminated water-soluble dendrimers were synthesized to establish their utility in drug delivery as well as conducting chemical reactions in their interiors **(Kaanumalle, et al., 2005)**. This might allow researchers to attach both targeting molecules and drug molecules to the same dendrimer, which could reduce negative side effects of medications on healthy cells **(Hermanson, 2008)**.

Dendrimers can also be used as a solubilizing agent. Since their introduction in the mid-1980s, this novel class of dendrimer architecture has been a prime candidate for host-guest chemistry **(Tomalia, Naylor, & Goddard(III), 1990)**. Dendrimers with a hydrophobic

core and hydrophilic periphery have shown to exhibit micelle-like behavior and have container properties in solution **(Frechet, 1994)**. The use of dendrimers as unimolecular micelles was proposed by Newkome in 1985. This analogy highlighted the utility of dendrimers as solubilizing agents **(Liu, Kono, & Fréchet, 2000) (Newkome, Yao, Baker, & Gupta, 1985)**. The majority of drugs available in the pharmaceutical industry are hydrophobic in nature and this property, in particular, creates major formulation problems. This drawback of drugs can be ameliorated by dendrimeric scaffolding, which can be used to encapsulate as well as to solubilize the drugs because of the capability of such scaffolds to participate in extensive hydrogen bonding with water **(Stevelmans, et al., 1996) (Gupta, Agashe, Asthana, & Jain, 2006) (Thomas, et al., 2005) (Bhadra D. , Bhadra, Jain, & Jain, 2002) (Asthana, Chauhan, Diwan, & Jain, 2005) (Bhadra D. , Bhadra, Jain, & Jain, 2003)**. Dendrimer labs throughout the planet are persistently trying to manipulate dendrimer's solubilizing trait, in their way to explore dendrimer as drug delivery **(Khopade, Caruso, Tripathi, Nagaich, & Jain, 2002) (Prajapati, Tekade, Gupta, Gajbhiye, & Jain, 2009)** and target specific carrier **(Chauhan, et al., 2003) (Kukowska-Latallo, et al., 2005) (Quintana, et al., 2002)**.

For dendrimers to be able to be used in pharmaceutical applications, they must surmount the required regulatory hurdles to reach the market. One dendrimer scaffold designed to achieve this is the Poly Ethoxy Ethyl Glycinamide (PEE-G) dendrimer **(Toms, et al., 2016) (Dendrimers - GlycoFineChem, n.d.)**. This dendrimer scaffold has been designed and shown to have high High-Performance Liquid Chromatography (HPLC) purity, stability, aqueous solubility and low inherent toxicity.

#### 1.2.6.1. Drug delivery:

Approaches for delivering unaltered natural products using polymeric carriers is of widespread interest, dendrimers have been explored for the encapsulation of hydrophobic compounds and for the delivery of anticancer drugs. The physical characteristics of dendrimers, including their monodispersity, water solubility, encapsulation ability, and a large number of functionalizable peripheral groups, make these macromolecules appropriate candidates for evaluation as drug delivery vehicles. There are three methods for using dendrimers in drug delivery: first, the drug is covalently attached to the periphery of the dendrimer to form dendrimer prodrugs, second the drug is coordinated to the outer functional groups *via* ionic interactions, or third the dendrimer acts as a unimolecular micelle by encapsulating a pharmaceutical through the formation of a dendrimer-drug supramolecular assembly **(Morgan, et al., 2006) (Tekade, Dutta, Gajbhiye, & Jain, 2009)**. The use of dendrimers as drug carriers by encapsulating hydrophobic drugs is a potential method for delivering highly active pharmaceutical compounds that may not be in clinical use due to their limited water solubility and resulting in suboptimal pharmacokinetics. Dendrimers have been widely explored for controlled delivery of antiretroviral bioactives **(Dutta & Jain, 2007)**. The inherent antiretroviral activity of dendrimers enhances their efficacy as carriers for antiretroviral drugs **(Dutta, Garg, & Jain, 2008) (Dutta, et al., 2007)**. The dendrimer enhances both the uptake and retention of compounds within cancer cells, a finding that was not anticipated at the onset of studies. The encapsulation increases with dendrimer generation and this method may be useful to entrap drugs with a relatively high therapeutic dose. Studies based on this dendritic polymer also open up new avenues of research into the further development of drug-dendrimer complexes specific for cancer and/or targeted organ system **(Search of: starpharma - List Results - ClinicalTrials.gov, n.d.)**. These encouraging results provide further impetus to

design, synthesize, and evaluate dendritic polymers for use in basic drug delivery studies and eventually in the clinic **(Morgan, et al., 2006) (Cheng, Wu, Li, & Xu, 2008)**. An example of this application is shown in Figure 1.7.

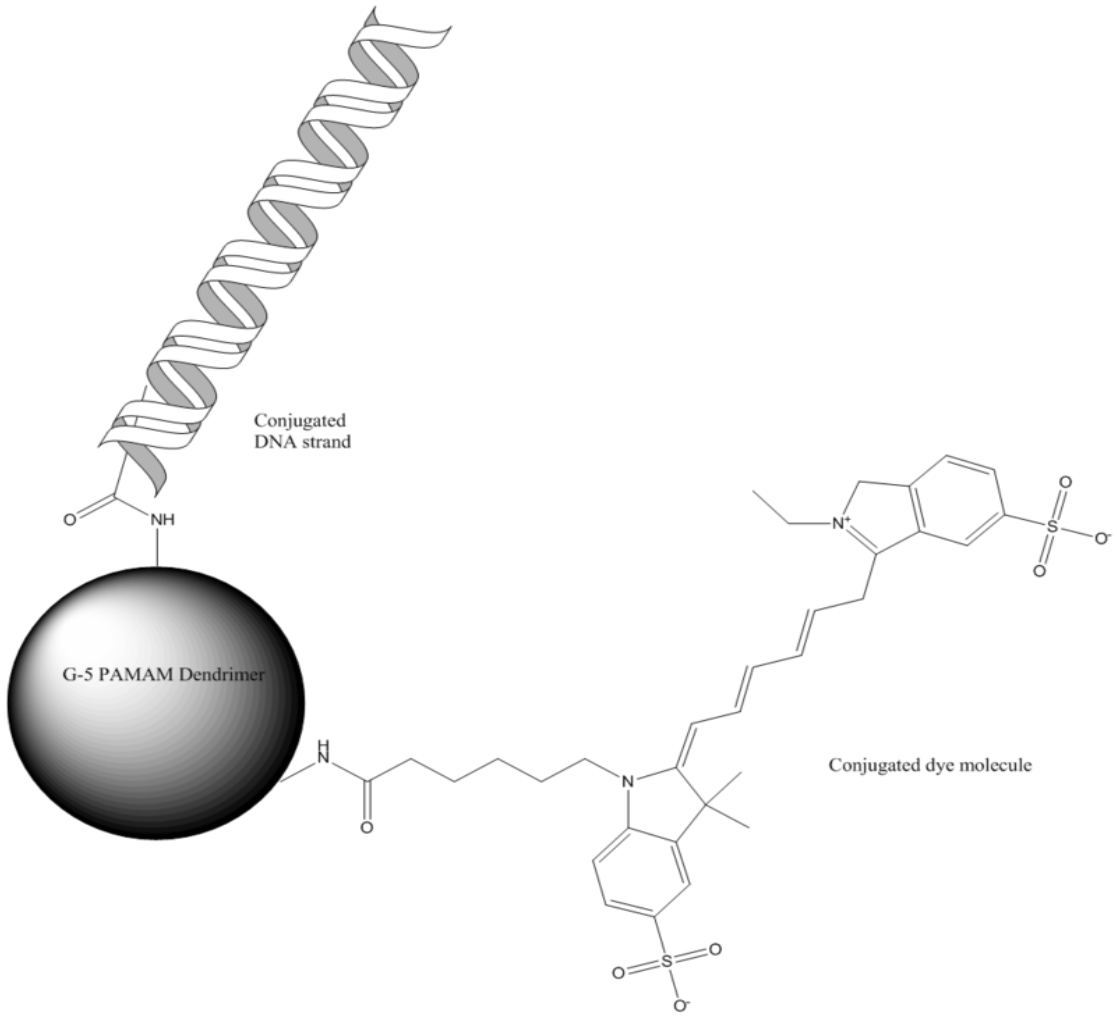


**Figure 1.7:** Schematic of a G5 PAMAM dendrimer conjugated to both a dye molecule and a strand of DNA.

### 1.2.6.2. Gene delivery:

The ability to deliver pieces of DNA to the required parts of a cell includes many challenges. Current research is being performed to find ways to use dendrimers to traffic genes into cells without damaging or deactivating the DNA. To maintain the activity of DNA during dehydration, the DNA-dendrimer complexes were encapsulated in a water-soluble polymer, and then deposited on or sandwiched in functional polymer films with a fast degradation rate to mediate gene transfection. Based on this method, PAMAM DNA-dendrimer complexes were used to encapsulate functional biodegradable polymer films for substrate-mediated gene delivery. Research has shown that the fast-degrading functional polymer has great potential for localized transfection **(Fu, Cheng, Zhang, & Zhuo, 2008) (Fu, Cheng, Zhang, & Zhuo, 2007) (Dutta, Garg, & Jain, 2008)**.

### 1.2.6.3. Sensors:

Dendrimers have potential applications in sensors. Studied systems include proton or potential of Hydrogen (pH) sensors using poly(propylene imine) **(Fernandes, Vieira, Queiroz, Guimarães, & Zucolotto, 2010)**, cadmium-sulfide/polypropylenimine tetrahexacontaamine dendrimer composites to detect fluorescence signal quenching **(Campos, Algarra, & Silva, 2010)**, and poly(propylenamine) first and second-generation dendrimers for metal cation photodetection amongst others **(Grabchev, Staneva, & Chovelon, 2010)**. Research in this field is vast and ongoing due to the potential for multiple detections and binding sites in dendritic structures.

#### 1.2.6.4. Blood substitution:

Dendrimers are also being investigated for use as blood substitutes. Their steric bulk surrounding a heme-mimetic center significantly slows degradation compared to free heme **(Twyman & Ge, 2006) (Twyman, Ellis, & Gittins, 2012)**, and prevents the cytotoxicity exhibited by free heme.

#### 1.2.6.5. Nanoparticles:

Dendrimers also are used in the synthesis of monodisperse metallic nanoparticles. PAMAM dendrimers are utilized for their tertiary amine groups at the branching points within the dendrimer. Metal ions are introduced to an aqueous dendrimer solution and the metal ions form a complex with the lone pair of electrons present at the tertiary amines. After complexion, the ions are reduced to their zerovalent states to form a nanoparticle that is encapsulated within the dendrimer. These nanoparticles range in width from 1.5 to 10 *nm* and are called dendrimer-encapsulated nanoparticles **(Scott, Wilson, & Crooks, 2005)**.

#### 1.2.6.6. Crop protection and agrochemicals:

Given the widespread use of pesticides, herbicides, and insecticides in modern farming, dendrimers are also being used by companies to help improve the delivery of agrochemicals to enable healthier plant growth and to help fight plant diseases **(Dendrimer technology licensed for herbicide, n.d.)**.

### 1.2.7. Types (Classifications) of dendrimers:

Dendrimer can be differentiated (classification) on the basis of their shape, end functional groups, internal cavities, structure, branching, solubility, chirality, attachment and maybe other properties. In this thesis, we focused on one type which is EDA-core PAMAM dendrimer.

#### 1.2.7.1. PAMAM dendrimer:

Poly(amido amine) dendrimers or PAMAM dendrimers are the most common class of dendrimers suitable for many materials science and biotechnology applications. PAMAM dendrimers consist of alkyl-diamine core and tertiary amine branches (see Figures 1.8 and 1.9). They are available in generations G(0-10) with 5 different core types and 10 functional surface groups. Most PAMAM dendrimers are supplied as solutions in methanol for improved long-term storage stability. They can be dried and reconstituted in other application-specific solvents.

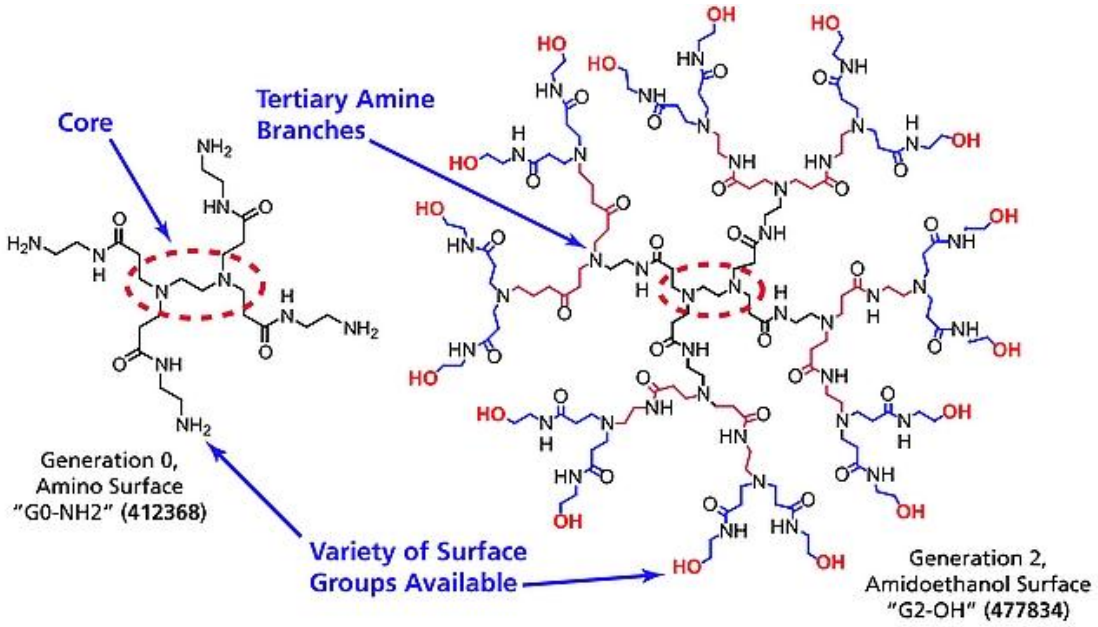


**Figure 1.8:** PAMAM dendrimer structures.

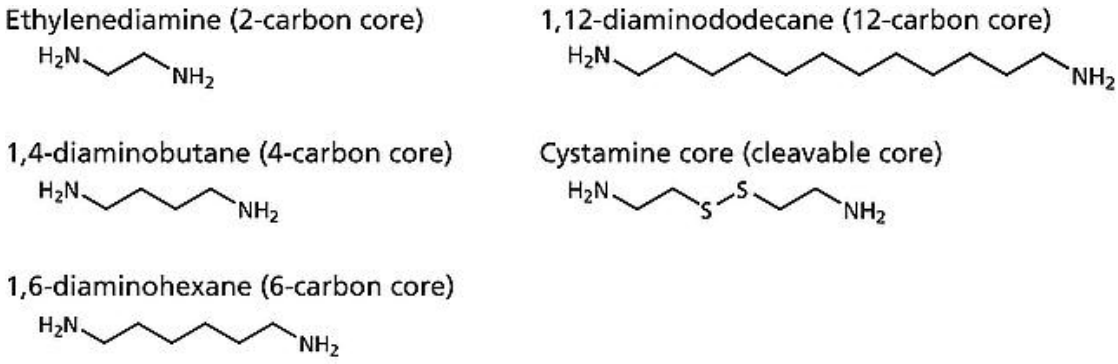


**Figure 1.9:** PAMAM dendrimer core types.

Nowadays, PAMAM dendrimers attract great attention due to their exceptional architecture, monodispersity, low toxicity and high positive charge. Such these vectors are characterized with respect to their ability to neutralize, bind and compact DNA. In gene therapy, the net positive charge of the PAMAM DNA-dendrimer complex plays an important role in determines the transfection efficiency because of the negative charge of the cell membrane. Another important aspect for gene therapy is that the bound DNA should be protected from *in vivo* degradation by the delivery vector. Using Atomic Force Microscopy (AFM) technique, Hosam and coworkers demonstrated that DNA delivered using the PAMAM dendrimer is protected from such degradation **(Abdelhady, et al., 2003)**. In addition to that, PAMAM dendrimers give better transfection efficiency compared with other delivery materials.

## 1.3 Deoxyribonucleic acid (DNA)

### 1.3.1. The definition:

DNA is a molecule that carries the genetic instructions used in the growth, development, functioning, and reproduction of all known living organisms and many viruses. DNA and Ribonucleic acid (RNA) are nucleic acids; alongside proteins, lipids and complex carbohydrates (polysaccharides), they are one of the four major types of macromolecules that are essential for all known forms of life. Most DNA molecules consist of two biopolymer strands coiled around each other to form a double helix.

The two DNA strands are called polynucleotides since they are composed of simpler monomer units called nucleotides **(Alberts, et al., 2014) (Purcell, n.d.)**. Each nucleotide is composed of one of four nitrogen-containing nucleobases (cytosine [C], guanine [G], adenine [A] or thymine [T]), a sugar called deoxyribose, and a phosphate group. The nucleotides are joined to one another in a chain by covalent bonds between the sugar of one nucleotide and the phosphate of the next, resulting in an alternating sugar-phosphate backbone. The nitrogenous bases of the two separate polynucleotide strands are bound together, according to base pairing rules (A with T and C with G), with hydrogen bonds to make double-stranded DNA (dsDNA).

The complementary nitrogenous bases are divided into two groups, pyrimidines, and purines. In a DNA molecule, the pyrimidines are thymine and cytosine, the purines are adenine and guanine.

DNA stores biological information. The DNA backbone is resistant to cleavage, and both strands of the double-stranded structure store the same biological information. This information is replicated as and when the two strands separate. A large part of DNA (more than 98% for humans) is non-coding, meaning that these sections do not serve as patterns for protein sequences.

The two strands of DNA run in opposite directions to each other and are thus antiparallel. Attached to each sugar is one of four types of nucleobases (informally, bases). It is the sequence of these four nucleobases along the backbone that encodes biological information. RNA strands are created using DNA strands as a template in a process called transcription. Under the genetic code, these RNA strands are translated to specify the sequence of amino acids within proteins in a process called translation.

Within eukaryotic cells, DNA is organized into long structures called chromosomes. During cell division these chromosomes are duplicated in the process of DNA replication, providing each cell its own complete set of chromosomes. Eukaryotic organisms (animals, plants, fungi, and protists) store most of their DNA inside the cell nucleus and some of their DNA in organelles, such as mitochondria or chloroplasts **(Russell, 2001)**. In contrast, prokaryotes (bacteria and archaea) store their DNA only in the cytoplasm. Within the eukaryotic chromosomes, chromatin proteins such as histones compact and organize DNA. These compact structures guide the interactions between DNA and other proteins, helping control which parts of the DNA are transcribed.

DNA usually occurs as linear chromosomes in eukaryotes and circular chromosomes in prokaryotes as Figure 1.10 shows. The set of chromosomes in a cell makes up its genome; the human genome has approximately 3 billion base-pairs (bp) of DNA arranged into 46 chromosomes **(Venter, et al., 2001)**. The information carried by DNA is

held in the sequence of pieces of DNA called genes. Most DNA molecules consist of two biopolymer strands coiled around each other to form a double helix.

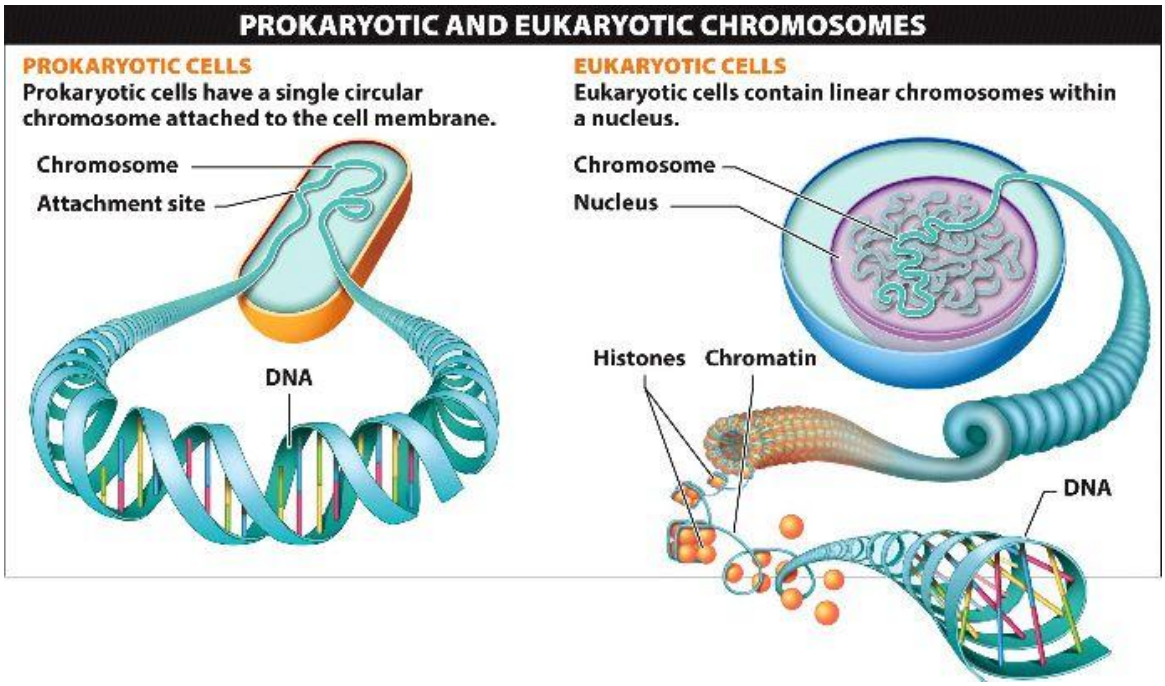


**Figure 1.10:** Eukaryote Vs. Prokaryote chromosomes (DNA) **(Chromosomes and Cell Division, n.d.)**.

### 1.3.2. History of the DNA molecule:

DNA was first isolated by Friedrich Miescher in 1869. Its molecular structure was first identified by James Watson and Francis Crick at the Cavendish Laboratory within the University of Cambridge in 1953, whose model-building efforts were guided by X-ray diffraction data acquired by Raymond Gosling, who was a post-graduate student of Rosalind Franklin. DNA is used by researchers as a molecular tool to explore physical laws and theories, such as the ergodic theorem and the theory of elasticity. The unique material properties of DNA have made it an attractive molecule for material scientists and engineers interested in micro- and nano-fabrication. Among notable advances in this field are DNA origami and DNA-based hybrid materials **(Mashaghi & Katan, 2013)**.

### 1.3.3. General characteristics of DNA molecule:

#### 1.3.3.1. The structure:

DNA is a long polymer made from repeating units called nucleotides **(Saenger, 1984) (Alberts, et al., 2002)**. The structure of DNA is dynamic along its length, being capable of coiling into tight loops, and other shapes **(Irobalieva, et al., 2015)**. In all species, it is composed of two helical chains, bound to each other by hydrogen bonds. Both chains are coiled around the same axis and have the same pitch of 34 ångströms (*Å*) (3.4 *nm*). The pair of chains has a radius of 10 *Å* (1.0 *nm*) **(Watson & Crick, 1953)**. According to another study, when measured in a different solution, the DNA chain measured 22 to 26 *Å* wide (2.2 to 2.6 *nm*), and one nucleotide unit measured 3.3 *Å* (0.33 *nm*) long **(Mandelkern, Elias, Eden, & Crothers, 1981)**. Although each individual nucleotide repeating unit is

very small, DNA polymers can be very large molecules containing millions to hundreds of millions of nucleotides. For instance, the DNA in the largest human chromosome, chromosome number 1, consists of approximately 220 million bp and would be 85 millimeters (*mm*) long if straightened **(Gregory, et al., 2006)**.

In living organisms, DNA does not usually exist as a single molecule, but instead as a pair of molecules that are held tightly together **(Watson & Crick, 1953) (Berg, Tymoczko, & Stryer, 2002)**. These two long strands entwine like vines, in the shape of a double helix. The nucleotide contains both a segment of the backbone of the molecule (which holds the chain together) and a nucleobase (which interacts with the other DNA strand in the helix). A nucleobase linked to a sugar is called a nucleoside and a base linked to a sugar and one or more phosphate groups is called a nucleotide. A polymer comprising multiple linked nucleotides (as in DNA) is called a polynucleotide **(Abbreviations and Symbols for Nucleic Acids, Polynucleotides and their Constituents, n.d.)**.

The backbone of the DNA strand is made from alternating phosphate and sugar residues **(Ghosh & Bansal, 2003)**. The sugar in DNA is 2-deoxyribose, which is a pentose (five-carbon) sugar. The sugars are joined together by phosphate groups that form phosphodiester bonds between the third and fifth carbon atoms of adjacent sugar rings. These asymmetric bonds mean a strand of DNA has a direction. In a double helix, the direction of the nucleotides in one strand is opposite to their direction in the other strand: the strands are antiparallel. The asymmetric ends of DNA strands are said to have a directionality of five prime (5′) and three prime (3′), with the 5′ end having a terminal phosphate group and the 3′ end a terminal hydroxyl group **(Berg, Tymoczko, & Stryer, 2002)**.

The DNA double helix is stabilized primarily by two forces: hydrogen bonds between nucleotides and base-stacking interactions among aromatic nucleobases **(Yakovchuk, Protozanova, & Frank-Kamenetskii, 2006)**. In the aqueous environment of the cell, the conjugated $\pi$ bonds of nucleotide bases align perpendicular to the axis of the DNA molecule, minimizing their interaction with the solvation shell. The four bases found in DNA are adenine (A), cytosine (C), guanine (G) and thymine (T). These four bases are attached to the sugar-phosphate to form the complete nucleotide, as shown for adenosine monophosphate. Adenine pairs with thymine and guanine pairs with cytosine. It was represented by A-T bp and G-C bp **(Tropp, 2011) (Carr, n.d.)**.

DNA exists in many possible conformations that include A-DNA, B-DNA, and Z-DNA forms (see Figure 1.13), although, only B-DNA and Z-DNA have been directly observed in functional organisms **(Ghosh & Bansal, 2003)**. The conformation that DNA adopts depends on the hydration level, DNA sequence, the amount and direction of supercoiling, chemical modifications of the bases, the type and concentration of metal ions, and the presence of polyamines in solution **(Basu, Feuerstein, Zarling, Shaffer, & Marton, 1988)**. The most important and most abundant form from these conformations is B-form. In this conformation, the highly negatively charged, Water-soluble and semi-flexible double helices (polymer chains) have a Persistence length ($l_p$) in the range of (30 - 100) *nm* in eukaryotic cells **(Smith, Finzi, & Bustamante, 1992)**.

Figures 1.11, 1.12 and 1.13 summarize the previous paragraphs (the structure of DNA).

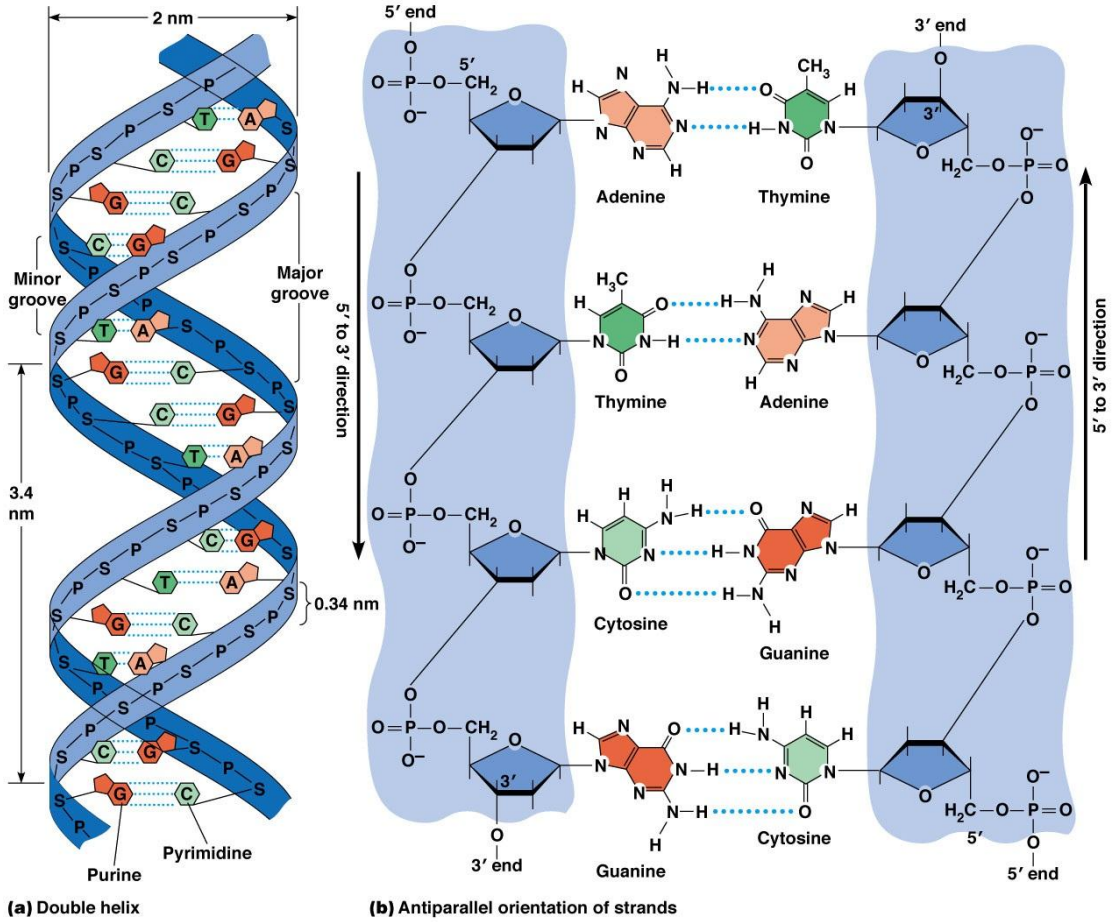


**Figure 1.11:** The DNA Double Helix. (a) This schematic diagram shows the sugar-phosphate chains of the DNA backbone, the complementary bp, the major and minor grooves, and several important dimensions. A = adenine, G = guanine, C = cytosine, T = thymine, P = phosphate, and S = sugar (deoxyribose). (b) One strand of a DNA molecule has its 5' and 3' ends oriented in one direction, whereas the 5' and 3' ends of its complement are in the opposite orientation. This illustration also shows the hydrogen bonds that connect the bases in AT and GC pairs **(Hardin & Bertoni, 2015)**.

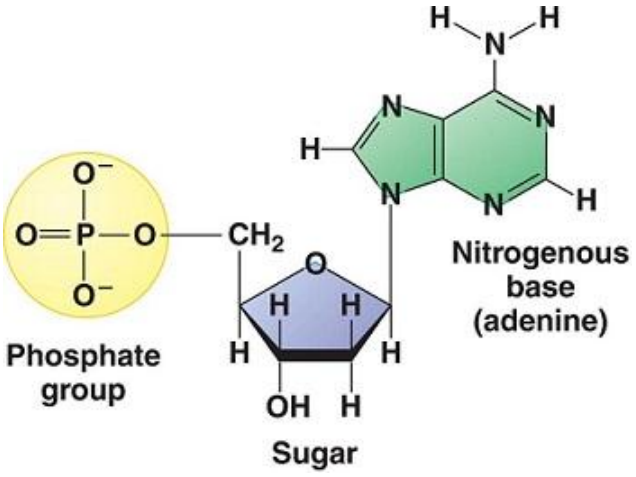


**Figure 1.12:** The structure of the nucleotide.

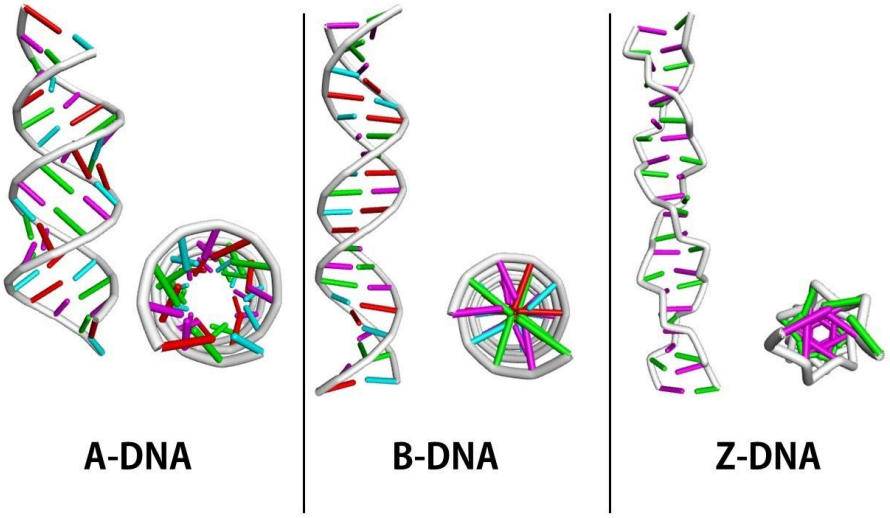


**Figure 1.13:** From left to right, the structures of A, B, and Z DNA.

### 1.3.3.2. Nucleobase classification:

The nucleobases are classified into two types: the purines, A and G, being fused five- and six-membered heterocyclic compounds, and the pyrimidines, the six-membered rings C and T **(Berg, Tymoczko, & Stryer, 2002)** (see Figure 1.14).

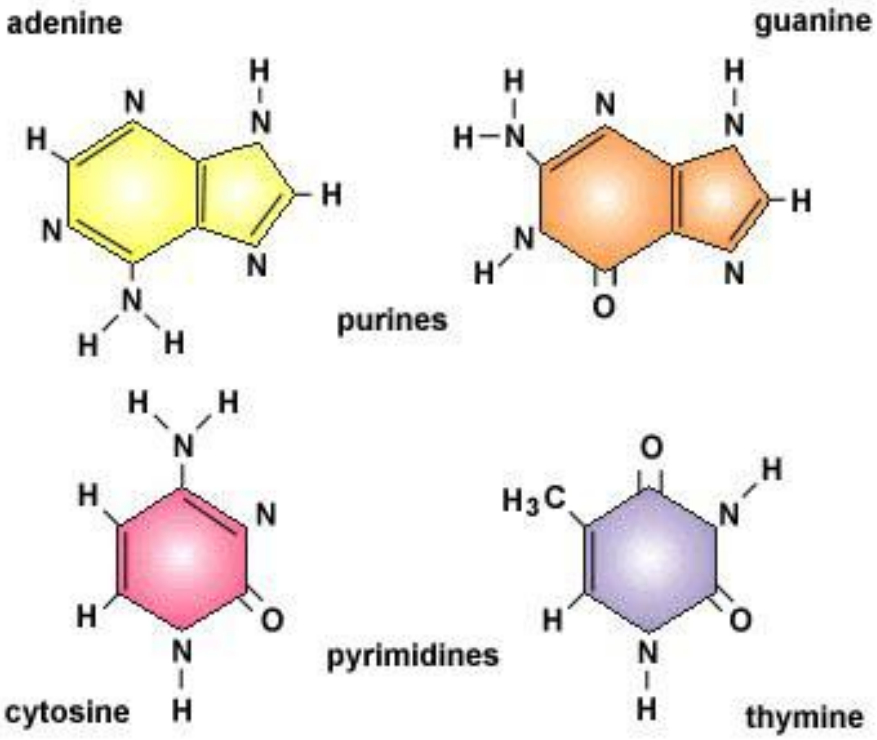


**Figure 1.14:** Major pyrimidine and purine bases of nucleic acids (DNA) and their structures.

DNA can be described as an LPE chain with negatively charged repeating units.

## 1.4 DNA-dendrimer complexation

### 1.4.1. Wrapping process and its degree (Thermodynamics of the Complex):

The major binding force for the DNA-dendrimer complex is the electrostatic interaction. Molecular dynamics (MD) simulations reveal that it takes first few nanoseconds for the DNA to form a stable complex with the dendrimer. Afterward, DNA engages to overcome different energetic hindrances and finds its optimal binding pattern on the dendrimer surface. DNA binding with dendrimers can be divided into a "tightly bound DNA" region and a "linker DNA" region as Fant and co-workers experiment study of DNA-dendrimer complexation suggests **(Fant, Esbjörner, Lincoln, & Nordén, 2008)**. The number of turns of DNA around dendrimer is maximum for the higher dendrimer generations, *i.e.*, the charge ratio between the dendrimer and DNA is maximum. On the other hand, with lower dendrimer generations, *i.e.*, with decreasing charge ratio, the number of turns of DNA around dendrimer decreases. Figure 1.15 shows the effect of generation on the number of attached monomers/atoms/beads (number of contacts) on dendrimer **(Nandy & Maiti, 2011)**.

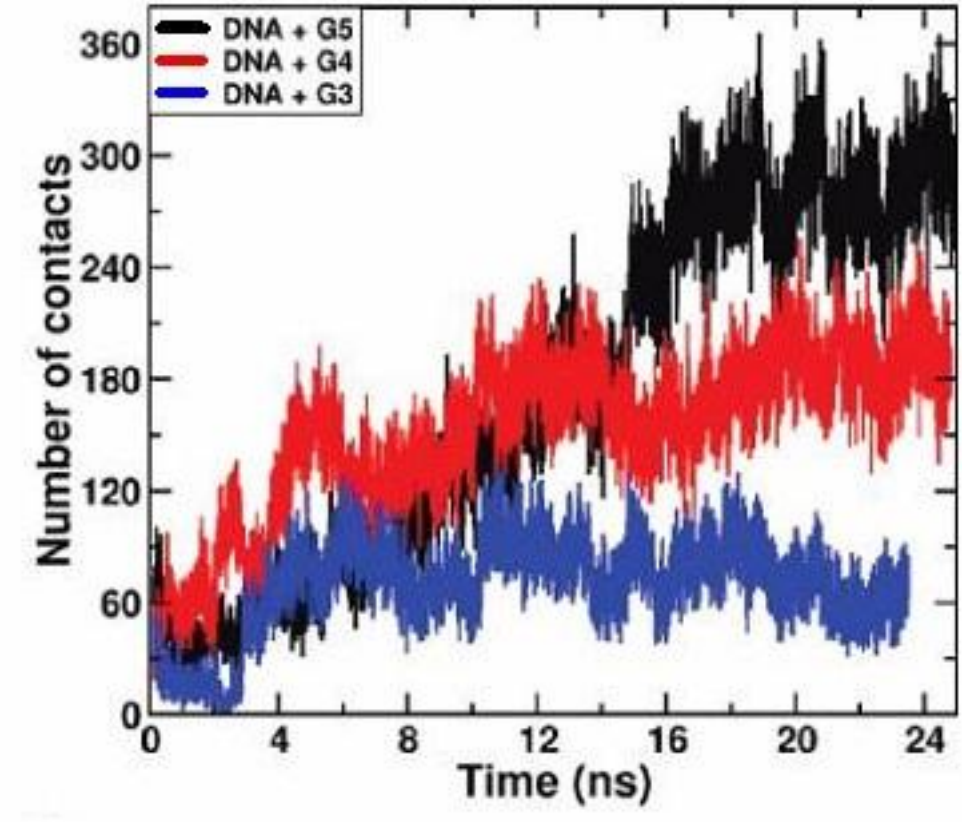


**Figure 1.15:** The number of attached monomers/atoms/beads of DNA on dendrimer as a function of simulation time **(Nandy & Maiti, 2011)**.

The electrostatic interaction that present between the cationic dendrimer and the anionic PE makes the DNA undergoes a transition from a semiflexible coil to a more compact conformation when it is mixed with PAMAM dendrimers in electrolyte solution **(Örberg, Schillén, & Nylander, 2007)**. Despite the DNA rigidity, strong electrostatic interactions cause linear DNA chain to wrap around the dendrimer and penetrate inside it, leading to the formation of a compact complex as a recent MD simulation showed **(Lee & Larson, 2009)**. It is known that, when a cationic polymer almost or completely neutralizes an ani-

onic DNA, the intermolecular interactions are electrostatic interaction and excluded volume (Lennard-Jones) interaction.

### 1.4.2. The effect of salt concentration:

For dendrimer, MD simulations generally conclude that charged dendrimers affected strongly by high ionic strength (high salts concentration) and form a contracted conformation, with a high degree of back-folding somewhat similar to what is observed upon increasing pH or poor solvation. Whereas at low salt conditions, the repulsive forces between the charged dendrimer fractions lead to an extended conformation in order to minimize charge repulsion in the structure (see Figure 1.16). There is a good quantity to capture the effect of the salt concentration on the dendrimer which is the radius of gyration ($R_g$) because it is very sensitive to the salt concentration. It increases monotonically when salt concentration is reduced because the electrostatic repulsion within the dendrimer molecule becomes stronger, and *vice versa*.

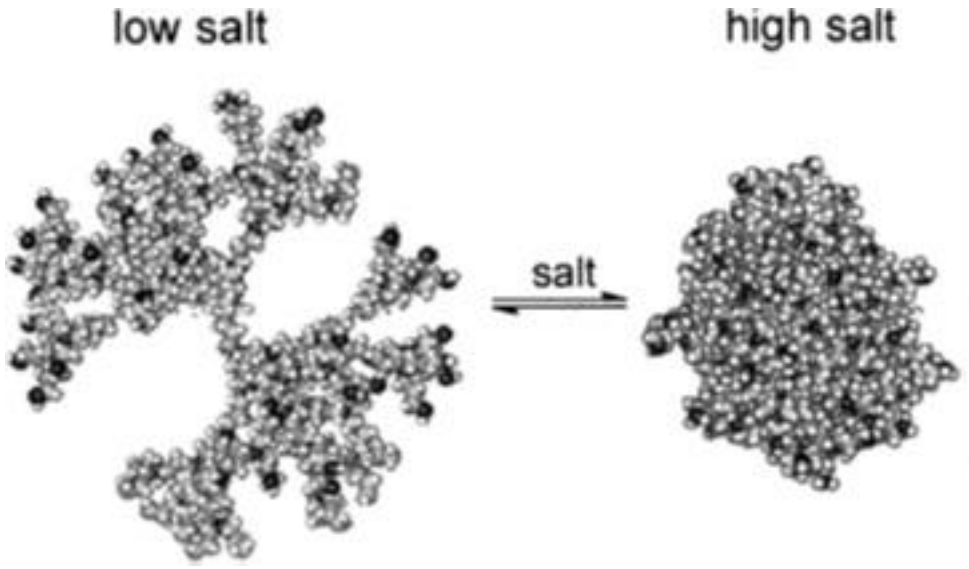


**Figure 1.16:** The three-dimensional conformational change of a Poly(propylene imine) (PPI) dendrimer upon increasing ionic strength **(Dendrimers: Design, Synthesis and Chemical Properties, 2006)**.

For DNA, the repulsive electrostatic interaction increases when salt concentration decreasing, therefore the DNA chain becomes straighter at lower salt concentration and the $R_g$ of it increases monotonically.

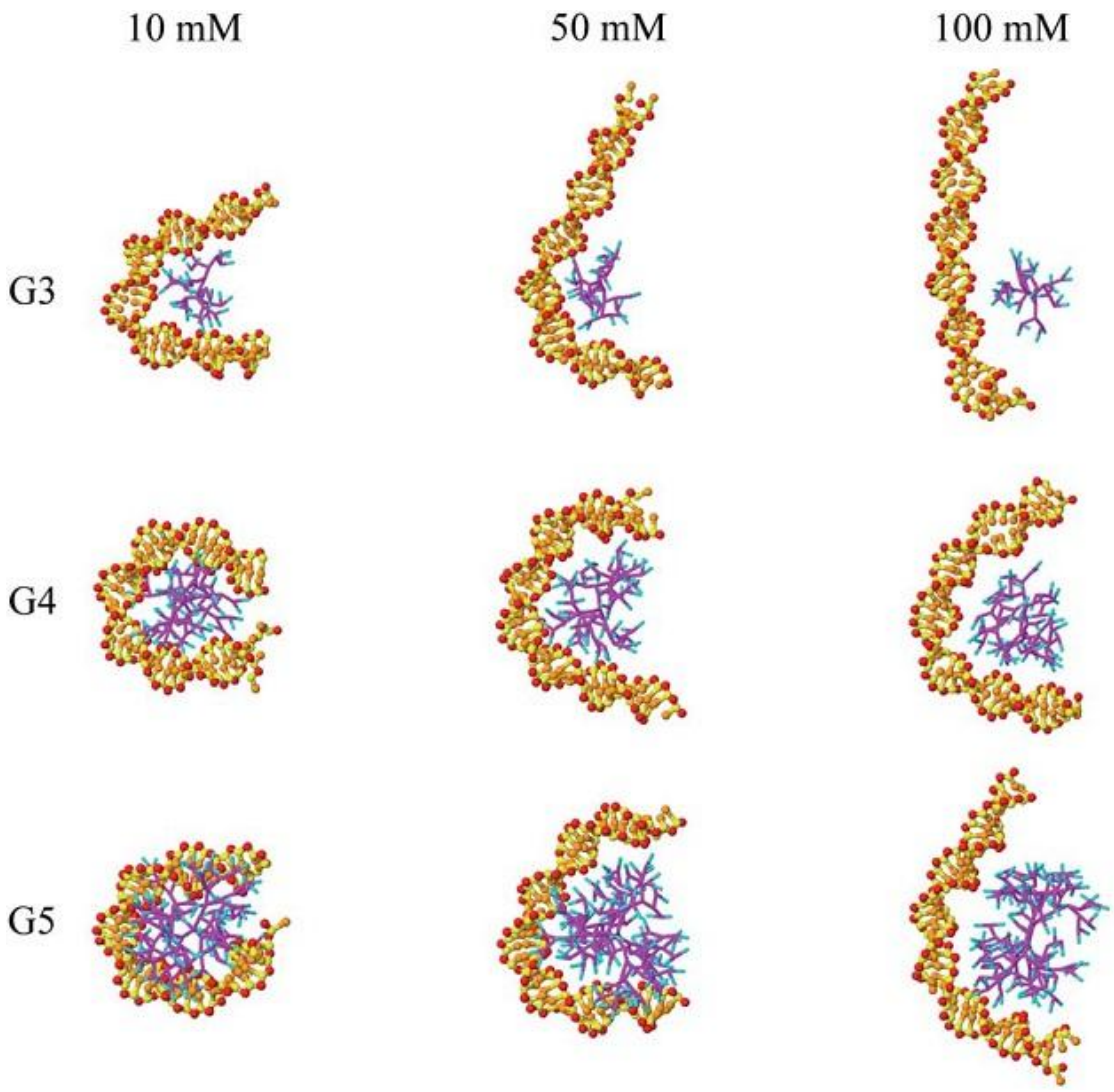


**Figure 1.17:** 38 base pair (bp) DNA condensed by G3, G4, and G5 dendrimers at salt concentrations of 10, 50, and 100 millimolar (*mM*) **(Yu & Larson, 2014)**.

For DNA-dendrimer complex, as shown in Figure 1.17, a DNA molecule wraps around a dendrimer tightly at a low salt concentration (10 *mM*) but is much straighter at a high salt concentration (100 *mM*) due to the stronger ion screening effects at higher salt concentration. For a given salt concentration the DNA compacts more tightly with a higher generation dendrimer. Therefore, a high generation dendrimer at high salt concentrations behaves like a lower generation dendrimer at lower salt concentration, in agreement with observations by Cryogenic-TEM (Cryo-TEM) **(Carnerup, Ainalem, Alfredssona, & Nylander, 2011)**. $R_g$ values of these complexes are very sensitive to the salt concentration and they decrease monotonically with decreasing salt concentration because of increased attraction between DNA and dendrimer at the lower salt concentration **(Yu & Larson, 2014)**.

### 1.4.3. The effect of pH:

For dendrimer, at high pH values, all amino groups of PAMAM dendrimer is deprotonated and the dendrimer is uncharged. This appears in an increased tendency of the terminal units to fold back into the dendrimer interior leading to a dense-core conformation and smaller radius. With reducing pH and in a first protonation step, primary amines of the

outer layer of the PAMAM dendrimer protonate independently **(Cakara, Kleimann, & Borkovec, 2003) (Niu, Sun, & Crooks, 2003)**. The result is a stable conformation with all primary amines protonated and all tertiary amines deprotonated. The arising of electrostatic repulsion between like-charged end groups reduces back folding of dendrimer branches and increases the radius. Lowering the pH of the solution further, PAMAM tertiary amino groups protonate **(Cakara, Kleimann, & Borkovec, 2003)**. This process leads to a stable state, where all amino groups are protonated (see Figure 1.18), with the exception of one central tertiary amino group. As a consequence, dendrimer branches are further extended due to the increase in intra-polymeric coulomb repulsions.

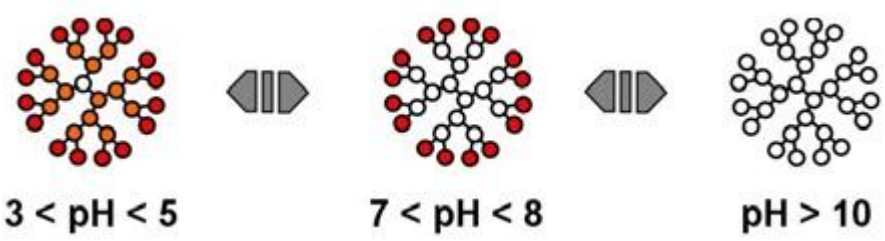


**Figure 1.18:** Schematic representation of the microscopic protonation mechanism for PAMAM dendrimer.

Table 1.2 and Figure 1.19 show the effect of pH values on G6-PAMAM dendrimer radius, total charge, and contributions of primary and tertiary amino groups **(Dootz, Toma, & Pfohl, 2011)**.

**Table 1.2:** Characteristic properties of G6-PAMAM dendrimer derived from the bead model at pH 5.5 and 8.5 **(Dootz, Toma, & Pfohl, 2011)**.

| pH values | Radius (R)(*nm*) | The contribution of primary amino groups (+*e*) | The contribution of tertiary amino groups (+*e*) | Total charge (+*e*) | Surface charge density (+*e*/*nm*$^2$) |
|---|---|---|---|---|---|
| 5.5 (Acidic) | 3.55 | 256 | 149 | 405 | 1.6-1.9 |
| 8.5 (Basic) | 3.04 | 160 | 0 | 160 | 1.46 |

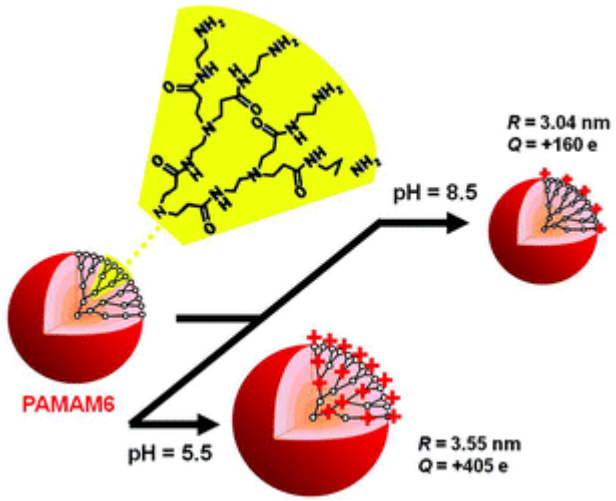


**Figure 1.19:** The effect of pH on G6-PAMAM dendrimer size and charge **(Dootz, Toma, & Pfohl, 2011)**.

For DNA, a process called depurination (hydrolysis of glycosidic bonds) occurs at low pH, whereas a process called denaturation which means deprotonate the DNA chain by pulling the hydrogen from its bases. Whatever, in this thesis, we do not study the effect of pH on the DNA chain.

For DNA-dendrimer complex, at high pH (pH >10) there is no formation of the complex because the dendrimer is uncharged. Whereas at neutral pH, the dendrimer is positively charged as previously explained, the strong electrostatics interaction helps the DNA strand collapse onto the dendrimer (see Figure 1.20). This electrostatic attraction is resisted by the elastic energy of the DNA due to bending, and when the electrostatic energy overcomes the elastic energy of bending, the collapse of the DNA onto dendrimer exists. At neutral pH, there is less penetration of DNA compared to a low pH. This means that at low pH when the complex is formed, too much of DNA penetration may complicate its release, and thus making its use as gene therapy material difficult (see Figure 1.28 in page 36). Nevertheless, at low pH condition may be better suited for the purpose of the DNA delivery inside cell since a larger fraction of DNA wrapped around dendrimer and therefore protected. If electrostatic interaction is the only major driving force in the DNA wrapping process, then lowering the solution pH further (which increases the DNA-dendrimer charge ratio) should accelerate the wrapping as proposed by various recent experiments **(Luo, Haverstick, Belcheva, Han, & Saltzman, 2002)**.

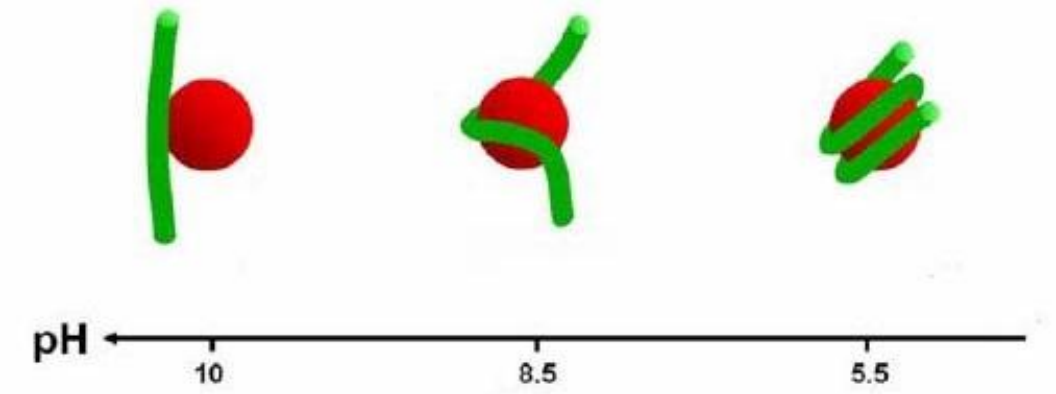


**Figure 1.20:** Different conformations of DNA-PAMAM dendrimer complex at different pH values (using simple models for both DNA chain and dendrimer).

### 1.4.4. LPE chain compaction by PAMAM dendrimer:

Two mechanisms of LPE chain compaction by the nanoscale object are usually found: the LPE either is freely adsorbed on the nanoscale objects or forms beads on a string-like object. These mechanisms depend on the size of the nanoscale object and the rigidity of the LPE chain. DNA condensation *in vitro* has attracted considerable attention due to the possibilities within non-viral gene delivery system **(Luo & Saltzman, 2000) (Kabanov, et al., 2000)**. In eukaryotic organisms, histone proteins are responsible for the packing of DNA within the nucleus, hence involved in the control of the genetic activity.

### 1.4.5. Transfection of DNA-dendrimer complex/aggregate in Gene therapy:

The free plasmid DNA is able to transfect into the living cells when given in a suitable way, but will normally be degraded in the systemic circulation, this means that the complexing of it is important. This complexing occurs with the help of a delivery system such as dendrimer which tends to compact, protect, and help the therapeutic nucleic acid to target the desired site of action. The most common strategy employed for the complexing of DNA is based on the electrostatic interaction between the anionic DNA chain and the cationic dendrimer molecule (see Figure 1.21). There are many factors that affect the transfection efficiency such as size, structure, charge density of these polymers, charge inversion, electrostatic interaction and pH value.

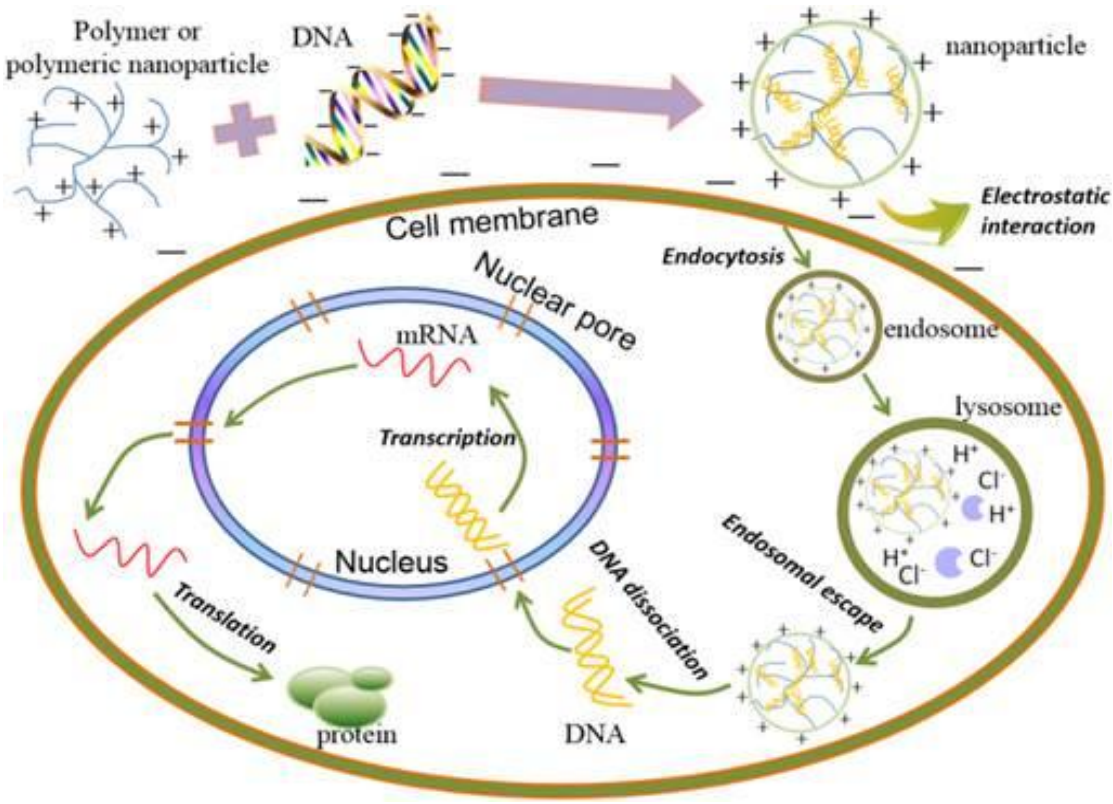


**Figure 1.21:** Gene delivery process of polymers **(Jin, Zeng, Liu, Deng, & He, 2014)**.

### 1.4.6. Importance of charge inversion:

The phenomenon of overcharge plays an important role in gene delivery. To deliver an LPE chain such as DNA from outside to the living cell, the charge of the DNA has to be screened, inverted or overcharged, because the cell membrane possesses the potential of the same sign as DNA, which prevents the penetration of the DNA through the cell membrane if it is not overcharged, thus for DNA to penetrate through the cell membrane, it has to be overcharged *via* complexation with oppositely charged macroion. Objects such as proteins, dendrimers, micelles, *etc.*, can be used as a vehicle for DNA. The formation of complexes DNA-cationic liposomes, when the nucleic acids are completely encapsulated within the positively charged lipid bilayers, is another example of the overcharging **(Lasic, Strey, Stuart, Podgornik, & Frederik, 1997)**. Around 90% of the negative charges on the DNA need to be neutralized for it to condense **(Bloomfield, 1997)**, for this reason, the cationic nature of the condensing agents is important in order to decreases the repulsion between the anionic phosphate groups of the DNA backbone, allowing condensation to occur.

## 1.5 Previous studies on DNA-dendrimer complexation

### 1.5.1. Theoretical (models) studies:

In 1999, the first theoretical models on sphere-LPE chain complexation were presented. Park and co-workers treated with the counter-intuitive appearance of spontaneous overcharging in PE-colloid complexes, a phenomenon which has been observed in experiments and simulations involving flexible chains adsorbing on oppositely charged cores. They showed that this overcharging can be accounted for in the Poisson-Boltzmann approxima-

tion; within this theory, overcharging is an entropic effect associated with the release of the counterions of the highly charged PE chain as it "overwinds" onto the rigid colloidal particle. Also, they found that increasing the rigidity of the PE chain leads eventually to undercharging of the complex **(Park, Bruinsma, & Gelbart, 1999)**.

Mateescu and co-workers considered the electrostatic interaction between a spherical macroion of charge Qq and an oppositely, highly charged PE of charge −Nq (N, Q > 0). They found that for $N \leq Q$ the PE fully collapses on the macroion, while for $N > Q$ only a partial collapse (up to neutralization of the macroion) is expected. They showed, however, that for $N > Q$, the amount of collapsed PE can be bigger than that required to neutralize the macroion, *i.e.*, the macroion can be overcharged. The overcharging increases with the diameter of the macroion (continuously or through multiple first-order transitions), until a total collapse of the PE takes place. They compared the predictions of their model with Monte Carlo (MC) simulations and suggested a possible mechanism for the overcharging of the octameric histone in the nucleosome **(Mateescu, Jeppesen, & Pincus, 1999)**.

Netz and Joanny studied the interaction of a charged, semiflexible polymer with an oppositely charged sphere. Both the effects of added salt (leading to a finite screening length) and of a bare stiffness of the polymer are taken into account. For intermediate salt concentration and high enough sphere charge, they obtained a strongly bound complex where the polymer completely wraps around the sphere. The complex may or may not exhibit charge reversal, depending on the sphere charge and salt concentration. Whereas the low-salt regime is dominated by the polymer-polymer repulsion and leads to a characteristic hump shape: the polymer partially wraps around the sphere, and the two polymer arms extend parallel and in opposite directions from the sphere. In the high-salt regime they found bent solutions, where the polymer partially wraps the sphere and the polymer ends extend in arbitrary directions from the sphere; in this regime, the wrapping transition is strongly discontinuous. This wrapping behavior agrees qualitatively well with the salt-induced release of DNA from nucleosomal core particles. The salt dependence of the wrapping transition for large salt concentrations agrees with experimental results for the complexation of synthetic PE with charged micelles. In their analysis they calculated the classical or optimal path of the polymer, using a perturbational scheme. This calculation is confirmed and augmented by scaling arguments, which in addition allow them to consider the effect of polymer fluctuations **(Netz & Joanny, 1999)**.

Nguyen and Shklovskii studied the complexation of a PE with an oppositely charged spherical macroion for both salt-free and salty solutions. They showed that when a PE winds around the macroion, its turns repel each other and form an almost equidistant solenoid, these repulsive correlations of turns lead to the charge inversion: more PE winds around the macroion than it is necessary to neutralize it. The charge inversion becomes stronger with increasing concentration of salt and can exceed 100%. Their analytical theory agrees with MC simulation results **(Nguyen & Shklovskii, 2001)**.

Schiessel and co-workers considered the complexation of highly charged semiflexible PE with oppositely charged macroions. On the basis of scaling arguments, they discussed how the resulting complexes depend on the $l_p$ of the PE, the salt concentration, and the sizes and charges of the chain and the macroions. They studied first the case of complexation with a single sphere and calculate the wrapping length of the chain. They then extended their consideration to complexes involving many wrapped spheres and studied cooperative effects.

They evaluated the mechanical properties of such a complex under an external deformation **(Schiessel, Bruinsma, & Gelbart, 2001)**.
Qamhieh and co-workers studied the interaction between positively charged PAMAM dendrimers of generation 4 and DNA for two DNA lengths; 2000 bp (L = 680 *nm*) and 4331 bp (L = 1472.5 *nm*) using a theoretical model by Schiessel for a semiflexible PE and hard spheres. They modified the model to take into account that the dendrimers are to be regarded as soft spheres, that is, the radius is not constant when the DNA interacts with the dendrimer. They showed that, for the shorter and longer DNA, the estimated optimal wrapping length, $l_{opt}$ is ≈ 15.69 and ≈ 12.25 *nm*, respectively, for dendrimers that retain their original size ($R_o$ = 2.25 *nm*) upon DNA interaction, however, the values of $l_{opt}$ for the dendrimers that were considered to have a radius of ($R = 0.4R_o$) 0.9 *nm* were 9.3 and 9.4 *nm* for the short and long DNA, respectively, and the effect due to the DNA length is no longer observed. For $l_{opt}$ = 10.88 *nm*, which is the length needed to neutralize the 64 positive charges of the G4 dendrimer, the maximum number of dendrimers per DNA ($N_{max}$) was ≈ 76 for the shorter DNA, which is larger than the corresponding experimental value of 35 for 2000 bp DNA. Whereas for the longer DNA, $N_{max}$ ≈ 160, which is close to the experimental value of 140 for the 4331 bp DNA. They observed the charge inversion of the dendrimer only when they retain their size or only slightly contract upon DNA interaction **(Qamhieh, Nylander, & Ainalem, 2009)** (see Figure 1.22, which is from a new study for Qamhieh **(Qamhieh, et al., 2014)**).

Qamhieh and Abu Khaleel developed and applied a theoretical model describing an LPEs and ion-penetrable spheres to investigate the interaction between linearized DNA and positively charged dendrimer of different generations. Throughout their study, they emphasized the effect of the medium's environments on the complexation of LPE chain with one dendrimer. They found that the wrapping degree of the chain around the dendrimer increases by increasing dendrimer's charge (decreasing pH), Bjerrum length ($l_B$), salt concentration, and decreases by increasing the rigidity of the chain. Also, they investigated the effect of (1:1) salt concentration on complexation of DNA plasmids with one dendrimer of different generations and found that the optimal wrapping length of the LPE chain around the dendrimer depends on dendrimer generation **(Qamhieh & Abu-Khaleel, 2014)** (see Figure 1.22, which is from new study for Qamhieh **(Qamhieh, et al., 2014)**).

In the same frame, Qamhieh and co-workers adopted and applied an analytical model developed by Schiessel *et al.* to provide further insight into the complexation between DNA (4331 bp) and positively charged PAMAM dendrimers of generations 1, 2, 4, 6 and 8, previously studied experimentally (see Figure 1.22).

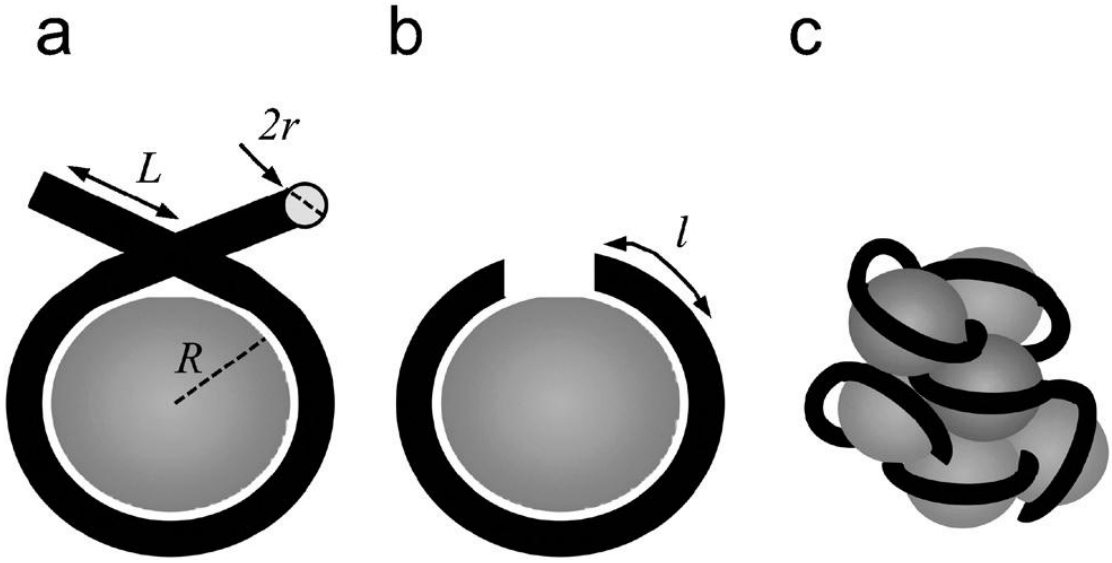


**Figure 1.22:** The proposed binding model between DNA, of contour length *L* and radius *r*, and PAMAM dendrimers modeled as hard spheres of radius *R*. In (a) a segment of a DNA molecule is shown to wrap around one dendrimer. The DNA segments linking to the next dendrimer in an aggregate are shown. In (b) a DNA-dendrimer complex consisting only of one dendrimer and the DNA segment of length, *l*, actually wrapping the dendrimer is visualized. In (c) the DNA-dendrimer aggregate consisting of the entire DNA molecule and a multiple of dendrimers is shown. The model is in accordance with the cooperative binding model proposed by Örberg **(Örberg, Schillén, & Nylander, 2007)** [ **(Qamhieh, et al., 2014)**].

As in previous studies for Qamhieh **(Qamhieh, Nylander, & Ainalem, 2009) (Qamhieh & Abu-Khaleel, 2014)**, the modified theoretical models applied describe the DNA as a semiflexible PE that interacts with dendrimers considered as either hard (impenetrable) spheres or as penetrable and soft spheres. They found that the number of DNA turns around one dendrimer, thus forming a complex, increases with the dendrimer size or generation as appears in Figure 1.23. The DNA penetration required for the complex to become charge neutral depends on dendrimer generation, where lower generation dendrimers require little penetration to give charge neutral complexes. High generation dendrimers display charge inversion for all considered dendrimer sizes and degrees of penetration. Consistent with the morphologies observed experimentally for DNA-dendrimer aggregates, where highly ordered rods and toroids are found for low generation dendrimers, the DNA wraps less than one turn around the dendrimer. Disordered globular structures appear for high generation dendrimers, where the DNA wraps several turns around the dendrimer. Particularly noteworthy is that the dendrimer generation 4 complexes, where the DNA wraps about one turn around the dendrimers, are borderline cases and can form all types of morphologies, Figure 1.24 explains this. The net-charges of the aggregate have been estimated using zeta potential measurements and are discussed within the theoretical framework **(Qamhieh, et al., 2014)**.

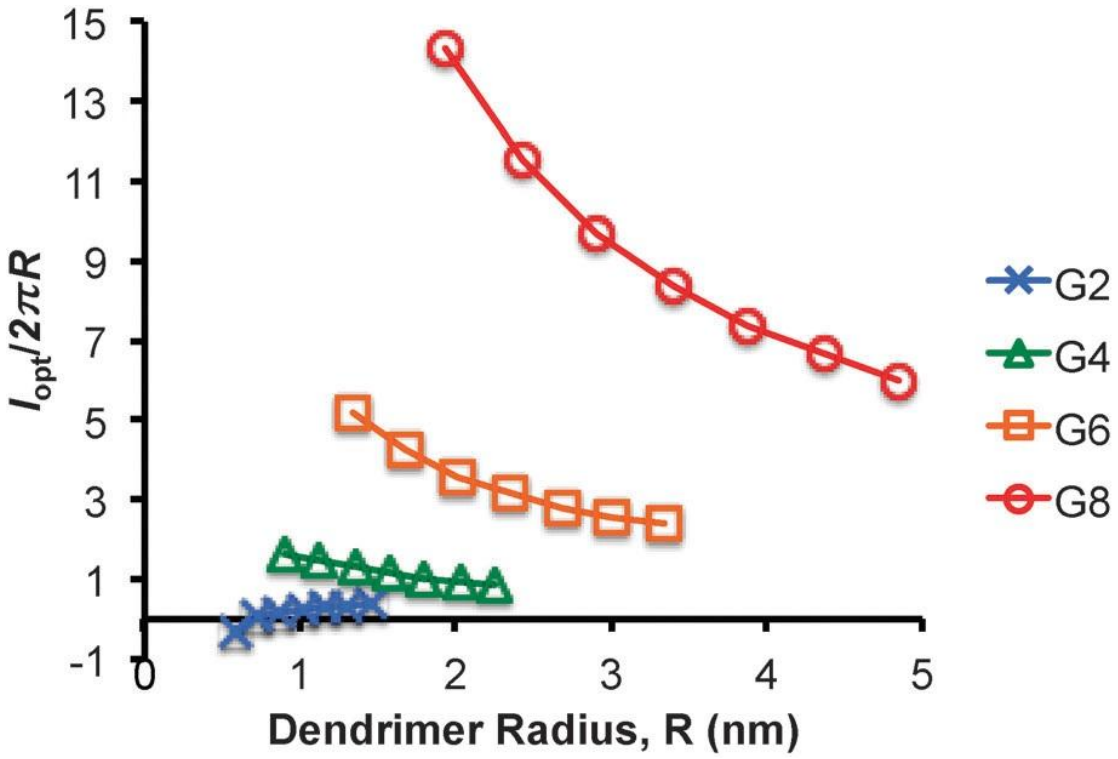


**Figure 1.23:** The ratio between the optimal DNA wrapping length and the circumference of the dendrimer, $l_{opt}/2\pi R$, as a function of dendrimer radius for different dendrimer generations, G **(Qamhieh, et al., 2014)**.

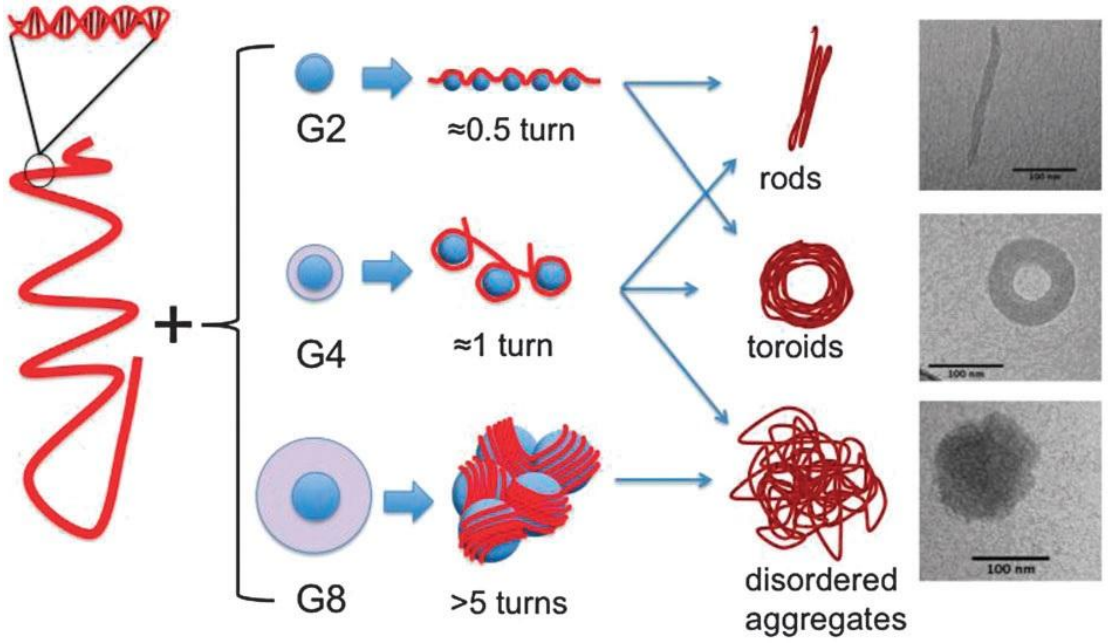


**Figure 1.24:** A schematic figure that depicts the relationship between the wrapping of the DNA and morphology of the formed complexes. The number of turns the DNA can wrap the dendrimer, *i.e.*, $l_{opt}/2\pi R$, are also indicated. Note that G4 is the border case, where different morphologies can form. The Cryo-TEM images are adopted from Ainalem **(Ainalem, et al., 2009)** [ **(Qamhieh, et al., 2014)**].

### 1.5.2. Experimental studies:

Örberg and co-workers investigated the interaction between a cationic PAMAM dendrimer of generation 4 and double-stranded salmon sperm DNA in 10 mM NaBr solution using Dynamic Light Scattering (DLS) and steady-state Fluorescence spectroscopy. They studied the structural parameters of the formed aggregates as well as the complex formation process in dilute solutions. They found that when DNA is mixed with PAMAM dendrimers, it undergoes a transition from a semiflexible coil to a more compact conformation due to the electrostatic interaction present between the cationic dendrimer and the anionic PE. The DLS results reveal that one salmon sperm DNA molecule forms a discrete aggregate in a dilute solution with several PAMAM dendrimers with a mean apparent hydrodynamic radius of 50 *nm* (see Figure 1.25). These discrete complexes coexist with free DNA at low molar ratios of dendrimer to DNA, which shows that cooperativity is present in the complex formation. They confirmed the formation of the complexes by agarose gel electrophoresis measurements. They also found that DNA in the complexes is significantly more protected against DNase catalyzed digestion compared to free DNA. Furthermore, they found that the number of dendrimers per DNA chain in the complexes is approximately equal 35 as determined by steady-state fluorescence spectroscopy **(Örberg, Schillén, & Nylander, 2007)**.

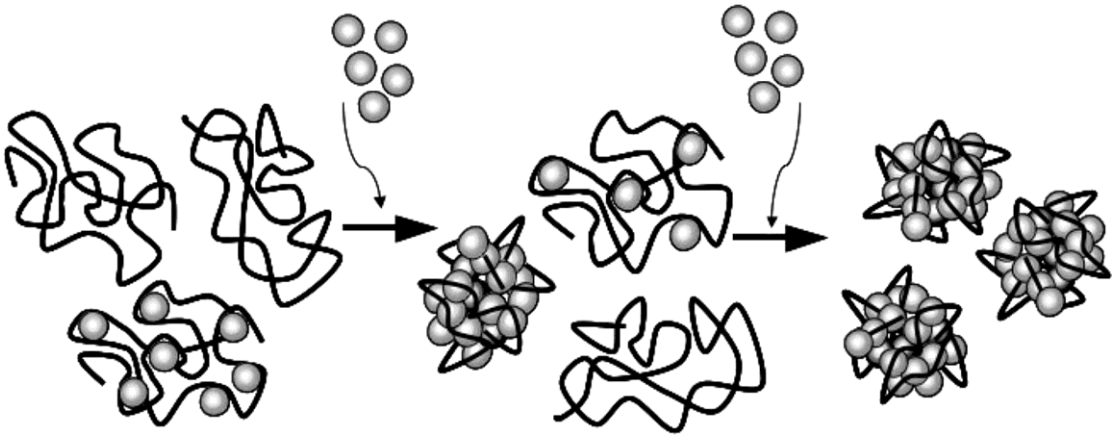

**Figure 1.25:** The proposed binding model for discrete aggregates formed between DNA and PAMAM dendrimers of generation 4 **(Örberg, Schillén, & Nylander, 2007)**.

Ainalem and co-workers presented novel results from a coherent and systematic study using Cryo-TEM, DLS and Fluorescence spectroscopy to reveal how the size, composition, and morphology of aggregates formed between DNA (4331 bp) and PAMAM dendrimers, are affected by dendrimer size and charge at low charge ratios (<1) in dilute solutions. They found that under such conditions the process is cooperative and kinetically controlled and well-defined structured aggregates are formed for lower dendrimer generations. The smaller sized dendrimers (G1 and G2), which have a lower total charge per molecule, allow the formation of well-structured rods and toroids. In contrast, globular and less defined aggregates, which are less stable against precipitation, are formed with higher generation dendrimers (see Figure 1.26). They also were able to directly visualize the cooperative nature of the condensation process as Cryo-TEM and DLS show that DNA-dendrimer aggregates, containing condensed DNA, coexist with free extended DNA chains. In fact, they also found that the apparent hydrodynamic radii of the DNA-dendrimer aggregates, obtained using DLS, are almost constant for charge ratios $\leq 1$. The fluorescence study

showed that the number of dendrimers bound per DNA chain decreases with the dendrimer generation but is independent of the charge ratio **(Ainalem, et al., 2009)**.

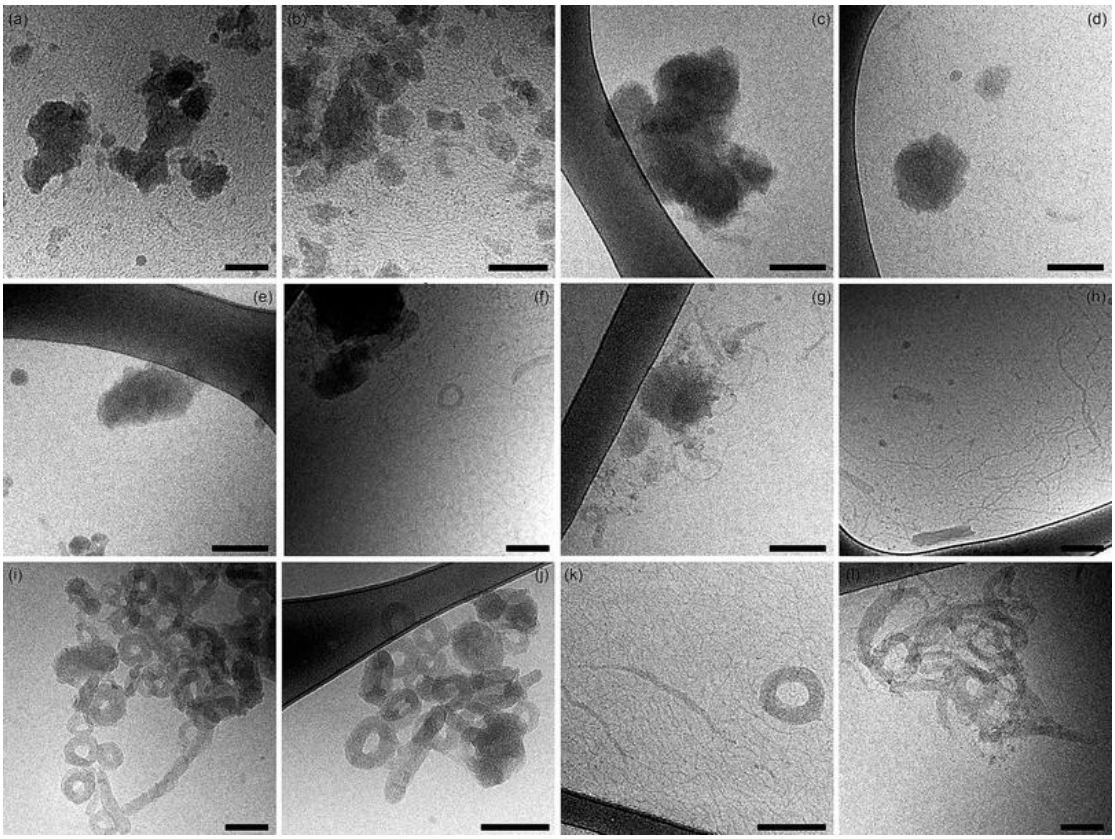


**Figure 1.26:** Cryo-TEM images of DNA-dendrimer aggregates in 10 *mM* NaBr where the morphology is seen to vary depending on dendrimer generation displayed is G8/DNA (a, b), G6/DNA (c, d), G4/DNA (e-h), G2/DNA (i, j), and G1/DNA (k, l). Scale bars are 100 *nm* in all images **(Ainalem, et al., 2009)**.

The dendrimer binding to DNA has been also found to be sufficiently strong. For increasing $r_{charge}$ values, the fluorescence emission intensity gradually decreases. This indicates that the amount of free DNA decreases for increased dendrimer concentrations. Ainalem and co-workers assumed that all dendrimers interact with DNA, for low $r_{charge}$ values, the mean resulting numbers of dendrimers per condensed DNA chain of 4331 bp are then 318, 16 and 5 for the G2, G6 and G8 of dendrimers respectively. According to the relation $r_{charge} = N_{exp}*Z_{dend}/Z_{DNA}$, these values correspond to mean charge ratios of 0.47 for G2, 0.59 for G6 and 0.61 for G8 (see Table 1.3) **(Ainalem, et al., 2009)**. Whereas Örberg and co-workers found that the mean resulting numbers of dendrimers per condensed salmon sperm DNA chain of 2000 bp (L = 680 *nm*) is 35 for G4 dendrimer, which corresponds to a charge ratio of 0.56 **(Örberg, Schillén, & Nylander, 2007)**.

**Table 1.3:** Calculated numbers of dendrimers in DNA-dendrimer aggregates using steady state Fluorescence spectroscopy for DNA of 4331 bp **(Ainalem, et al., 2009)**.

| Dendrimer generation | Charge ratio ($r_{charge}$) | Free DNA (%) | Dendrimers per DNA |
|---|---|---|---|
| G2 | 0.0 | 100 | 0 |
| | 0.086 | 87.5 | 303 |
| | 0.13 | 76.9 | 299 |
| | 0.17 | 69.8 | 305 |
| | 0.43 | 37.1 | 365 |
| G6 | 0.0 | 100 | 0 |
| | 0.086 | 79.0 | 14 |
| | 0.13 | 71.9 | 15 |
| | 0.17 | 63.9 | 16 |
| | 0.43 | 20.4 | 18 |
| G8 | 0.0 | 100 | 0 |
| | 0.086 | 86.0 | 5 |
| | 0.13 | 78.9 | 5 |
| | 0.17 | 71.5 | 5 |
| | 0.43 | 33.8 | 6 |

Carnerup and co-workers studied the condensation of DNA and PAMAM dendrimers of generation 1, 2, 4, 6, and 8 as a function of salt concentration in order to reveal the forces that control the aggregate size and morphology. They found that for the lower generation dendrimers (1, 2, and 4) a dramatic increase in aggregate size occurs as a result of an increase in salt concentration. Toroidal aggregates having an outer diameter of up to several hundreds of *nm* are observed. For the higher generation 6 dendrimers, the size of the condensed DNA aggregates does not change, however, an alteration in morphology is seen at high salt concentration, as more rod-like aggregates are observed (see Figure 1.27). The size and morphology of generation 8 dendrimers are seemingly insensitive to salt concentration. They believed that the effective neutralization of the dendrimer and DNA charge in the aggregate is the reason for the observed effects. They further showed that the 2D hexagonal lattice spacing observed in toroids is close to constant irrespective of the size of the cation responsible for the DNA condensation **(Carnerup, Ainalem, Alfredssona, & Nylander, 2011)**.

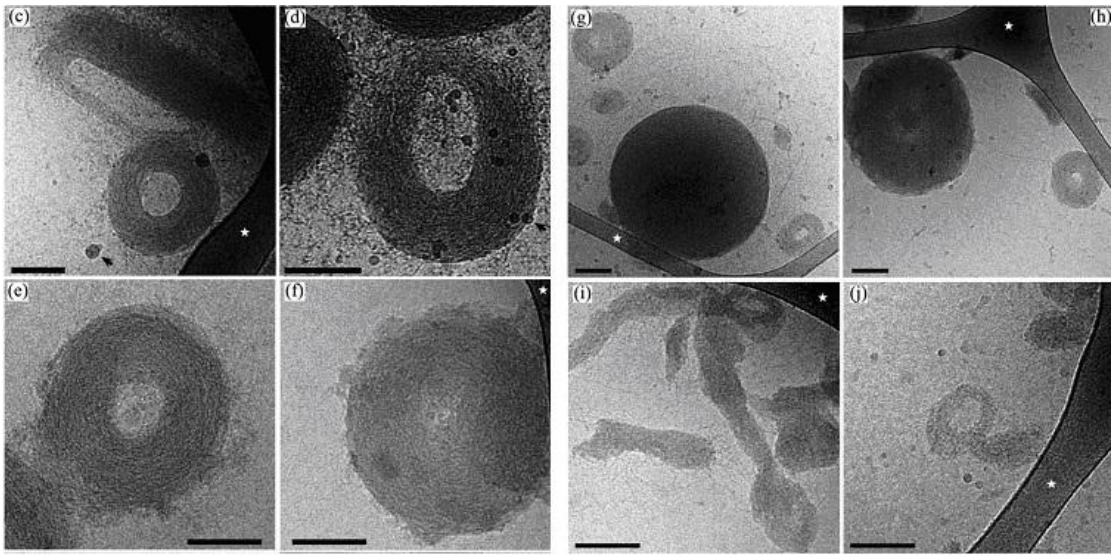


**Figure 1.27:** Cryo-TEM micrographs of Gx/DNA aggregates condensed in 150 *mM* NaBr: (c-d) G1/DNA, (e and f) G2/DNA, (g and h) G4/DNA and (i and j) G6/DNA compared to Figure 1.26 at 10 *mM* NaBr. Scale bars are 100 *nm* in all images **(Carnerup, Ainalem, Alfredssona, & Nylander, 2011)**.

### 1.5.3. Computer simulation studies:

Employing computer simulation and theory, Welch and Muthukumar presented a molecular-level picture of the guest-host dendrimer-LPE aggregates and the conditions necessary for forming them. Specifically, they examined the equilibrium and dynamic complexation behavior of a monocentric dendrimer with charged terminal groups to a flexible, oppositely charged PE. They noted Three different types of complexes depending upon the solution ionic strength and the sizes of the dendrimer and chain. Also, they found that a dendrimer may encapsulate a chain, a chain and a dendrimer may mutually interpenetrate, or a unique "chain-walking" phenomenon may be observed. In addition, they discussed the critical conditions for complexation, density profiles of the PE and the dendrimer in the complex, and the curious dynamics observed. Furthermore, they proposed a closed formula to describe the critical conditions for complexation between a dendrimer and a PE **(Welch & Muthukumar, 2000)**.

Luylin and co-workers carried out Brownian Dynamics (BD) computer simulations of complexes formed by charged dendrimers and oppositely charged linear polymer chains of different degree of polymerization ($N_{ch}$). They used bead-rod freely jointed models in the Debye-Hückel approximation without hydrodynamic interactions. They calculated mean-square radii of gyration together with the radial density distribution functions separately for a complex, a dendrimer, and a linear chain in a complex. They found that the mean-square $R_g$, the different monomer radial distribution functions, and the static structure factor for a dendrimer in a complex with long enough chains are very close to those for a single neutral dendrimer, and the monomers of the linear chains with $N_{ch}$ equal to the number of the dendrimer's terminal charged groups are located very close to these terminal groups. They found also for longer chains the total number of the chain monomers adsorbed onto a dendrimer exceeds the number that is necessary for a dendrimer neutralization, and the overcharging phenomenon is observed. They compared their results with predictions of the correlation theory **(Lyulin, Darinskii, & Lyulin, 2005)**.

Maiti and Bagchi studied the sequence-dependent complexation between oligonucleotides (single-strand DNA or ssDNA) and various generation EDA cored PAMAM dendrimers through Atomistic MD (AAMD) simulations accompanied by free energy calculations and inherent structure determination (see Figure 1.28). Simulations revealed the formation of a stable complex and provided a detailed molecular level understanding of the structure and dynamics of such a complexation. They found that the reaction free energy surface in the initial stage is funnel-like, with a significant barrier arising in the late stage due to the occurrence of misfolded states of DNA. Complexation showed surprisingly strong sensitivity to the ssDNA sequence, which is found to arise from a competition between enthalpic versus entropic rigidity of ssDNA **(Maiti & Bagchi, 2006)**.

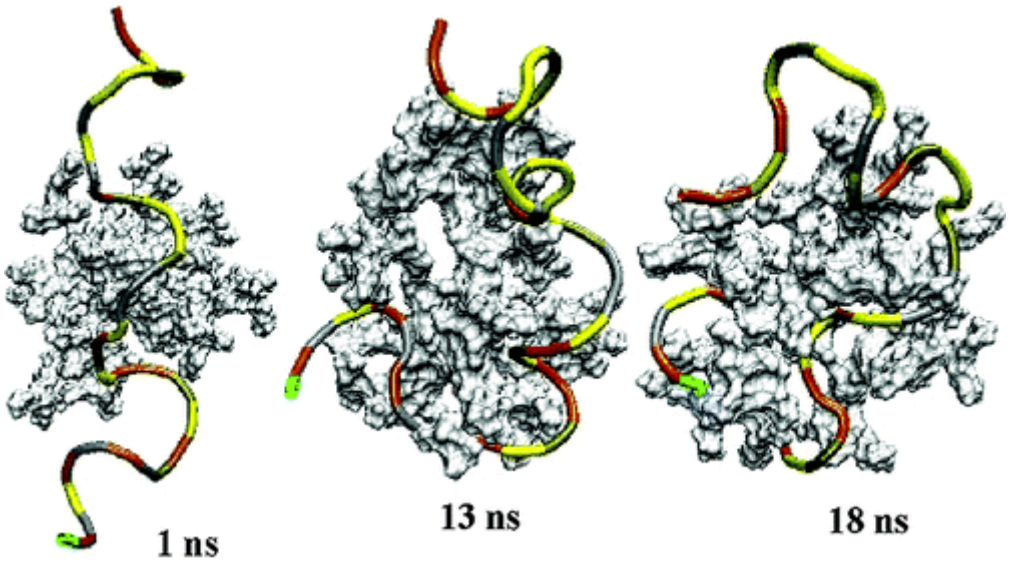


**Figure 1.28:** Several snapshots in a few *ns* of formation of DNA-dendrimer complex **(Maiti & Bagchi, 2006)**.

Given the exceptional potential of dendrimer macromolecules for numerous biomedical applications, Luylin and co-workers also performed extensive Coarse-Grained (CG) MD simulations to investigate the role of electrostatic interactions in complexes comprised of cationic dendrimers with oppositely charged LPE (see Figure 1.29). For this purpose, they varied the nature of the PE chain by considering both mono- and divalent chains and studied these cases for different valency of counterions. They also varied systematically the dielectric properties of the solvent and included counterions as well as solvent molecules explicitly in the model. They found that the complexation of an LPE with a dendrimer leads to a remarkable condensation of the complex. Furthermore, the formation of the complex gives rise to a considerable dehydration of the chain, the dehydration becoming more pronounced when the electrostatic interactions strengthen. Thus, charged dendrimers clearly demonstrate the ability for efficient compaction of guest chains and protective screening of the chains from the surrounding medium, the two well-known prerequisites for vehicle-mediated delivery of drugs and genes into cells. In addition, their study indicates noticeable effects of counterions on the structure of dendrimer-chain complexes. These effects become more pronounced with increasing strength of electrostatic interactions **(Lyulin, Vattulainen, & Gurtovenko, 2008)**.

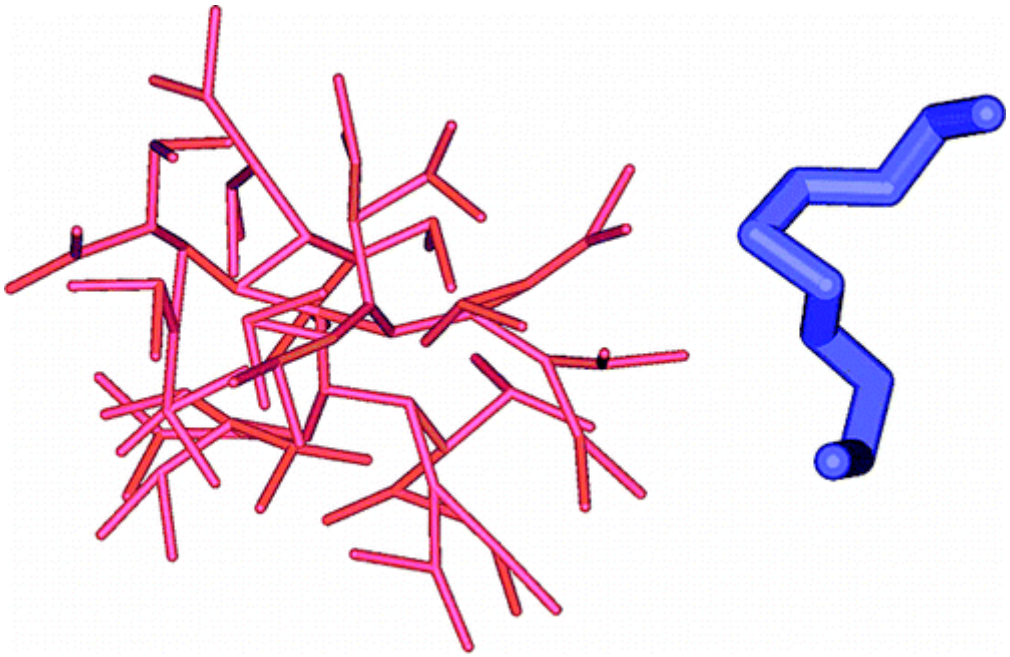

**Figure 1.29:** CG models for dendrimer and the LPE chain **(Lyulin, Vattulainen, & Gurtovenko, 2008)**.

Complexes of fully ionized third generation dendrimers with oppositely charged LPE chains are studied by Larin and co-workers using BD method. A freely jointed model of a dendrimer and a linear chain is used. Electrostatic interactions are considered within the Debye-Hückel approximation with the Debye radius exceeding the dimensions of a dendrimer (see Figure 1.30). In these systems, the phenomenon of charge inversion is observed, and the degree of "overcharging" is higher as compared with that taking place in analogous complexes formed by dendrimers in which only terminal groups are charged. The dependence of the number of chain units adsorbed on a dendrimer on the PE chain length is nonmonotonic and agrees qualitatively with the predictions of the theory proposed by Nguyen and Shklovskii for a complex composed of a spherical macroion with an oppositely charged linear chain. This nonmonotonic character also manifests itself for certain other structural characteristics of the complexes. Upon the formation of a complex, a chain is shown to penetrate deeply into a dendrimer **(Larin, Lyulin, Lyulin, & Darinskii, 2009)**. In another study for them, they studied the complexes formed by two dendrimers with charged terminal groups and oppositely charged long LPE using BD simulations (see Figure 1.31). They investigated the structural properties of the complexes and their dependence on the LPE chain length. They also observed that dendrimers in the considered complexes are sufficiently overcharged, *i.e.*, the number of adsorbed LPE monomers is larger than required for the neutralization. The degree of overcharging increases with the increase of the LPE length and is accompanied by the linker appearance until saturation in overcharging is reached. In addition to that, they observed the nonmonotonic dependence of the linker size on the LPE length. They developed the correlation theory to describe the structural properties of the complexes formed by two macroions and a PE chain **(Larin, Darinskii, Lyulin, & Lyulin, 2010)**.

**(a)**

**(b)**

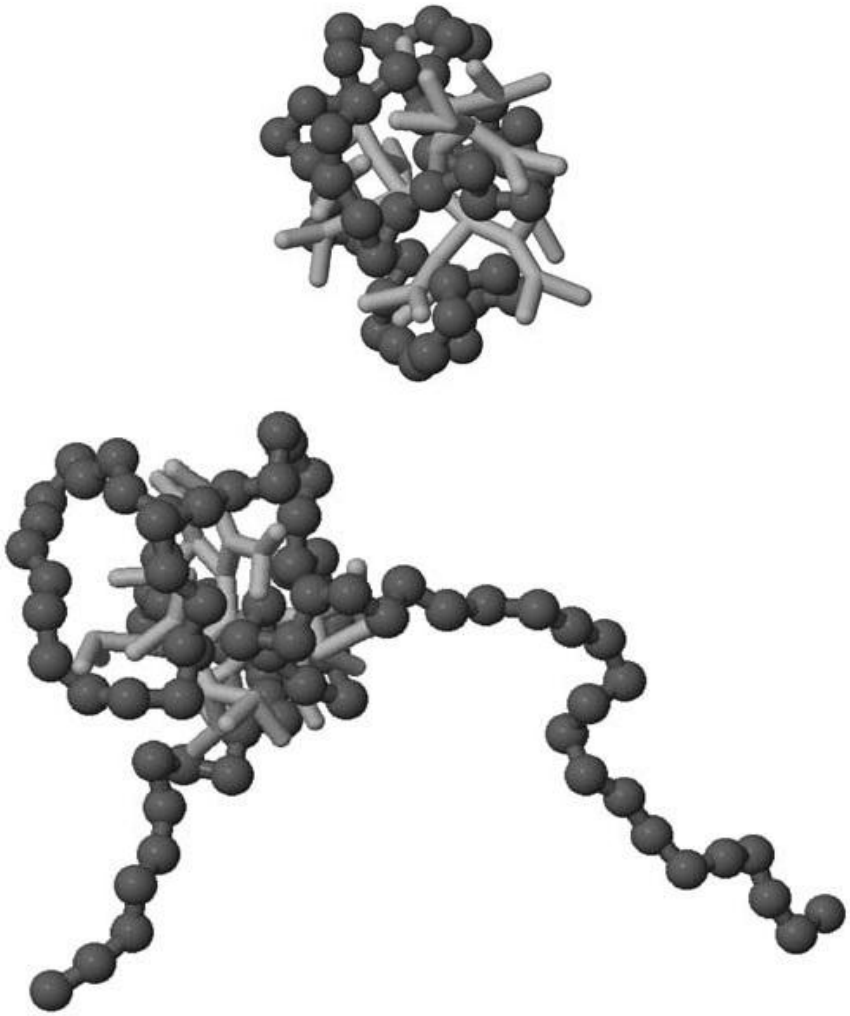

**Figure 1.30:** Instant configurations of the complexes formed by the fully charged G3 dendrimer containing PE chains with length $N_{ch}$ = (a) 48 and (b) 80. A dendrimer is shown as light gray rods, chain units are shown as dark gray spheres **(Larin, Lyulin, Lyulin, & Darinskii, 2009)**.

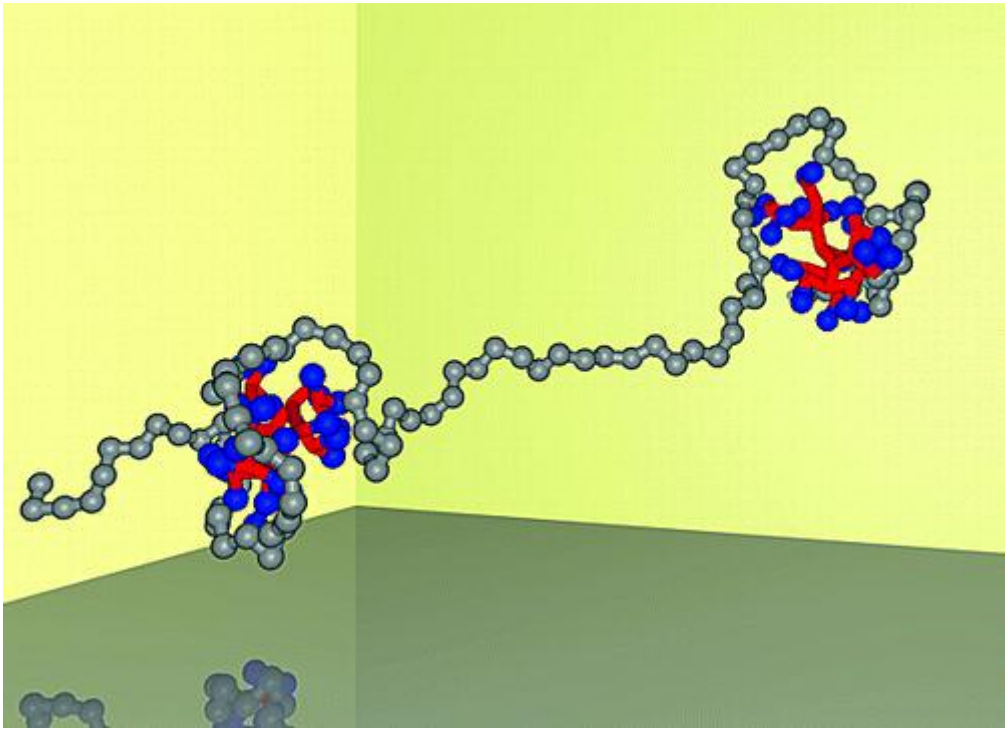

**Figure 1.31:** The complex formed by two dendrimers with charged terminal groups and oppositely charged long LPE using BD simulations **(Larin, Darinskii, Lyulin, & Lyulin, 2010)**.

New MD simulation methodologies such as the CG models for bio-systems and the technological advances in computers and their computing power have enabled scientists and researchers to develop their studies and perform better and more accurate MD simulations. Tian and Ma employed extensive CGMD simulation to study the influence of rigidity of the LPE chain on dendrimer-LPE complexes (see Figure 1.32). They found that the size of PE chain increases and its shape changes from oblate to prolate concomitant with the interesting conformation transformations from "coil"-like to "U"-like or "V"-like and further to "rod"-like as the stiffness of the PE chain is increased. They also find that, as a soft nanoparticle, the changes of the size and the shape of charged dendrimer depend not only on the stiffness of the PE chain but also on $l_B$ of the system. This can be explained in terms of two competing interaction energies: the bending energy and the electrostatic attractive energy. Furthermore, they witness that the effective charge of dendrimer exists a jump at both Bjerrum lengths ($l_B$) studied, but the overcharge only appears at the large $l_B$. Moreover, they propose that there may exist an optimum stiffness of bioactive guest in the complexes for delivery and release **(Tian & Ma, 2010)**.

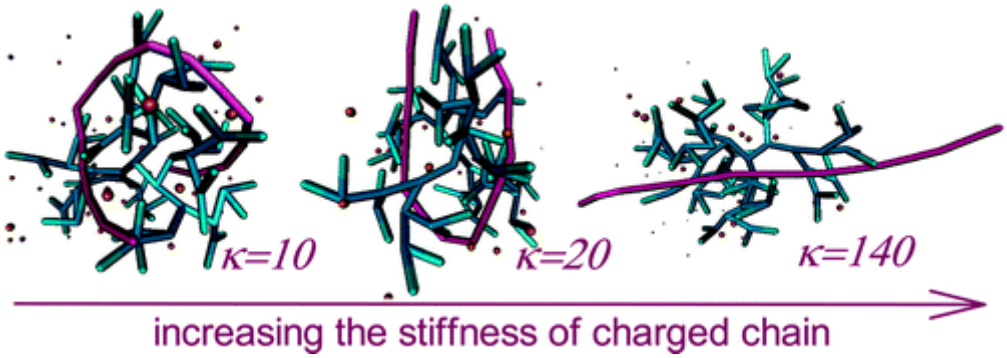


**Figure 1.32:** The influence of rigidity of the LPE chain on LPE-dendrimer complexes **(Tian & Ma, 2010)**.

Yu and Larson used MC simulations to determine the influence of PAMAM dendrimer size and charge on its interactions with dsDNA conformation and interaction strength. To achieve a compromise between simulation speed and molecular detail, they combined the CG DNA model of de Pablo *et al.* which resolves each DNA base using three beads - and thereby retains the double-helix structure - with a dendrimer model with resolution similar to that of the DNA. They found that the resulting predictions of the effects of dendrimer generation, dendrimer surface charge density, and salt concentration on DNA-dendrimer complexes are in agreement with both experiments and AAMD simulations. They showed that DNA wraps a fully charged G5 or G6 dendrimer at a low salt concentration (10 *mM*) similarly to a histone octamer, and for the G5 dendrimer, they got the DNA superhelices with both handednesses. Whereas at salt concentrations above 50 *mM*, or when a high fraction of dendrimer surface charges are neutralized by acetylation, they found that DNA adhered but does not compactly wrap the dendrimer, in agreement with experimental findings. They also were able to simulate pairs of dendrimers binding to the same DNA strand. Thus, their mesoscale simulation not only elucidates DNA-dendrimer interactions but also provides a methodology for efficiently simulating chromatin formation and other cationic macroion-DNA complexes **(Yu & Larson, 2014)** (return to Figure 1.17 in page 23).

## 1.6 Statement of the problem

This Thesis/Research aimed to study the complexation of dsDNA with EDA-core PAMAM dendrimer using BD simulations. Specifically, it seeks to answer the following sub-problems:

1. Is our model for dsDNA chain valid? (through calculating the translational diffusion coefficient ($D_t$) and the persistence length ($l_p$) of the dsDNA chain).
2. How the salt concentration affects the persistence length ($l_p$) of the dsDNA chain?
3. How is the complexation of the dsDNA chain with dendrimer affected by both salt concentration and pH?
4. In dsDNA-two dendrimer aggregate, how the salt concentration and the dsDNA chain length affect the linker between dendrimers and the adsorbed part of the dsDNA chain onto dendrimers surfaces? also, does the over-charging phenomenon appear? and how it depends on the dsDNA chain length and the salt concentration?
5. How the different generations of dendrimer affect the morphology of the dsDNA-dendrimer aggregate at 10 *mM* salt concentration?

# Chapter Two

## Models and Method

# 2 Chapter Two: Models and Method

## 2.1 Introduction

In this study, we used the single strand bead-spring and the charged hard sphere models to describe the B-form dsDNA chain and the EDA-core PAMAM dendrimer respectively (see Figure 2.1).

**(a)**

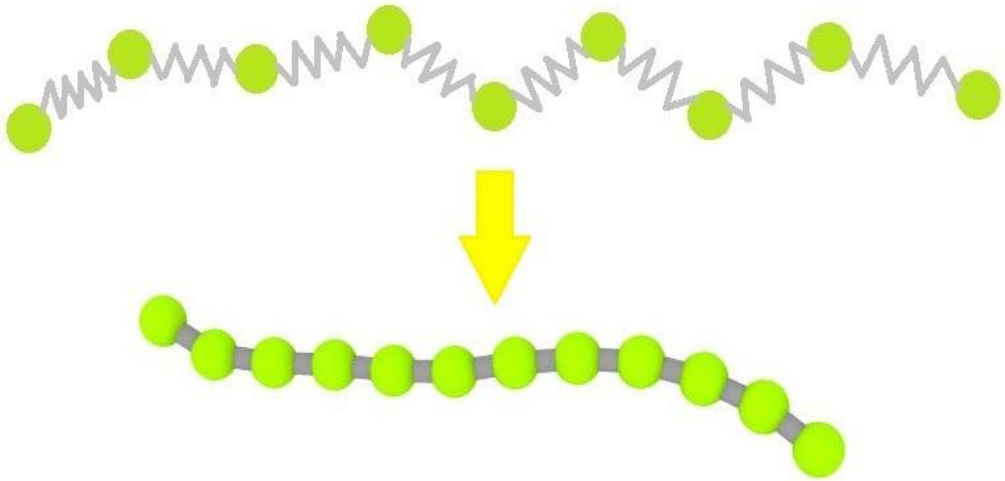

**(b)**

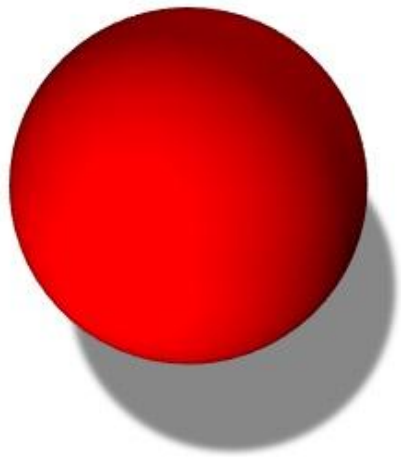

**Figure 2.1:** The models we used: (a) for dsDNA chain and (b) for EDA-core PAMAM dendrimer.

## 2.2 Models

### 2.2.1. DNA model:

We used the single strand bead-spring model to simulate the B-form dsDNA. Each bead represents 6 bp with a radius equal to 8.0 *Å*, a mass equal to 3900.0 *g/mol* and total charge equal to -12*e* except for the ends of the chain the total charge of the bead equal to -14*e* (-2*e* come from 5' end of the B-form dsDNA). For completeness, we listed all equations (force field) used in the next four pages. [The constants used in these equations and further details about this model (force field) can be found in the simulated systems (summary of all parameters) part (section 2.3).]

The bonded interactions of our force field are given by:

$$U_{bond} = K_{bond}(r - r_0)^2 \qquad (2.1)$$

Where $K_{bond}$ is the linear spring constant (in *Kcal/mol.Å*$^2$), $r$ is the length of the bond between the $i_{th}$ and the $(i+1)_{th}$ dsDNA beads and $r_0$ is the equilibrium bond distance (in *Å*).

$$U_{angle/bend} = K_{angle/bend}(\theta - \theta_0)^2 \qquad (2.2)$$

Where $K_{angle/bend}$ is the angular spring constant (in *Kcal/mol.rad*$^2$), $\theta$ is the angle between the $(i-1)_{th}$, the $i_{th}$ and the $(i+1)_{th}$ dsDNA beads and $\theta_0$ is the equilibrium angle (in degrees $^o$).

Here $U_{bond}$ and $U_{angle/bend}$ (in *Kcal/mol*) represent bond stretch energy and bending energy respectively. For clarification, Figure 2.2 shows the graph of these two potentials with $r_0 = 0$ Å and $\theta_0 = 0$ °.

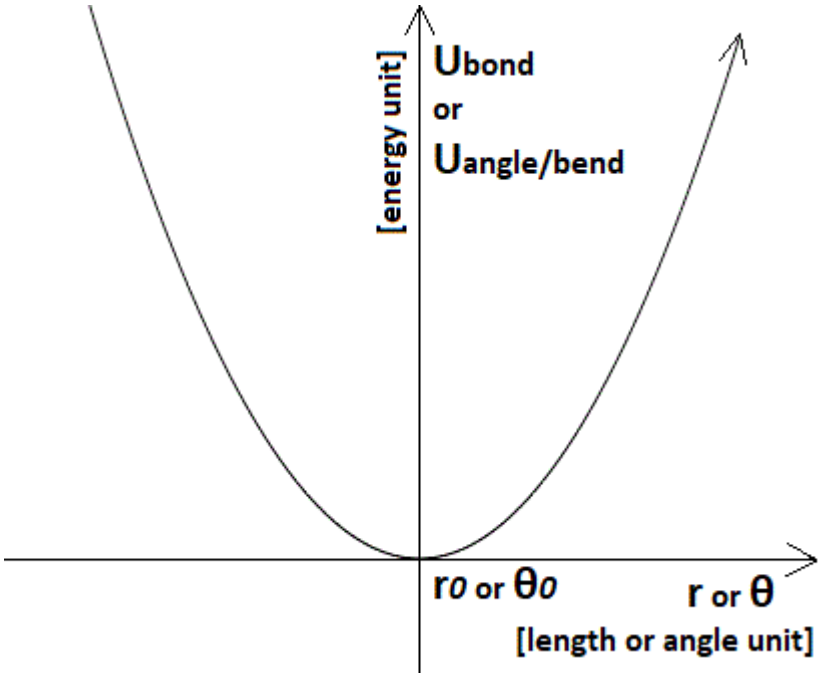


**Figure 2.2:** The bonded interactions of our force field for dsDNA chain with $r_0 = 0$ Å and $\theta_0 = 0$ °.

The nonbonded, pairwise interactions between dsDNA beads which are the excluded volume potential and the electrostatic repulsions were included in the truncated Lennard-Jones potential ($U_{LJ}$) and the Debye-Hückel potential ($U_{elec}$) (in *Kcal/mol*) respectively.

$$U_{LJ} = 4\varepsilon\left[\left(\frac{\sigma}{r}\right)^{12} - \left(\frac{\sigma}{r}\right)^{6}\right], \quad r < r_{cutoff} \qquad (2.3)$$

Where $\varepsilon$ is the depth of the potential well (in *Kcal/mol*), $\sigma$ is the finite distance at which the inter-bead potential is zero, $r$ is the distance between dsDNA beads and $r_{cutoff}$ is the cutoff radius of this potential (in *Å*). The minimum of this potential occurs at $r_m = 2^{1/6}\sigma \approx 1.122\sigma$ (Å) and equal to $-\varepsilon$ $(Kcal/mol)$.

$$U_{elec} = \frac{Cq_iq_j}{\epsilon r} exp^{(-\kappa r)}, \;\; r < r_{cutoff} \tag{2.4}$$

Where $C$ is an energy-conversion constant (is set by the simulation program according to the type of units used - see the Simulation method section below), $q_i$ and $q_j$ are the number of charges on the two beads (multiple of electron charge (*e*)), $\epsilon$ is the dielectric constant (*unitless*), $r$ is the distance between dsDNA beads, $r_{cutoff}$ is the cutoff radius of this potential (in *Å*) and $\kappa$ is the inverse of the Debye length (in $Å^{-1}$) which is defined by:

$$\kappa^{-1} = \sqrt{\frac{\epsilon_0 \epsilon(T,C) k_B T}{2N_A {e_c}^2 I}} = \frac{1}{\sqrt{8\pi l_B N_A I}} \tag{2.5}$$

$$Where\ l_B = \frac{{e_c}^2}{4\pi\epsilon_0\epsilon(T,C)k_BT}$$

Where $\epsilon_0$ is the vacuum permittivity (in $C^2/N.Å^2$), and $\epsilon(T,C)$ is the temperature *(T)* and salt concentration *(C)*-dependent dielectric constant (*unitless*), $k_B$ is the Boltzmann constant (in *N.Å/K*), *T* is the temperature (in *K*), $N_A$ is the Avogadro's number (in $mol^{-1}$), $e_c$ is the elementary charge (in *C*), *I* is the molar ionic strength (here in $mol/Å^3$), *i.e.*, a measure of the concentration of ions in that solution, that is given by this relation:

$$I = \frac{1}{2}\sum_{i=1}^{n} c_i z_i^2 \tag{2.6}$$

Where one half is because we are including both cations and anions, $c_i$ is the molar concentration of ion *i* (in *M*, *mol/L*), $z_i$ is the charge number of that ion, and the sum is taken over all ions in the solution. For a 1:1 electrolyte such as sodium chloride (NaCl) that we used, where each ion is singly-charged, the ionic strength is equal to the concentration. And $l_B$ is the Bjerrum length of the medium (in *Å*) which equal to 7.1 *Å* for water at 25 °*C*.

The definition of $\varepsilon(T,C)$ is:

$$\varepsilon(T,C) = \varepsilon(T)a(C) \tag{2.7}$$

Where $\varepsilon(T)$ is the static (zero-frequency) dielectric constant at absolute temperature *T* (in *K*), and $a(C)$ is the salt correction (NaCl which is the monovalent salt we considered in our study or any monovalent salt can give the same effect) for a solution with molarity $C$ (in *M*) **(Sambriski, Schwartz, & de Pablo, 2009)**. These contributions are given by:

$$\varepsilon(T) = 249.4 - 0.788 \times T + 7.20 \times 10^{-4} \times T^2 \quad (2.8)$$

And

$$a(C) = 1.000 - 0.2551 \times C + 5.151 \times 10^{-2} \times C^2 - 6.889 \times 10^{-3} \times C^3 \quad (2.9)$$

Since all the simulations were carried out at 25 °*C* which equivalent to 298.15 *K*, the dielectric constant only depends on the salt concentration.

The meaning of $r_{cutoff}$ for the nonbonded potentials is that they are ignored when they calculated at a distance greater than the cutoff radius.

Figures 2.3 and 2.4 explain the nonbonded potentials.

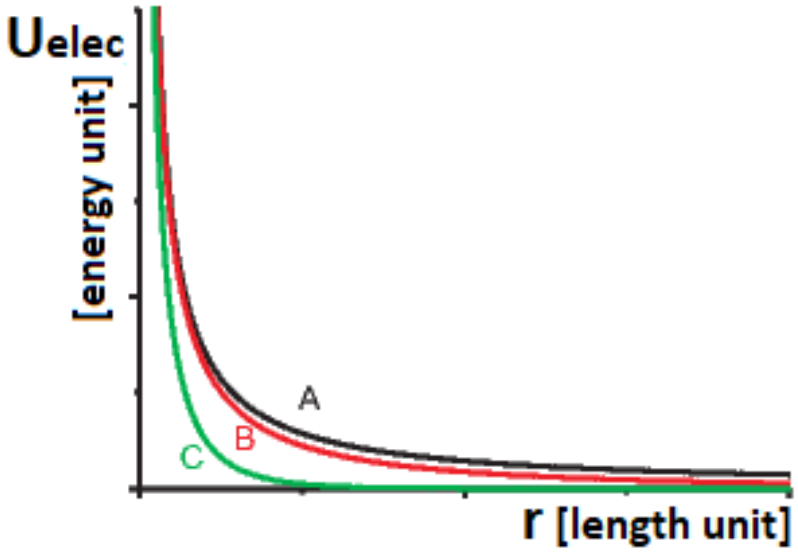


**Figure 2.3:** Debye-Hückel potential for different Debye lengths ($\kappa^{-1}$).

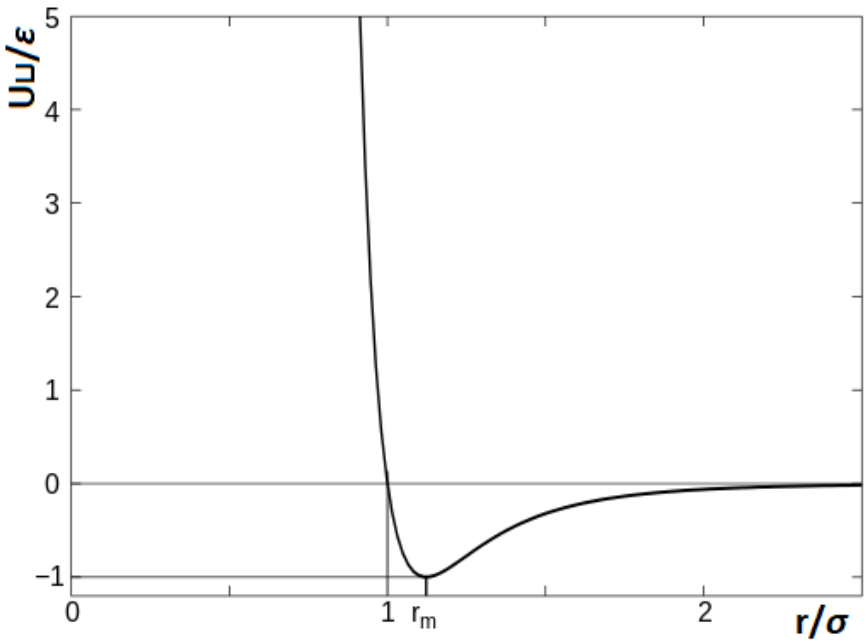


**Figure 2.4:** Lennard-Jones potential (the excluded volume potential).

Figure 2.5 illustrates our model (force field) for dsDNA chain.

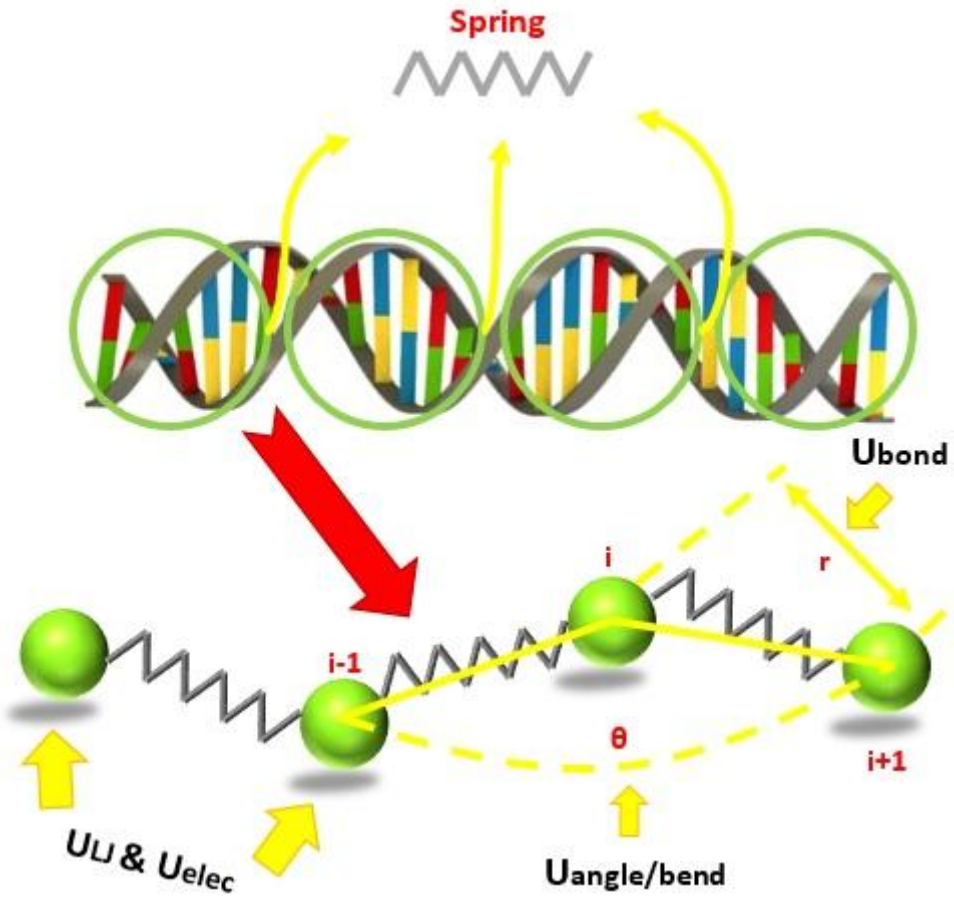


**Figure 2.5:** Our bead-spring model (force field) for dsDNA chain.

### 2.2.2. Dendrimer model:

In this Thesis/Research, we modeled the EDA-core PAMAM dendrimer by a (positive) charged hard sphere (return to Figure 2.1.b in page 42). Table 2.1 contains the physical data for the EDA-core PAMAM dendrimer used in our work.

**Table 2.1:** Physical data for EDA-core PAMAM dendrimer*.

| G | Mass (*g/mol*) | R (*Å*)** | Z(*e*)** |
|---|---|---|---|
| G2 | 3256.0 | 14.5 | 16.0 |
| G4 | 14215.0 | 22.5 | 64.0 |
| G6 | 58048.0 | 33.5 | 256.0 |
| G7 | 116493.0 | 40.5 | 512.0 |

* G denotes the dendrimer generation and Z specifies the number of primary amines (charged groups) on the dendrimer surface. The radius as reported by the **(manufacturer Sigma)** is R.
** We considered in our work that these values change under the effect of some factors like pH.

### 2.2.3. DNA-dendrimer interactions:

Since the attractive force between the dsDNA chain and the dendrimer is dominated by electrostatic interactions, for simplicity, we only considered two different forces between dsDNA and dendrimer, namely the electrostatic and excluded volume forces. We again used the Debye-Hückel potential to model the electrostatic attraction between the dsDNA chain and the dendrimer (Eqns. 2.4 and 2.5). Compared to the dendrimer sphere and the dsDNA beads, the salt ions and water molecules are small enough that an implicit model for their effect hopefully provides an adequate description. In other words, we mimicked the effect of solvent (water) and ions through epsilon ($\varepsilon$) and kappa ($\kappa$) parameters in the Debye-Hückel potential.

The excluded volume potential between the dsDNA beads and the dendrimer was modeled by a truncated Lennard-Jones potential (Eqn. 2.3).

Figure 2.6 summarizes the DNA-dendrimer interactions.

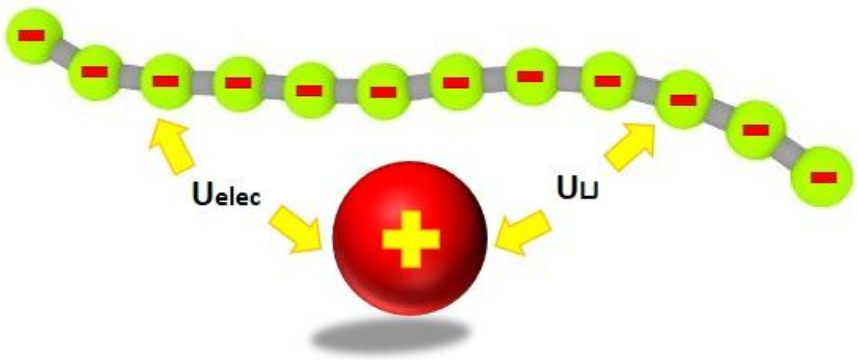


**Figure 2.6:** DNA-dendrimer interactions.

### 2.3 Simulated systems (Summary of all parameters)

#### 2.3.1. dsDNA systems:

**Table 2.2:** Simulated dsDNA chain systems prepared to study the salt concentration effect on the persistence length of the dsDNA chain.

<table>
<tr><th rowspan="2">[$Na^+$] mM</th><th rowspan="2"># of bps</th><th rowspan="2"># of beads</th><th rowspan="2">Total charge (e)</th><th colspan="2">Forcefield parameters*</th></tr>
<tr><th>Bonded</th><th>Nonbonded</th></tr>
<tr><td rowspan="13">10<br>&<br>150<br>&<br>1000</td><td rowspan="4">72</td><td rowspan="4">12</td><td rowspan="4">-148</td><td>$K_{bond}$ = 50.0 Kcal/mol.Å$^2$</td><td rowspan="13">$\sigma = 2R_{bead}$ = 16.000 Å<br>$\varepsilon$ = 0.700 Kcal/mol<br><br>$r_{cutoff}$ (LJ) = 71.000 Å**<br><br>$r_{cutoff}$ (elec) [72bp] = 979.200 Å<br>$r_{cutoff}$ (elec) [144bp] = 979.200 Å<br>$r_{cutoff}$ (elec) [288bp] = 1958.400 Å<br>$r_{cutoff}$ (elec) [432bp] = 2937.600 Å</td></tr>
<tr><td>$r_0$ = 20.800 Å</td></tr>
<tr><td>$K_{angle/bend}$ = 7.0 Kcal/mol.rad$^2$</td></tr>
<tr><td>$\theta_0$ = 180.000 °</td></tr>
<tr><td rowspan="4">144</td><td rowspan="4">24</td><td rowspan="4">-292</td><td>$K_{bond}$ = 50.0 Kcal/mol.Å$^2$</td></tr>
<tr><td>$r_0$ = 20.591 Å</td></tr>
<tr><td>$K_{angle/bend}$ = 7.0 Kcal/mol.rad$^2$</td></tr>
<tr><td>$\theta_0$ = 180.000 °</td></tr>
<tr><td rowspan="4">288</td><td rowspan="4">48</td><td rowspan="4">-580</td><td>$K_{bond}$ = 50.0 Kcal/mol.Å$^2$</td></tr>
<tr><td>$r_0$ = 20.494 Å</td></tr>
<tr><td>$K_{angle/bend}$ = 4.0 Kcal/mol.rad$^2$</td></tr>
<tr><td>$\theta_0$ = 180.000 °</td></tr>
<tr><td rowspan="4">432</td><td rowspan="4">72</td><td rowspan="4">-868</td><td>$K_{bond}$ = 50.0 Kcal/mol.Å$^2$</td></tr>
<tr><td>$r_0$ = 20.462 Å</td></tr>
<tr><td>$K_{angle/bend}$ = 3.0 Kcal/mol.rad$^2$</td></tr>
<tr><td>$\theta_0$ = 180.000 °</td></tr>
<tr><td># of bps</td><td colspan="4">Simulation box volume [x × y × z] (Å$^3$)</td></tr>
<tr><td>72</td><td colspan="4" rowspan="2">979.200 × 979.200 × 979.200</td></tr>
<tr><td>144</td></tr>
<tr><td>288</td><td colspan="4">1958.400 × 1958.400 × 1958.400</td></tr>
<tr><td>432</td><td colspan="4">2937.600 × 2937.600 × 2937.600</td></tr>
<tr><td></td><td colspan="5">Simulation time (μs)</td></tr>
<tr><td></td><td colspan="5">3.250 (The first 0.750 μs is for equilibrium)</td></tr>
</table>

* Wherever we used these dsDNA chains, we used these parameters except the cutoff radii for both LJ and electrical potentials.
** $r_{cutoff}$ $(LJ) = 10.00 l_B$, where $l_B$ = 7.100 *Å* (For water at 25 °*C*).

### 2.3.2. dsDNA-dendrimer complex systems:

**Table 2.3:** Simulated dsDNA-dendrimer complex systems prepared to study the salt concentration effect on the DNA-dendrimer complex.

| $[Na^+]$ *mM* | dsDNA | Dendrimer | | | | DNA-dendrimer interactions parameters* | $r_{charge}$** |
|---|---|---|---|---|---|---|---|
| | # of bps | # | G | R (*Å*) | Charge (*e*) | | |
| 10 & 150 & 1000 | 144 | 1 | G6 | 33.5 | 256.0 | $\sigma$ = 48.600 *Å* | 0.876 |
| | | | | | | $\varepsilon$ = 1.100 *Kcal/mol* | |
| | | | | | | $r_{cutoff}$ *(LJ)* = 71.000 *Å* | |
| | | | | | | $r_{cutoff}$ *(elec)* = 979.200 *Å* | |
| | 288 | 1 | G7 | 40.5 | 512.0 | $\sigma$ = 55.600 *Å* | 0.882 |
| | | | | | | $\varepsilon$ = 1.300 *Kcal/mol* | |
| | | | | | | $r_{cutoff}$ *(LJ)* = 71.000 *Å* | |
| | | | | | | $r_{cutoff}$ *(elec)* = 1958.400 *Å* | |
| | # of bps | Simulation box volume [x × y × z] ($Å^3$) | | | | | |
| | 144 | 979.200 × 979.200 × 979.200 | | | | | |
| | 288 | 1958.400 × 1958.400 × 1958.400 | | | | | |
| | # of bps | Simulation time ($\mu s$) | | | | | |
| | 144 | 3.250 (The first 0.750 $\mu s$ is for equilibrium) | | | | | |
| | 288 | 4.250 (The first 1.750 $\mu s$ is for equilibrium) | | | | | |

* ($\sigma$, $\varepsilon$) here for DNA-dendrimer interactions; those of dsDNA chains are the same as in Table 2.2 in page 48, also, here $\sigma = R_{dsDNA} + R_D + l_B$ *Å* and $r_{cutoff}$ $(LJ) = 10.00 l_B$.
** The definition of $r_{charge}$ is given by:

$$r_{charge} = \frac{N_D Z_D}{Z_{dsDNA}} \ (unitless) \qquad (2.10)$$

Where $N_D$ is the number of the dendrimers, $Z_D$ is the dendrimer charge number and $Z_{dsDNA}$ is the charge number of the dsDNA molecule.

Table 2.4 contains information about the simulation system prepared to study the pH effect on the DNA-dendrimer complex. We introduced this effect through changing the values of the radius and the charge of the dendrimer.

**Table 2.4:** Simulated dsDNA-dendrimer complex system prepared to study the pH effect on the DNA-dendrimer complex.

| pH value | dsDNA | Dendrimer* | | | | DNA-dendrimer interactions parameters** | $r_{charge}$ |
|---|---|---|---|---|---|---|---|
| | # of bps | # | G | R (*Å*) | Charge (*e*) | | |
| Acidic ≤ 4 | 144 | 1 | G6 | 30.89 | 510.0 | $\sigma(DNA) = 2R_{dsDNA} + (1/3)l_B = 18.370$ *Å*<br>$\sigma(DNA\text{-}G6) = R_{dsDNA} + R_{G6} + 1.50l_B = 49.540$ *Å* | 1.746 |
| | | | | | | $\varepsilon(DNA\text{-}G6) = 1.100$ *Kcal/mol* | |
| | | | | | | $r_{cutoff}\,(LJ) = 71.000$ *Å* | |
| | | | | | | $r_{cutoff}\,(elec) = 979.200$ *Å* | |
| Neutral ~ 7 | | | | 27.28 | 256.0 | $\sigma(DNA) = 2R_{dsDNA} = 16.000$ *Å*<br>$\sigma(DNA\text{-}G6) = R_{dsDNA} + R_{G6} + 1.00l_B = 42.380$ *Å* | 0.876 |
| | | | | | | $\varepsilon(DNA\text{-}G6) = 1.100$ *Kcal/mol* | |
| | | | | | | $r_{cutoff}\,(LJ) = 71.000$ *Å* | |
| | | | | | | $r_{cutoff}\,(elec) = 979.200$ *Å* | |
| Basic ≥ 12 | | | | 26.76 | 0.0 | $\sigma(DNA) = 2R_{dsDNA} = 16.000$ *Å*<br>$\sigma(DNA\text{-}G6) = R_{dsDNA} + R_{G6} = 34.760$ *Å* | 0.000 |
| | | | | | | $\varepsilon(DNA\text{-}G6) = 1.100$ *Kcal/mol* | |
| | | | | | | $r_{cutoff}\,(LJ) = 71.000$ *Å* | |
| | | | | | | $r_{cutoff}\,(elec) = 979.200$ *Å* | |
| Simulation box volume [x × y × z] ($Å^3$) | | | | | | | |
| 979.200 × 979.200 × 979.200 | | | | | | | |
| Simulation time ($\mu s$) | | | | | | | |
| 3.250 (The first 0.750 $\mu s$ is for equilibrium) | | | | | | | |

* The values of R and Charge as reported in Maiti and co-workers article **(Maiti, Çağ ın, Lin, & Goddard, 2005)**.

** ($\varepsilon$) for dsDNA chains is the same as in Table 2.2 in page 48, also, here $r_{cutoff}\,(LJ) = 10.00l_B$.

### 2.3.3. dsDNA-dendrimer aggregate systems (Linker/Tail(s) study):

**Table 2.5:** Simulated dsDNA-dendrimer aggregate systems prepared to study the salt concentration effect on the linker between two dendrimers (G4 and G6) in DNA-dendrimer aggregate.

| $[Na^+]$ *mM* | dsDNA | Dendrimer | | | | DNA-dendrimer interactions parameters* |
|---|---|---|---|---|---|---|
| | # of bps | # | G | R (*Å*) | Charge (*e*) | |
| 10 & 75 & 120 | 144 | 3 | G4 & G6 | 22.5 (G4) 33.5 (G6) | 64.0 (G4) 256.0 (G6) | $\sigma(DNA\text{-}G4) = R_{dsDNA} + R_{G4} + 0.50l_B = 34.050$ *Å*<br>$\sigma(DNA\text{-}G6) = R_{dsDNA} + R_{G6} + 1.00l_B = 48.600$ *Å*<br>$\sigma(Gx\text{-}Gx) = R_{Gx} + R_{Gx}$ *Å* |
| | | | | | | $\varepsilon(DNA\text{-}Gx) = 1.100$ *Kcal/mol*<br>$\varepsilon(Gx\text{-}Gx) = 0.700$ *Kcal/mol* |
| | | | | | | $r_{cutoff}\,(LJ) = 106.500$ *Å* |
| | | | | | | $r_{cutoff}\,(elec) = 979.200$ *Å* |
| | 288 | | | | | $\sigma(DNA\text{-}G4) = R_{dsDNA} + R_{G4} + 0.50l_B = 34.050$ *Å*<br>$\sigma(DNA\text{-}G6) = R_{dsDNA} + R_{G6} + 1.00l_B = 48.600$ *Å*<br>$\sigma(Gx\text{-}Gx) = R_{Gx} + R_{Gx}$ *Å* |
| | | | | | | $\varepsilon(DNA\text{-}Gx) = 1.100$ *Kcal/mol*<br>$\varepsilon(Gx\text{-}Gx) = 0.700$ *Kcal/mol* |
| | | | | | | $r_{cutoff}\,(LJ) = 106.500$ *Å* |
| | | | | | | $r_{cutoff}\,(elec) = 1958.400$ *Å* |
| | 432 | | | | | $\sigma(DNA\text{-}G4) = R_{dsDNA} + R_{G4} + 0.50l_B = 34.050$ *Å*<br>$\sigma(DNA\text{-}G6) = R_{dsDNA} + R_{G6} + 1.00l_B = 48.600$ *Å*<br>$\sigma(Gx\text{-}Gx) = R_{Gx} + R_{Gx}$ *Å* |
| | | | | | | $\varepsilon(DNA\text{-}Gx) = 1.100$ *Kcal/mol*<br>$\varepsilon(Gx\text{-}Gx) = 0.700$ *Kcal/mol* |
| | | | | | | $r_{cutoff}\,(LJ) = 106.500$ *Å* |
| | | | | | | $r_{cutoff}\,(elec) = 2937.600$ *Å* |
| | # of bps | Simulation box volume [x × y × z] ($Å^3$) | | | | |
| | 144 | 979.200 × 979.200 × 979.200 | | | | |
| | 288 | 1958.400 × 1958.400 × 1958.400 | | | | |
| | 432 | 2937.600 × 2937.600 × 2937.600 | | | | |
| | Simulation time ($\mu s$) | | | | | |
| | 5.000 (The first 2.500 $\mu s$ is for equilibrium) | | | | | |

* ($\sigma$, $\varepsilon$) for dsDNA chains are the same as in Table 2.2 in page 48, also, here $r_{cutoff}\,(LJ) = 15.00l_B$.

### 2.3.4. dsDNA-dendrimer aggregate systems (Morphology study):

**Table 2.6:** dsDNA-dendrimer aggregate systems prepared to study the effect of dendrimer generation on the morphology of dsDNA-dendrimer aggregate at $[Na^+]$ = 10 *mM*.

<table>
<tr><td colspan="8">dsDNA</td></tr>
<tr><td rowspan="2"># of bps</td><td rowspan="2"># of beads</td><td rowspan="2">Total charge (e)</td><td colspan="5">Forcefield parameters</td></tr>
<tr><td colspan="3">Bonded</td><td colspan="2">Nonbonded</td></tr>
<tr><td rowspan="4">1080</td><td rowspan="4">180</td><td rowspan="4">-2164</td><td colspan="3">$K_{bond}$ = 50.0 Kcal/mol.Å$^2$</td><td colspan="2" rowspan="8">$\sigma = 2R_{bead}$ = 16.000 Å<br>$\varepsilon$ = 0.700 Kcal/mol</td></tr>
<tr><td colspan="3">$r_0$ = 20.424581 Å</td></tr>
<tr><td colspan="3">$K_{angle/bend}$ = 3.0 Kcal/mol.rad$^2$</td></tr>
<tr><td colspan="3">$\theta_0$ = 160.000 °</td></tr>
<tr><td rowspan="4">4332</td><td rowspan="4">722</td><td rowspan="4">-8668</td><td colspan="3">$K_{bond}$ = 50.0 Kcal/mol.Å$^2$</td></tr>
<tr><td colspan="3">$r_0$ = 20.406103 Å</td></tr>
<tr><td colspan="3">$K_{angle/bend}$ = 3.0 Kcal/mol.rad$^2$</td></tr>
<tr><td colspan="3">$\theta_0$ = 160.000 °</td></tr>
<tr><td rowspan="2"># of bps</td><td colspan="4" rowspan="2">Dendrimer</td><td rowspan="2">DNA-dendrimer interactions parameters</td><td rowspan="2">$r_{charge}$</td></tr>
<tr></tr>
<tr><td></td><td>G</td><td>#</td><td>R (Å)</td><td>Charge (e)</td><td></td><td></td></tr>
<tr><td rowspan="4">1080</td><td rowspan="6">G2</td><td rowspan="4">79</td><td rowspan="4">14.5</td><td rowspan="4">16.0</td><td>$\sigma(DNA\text{-}G2) = R_{dsDNA} + R_{G2} + 0.25l_B$ = 24.275 Å<br>$\sigma(G2) = 2R_{G2}$ Å</td><td rowspan="4">0.584</td></tr>
<tr><td>$\varepsilon(DNA\text{-}G2)$ = 1.100 Kcal/mol<br>$\varepsilon(G2)$ = 0.700 Kcal/mol</td></tr>
<tr><td>$r_{cutoff}$ (LJ) = $20.00l_B$ = 142.000 Å</td></tr>
<tr><td>$r_{cutoff}$ (elec) = 7344.000 Å</td></tr>
<tr><td rowspan="2">1080</td><td rowspan="2">35</td><td rowspan="4">22.5</td><td rowspan="4">64.0</td><td>$\sigma(DNA\text{-}G4) = R_{dsDNA} + R_{G4} + 0.50l_B$ = 34.050 Å<br>$\sigma(G4) = 2R_{G4}$ Å</td><td rowspan="2">1.035</td></tr>
<tr><td>$\varepsilon(DNA\text{-}G4)$ = 1.100 Kcal/mol<br>$\varepsilon(G4)$ = 0.700 Kcal/mol</td></tr>
<tr><td rowspan="2">4332</td><td rowspan="2">140</td><td>$r_{cutoff}$ (LJ) = $20.00l_B$ = 142.000 Å</td><td rowspan="2">1.033</td></tr>
<tr><td>$r_{cutoff}$ (elec) [35] = 7344.000 Å<br>$r_{cutoff}$ (elec) [140] = 29457.600 Å</td></tr>
<tr><td rowspan="3">1080</td><td rowspan="3">G6</td><td rowspan="2">4</td><td rowspan="3">33.5</td><td rowspan="3">256.0</td><td>$\sigma(DNA\text{-}G6) = R_{dsDNA} + R_{G6} + 1.00l_B$ = 48.600 Å<br>$\sigma(G6) = 2R_{G6}$ Å</td><td rowspan="2">0.473</td></tr>
<tr><td>$\varepsilon(DNA\text{-}G6)$ = 1.100 Kcal/mol<br>$\varepsilon(G6)$ = 0.700 Kcal/mol</td></tr>
<tr><td>8</td><td>$r_{cutoff}$ (LJ) = $20.00l_B$ = 142.000 Å<br>$r_{cutoff}$ (elec) = 7344.000 Å</td><td>0.946</td></tr>
<tr><td># of bps</td><td colspan="7">Simulation box volume [x × y × z] (Å$^3$)</td></tr>
<tr><td>1080</td><td colspan="7">7344.000 × 7344.000 × 7344.000</td></tr>
<tr><td>4332</td><td colspan="7">29457.600 × 29457.600 × 29457.600</td></tr>
<tr><td>G</td><td colspan="7">Simulation time (μs)</td></tr>
<tr><td>2</td><td colspan="7">27.500</td></tr>
<tr><td rowspan="2">4</td><td colspan="7">[#35]: 27.500</td></tr>
<tr><td colspan="7">[#140]: 40.000</td></tr>
<tr><td rowspan="2">6</td><td colspan="7">[#4]: 13.750</td></tr>
<tr><td colspan="7">[#8]: 40.000</td></tr>
</table>

## 2.4 Simulation method

### 2.4.1. The simulator used (LAMMPS):

We employed a BD simulation method using a program called "Large-scale Atomic/Molecular Massively Parallel Simulator (LAMMPS) **[version 22Sep2017]**" **(Plimpton, 1995)** to simulate our systems illustrated previously (see Appendix A for how to download, install and prepare LAMMPS to run). We used a time step equal to 25.0 *fs*, a real style for units, a full style for atoms (wherever we use the word "atom", we mean any entity in our systems like dsDNA bead or dendrimer sphere), neighbor skin equal to 3.0 *Å* for building neighbor lists and periodic boundary conditions were not used. Also, we full weighted the pairwise interactions (Nonbonded) between pairs of atoms that are permanently bonded to each other, either directly or *via* one or two intermediate bonds. Furthermore, at the beginning of each simulation and for a specific period of time illustrated in the "Simulated systems" part previously, we minimized the energy of the system using the Polak-Ribiere version of the conjugate gradient (CG) algorithm ("*cg*" minimization style that LAMMPS offered) (for more information about LAMMPS input files and commands see Appendix B). Remember, we introduced the solvent and salt ions implicitly in our work.

### 2.4.2. Brownian Dynamics (BD) using LAMMPS (An explanation):

LAMMPS program does a BD simulation throughout applying a Langevin thermostat (Langevin Dynamics (LD)) and constant NVE integration. Langevin thermostat used to perform a simulation in the NVT ensemble as described in Schneider and Stoll paper **(Schneider & Stoll, 1978)** to a group of atoms which models an interaction with a background implicit solvent and the constant NVE integration used to update position and velocity for atoms in the group each timestep. *V* is volume; *E* is energy; *N* is the number of atoms/beads/spheres; *T* is the temperature.

In BD, the total force on each atom will have the form:

$$\begin{aligned} F &= F_c + F_f + F_r \\ F_f &= -\left(m/damp\right) v \\ F_r &\propto \sqrt{k_B T m/dt \times damp} \end{aligned} \tag{2.11}$$

Where:

$F_c$ is the conservative force computed *via* the usual inter-particle interactions.
$F_f$ is a frictional drag or viscous damping term proportional to the particle's velocity. The proportionality constant for each atom is computed as $m/damp$, where $m$ is the mass of the atom and (in *g/mol*) $damp$ is the damping factor specified by the user. The $damp$ parameter is specified in time units (*fs*) and determines how rapidly the temperature is relaxed. For example, a value of 100.0 means to relax the temperature in a timespan of (roughly) 100-time units (*fs* that we used). The $damp$ factor can be thought of as inversely related to the viscosity of the solvent. *I.e.*, a small relaxation time implies a hi-viscosity solvent and *vice versa*.
$F_r$ is a force due to solvent atoms at a temperature *T* randomly bumping into the particle/atom. As derived from the fluctuation/dissipation theorem, its magnitude as shown

above is proportional to *sqrt*($k_B T m/dt \times damp$), where $k_B$ is the Boltzmann constant (in *Kcal/mol.K*), $T$ is the desired temperature (in *K*), $m$ is the mass of the particle (in *g/mol*), $dt$ is the timestep size and $damp$ is the damping factor (in *fs*). Random numbers are used to randomize the direction and magnitude of this force as described in Dunweg and Paul paper **(Dunweg & Paul, 1991)**, where a uniform random number is used (instead of a Gaussian random number) for speed.

To relate the constant of frictional drag force ($m/damp$) of this thermostat to BD one that depends on the dynamic viscosity of the solvent and the diameter of the atom ($3\pi\eta d$) we did the following:

$$m/damp = 3\pi\eta d \rightarrow damp = m/3\pi\eta d \qquad (2.12)$$

Where $\eta$ is the dynamic viscosity of the frictional fluid (solvent) (in *g/fs.Å*) and $d$ is the diameter of the atom (in *Å)*. According to this relation and in a specific solvent the damp parameter depends on the atom types since they have different sizes or masses. In our models, *e.g.*, the damp parameter for the dsDNA bead is roughly equal to *482.5 fs* and for G6 dendrimer with *R = 33.5 Å* is approximately equal to *1715.2 fs*. By using scaling factors that LAMMPS offered, we fitted this damping parameter for different atom types (dendrimer generations) in our simulation systems.

We run the Gronbech-Jensen/Farago time-discretization of the Langevin model. As described in their papers **(Grønbech-Jensen & Farago, 2013) (Grønbech-Jensen, Hayre, & Farago, 2014)**, the purpose of this method is to enable longer timesteps to be used (up to the numerical stability limit of the integrator), while still producing the correct Boltzmann distribution of atom positions. It is implemented within LAMMPS, by changing how the random force is applied so that it is composed of the average of two random forces representing half-contributions from the previous and current time intervals.

For all our simulation systems, we set the temperature of this thermostat equal to 298.15 *K* (25 °*C*) and the random number seed for Langevin integrator equal to 12345. Since we had only the translational degrees of freedom for the atoms, the thermostat effect is only applied to them.

We performed these simulations on different PCs such as Intel Core i5 and Core i7 (2 cores and 4 threads) laptops, and Google virtual machines with 8 or 12 or 32 cores/threads from Google cloud.

## 2.5 Analysis of the results (Methods, Quantities, and Equations)

In this section we put the methods and equations of the quantities we used in our results such as the translational diffusion coefficient of DNA chain ($D_t$), the persistence length of DNA chain ($l_p$), the radius of gyration ($R_g$) of DNA chain or DNA-dendrimer complex, the distance between centers of masses of DNA chain and dendrimer ($D_{coms}$), the fraction of adsorption DNA beads onto dendrimer surface ($\omega$), the order (curvature) parameter of DNA-dendrimer complex ($\gamma$), the not adsorbed DNA beads (it can be in-between adsorbed ones or linker or tail/s) in (G4-G6)-dendrimers-DNA aggregate and the toroidal parameter ($\tau$) for DNA-dendrimer aggregate.

### 2.5.1. The translational diffusion coefficient ($D_t$):

We used a plugin called "Diffusion Coefficient Tool" **(Giorgino, 2015)** for a program called "Visual Molecular Dynamics (VMD) **[version 1.9.4a12]**" **(Humphrey, Dalke, & Schulten, 1996)** to compute the Mean-Squared Displacement (MSD) and the translational diffusion coefficient ($D_t$) for the DNA chain according to the following:

$$MSD(\tau) = \langle |\boldsymbol{r}(\tau) - \boldsymbol{r}(0)|^2 \rangle \tag{2.13}$$

The average, written explicitly, is done over windows of span $\tau$ (lag time) that can be constructed in the interval $[w_f \dots w_t]$. To reduce computation requirements, this average will be done with a stride of $w_s$ (*i.e.*, only one window every $w_s$ will be considered):

$$MSD(\tau) = \underbrace{\frac{w_s}{w_t - w_f - \tau} \sum_{t_0 = w_f \text{ every } w_s}^{w_t - \tau - 1} \underbrace{\frac{1}{N} \sum_{i=1}^{N} (\boldsymbol{r}_i(t_0 + \tau) - \boldsymbol{r}_i(t_0))^2}_{Average\ over\ selected\ atoms}}_{Average\ over\ intervals\ of\ span\ \tau} \tag{2.14}$$

Where $\boldsymbol{r}_i(t_0 + \tau)$ and $\boldsymbol{r}_i(t_0)$ are the position vectors of the atom i (in the selection) at time $t_0 + \tau$ and $t_0$ respectively, $N$ is the number of atoms (rather, molecules since the tool needs to select one atom per molecule in the simulation) in the selection.
When the center of mass (COM) drift subtraction is enabled, the following replacement is applied to the above formula:

$$\boldsymbol{r}(t) \rightarrow \boldsymbol{r}(t) - \boldsymbol{r}_0(t) \tag{2.15}$$

Where $\boldsymbol{r}_0(t)$ is the position vector of the COM of the selected atoms at time $t$:

$$\boldsymbol{r}_0(t) = \sum_{i=1}^{N} \boldsymbol{r}_i(t)/N \tag{2.16}$$

In our work, we selected one atom in the dsDNA chain through "index 0", *i.e.*, $N$ = 1 atom (the first bead in the dsDNA chain (molecule)) (see Appendix C ($D_t$ section) to get more about how we used this plugin/tool), we disabled COM drift subtraction because we have one molecule (one atom in the selection), set the interval $[w_f \dots w_t] = [0 \dots 999]$ (1000) frames, $w_s = 1$ frame and changed $\tau$ from 1000/10 = 100 to 1000/2 = 500 by a step equal to 1000/50 = 20, hence there are 21 values for $\tau$ and $MSD(\tau)$ for each DNA simulation system.
Then we calculated $D_t$ using the following relation (Einstein relation) as the tool do:

$$D_t(\tau) = \frac{MSD(\tau)}{2n\tau} \tag{2.17}$$

Where $D_t(\tau)$ is the translational diffusion coefficient at lag time $\tau$, $n$ is the space dimension of the system (=3) (*unitless*). Again, we have 21 values for $D_t(\tau)$ as $MSD(\tau)$ and $\tau$.

### 2.5.2. The persistence length ($l_p$):

Let us define the angle $\theta$ between a unit vector that is tangent to the DNA chain at position *0* (zero) and a unit tangent vector at a distance *s* away from position *0*, along the contour of the chain. It can be shown that the expectation value of the cosine of the angle falls off exponentially with distance:

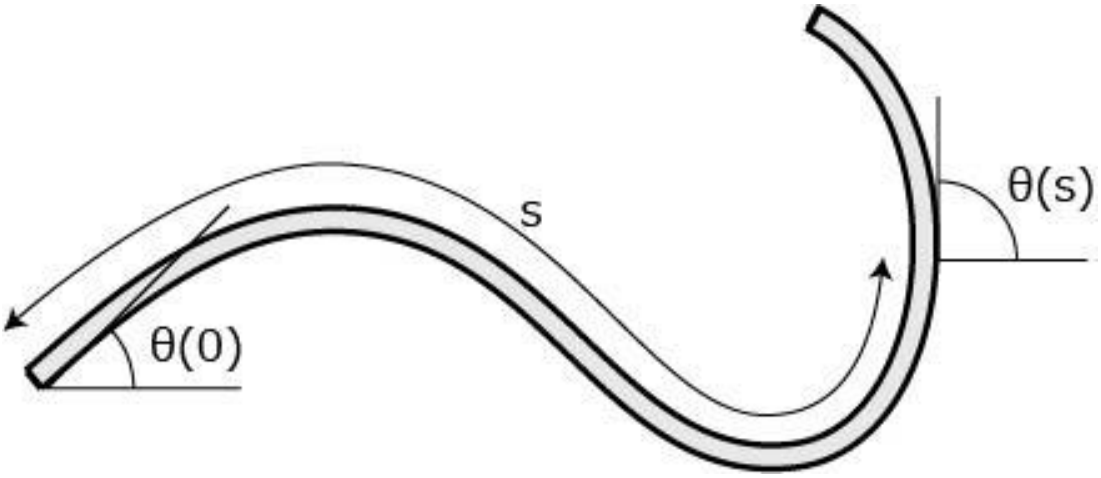


**Figure 2.7:** Schema shows the unit tangent vectors to the DNA chain at positions *0* and *s* along the contour of the chain respectively, $\theta = \theta(s) - \theta(0)$.

$$\langle \hat{\boldsymbol{u}}(0) \cdot \hat{\boldsymbol{u}}(s) \rangle = \langle \cos(\theta) \rangle = e^{-s/l_p} \\ \rightarrow s = -l_p ln(\langle \cos(\theta) \rangle) \tag{2.18}$$

Where $\hat{\boldsymbol{u}}(0)$ is the unit tangent vector (*unitless*) at position *0* (zero), $\hat{\boldsymbol{u}}(s)$ is the unit tangent vector (*unitless*) at relative position *s* along the DNA chain, $\theta$ is the angle between them, $l_p$ is the persistence length and $\langle \quad \rangle$ denotes the average over all starting or ending positions and/or time steps/frames. In our work, we set the starting point the mid of first bond (between bead 1 & 2 in the DNA chain) and the ending points the mid of all bonds in the DNA chain, hence we have ($N_{dsDNA\text{-}beads} - 1$) values for *s* and $\cos(\theta)$ in each time step/frame and the average is over time steps/frames only.

The $l_p$ in DNA exhibits a dependence on the ionic strength of the solution. Although it is usually understood that DNA becomes more flexible with increasing salt concentration (due to an enhanced shielding of repulsive bead-bead interactions), the issue of whether to attribute the stiffness to electrostatics alone has not been fully resolved. A reasonable representation for the dependence of $l_p$ on ionic strength is attained by using the nonlinear Poisson-Boltzmann theory for uniformly charged cylinders,

$$l_p = l_{p0} + l_{pe} = l_{p0} + \frac{1}{4l_B/(\kappa^{-1})^2} \tag{2.19}$$

Where the total $l_p$ is taken as the sum of a non-electrostatic length scale $l_{p0}$ and an electrostatic length scale $l_{pe}$. The electrostatic contribution is accounted for by the Debye length, $\kappa^{-1}$, and the Bjerrum length, $l_B$, that have been defined in Eqn. 2.5. This treatment has

been shown to describe simulation data from Eqn. 2.18 for the dependence of DNA flexibility on ionic strength **(Sambriski, Schwartz, & de Pablo, 2009)**.

See Appendix C ($l_p$ section) to get a closer look at the C language code we wrote for this quantity.

### 2.5.3. The radius of gyration ($R_g$):

We wrote a Tcl code (script) used by VMD to compute this quantity for a specific group of atoms according to this relation:

$$R_g = \sqrt{\frac{\sum_i^n m_i \, |\boldsymbol{r}_i - \boldsymbol{r}_{cm}|^2}{\sum_i^n m_i}} \tag{2.20}$$

Where $m_i$ is the mass of the $i_{th}$ atom in the group, $\boldsymbol{r}_i$ is the $i_{th}$ atom position in the group, $\boldsymbol{r}_{cm}$ is the position of the COM of the group that given by the relation:

$$\boldsymbol{r}_{cm} = \frac{\sum_i^n m_i \, \boldsymbol{r}_i}{\sum_i^n m_i} \tag{2.21}$$

and the sum of the two definitions is over all atoms in the group.

See Appendix C ($R_g$ section) to get a closer look at the code we wrote for this quantity.

### 2.5.4. The distance between COMs ($D_{coms}$):

We wrote a Tcl code (script) used by VMD program to compute this quantity between DNA chain COM and dendrimer COM.

See Appendix C ($D_{coms}$ section) to get a closer look at the code we wrote for this quantity.

### 2.5.5. The fraction of adsorption DNA beads onto dendrimer surface ($\omega$):

In the DNA-dendrimer complex, the bead of DNA chain was considered as "adsorbed onto dendrimer surface" when the distance between its center and dendrimer center is less than the sum of their radii plus $2.000 l_B$.

See Appendix C ($\omega$ section) to get a closer look at the C language code we wrote for this quantity.

### 2.5.6. The order (curvature) parameter of DNA-dendrimer complex ($\gamma$):

To quantify the arrangement of adsorbed DNA segments (beads) on the dendrimer surface, we used a curvature order parameter $\gamma$ (*unitless*) **(Yu & Larson, 2014)** defined by:

$$\gamma = \frac{\left|\sum_{(i)} \hat{\boldsymbol{r}}_{i,i+1} \times \hat{\boldsymbol{r}}_{i+1,i+2}\right|}{N_d} \qquad (2.22)$$

Where $\hat{\boldsymbol{r}}_{i,i+1}$ is a unit distance vector (*unitless*) between the $i_{th}$ and the $(i+1)_{th}$ DNA beads, $\hat{\boldsymbol{r}}_{i+1,i+2}$ is also a unit distance vector (*unitless*) between the $(i+1)_{th}$ and the $(i+2)_{th}$ DNA beads, $N_d$ is the number of the adsorbed DNA beads onto dendrimer surface and × denotes a vector product.

This equation only accounts for the cross product of adjacent vectors $\hat{\boldsymbol{r}}_{i,i+1}$ and $\hat{\boldsymbol{r}}_{i+1,i+2}$ for which the $i_{th}$, $(i+1)_{th}$, $(i+2)_{th}$ DNA beads were all adsorbed onto the dendrimer (the $i_{th}$ bead of DNA was considered as "adsorbed" when the distance between its center and dendrimer center is less than the sum of their radii plus $2.0l_B$). $\gamma$ defined in Eqn. 2.22 is equal to zero when the DNA conformation is straight, and when it is randomly coiled. $\gamma$ would be unity if the backbone of the DNA were to bend an angle of 90° at each bead, always in the same direction, forming a tight helix. When $N_d$ equal zero, *i.e.*, there is no adsorbed dsDNA beads onto dendrimer surface $\gamma$ becomes undefined, *i.e.*, division by zero, in this case, we set $\gamma$ equal to zero.

See Appendix C ($\gamma$ section) to get a closer look at the C language code we wrote for this quantity.

### 2.5.7. The not adsorbed DNA beads (it can be in-between adsorbed ones or linker or tail/s) in DNA-(G4-G6)-dendrimers aggregate:

In the DNA-(G4-G6)-dendrimers aggregate, the DNA chain beads that are not adsorbed onto dendrimers surfaces can consider to be an in-between adsorbed beads or linker or tail/s.

See Appendix C (*In/L/T* section) to get a closer look at the C language code we wrote for this quantity.

### 2.5.8. The toroidal parameter ($\tau$):

In order to distinguish the rod-like, toroidal and globular DNA-dendrimer aggregate, we evaluated the toroidal parameter $\tau$ (*unitless*) **(Angelescu, Bruinsma, & Linse, 2006)** defined as:

$$\tau = \left\langle \frac{1}{18-1} \left[ \sum_{\alpha=x,y,z} \left( \sum_{\substack{i=0 \\ i+=\left\lfloor \frac{N_b}{18} \right\rfloor}}^{\leq N_b} \frac{\left( \boldsymbol{r}_{i,i+\left\lfloor \frac{N_b}{18} \right\rfloor} \times \boldsymbol{r}_{i+\left\lfloor \frac{N_b}{18} \right\rfloor, i+\left\lfloor \frac{N_b}{9} \right\rfloor} \right)_\alpha}{\left| \boldsymbol{r}_{i,i+\left\lfloor \frac{N_b}{18} \right\rfloor} \times \boldsymbol{r}_{i+\left\lfloor \frac{N_b}{18} \right\rfloor, i+\left\lfloor \frac{N_b}{9} \right\rfloor} \right|} \right)^2 \right]^{1/2} \right\rangle \qquad (2.23)$$

Where $\boldsymbol{r}_{i,i+\left\lfloor\frac{N_b}{18}\right\rfloor}$ is the distance vector between $i_{th}$ and $\left(i+\left\lfloor\frac{N_b}{18}\right\rfloor\right)_{th}$ DNA beads, $\boldsymbol{r}_{i+\left\lfloor\frac{N_b}{18}\right\rfloor,i+\left\lfloor\frac{N_b}{9}\right\rfloor}$ is also the distance vector between $\left(i+\left\lfloor\frac{N_b}{18}\right\rfloor\right)_{th}$ and $\left(i+\left\lfloor\frac{N_b}{9}\right\rfloor\right)_{th}$ DNA beads, $N_b$ is the number of DNA beads in the aggregate, $\lfloor\ \rfloor$ denotes the floor function, $\times$ denotes a vector product and $\langle\ \rangle$ denotes the average over all time steps/frames in the simulation. $\tau$ approaches 1 when the aggregate has an ideal toroid shape and fluctuates around $1/(18-1)$ for a disordered (random) shape. Note, when ($i = 0$), $\boldsymbol{r}_{i,i+\left\lfloor\frac{N_b}{18}\right\rfloor} = \boldsymbol{r}_{1,\left\lfloor\frac{N_b}{18}\right\rfloor}$ not $\boldsymbol{r}_{0\left\lfloor\frac{N_b}{18}\right\rfloor}$ because the first id of the DNA beads is 1, and the summation stops when *i* becomes greater than $N_b$.

See Appendix C ($\tau$ section) to get a closer look at the C language code we wrote for this quantity.

# Chapter Three

## Results and Discussions

# 3 Chapter Three: Results and Discussions

In our work that has been done on the operating system Ubuntu **[Version 16.04 LTS] (Ubuntu, n.d.)** , we used the LibreOffice program **[version 5.1.6.2] (Home | LibreOffice, n.d.)** and the Scientific Data Analysis and Visualization (SciDAVis) program **[version 1.22] (SciDAVis, n.d.)** for analyzing and graphing the theoretical results, the Open Visualization Tool (Ovito) program **[version 3.0.0-dev46] (Stukowski, 2010)** for Visualizing the simulation systems results and generating PNG-formatted snapshots for them and the Pinta program **[version 1.6] (Pinta, n.d.)** for editing some simulation snapshots. Note, we generated PDF-formatted graphs by SciDAVis program, so we used the website (http://pdf2png.com/) to convert them to PNG-formatted graphs.

## 3.1 dsDNA simulations

In order to validate our model for dsDNA chain, we did the following calculations:

### 3.1.1. Translational diffusion coefficient ($D_t$):

#### 3.1.1.1. Effect of salt concentration:

To calculate the translational diffusion coefficient ($D_t$) of the dsDNA chain, we must calculate the Mean Squared Displacement (MSD) of the chain before. Figures 3.1 and 3.2 show, as an example, the graphs of MSD for all dsDNA chains and $D_t$ for 144 bp dsDNA chain both at 150 *mM* salt concentration versus lag time ($\tau$), *i.e.*, the span of windows used to average the *MSD* over the whole-time (frames) interval of the simulation (return to $D_t$ section in chapter two for more information). The values of *MSD* and $D_t$ are obtained from 1000 frames (time interval), as we said in their section in the previous chapter, which equal to $1 \times 10^8$ Brownian Dynamics step (BDS) after $3 \times 10^7$ BDS equilibration.

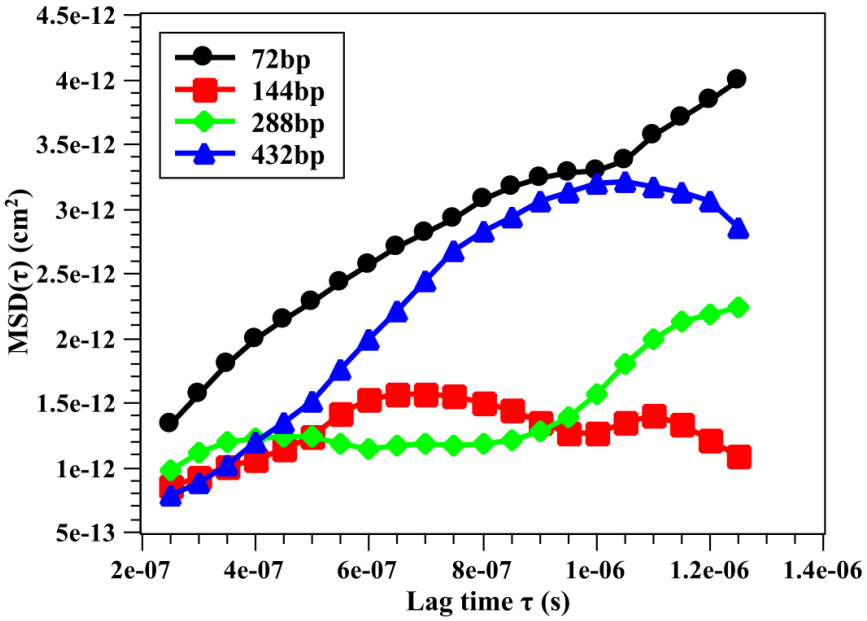


**Figure 3.1:** Mean squared displacement (*MSD*) Vs. lag time ($\tau$) for all dsDNA chains at $[Na^+]$ = 150 *mM*.

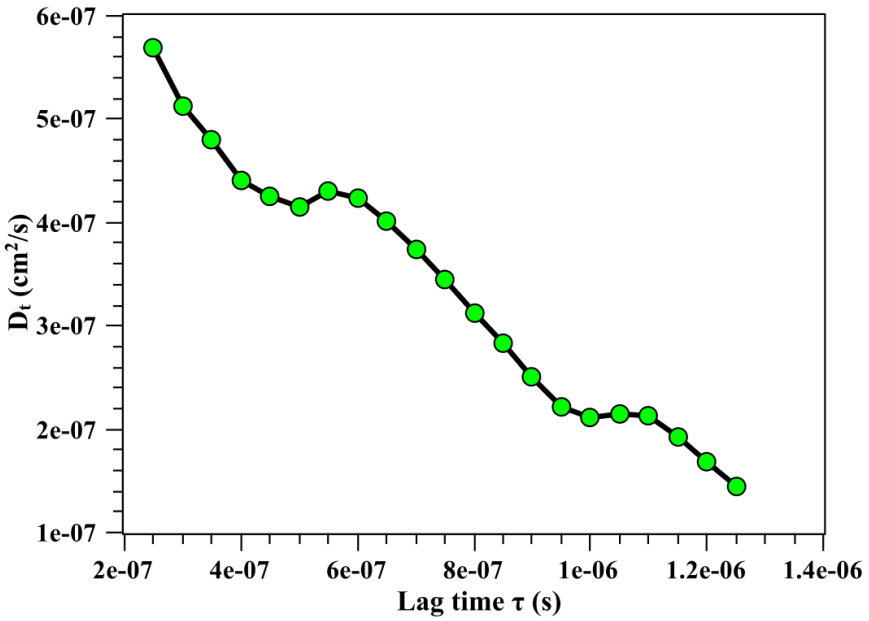


**Figure 3.2:** Translational diffusion coefficient ($D_t$) Vs. lag time ($\tau$) for 144 bp dsDNA chain at $[Na^+]$ = 150 *mM*.

Table 3.1 summarizes the calculations of $D_t$ for all dsDNA chains at different salt concentrations.

**Table 3.1:** The average of translational diffusion coefficient ($D_t$) over 21 sampling points for all dsDNA chains at different salt concentrations.

| $[Na^+]$ (*mM*) | # of dsDNA bps | $<D_t> \times 10^{-7}$ ($cm^2/s$) |
|---|---|---|
| 10 | 72 | 6.8 ± 0.3 |
| | 144 | 3.0 ± 0.2 |
| | 288 | 3.4 ± 0.2 |
| | 432 | 4.73 ± 0.12 |
| 150 | 72 | 6.7 ± 0.3 |
| | 144 | 3.3 ± 0.3 |
| | 288 | 3.5 ± 0.3 |
| | 432 | 5.19 ± 0.12 |
| 1000 | 72 | 6.7 ± 0.3 |
| | 144 | 3.4 ± 0.3 |
| | 288 | 3.6 ± 0.3 |
| | 432 | 5.22 ± 0.12 |

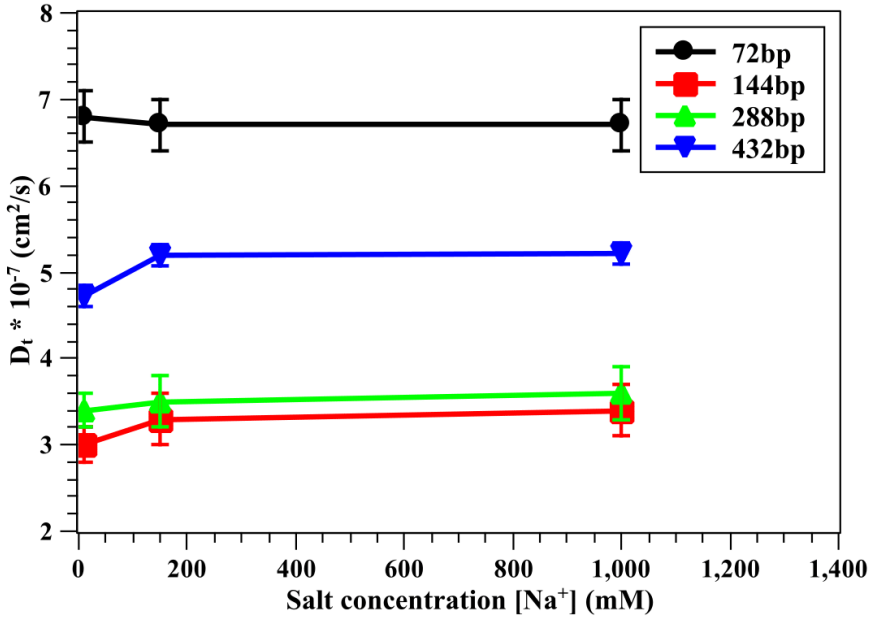


**Figure 3.3:** Translational diffusion coefficient ($D_t$) Vs. salt concentration for all dsDNA chains.

As shown in Table 3.1 and Figure 3.3, for 72 bp dsDNA chain, $D_t$ decreases with increasing salt concentration from 10 to 150 *mM*, *i.e.*, its movement (diffusivity) in the solution becomes slower, while it increases for the other chains. It approximately remains constant with increasing salt concentration from 150 to 1000 *mM* for all dsDNA chains.

### 3.1.1.2. The effect of dsDNA length (base pairs (bps) number):

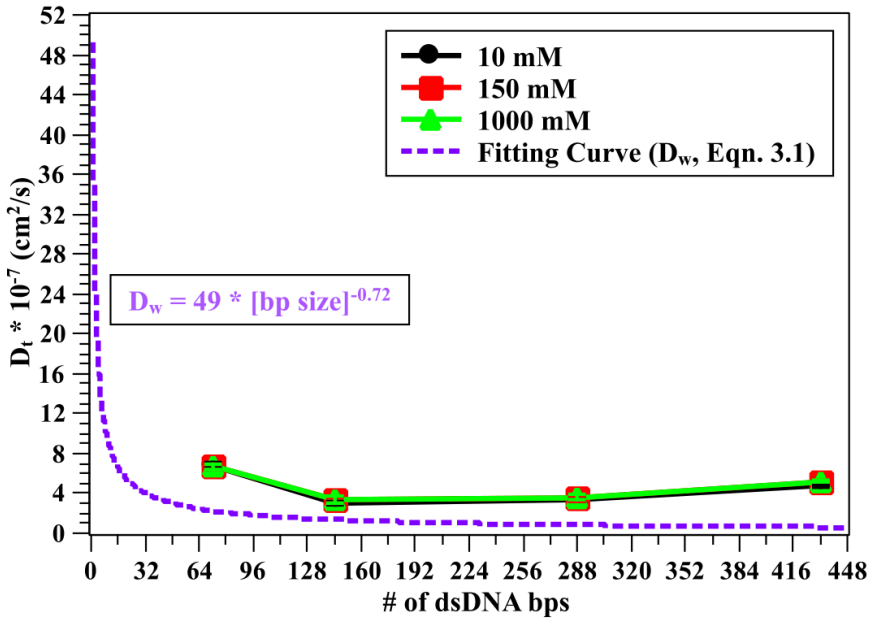


**Figure 3.4:** Translational diffusion coefficient ($D_t$) Vs. the number of bps in the dsDNA chain for all dsDNA chains at different salt concentrations.

Figure 3.4 tells us that $D_t$ decreases with increasing the number of bps in the dsDNA chain from 72 to 144 bp, then becomes almost constant when the number of bps in the dsDNA chain increases more and more, *i.e.*, the shorter dsDNA chain is more diffusive in the solution than the longer one at the same salt concentration due to increasing the friction between the longer dsDNA chain and the molecules in the solution (the solvent and the salt).

An experimental study for Lukacs and co-workers **(Lukacs, et al., 2000)** showed that the translational diffusion coefficient of dsDNA in water ($D_w$) decreased from $53 \times 10^{-8}$ to $0.81 \times 10^{-8}$ $cm^2/s$ for sizes 21-6000 bp, and they related $D_w$ empirically to DNA size (in bp) according to the following equation:

$$D_w = 4.9 \times 10^{-6} \frac{cm^2}{s} \times [bp\ size]^{-0.72} \qquad (3.1)$$

Although our results for $D_t$ are in NaCl solution instead of water, the $D_t$ behavior with the dsDNA chain length are in good agreement with the previous study results (return to Figure 3.4).

Error bars (*i.e.*, error in $D_t$) in Figures 3.3 and 3.4 are the standard errors of the means over the 21 sampling points.

### 3.1.2. The stiffness of dsDNA chain (Persistence length ($l_p$)):

The persistence length ($l_p$) of the dsDNA chain is related to its stiffness, *i.e.*, its angle/bending force constant $k_{angle/bend}$, by the following relation:

$$k_{angle/bend} = k_B T l_p / r_0 \qquad (3.2)$$

Where $k_B$ is the Boltzmann constant (in *Kcal/mol.K*), $T$ is the temperature (in *K*) and $r_0$ is the equilibrium bond distance (length) between beads in the dsDNA chain (in *Å* and $l_p$ in *Å*) (return to DNA model section in chapter two for more information).

#### 3.1.2.1. Effect of salt concentration:

Using Eqn. 2.18, we calculated the averages of the values of the dot product between unit tangent vectors (*i.e.*, $cos(\theta)$) (see Figure 3.5) that are tangent to the dsDNA chain and separated by ($s$) distance along the contour of the chain and also the averages of the values of ($s$) from 100 sampling points (frames) from $1 \times 10^8$ BDS every $1 \times 10^6$ BDS after $3 \times 10^7$ BDS equilibration for all dsDNA chains, then fitted them linearly in order to calculate the slope which is equal to - $l_p$ (the persistence length). (see Figure 3.6) (come back to the persistence length section in the analysis of the results in chapter two).

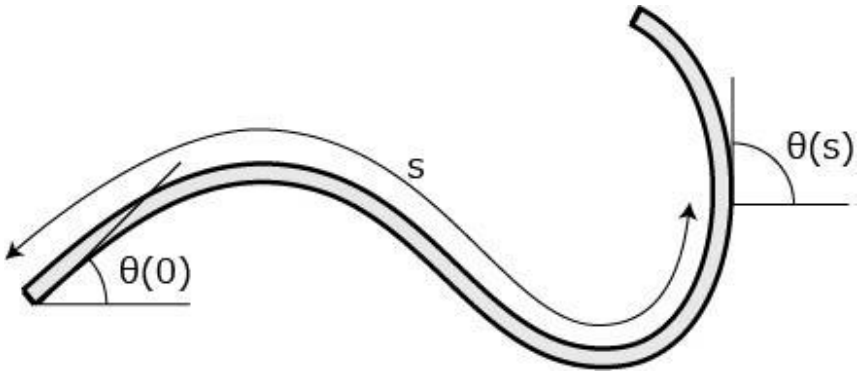


**Figure 3.5:** Schema shows the unit tangent vectors to the dsDNA chain at positions *0* and *s* along the contour of the chain respectively, $\theta = \theta(s) - \theta(0)$.

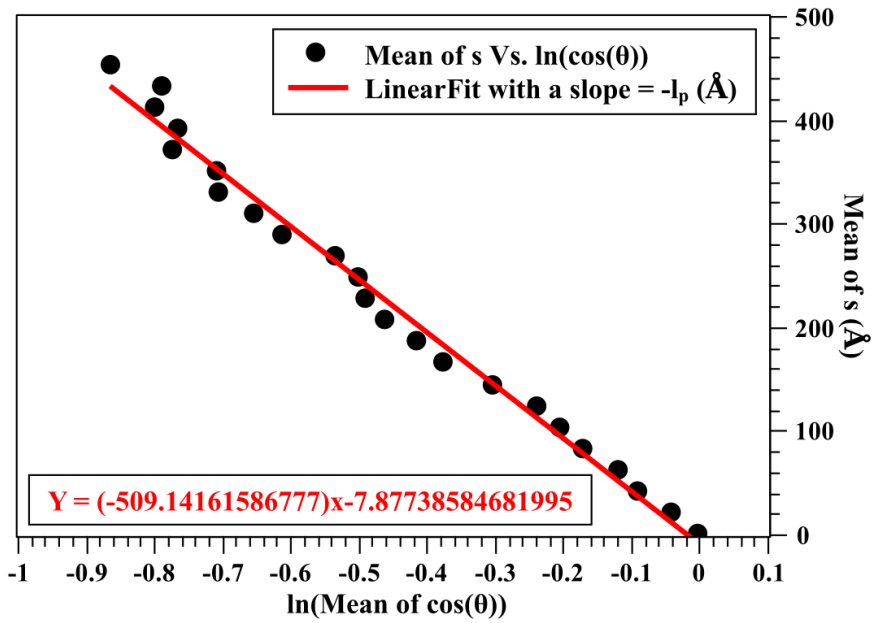


**Figure 3.6:** From Eqn. 2.18, <*s*> for 144 bp dsDNA chain with its linear fit Vs. *ln(<cos(θ)>)* at 150 *mM* salt concentration.

Table 3.2 contains the values of $l_p$ for all dsDNA chains at different salt concentrations.

**Table 3.2:** The values of the persistence length ($l_p$) for all dsDNA chains at different salt concentrations.

| $[Na^+]$ (*mM*) | # of bps | $l_p$ (*nm*) |
|---|---|---|
| 10 | 72 | 87 ± 7 |
| | 144 | 89.7 ± 1.6 |
| | 288 | 133 ± 6 |
| | 432 | 210 ± 30 |
| 150 | 72 | 48 ± 3 |
| | 144 | 50.9 ± 1.2 |
| | 288 | 41 ± 4 |
| | 432 | 44 ± 8 |
| 1000 | 72 | 47 ± 3 |
| | 144 | 50.4 ± 1.2 |
| | 288 | 39 ± 4 |
| | 432 | 41 ± 8 |

As shown in Table 3.2, $l_p$ decreases when the salt concentration increases because the electrostatic repulsion between the dsDNA beads becomes stronger at lower salt concentrations, hence, the dsDNA chain becomes straighter. To capture the effect of salt concentration on $l_p$ of dsDNA chain more clearly, we fitted the results in Table 3.2 with Eqn. 2.19, which describes the dependence of $l_p$ in DNA on the ionic strength of the solution, in Figure 3.7.

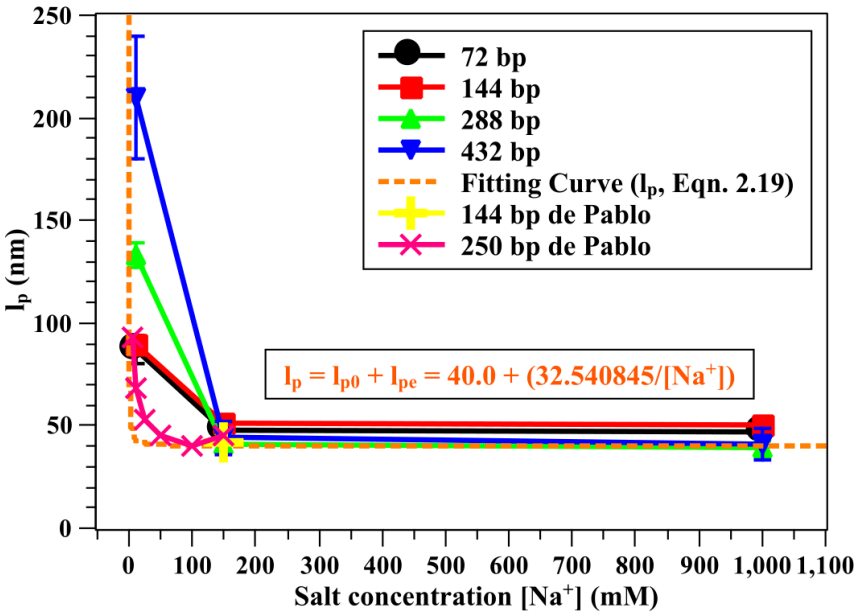


**Figure 3.7:** Persistence length ($l_p$) Vs. salt concentration ([$Na^+$]) with $l_{p0}$ = 40.0 *nm*, $l_B$ = 0.71 *nm* and ($\kappa^{-1}$ (*nm*) = 0.304/$\sqrt{[Na^+]\ (in\ M)}$) in Eqn. 2.19.
It clearly appears in Figure 3.7 that the behavior of $l_p$ with salt concentration is in agreement with Eqn. 2.19, *i.e.*, $l_p$ decreases according to Eqn. 2.19 with increasing the salt concentration, which means that in the high salt concentration (≥ 150 mM) only the non-electrostatic contribution of the persistence length remains, which is constant. Error bars (*i.e.*, error in $l_p$) are the calculated errors from previous step (linear fitting of <*s*> with *ln(<cos(θ)>)*).

Table 3.3 shows some of de Pablo and co-worker's results for the persistence length of the dsDNA chains in their replica exchange molecular dynamics (REMD) simulation study **(Sambriski, Schwartz, & de Pablo, 2009)**.

**Table 3.3:** The persistence length ($l_p$) for 144 and 250 bp dsDNA chains at different salt concentrations from de Pablo and co-workers study **(Sambriski, Schwartz, & de Pablo, 2009)**.

| # of dsDNA bps | Salt concentration ([$Na^+$] *M*) | $l_p$ (*nm*) |
|---|---|---|
| 144 | 0.150 | 42 ± 4 |
| 250 | 0.005 | 93 ± 5 |
| | 0.010 | 68 ± 4 |
| | 0.025 | 53 ± 3 |
| | 0.050 | 45 ± 6 |
| | 0.100 | 40 ± 2 |
| | 0.150 | 45 ± 6 |

Empirically, dsDNA is observed to exhibit a persistence length $l_p$ ~ 50 nm at T = 300 K in [$Na^+$] = 150 mM. For these same conditions, our model yields 41 *nm* < $l_p$ < 50.9 *nm*, which

is in reasonable agreement with both Baumann and co-workers experimental study **(Baumann, Smith, Bloomfield, & Bustamante, 1997)** and de Pablo and co-worker simulation study **(Sambriski, Schwartz, & de Pablo, 2009)**.

**(a)**

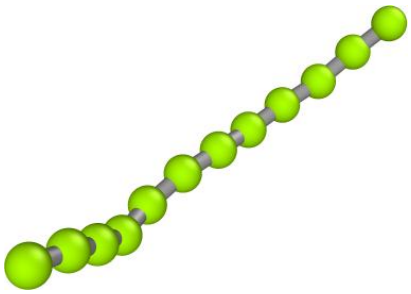

**(b)**

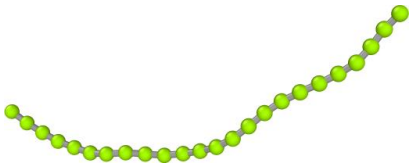

**(c)**

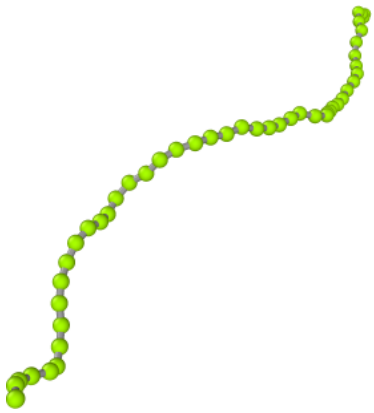

**(d)**

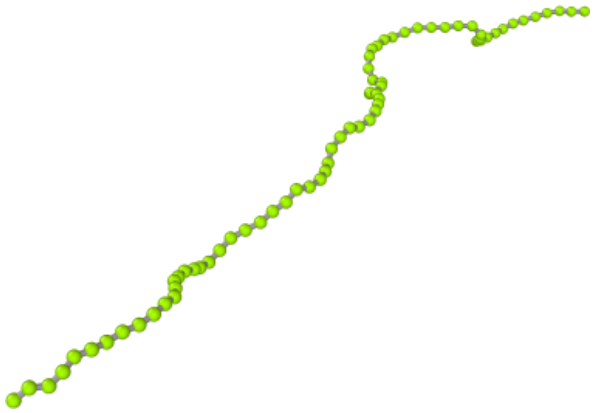

**Figure 3.8:** Snapshots for dsDNA chains simulations after $1 \times 10^8$ BDS (after $3 \times 10^7$ BDS equilibration); (a) 72bp-12b at $[Na^+]$ = 10 *mM*. (b) 144bp-24b at $[Na^+]$ = 150 *mM*, (c) 288bp-48b at $[Na^+]$ = 1000 *mM* and (d) 432bp-72b at $[Na^+]$ = 1000 *mM*.

From our results for $D_t$ and $l_p$ which are in good agreement with previous experimental and simulation studies, we can say that our model for dsDNA is approximately valid, *i.e.*, the bead-spring chain in our study represents or acts as the dsDNA chain.

## 3.2 dsDNA-dendrimer complex simulations

We calculated the radius of gyration ($R_g$), distance between COMs of the dsDNA and the dendrimer ($D_{coms}$), fraction of adsorption dsDNA beads onto dendrimer surface ($\omega$) and the order (curvature) parameter of dsDNA-dendrimer complex ($\gamma$) for each dsDNA-dendrimer complex under the effect of both salt concentration and pH from 100 sampling points (frames) from $1 \times 10^8$ BDS every $1 \times 10^6$ BDS after $3 \times 10^7$ BDS equilibration for 144bp-G6 system and $7 \times 10^7$ BDS equilibration for 288bp-G7 system.

### 3.2.1. Effect of salt concentration:

Figures 3.9, 3.10, 3.11, 3.12, and 3.13 collect the graphs of the previously mentioned quantities and the dsDNA-dendrimer complex systems snapshots as functions of salt concentration.

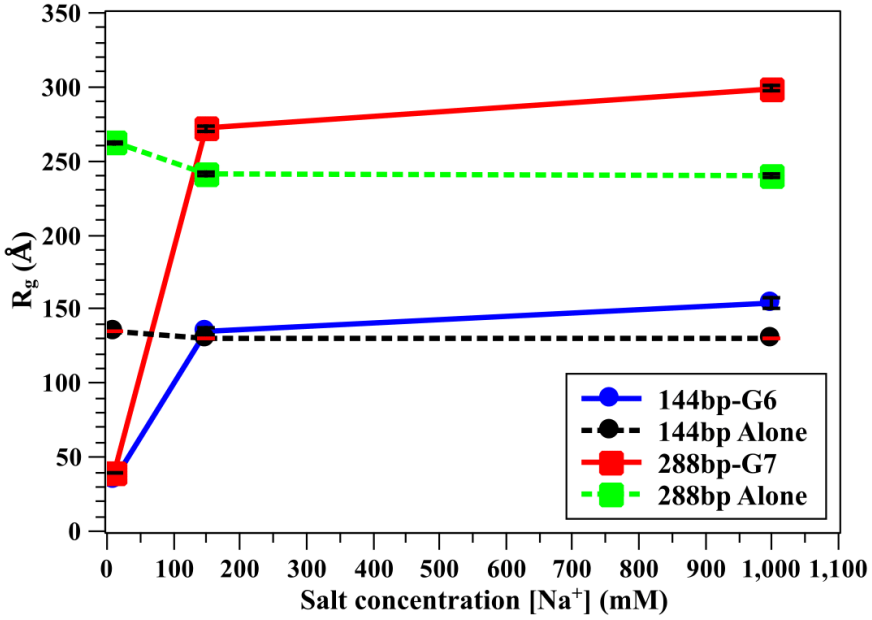


**Figure 3.9:** Radius of gyration ($R_g$) of dsDNA chains alone as well as dsDNA-dendrimer complexes as function of salt concentration.

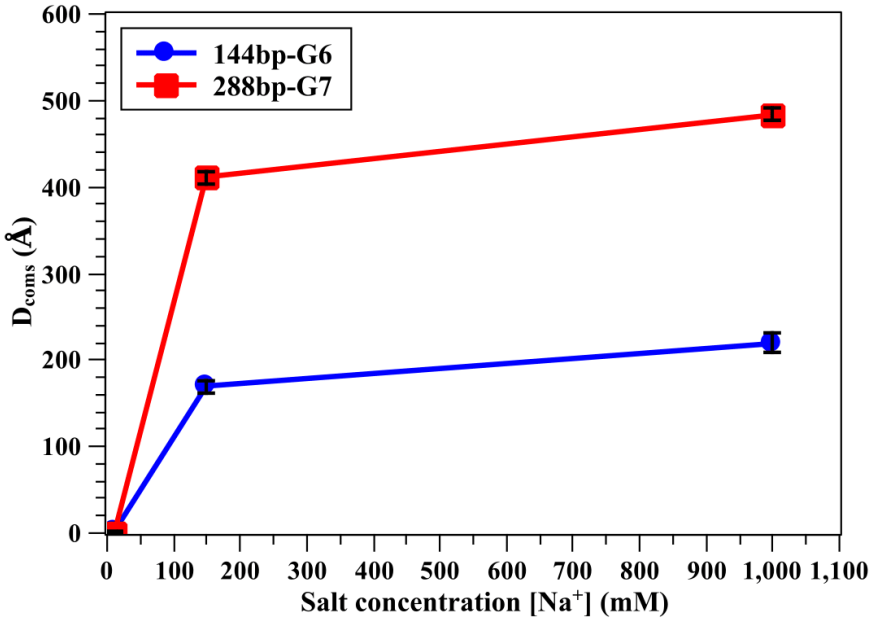


**Figure 3.10:** Distance between COMs of dsDNA chain and dendrimer ($D_{coms}$) in the complexes as function of salt concentration.

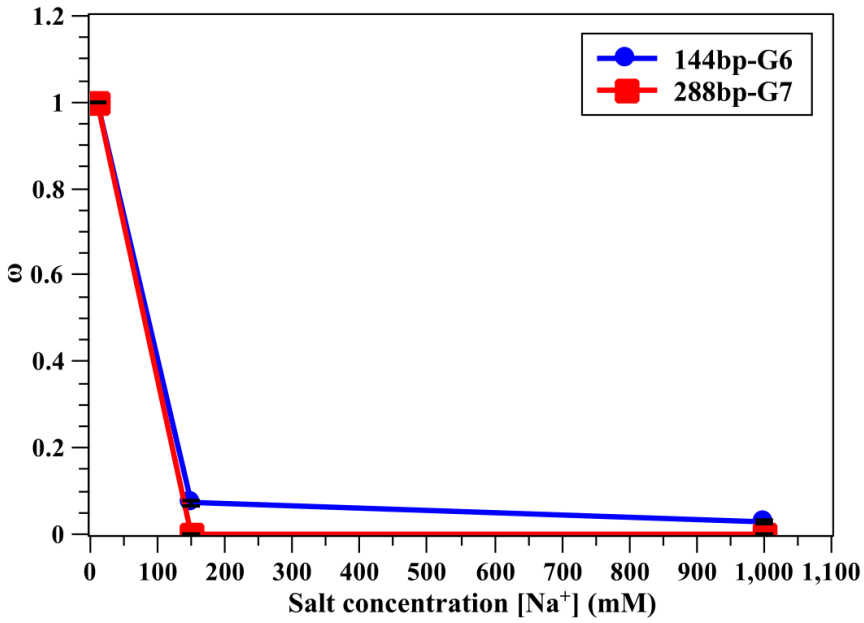


**Figure 3.11:** Fraction of adsorption dsDNA beads onto dendrimer surface ($\omega$) in the complexes as function of salt concentration.

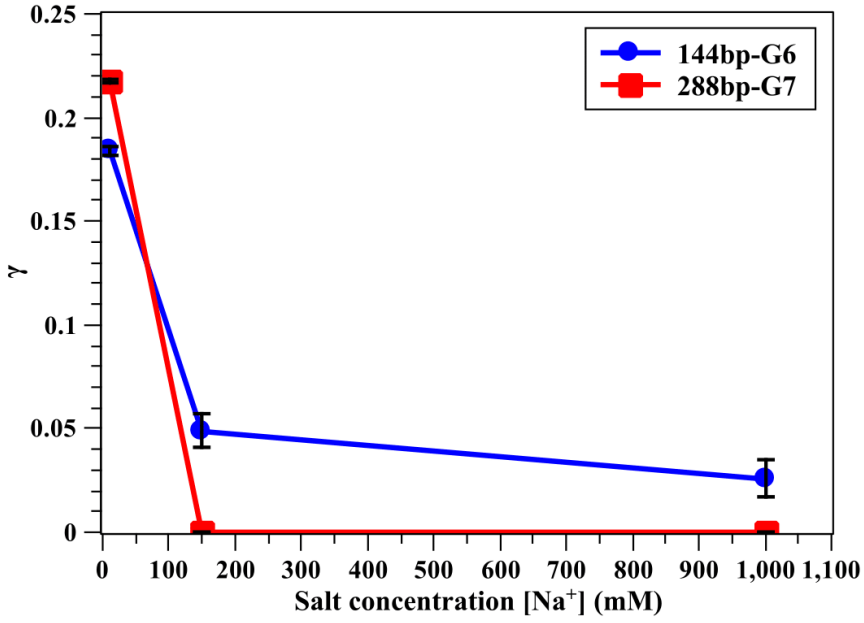


**Figure 3.12:** Order (curvature) parameter ($\gamma$) of the dsDNA-dendrimer complexes as function of salt concentration.

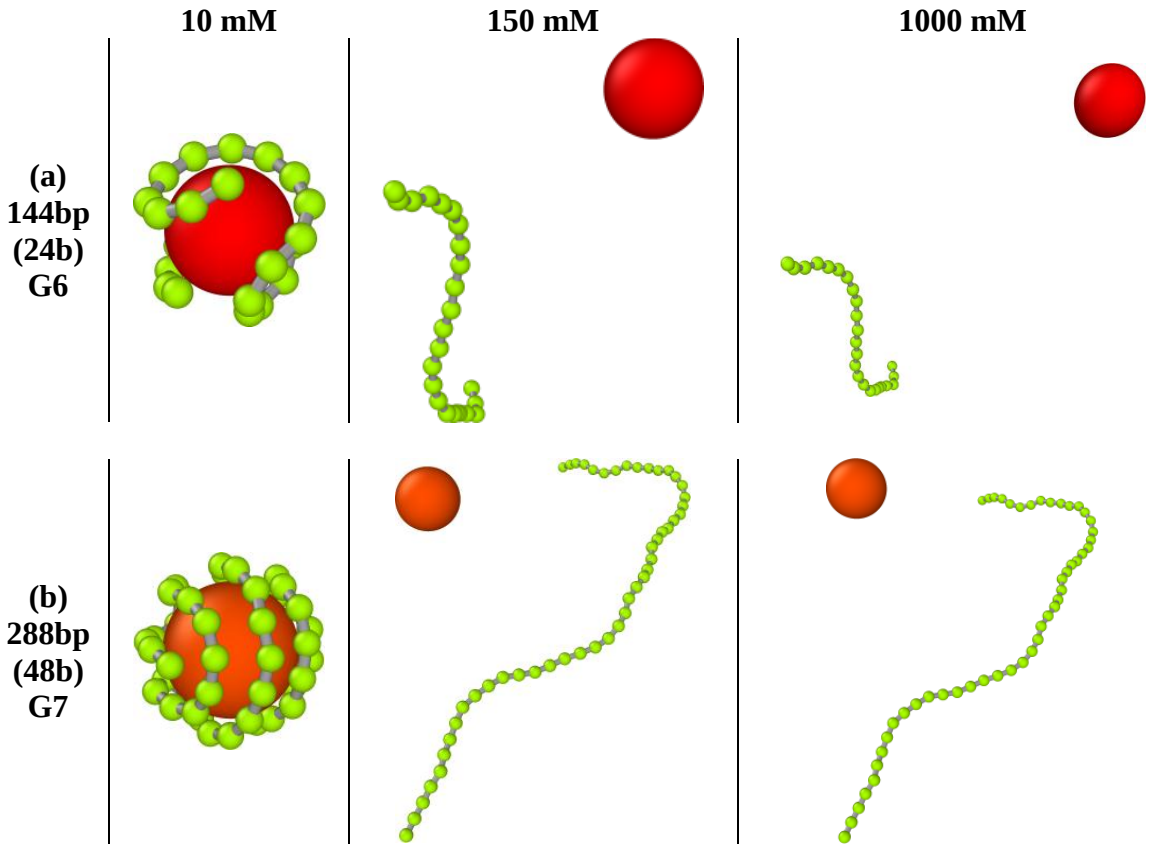


**Figure 3.13:** Snapshots of (a)144/(b)288bp dsDNA-G6/7 dendrimer interaction after $1 \times 10^8$ BDS (after $3 \times 10^7$ BDS equilibration for 144bp-G6 system and $7 \times 10^7$ BDS equilibration for 288bp-G7 system) at $[Na^+]$ = 10, 150 and 1000 *mM*.

Figures 3.9 and 3.13 show that a dsDNA molecule wraps around a dendrimer tightly at low salt concentration (10 *mM*) but is much straighter at high salt concentration (150 & 1000 *mM*), due to the stronger ion screening effects at higher salt concentration. The radius of gyration ($R_g$) of complexes decreases monotonically with decreasing salt concentration because of increased attraction between dsDNA and dendrimer at the lower salt concentration, while the $R_g$ of the dsDNA chains alone increase with decreasing salt concentration, due to the high electrostatic repulsion between the dsDNA beads.

As shown by Figures 3.10 and 3.13, the distance between COMs of the dsDNA chain and the dendrimer ($D_{coms}$) in all complexes increases monotonically with increasing salt concentration, *i.e.*, dissociation of the complex, because of the weak of the electrostatic attraction between the dsDNA chain and the dendrimer at a higher salt concentration.

In all dsDNA-dendrimer complexes, and as appearing in Figures 3.11 and 3.13, the fraction of adsorption dsDNA beads onto dendrimer surface ($\omega$) decreases monotonically with increasing salt concentration, *i.e.*, dissociation of the complex, as expected due to the stronger ion screening effects at higher salt concentration.

As shown by Figures 3.12 and 3.13, the order (curvature) parameter of the dsDNA-dendrimer complex ($\gamma$), which in our study is considered as a measure of the order (curvature) of the adsorbed dsDNA beads onto the dendrimer surface in the complex, decreases in all complexes with increasing salt concentration. In other words, when $\gamma \leq 0.05$, a disorder complex forms (where the dsDNA chain is adsorbed to the dendrimer surface random-

ly **(Cao, Zuo, Ma, Li, & Zhang, 2011)**) and when it equal zero no complex formed, based on this, our results show that we have an order complexes at low salt concentration and at a high one no complexes are formed because of the screening effects of salt ions, also, the complex formed from the dsDNA chain with G7 of the dendrimer at a low salt concentration (10 *mM*) is more order than the G6 one, this likely because of the increasing of the surface area of the G7 dendrimer.

Error bars in Figures 3.9, 3.10, 3.11, and 3.12 are the standard errors of the means over 100 sampling points.

For $R_g$, $\omega$ and $\gamma$, Figures 3.14 and 3.15 show their behavior with salt concentration as reported in Yu and Larson MC simulation study **(Yu & Larson, 2014)**.

**(a)**

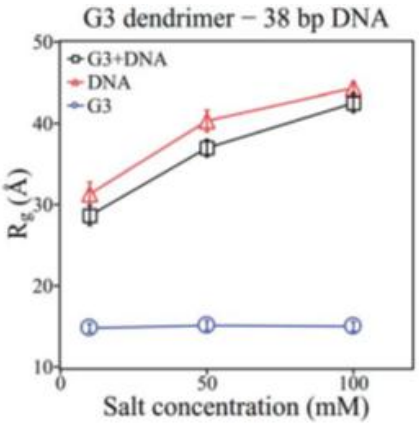


**(b)**

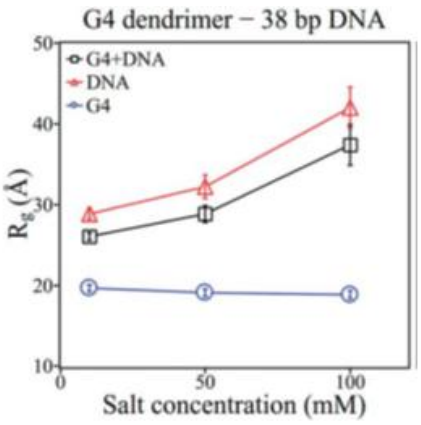


**(c)** **(d)**

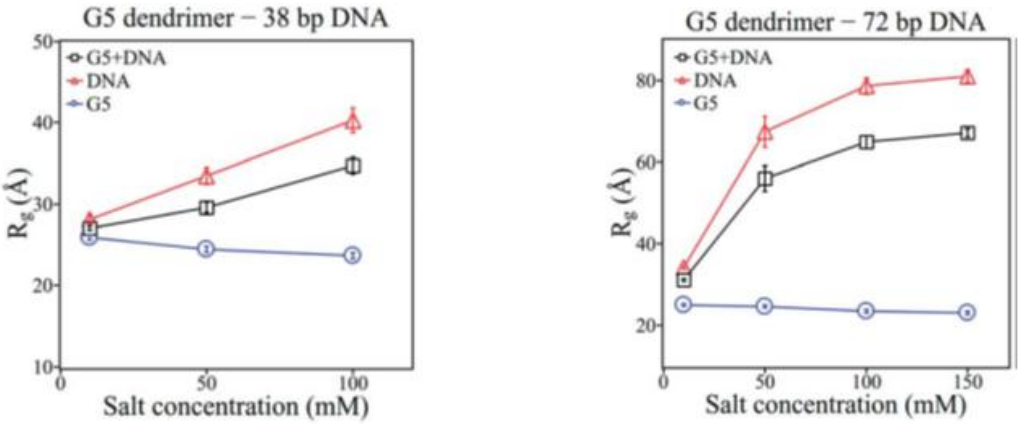


**Figure 3.14:** $R_g$ of complexes (black) as well as of dendrimers (blue) and DNA molecules (red) within those complexes as functions of salt concentration. (a) G3–38 bp DNA, (b) G4–38 bp DNA, (c) G5–38 bp DNA, (d) G5–72 bp DNA. (The error bars are standard deviations) **(Yu & Larson, 2014)**.

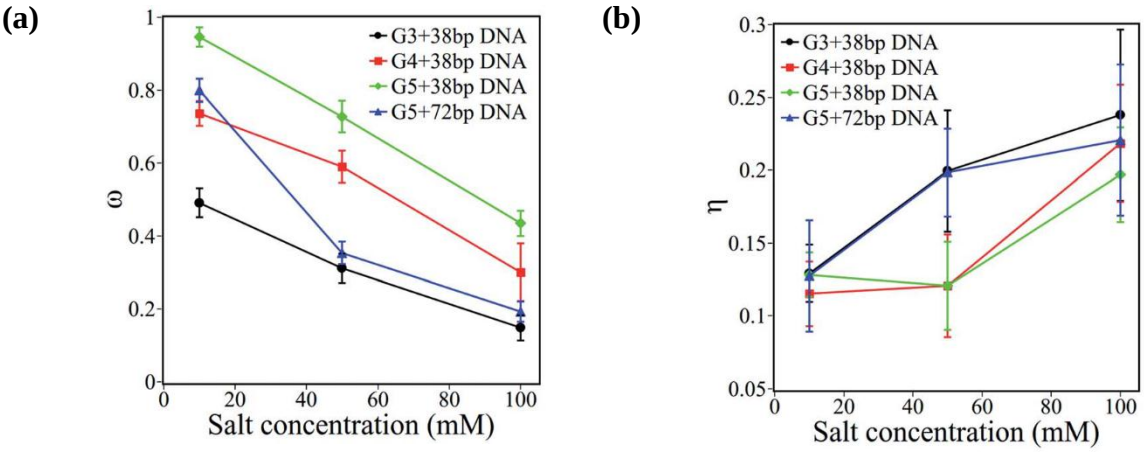


**Figure 3.15:** (a) Fraction $\omega$ of adsorbed DNA phosphate beads and (b) order parameter $\eta$ in dendrimer–DNA complexes as functions of salt concentration. The error bars represent standard deviations taken over 500 sampling points of the simulation [$\eta$ here is $\gamma$ in our study] **(Yu & Larson, 2014)**.

For $R_g$ and $\omega$, and although our results are for different generations of PAMAM dendrimer and at different salt concentrations, they behave like Yu and Larson's ones, but for $\gamma$ ($\eta$ in Yu and Larson study), our results behave in a reverse way with Yu and Larson's ones, and we can relate this to two reasons, the first is the differences between our models for dsDNA chain and dendrimer and Yu and Larson's ones, while the second is the difference in the scale of salt concentration used to calculate $\gamma$ (or $\eta$).

### 3.2.2. The effect of pH:

We ignored this effect on the dsDNA chain, and we took it only on the dendrimer through changing its radius and charge (return to pages 23-26 in chapter one for more about this).

Figures 3.16, 3.17, 3.18, 3.19, and 3.20 contain the graphs of the same quantities studied in salt concentration effect and the dsDNA-dendrimer complex systems snapshots as functions of pH.

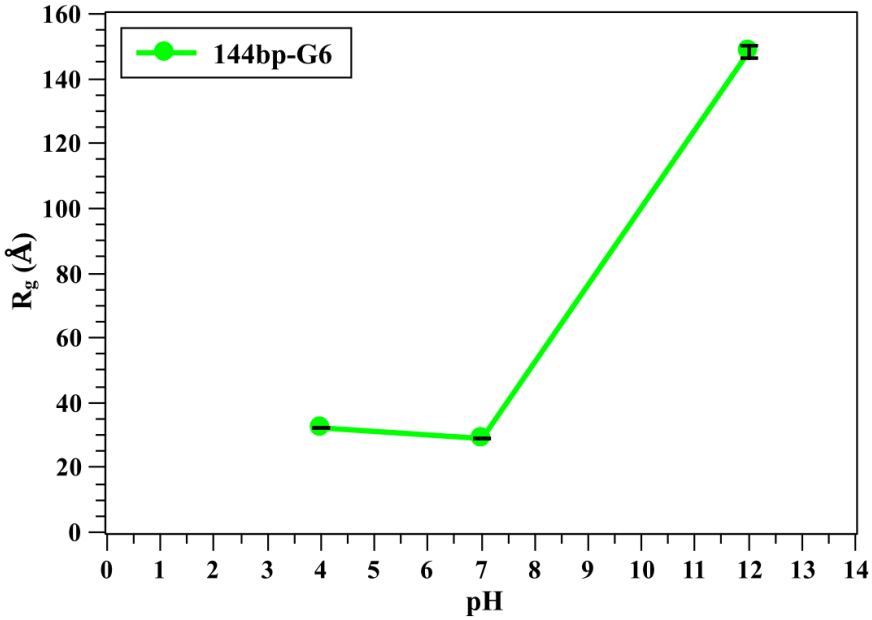


**Figure 3.16:** Radius of gyration ($R_q$) of dsDNA-dendrimer complex as function of pH.

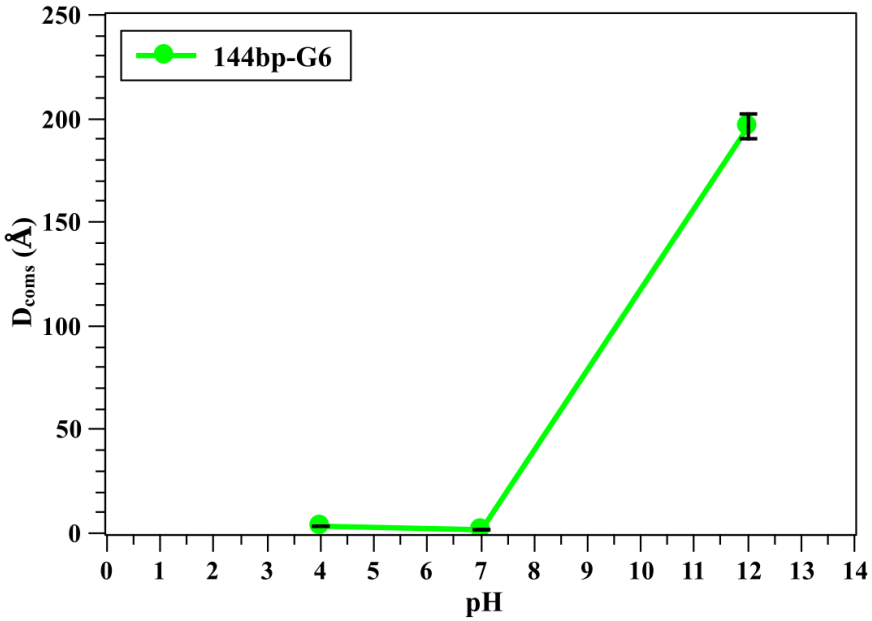


**Figure 3.17:** Distance between COMs of dsDNA chain and dendrimer ($D_{coms}$) in the complex as function of pH.

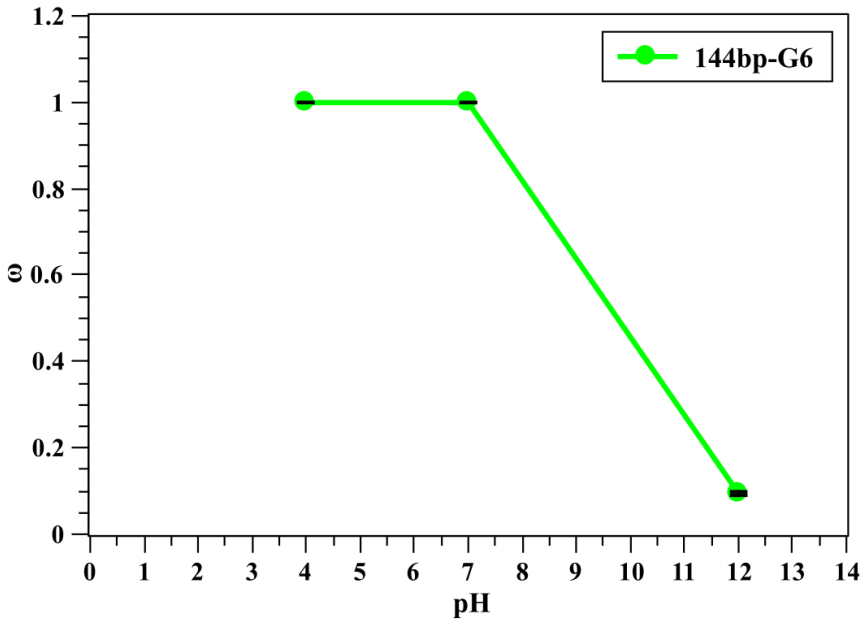


**Figure 3.18:** Fraction of adsorption dsDNA beads onto dendrimer surface ($\omega$) in the complex as function of pH.

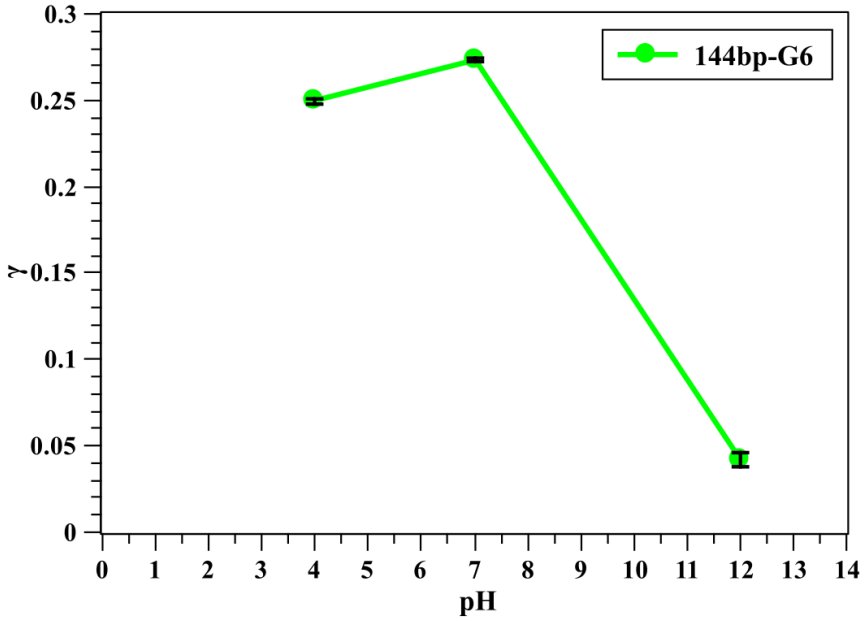


**Figure 3.19:** Order (curvature) parameter ($\gamma$) of the dsDNA-dendrimer complex as function of pH.

**Acidic ( ≤ 4)** **Neutral ( ~ 7)** **Basic ( ≥ 12)**

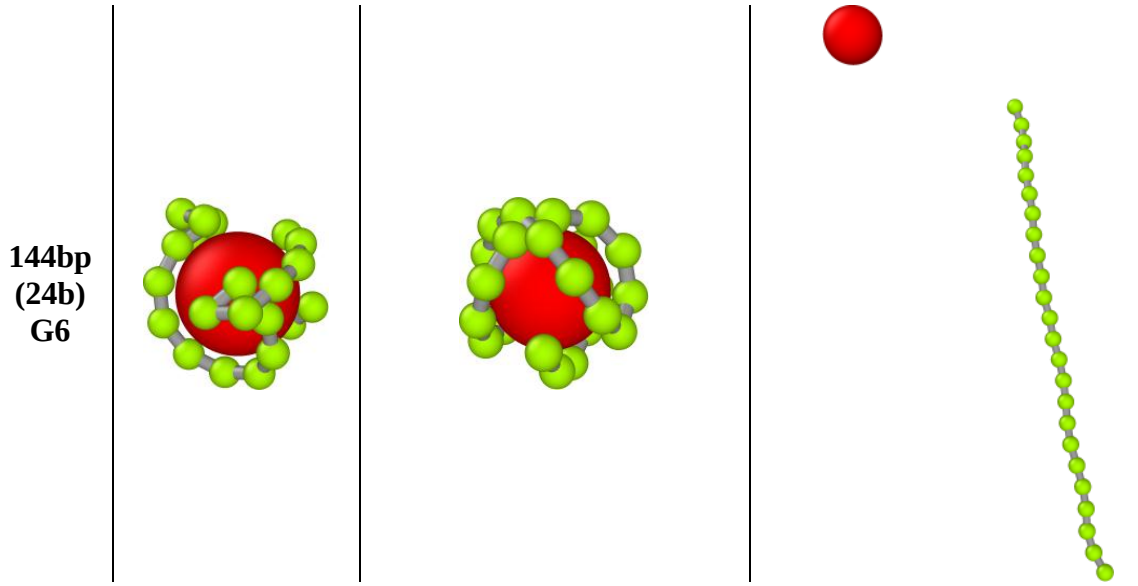


**Figure 3.20:** Snapshots of 144bp dsDNA-G6 dendrimer interaction after $1 \times 10^8$ BDS (after $3 \times 10^7$ BDS equilibration) at pH $\leq 4$, ~ 7 and $\geq 12$.

As shown by Figures 3.16 and 3.20, a dsDNA molecule wraps around a dendrimer closely at pH $\leq 7$ and forms a complex with it, while no complex formed at high pH ($\geq 12$), due to the deprotonation process in the dendrimer (becomes uncharged) at higher pH. The radius of gyration ($R_g$) of complex approximately remains constant at pH $\leq 7$ (in the acidic and neutral regions) and increases with increasing pH because of decreased attraction between dsDNA and dendrimer at the higher pH.
Figures 3.17 and 3.20 clarify that the distance between COMs of the dsDNA chain and the dendrimer ($D_{coms}$) in the complex approximately remains constant at pH $\leq 7$ (in the acidic and neutral regions) and increases with increasing pH, *i.e.*, dissociation of the complex, because of the weak of the electrostatic attraction between the dsDNA chain and the dendrimer at a higher pH as a result of the deprotonation process in the dendrimer (becomes un-charged) at higher pH.

It appears in Figures 3.18 and 3.20 that the fraction of adsorption dsDNA beads onto dendrimer surface ($\omega$) of the complex remains constant at pH $\leq 7$ (in the acidic and neutral regions) and decreases with increasing pH, *i.e.*, dissociation of the complex, as expected due to the same reason that we mentioned in the previous paragraphs.

As shown in Figures 3.19 and 3.20, the order (curvature) parameter of the dsDNA-dendrimer complex ($\gamma$) increases with increasing pH from $\leq 4$ to ~ 7 and then decreases with increasing pH. Based on what we said for $\gamma$ in salt concentration effect part, our results show that the order of the complex decreases when pH decreases below 7, due to more severe bending of the dsDNA as a result of the strong attraction between the dsDNA chain and the dendrimer at low pH due to the protonation process in the dendrimer (*i.e.*, increasing its charge) at the lower pH, and at a high one no complex is formed because of the deprotonation process in the dendrimer (*i.e.*, becomes uncharged) at the higher pH.

Error bars in Figures 3.16, 3.17, 3.18, and 3.19 are the standard errors of the means over 100 sampling points.

### 3.3 dsDNA-dendrimer aggregate simulations (Linker/Tail(s) study)

We calculated the number of adsorbed dsDNA beads onto dendrimers surfaces and the number of not adsorbed ones (it can be in-between adsorbed or linker or tail/s) for each dsDNA-dendrimer aggregate in this study under the effect of both salt concentration and dsDNA length (the number of bps in the dsDNA chain) from 100 sampling points (frames) from $1 \times 10^8$ BDS every $1 \times 10^6$ BDS after $1 \times 10^8$ BDS equilibration.

#### 3.3.1. Effect of salt concentration:

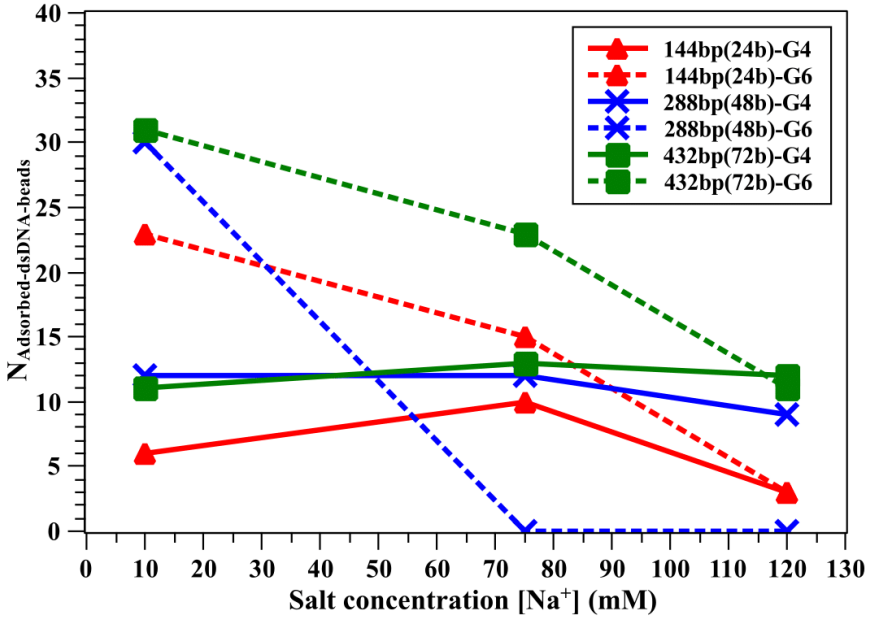


**Figure 3.21:** The number of adsorbed dsDNA beads onto dendrimers surfaces in the dsDNA-(G4-G6)-dendrimers aggregate Vs. salt concentration.

Figure 3.21 explains how the number of adsorbed dsDNA beads onto dendrimers surfaces in the dsDNA-(G4-G6)-dendrimers aggregate changes with variating salt concentration, we can roughly say that increasing salt concentration leads to decrease the number of adsorbed dsDNA beads, due to the weak of the electrostatic attraction between the dsDNA beads and the dendrimers at higher salt concentration. In other words, increasing salt concentration more and more causes dissociation of the aggregate. The total number of adsorbed dsDNA beads onto dendrimers surfaces in the aggregate may exceed the dsDNA beads number because the same dsDNA bead can be considered as adsorbed to the two dendrimers if it obeys the condition of adsorption for the two dendrimers (return to Linker/Tail(s) analysis section in chapter two).

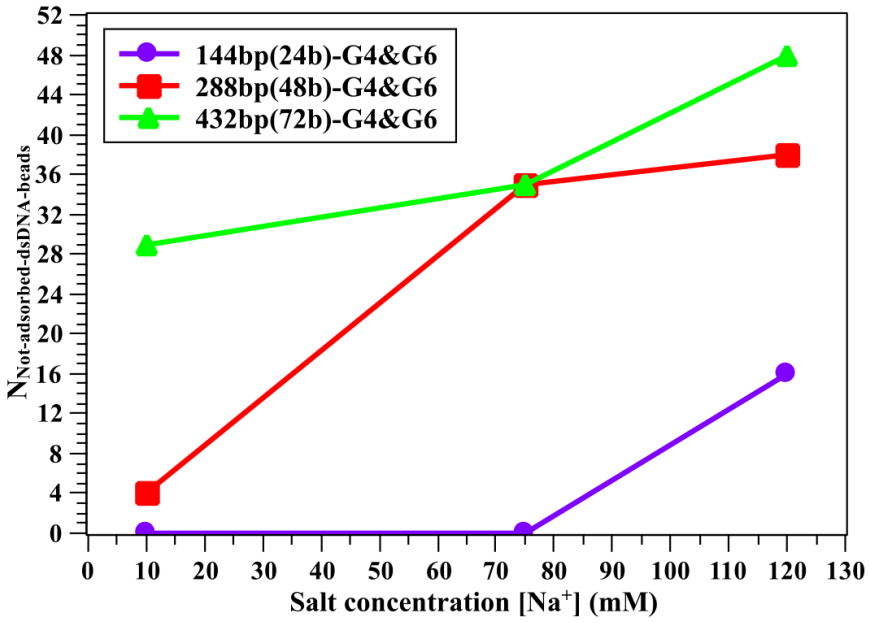

**Figure 3.22:** The number of not adsorbed dsDNA beads (it can be in-between adsorbed ones or linker or tail/s) in the dsDNA-(G4-G6)-dendrimers aggregate Vs. salt concentration.

As shown in Figure 3.22, the not adsorbed dsDNA beads (*i.e.*, not adsorbed onto dendrimers surfaces) number (it can be in-between adsorbed ones or linker or tail/s) in the dsDNA-(G4-G6)-dendrimers aggregate increases with increasing salt concentration, *i.e.*, increasing salt concentration increases the linker between dendrimers and/or the tail/s in the aggregate. This is because of decreasing the number of adsorbed dsDNA beads.

### 3.3.2. Effect of dsDNA length (base pairs (bps) number):

In Figure 3.23, the total number of adsorbed dsDNA beads onto dendrimers surfaces in the dsDNA-(G4-G6)-dendrimers aggregate almost increases with increasing dsDNA length (the number of bps in the dsDNA chains). The same thing happens for the not adsorbed dsDNA beads (it can be in-between adsorbed ones or linker or tail/s), *i.e.*, the linker between the dendrimers and/or the tail/s in the aggregate increases with increasing the number of bps in the dsDNA chain (see Figure 3.24).

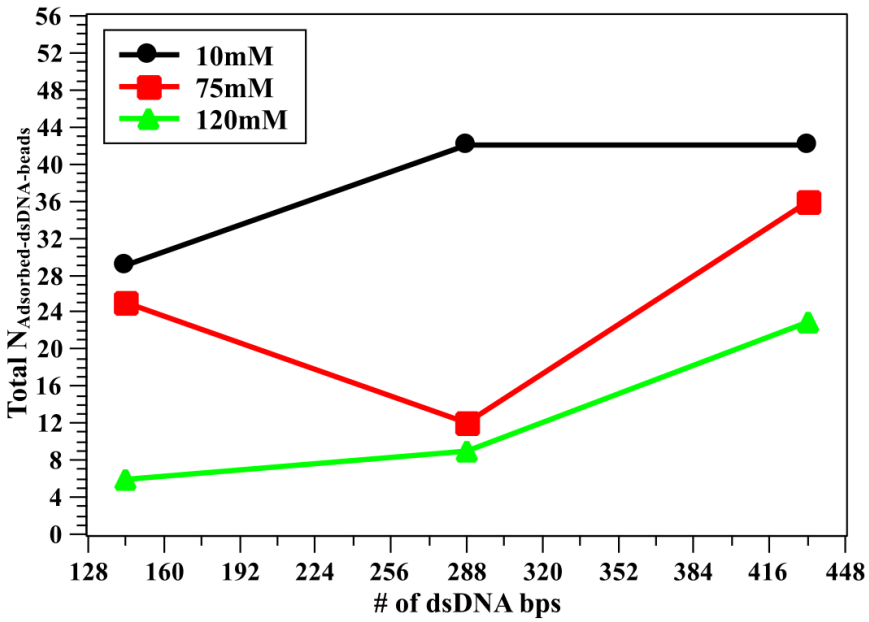


**Figure 3.23:** The total number of adsorbed dsDNA beads onto dendrimers surfaces in the dsDNA-(G4-G6)-dendrimers aggregate Vs. the number of bps in the dsDNA chains at different salt concentrations.

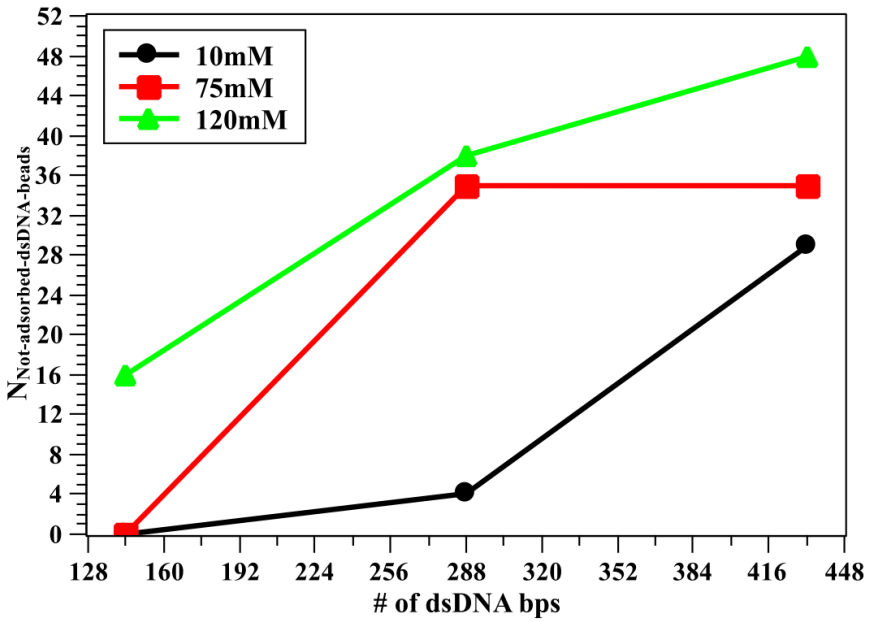


**Figure 3.24:** The number of not adsorbed dsDNA beads (it can be in-between adsorbed ones or linker or tail/s) in the dsDNA-(G4-G6)-dendrimers aggregate Vs. the number of bps in the dsDNA chains at different salt concentrations.

Figure 3.25 contains the snapshots of the dsDNA-(G4-G6)-dendrimers aggregate at different salt concentrations, which clarify what previous graphs show.

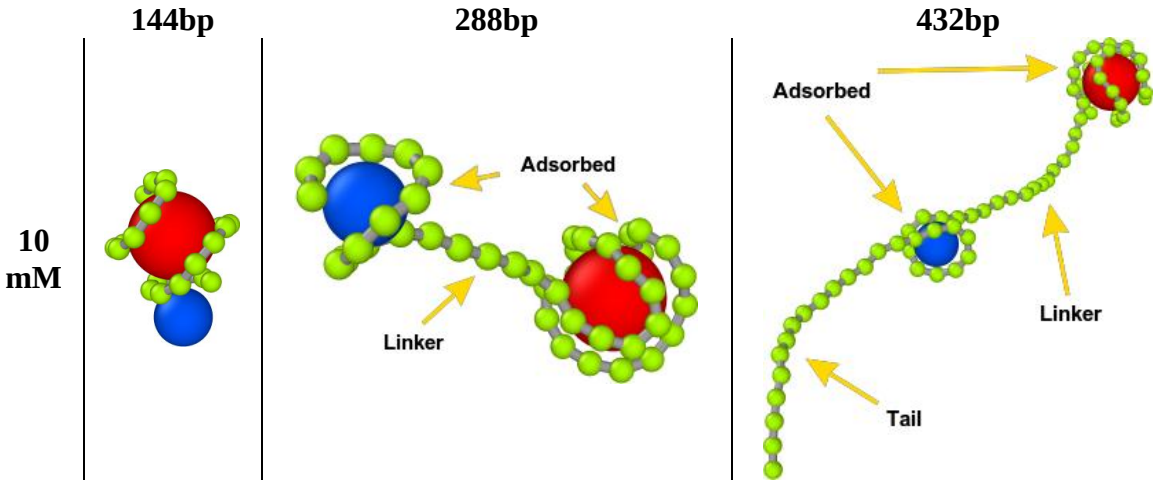

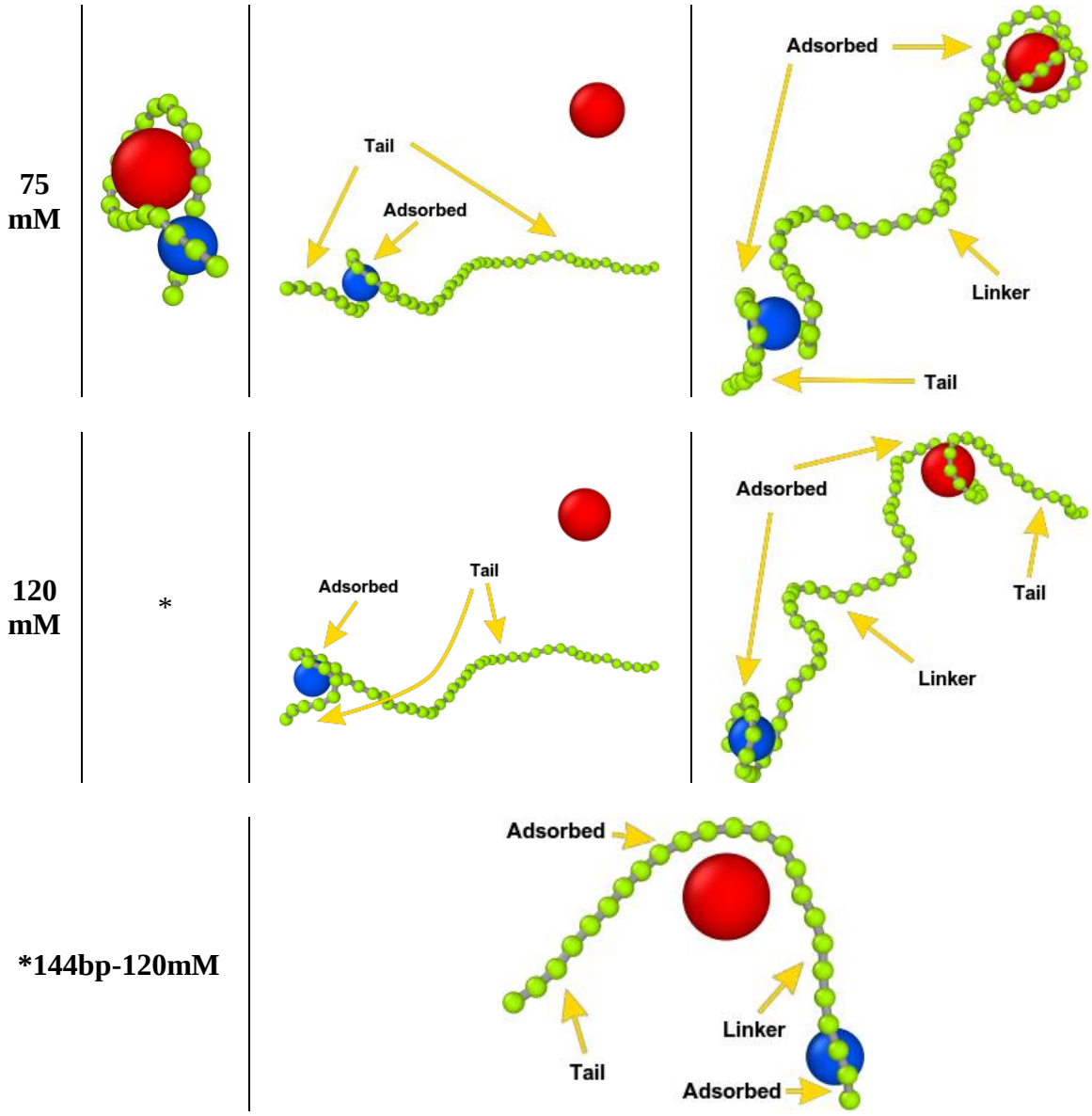


**Figure 3.25:** Snapshots of the dsDNA-(G4-G6)-dendrimers aggregate at different salt concentrations after $1 \times 10^8$ BDS (after $1 \times 10^8$ BDS equilibration).

For 288 bp dsDNA in both 75 and 120 *mM*, we can see from Figure 3.25 that the dsDNA beads did not adsorb onto the G6 dendrimer surface, hence the linker between the two dendrimers did not form in the aggregate, this probably because that the G6 dendrimer went away from the dsDNA chain and due to the salt concentration, the electrostatic attraction force became weak to pull the G6 dendrimer to the dsDNA chain.

As shown in Figures 3.23 and 3.25, for both effects (*i.e.*, salt concentration and dsDNA chain length), the overcharge phenomenon, *i.e.*, the total number of adsorbed dsDNA beads onto the dendrimers surfaces in the aggregate exceeds the one needed to neutralize the dendrimers charges, appears at some cases such as at 10 and 75 *mM* salt concentration for both 288 and 432 bp dsDNA chains and at 120 *mM* salt concentration for 288 bp dsDNA chain. We can conclude this by multiplying the total number of adsorbed dsDNA beads by the bead charge which equals to -12 *e* and checks if the total charge of the adsorbed beads exceeds the sum of two dendrimers charge (64 *e* for G4 and 256 *e* for G6).

Larin and co-workers observed, in their BD simulation study for the complexes formed by two dendrimers with charged terminal groups and oppositely charged long linear polyelectrolyte (LPE) **(Larin, Darinskii, Lyulin, & Lyulin, 2010)**, that dendrimers in the considered complexes are sufficiently overcharged; *i.e.*, the number of adsorbed LPE monomers is larger than required for the neutralization, and the degree of overcharging increases with the increase of the LPE length and is accompanied by the linker appearance until saturation in overcharging is reached. Also, they observed a nonmonotonic dependence of the linker size on the LPE length (return to Figure 1.31 in page 39).

Luylin and co-workers found in their BD simulation study that for longer LPE chains the total number of the chain monomers adsorbed onto a dendrimer exceeds the number that is necessary for a dendrimer neutralization, and they observed the overcharging phenomenon **(Lyulin, Darinskii, & Lyulin, 2005)**.

Based on what Larin and co-workers and Luylin and co-workers observed in their study, our linker and overcharging phenomena results are in good agreement with their results, *i.e.*, we observed the overcharged dendrimers in our aggregates and the degree of overcharging appears when the number of bps in the dsDNA chain exceeds 144 and remains constant when the number of bps in the dsDNA chain increases from 288 to 432, also the linker increases with increasing the dsDNA chain length (increasing the number of bps).

### 3.4 dsDNA-dendrimer aggregate simulations (Morphology study)

Here, we calculated the toroidal parameter ($\tau$) for each dsDNA-dendrimer aggregate in this part of our study in order to recognize the rod-like, toroidal and globular morphologies of the aggregates. All simulations in this study part are at 10 *mM* salt concentration.

The number of BDS used in $\tau$ calculations for each dsDNA-dendrimer aggregate is in Table 3.4.

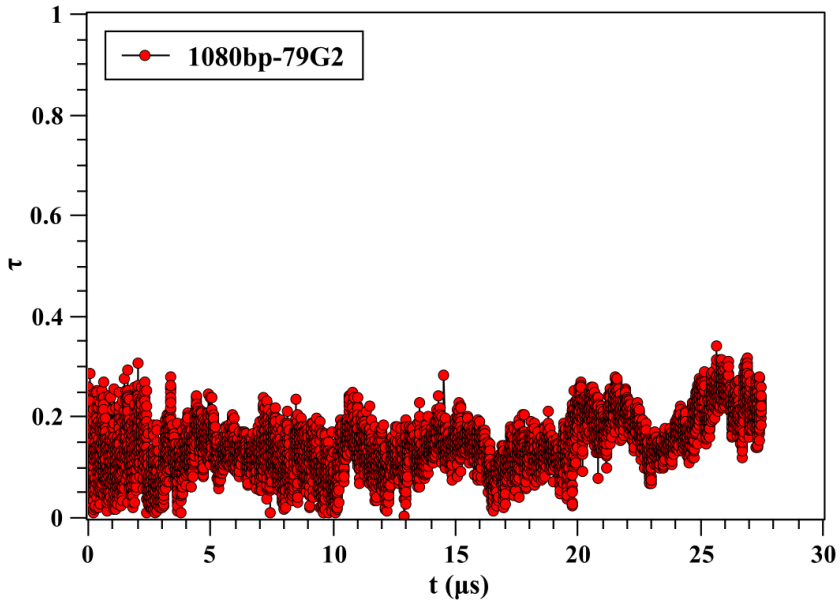


**Figure 3.26:** Toroidal parameter ($\tau$) Vs. time for 1080bp-dsDNA-79G2-dendrimer aggregate.

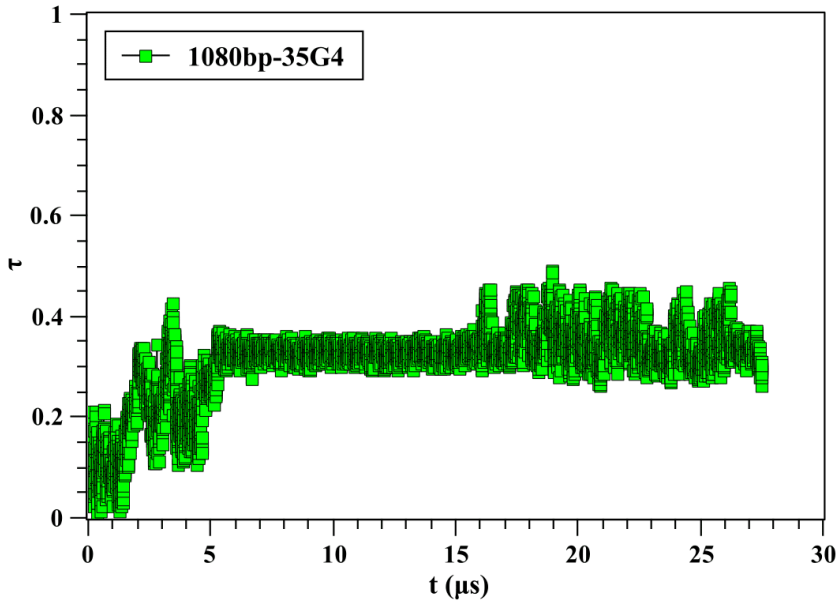


**Figure 3.27:** Toroidal parameter ($\tau$) Vs. time for 1080bp-dsDNA-35G4-dendrimer aggregate.

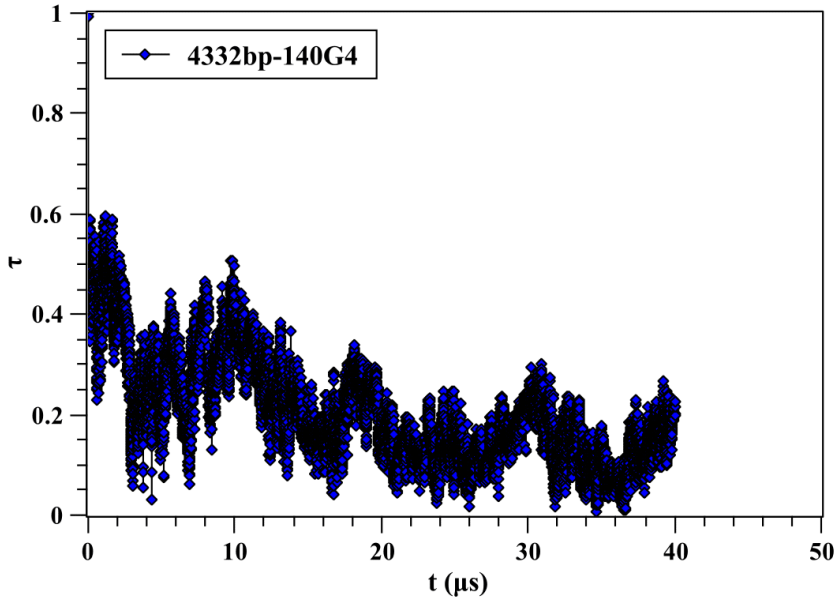


**Figure 3.28:** Toroidal parameter ($\tau$) Vs. time for 4332bp-dsDNA-140G4-dendrimer aggregate.

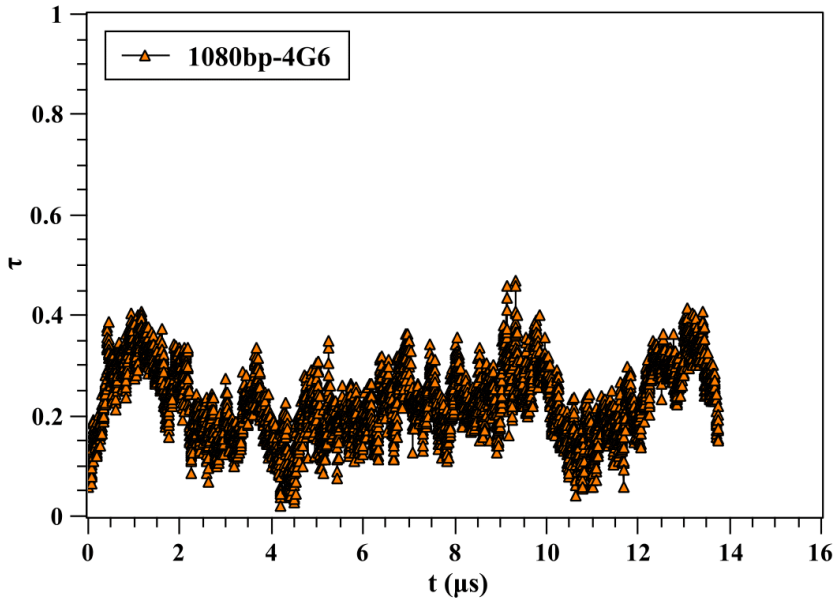


**Figure 3.29:** Toroidal parameter ($\tau$) Vs. time for 1080bp-dsDNA-4G6-dendrimer aggregate.

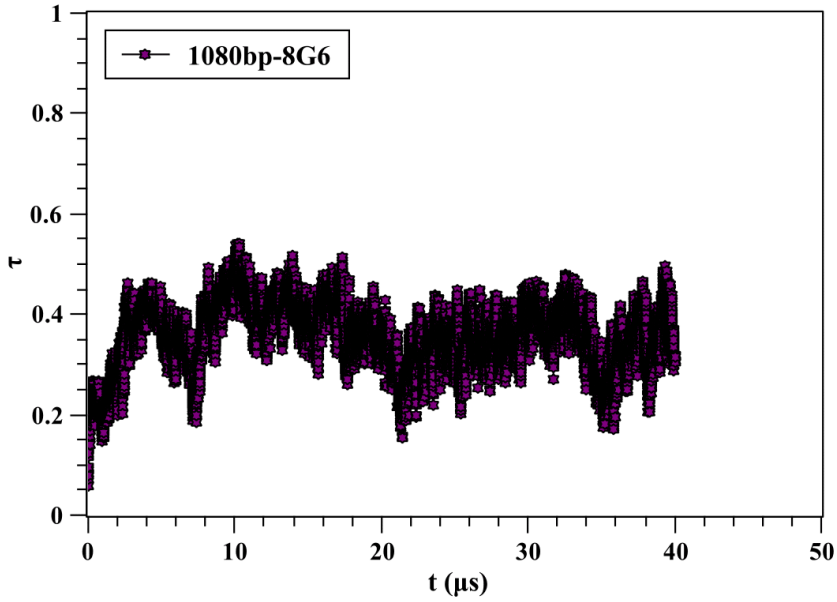


**Figure 3.30:** Toroidal parameter ($\tau$) Vs. time for 1080bp-dsDNA-8G6-dendrimer aggregate.

**Table 3.4:** Average toroidal parameter ($<\tau>$) for each dsDNA-dendrimer aggregate in morphology study part and the number of BDS used in its calculation.

| dsDNA-dendrimer aggregate | $<\tau>$ | Average over |
|---|---|---|
| 1080bp-79G2 | 0.1437 ± 0.0005 | $10.999 \times 10^8$ BDS (~27.5 $\mu s$) |
| 1080bp-35G4 | 0.3128 ± 0.0007 | $10.999 \times 10^8$ BDS (~27.5 $\mu s$) |

| | | |
|---|---|---|
| 4332bp-140G4 | 0.2067 ± 0.0008 | $16 \times 10^8$ BDS (40.0 $\mu s$) |
| 1080bp-4G6 | 0.2277 ± 0.001 | $55 \times 10^7$ BDS (13.75 $\mu s$) |
| 1080bp-8G6 | 0.3576 ± 0.0005 | $16 \times 10^8$ BDS (40.0 $\mu s$) |

According to Eqn. 2.23, $\tau$ approaches 1 when the aggregate has an ideal toroid shape and fluctuates around 1/(18-1) for a disordered (random) shape, therefore from Figures 3.26, 3.27, 3.28, 3.29, and 3.30 and Table 3.4, we can conclude that all of the aggregates in the morphology study part, at the final step/frame reached in their simulations, are far from the toroidal shape and they have disordered (randomly) shapes, but to see the shapes more clearly, we took snapshots of the initial, in-between and final shapes for all of these aggregates, Figures 3.31, 3.32, 3.33, 3.34, 3.35, 3.36, and 3.37 show them.

**(a)**

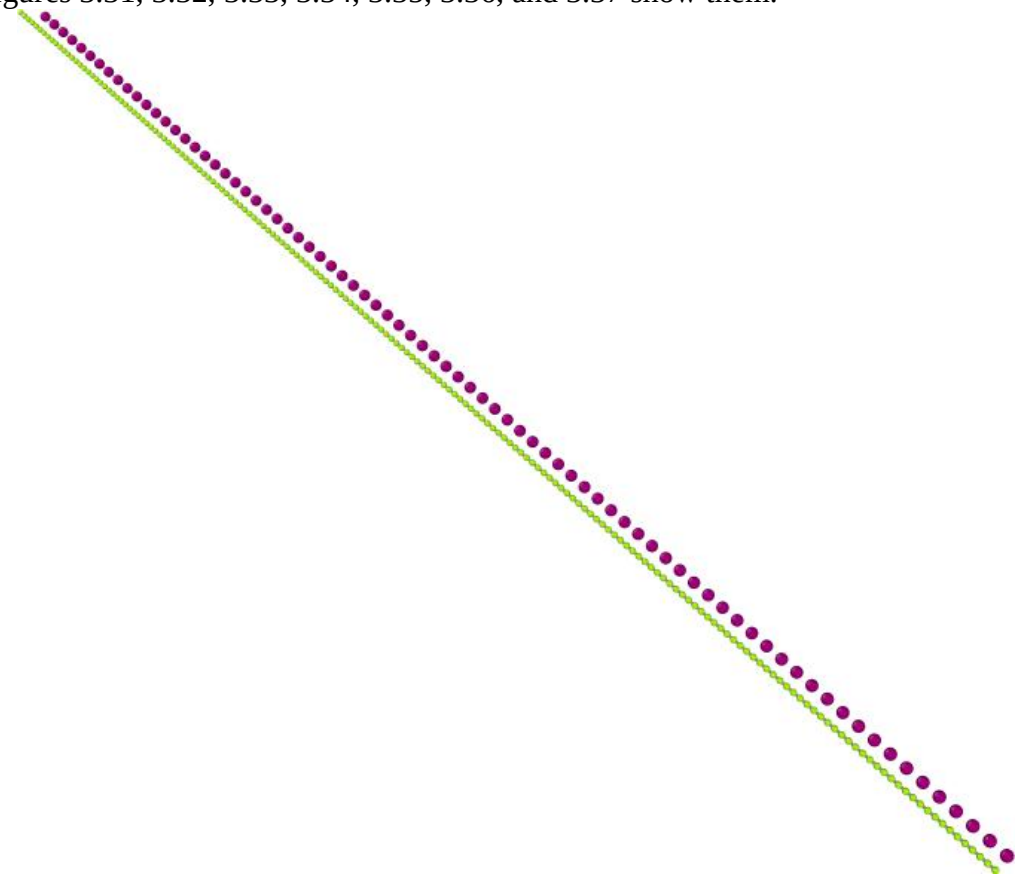

**(b)**

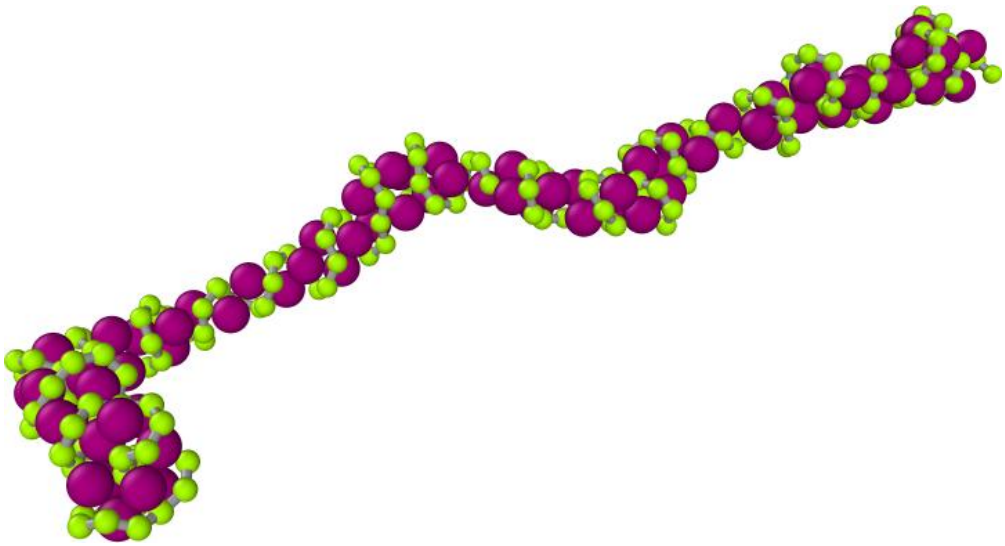

**Figure 3.31:** Snapshots of 1080bp-dsDNA-79G2-dendrimer aggregate; (a) the initial configuration and (b) after $10.999 \times 10^8$ BDS (~27.5 $\mu s$).

It obviously appears in Figure 3.31 that the final shape of 1080bp-dsDNA-79G2-dendrimer aggregate is a rod-like shape.

**(a)**

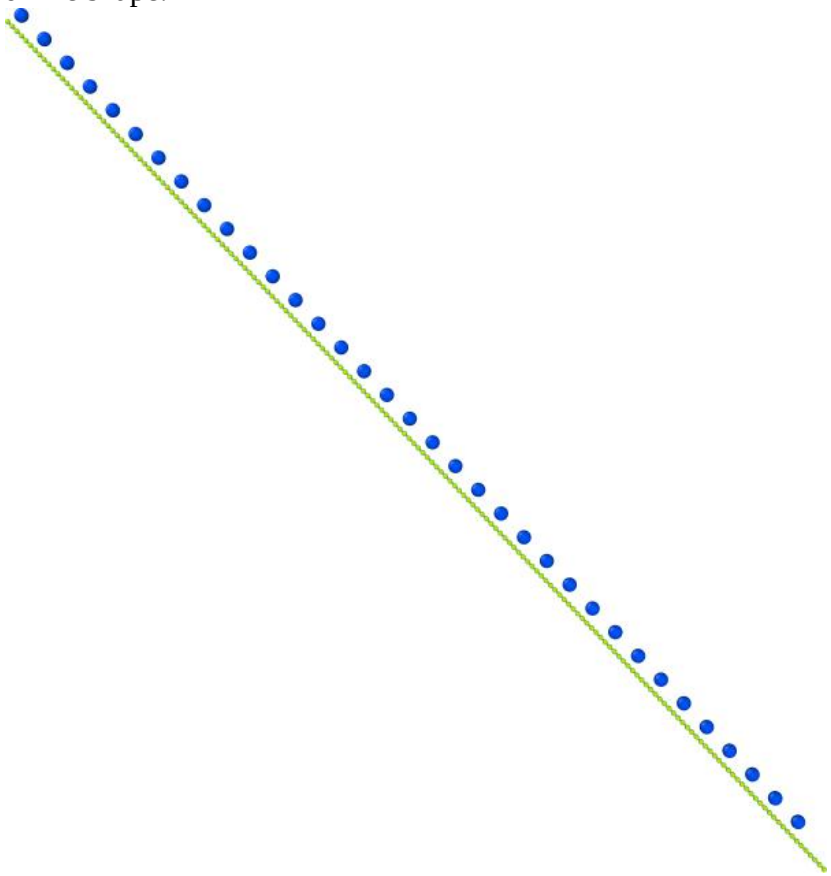

**(b)**

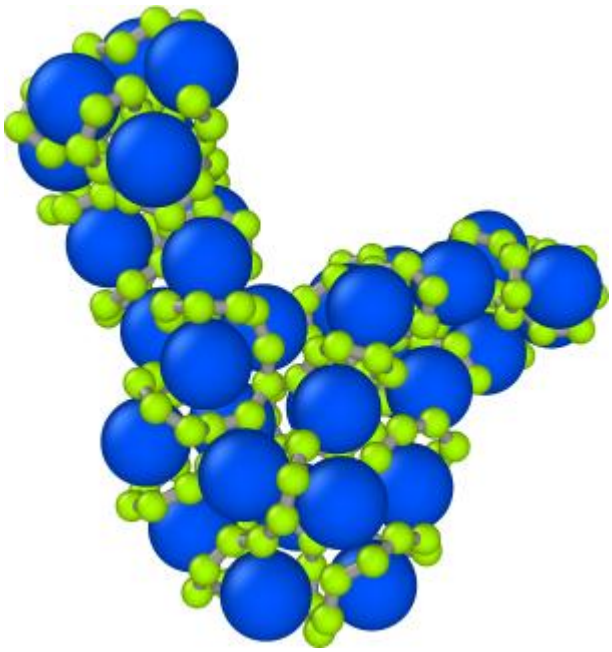

**Figure 3.32:** Snapshots of 1080bp-dsDNA-35G4-dendrimer aggregate; (a) the initial configuration and (b) after $10.999 \times 10^8$ BDS (~27.5 $\mu s$).

Figure 3.32 shows that the final shape of 1080bp-dsDNA-35G4-dendrimer aggregate is an almost globular shape.

**(a)**

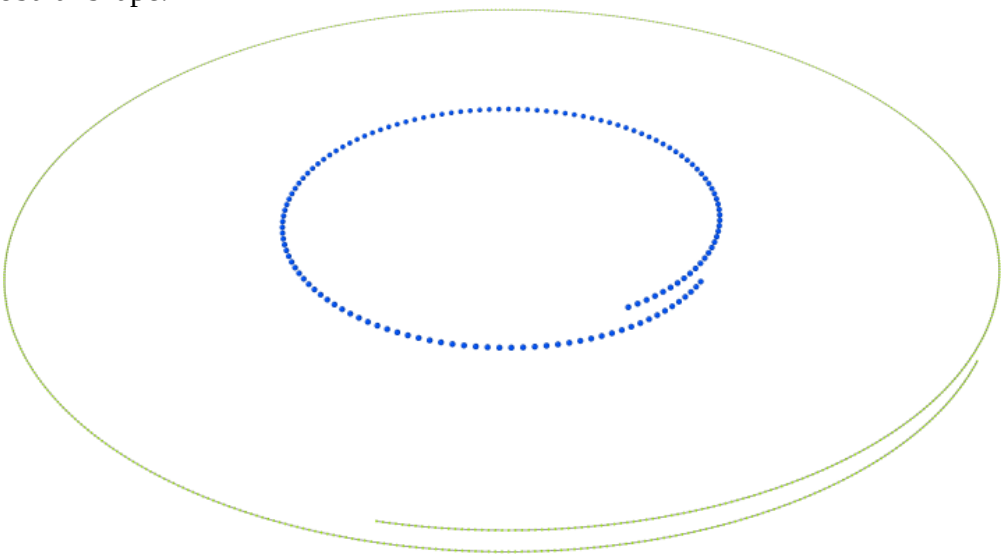

**(b)**

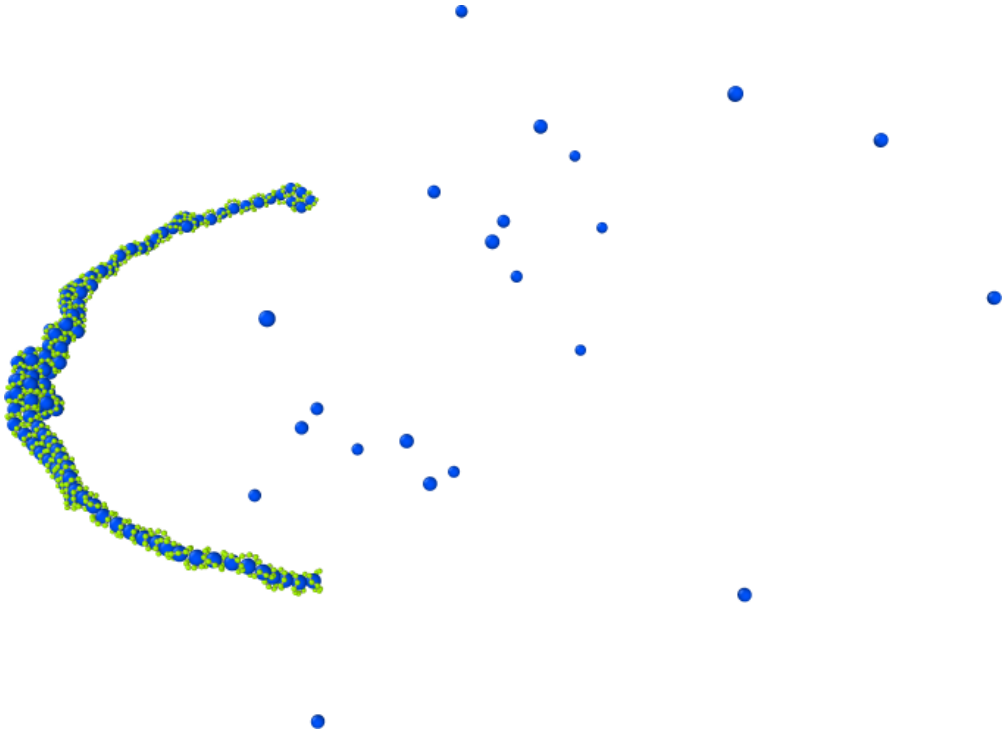

**Figure 3.33:** Snapshots of 4332bp-dsDNA-140G4-dendrimer aggregate; (a) the initial configuration and (b) after $4 \times 10^8$ BDS (10.0 $\mu s$).

**(a)**

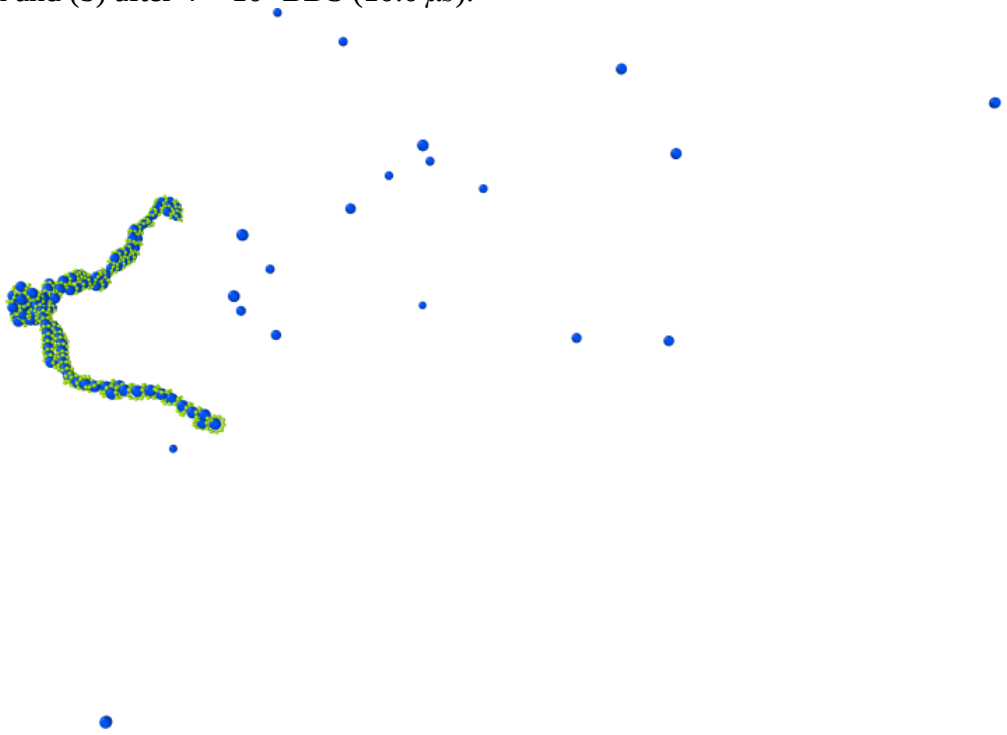

**(b)**

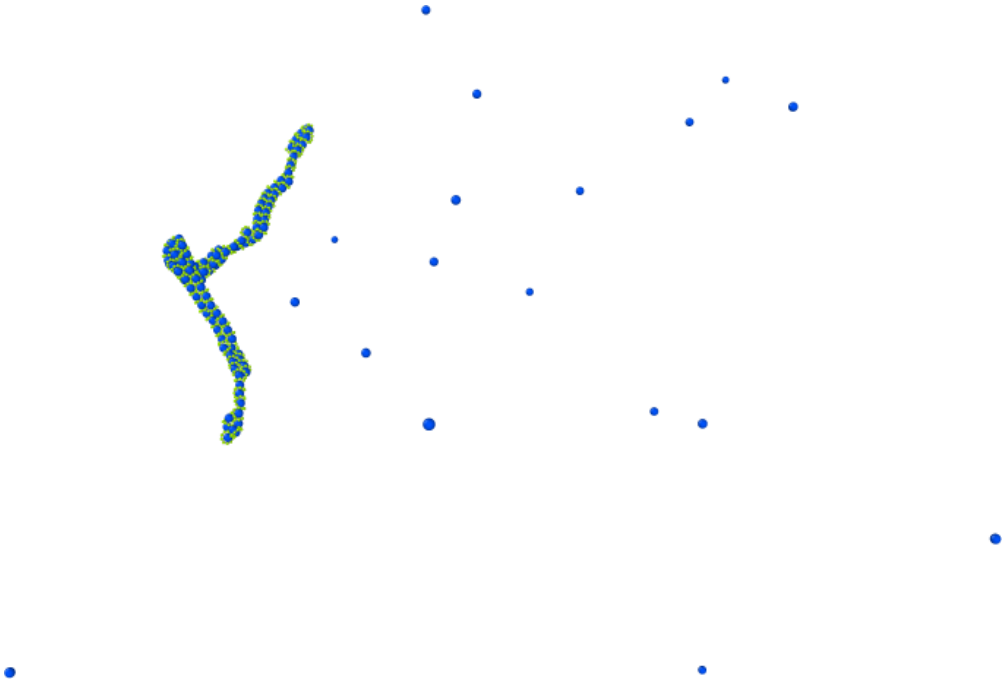

**Figure 3.34:** Snapshots of 4332bp-dsDNA-140G4-dendrimer aggregate; (a) after $8 \times 10^8$ BDS (20.0 $\mu s$) and (b) after $16 \times 10^8$ BDS (40.0 $\mu s$).

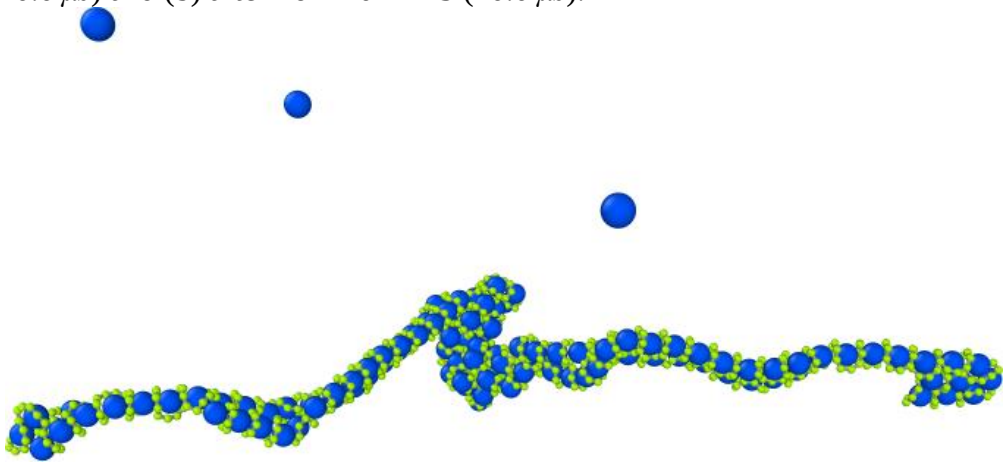

**Figure 3.35:** Snapshots of 4332bp-dsDNA-140G4-dendrimer aggregate after $16 \times 10^8$ BDS (40.0 $\mu s$) (zoomed in).

We know from Qamhieh and co-workers theoretical study **(Qamhieh, et al., 2014)** and Ainalem and co-workers experimental study **(Ainalem, et al., 2009)** that the dsDNA-G4-dendrimer aggregate could take a rod-like or toroidal or globular shape since it is the border case, *i.e.*, where different morphologies can form, therefore we set the initial configuration of 4332bp-dsDNA-140G4-dendrimer aggregate to toroidal shape, as seen in Figure 3.33.a, in order to reduce the time needed to reach the final toroidal shape (within equilibrium region), but the aggregate went far from toroidal shape to rod-like one (see Figures 3.33.b, 3.34.a, 3.34.b, and 3.35).

For dsDNA-G4-dendrimer aggregate systems (in Figures 3.32, 3.33, 3.34 and 3.35), we got globular and rod-like morphologies and we did not get the toroidal one. We think that the reason that we got two morphologies for the same generation of dendrimer aggregates is the difference in the number of dsDNA beads and the number of dendrimers in both aggre-

gates. For the rod-like morphology we have 1080 bp dsDNA beads with 35 G4 dendrimers, and for the globular morphology, we have 4332 bp dsDNA beads with 140 G4 dendrimers.

Figures 3.36 and 3.37 show that the final morphologies of 1080bp-dsDNA-4G6-dendrimer and 1080bp-dsDNA-8G6-dendrimer aggregates are approximately rod-like shapes.

Only the 1080bp-dsDNA-35G4-dendrimer and 1080bp-dsDNA-4G6-dendrimer aggregates systems reached the equilibrium, while the other systems did not reach, *i.e.*, the total energy of these systems is keeping decrease with time, which means that they need more time to reaches the equilibrium.

Qamhieh and co-workers said in their theoretical study that highly ordered rods and toroids are found for low generation dendrimers, where the DNA wraps less than one turn around the dendrimer, and disordered globular structures appear for high generation dendrimers, where the DNA wraps several turns around the dendrimer **(Qamhieh, et al., 2014)**. While Ainalem and co-workers found in their experimental study that well-defined structured aggregates are formed for lower dendrimer generations. The smaller sized dendrimers (G1 and G2), which have a lower total charge per molecule, allow the formation of well-structured rods and toroids. In contrast, globular and less defined aggregates, which are less stable against precipitation, are formed with higher generation dendrimers **(Ainalem, et al., 2009)** (return to Figure 1.24 in page 31).
Based on what stated in the previous studies, we can say that the rod-like morphology we obtained for dsDNA-G2-dendrimer and rod-like and globular morphologies we got for dsDNA-G4-dendrimer aggregates are in good agreement with their results, but the one we got for dsDNA-G6-dendrimer aggregates are not (*i.e.*, we did not get globular morphology) because of two reasons, as we think, the first one is, the limits of our models for both dsDNA chain and the dendrimer such as fixed size, fixed surface area, and dendrimer's impenetrability, whereas the second one is that the simulations at this part of study need more time to reach its equilibrium.

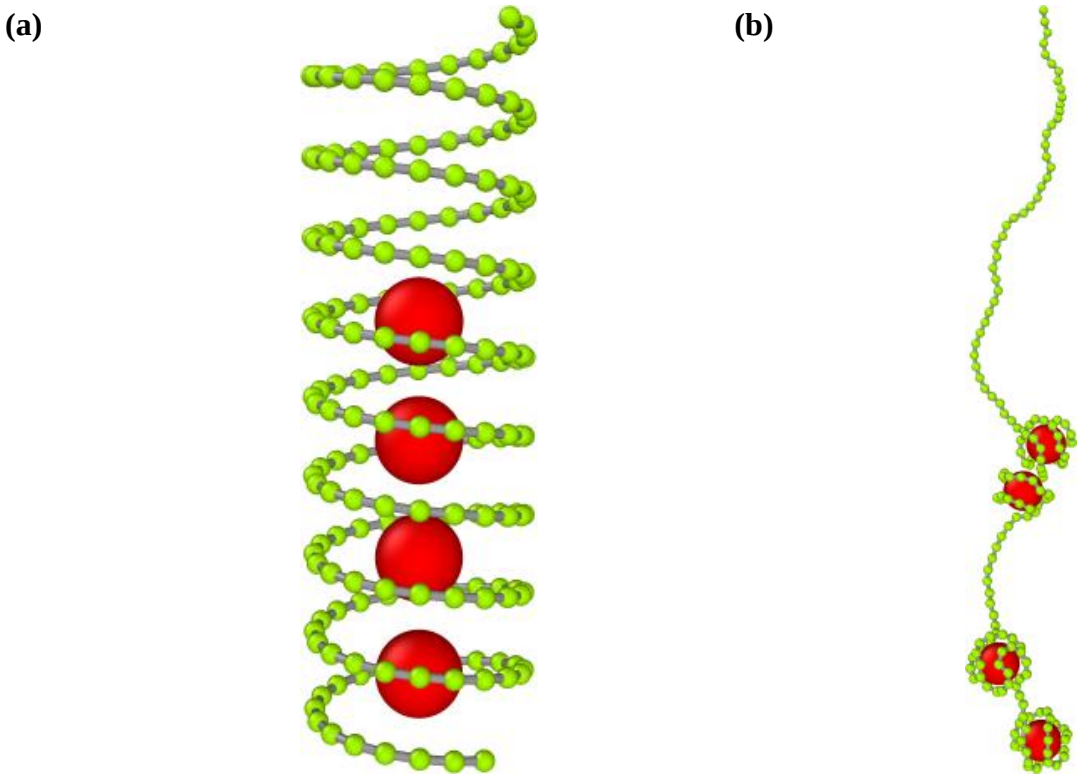


**Figure 3.36:** Snapshots of 1080bp-dsDNA-4G6-dendrimer aggregate; (a) the initial configuration and (b) after $55 \times 10^7$ BDS (13.75 $\mu s$).

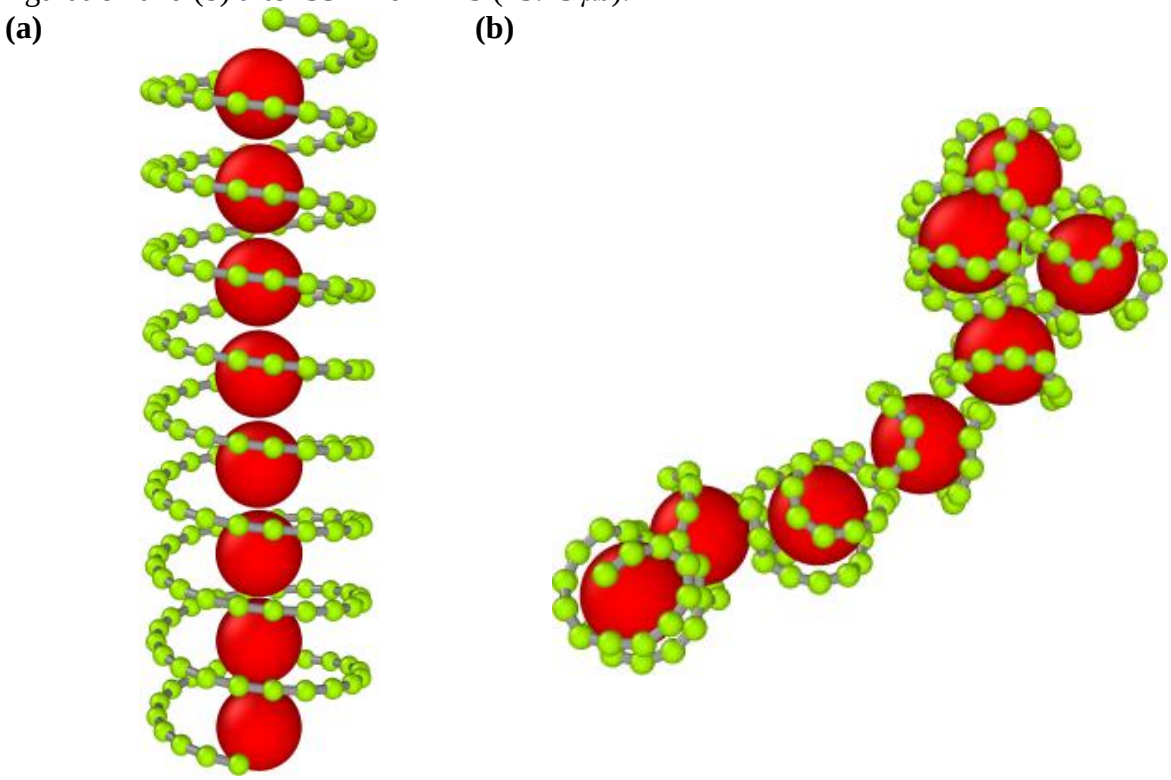


**Figure 3.37:** Snapshots of 1080bp-dsDNA-8G6-dendrimer aggregate; (a) the initial configuration and (b) after $16 \times 10^8$ BDS (40.0 $\mu s$).

# Chapter Four

# Conclusion and Future Work

# 4 Chapter Four: Conclusion and Future Work

## 4.1 Conclusion

For the dsDNA chain, we found a non-monotonic dependence of its translational diffusion coefficient (*i.e.*, its diffusivity) on the low salt concentration for different dsDNA chain lengths, whereas the high salt concentration has almost no effect on the translational diffusion coefficient of the dsDNA chain. Also, we concluded that the shorter dsDNA chain, *i.e.*, that has the smaller number of bps, is more diffusive in the solution than the longer one at the same salt concentration. The behavior of the translational diffusion coefficient of the dsDNA chain versus the dsDNA chain length is in good agreement with Lukacs and co-workers experimental study **(Lukacs, et al., 2000)**. The persistence length of the dsDNA chain is affected by the salt concentration as reported in de Pablo and co-workers study results **(Sambriski, Schwartz, & de Pablo, 2009)**, *i.e.*, it increases with decreasing salt concentration from 150 to 10 *mM*, while the high salt concentration ($\geq$ 150 *mM*) has approximately no effect on the persistence length, *i.e.*, only the non-electrostatic contribution of the persistence length remains, which is constant. From these results, we concluded that our model for the dsDNA chain is well fit.

For the dsDNA-dendrimer complex, we can conclude that the dsDNA chain strongly wraps around the dendrimer at both low salt concentration (below 150 *mM*) and pH $\leq$ 7, whereas in both of high salt concentration and high pH, no wrapping occurs, *i.e.*, no complex is formed. Also, the dsDNA-high generation dendrimer complex is more order than the low one at a low salt concentration (10 *mM*), and the order of the dsDNA-dendrimer complex at neutral pH is better than it at other pH values. Some of these results are in good agreement with Yu and Larson's computer simulation study for different generations of PAMAM dendrimer **(Yu & Larson, 2014)**.

In the Linker/Tail(s) study, we can agree that the number of adsorbed dsDNA beads onto the dendrimer surface decreases as a result of increasing the salt concentration and increases with increasing the number of bps in the dsDNA chain, while the number of not adsorbed dsDNA beads (it can be in-between adsorbed ones/Linker/Tail(s)) increases with the increase in both of salt concentration and the number of bps in the dsDNA chain. Also, for longer dsDNA chains, we observed the overcharge phenomenon for the dendrimers in the aggregates and its degree depends on the dsDNA chain length (*i.e.*, the number of bps). These results are in good agreement with Larin and co-workers' **(Larin, Darinskii, Lyulin, & Lyulin, 2010)** and Luylin and co-workers' **(Lyulin, Darinskii, & Lyulin, 2005)** computer simulation study.

Using our models for the dsDNA and the dendrimer and at a low salt concentration (10 *mM*), we can deduce that the morphologies we obtained for the dsDNA-dendrimer aggregates show a good dependence on the low dendrimer generations (G2 and G4), so as a result, we got a rod-like morphology for the dsDNA-G2 and G4-dendrimer aggregates, and also a globular one for the dsDNA-G4-dendrimer aggregate in good agreement with Qamhieh and co-workers' theoretical study **(Qamhieh, et al., 2014)** and Ainalem and co-workers' experimental study **(Ainalem, et al., 2009)**, but for high generation (G6), we obtained almost rod-like morphologies, which do not agree with the previous studies.

## 4.2 Future Work

We can say that our study is a simple study because of the simplicity of the models used for the dsDNA chain and the dendrimer, but such a study opens the way for us to develop our previous models to more complex models such as CG and AA ones so as to keep up with the theoretical studies and experimental results in this area and to arrive at a good accuracy in the interpretation of what happens in such systems and what affects them and how it affects so that we can form a good and sufficient view in order to build a vehicle able to carry the DNA chain and effectively participate in drug delivery and gene therapy.

# Appendices

# 5 Appendices

## 5.1 Appendix A: Setup of LAMMPS

We compiled LAMMPS **[version 22Sep2017]** from source code on many PCs that have the operating system Ubuntu **[version 16.04.4 LTS]** using Intel ® Parallel Studio XE **[version: 2017 Update 4 for Linux (Cluster Edition)/Student Version]**.
To install LAMMPS as we did (exactly) and prepare it to run simulations follow the next steps:

1. Download Ubuntu **[version 16.04.4 LTS]** from the following link:

http://releases.ubuntu.com/xenial/ubuntu-16.04.4-desktop-amd64.iso

Then install it on your machine/PC.

2. Download Intel ® Parallel Studio XE **[version: 2017 Update 4 for Linux (Cluster Edition)/Student Version]** from the following link and get its license using student e-mail (*i.e.*, @XXX.edu):

https://software.intel.com/en-us/parallel-studio-xe/choose-download/student-linux-fortran

Then install it by following its installation guide.

Important note: This product needs pre-request packages to be installed on your Ubuntu OS, some of them are mandatory and the others are optional, but we advise you to install all of them before installing this product.

3. Download LAMMPS **[version 22Sep2017]** from the following link:

http://lammps.sandia.gov/tars/lammps-22Sep17.tar.gz

And un-compress it. Then (carefully) follow its online manual (the online manual is for the latest stable version of LAMMPS, so pay attention to differences) to making it with the optional packages (ASPHERE, BODY, CLASS2, COMPRESS, CORESHELL, GRANULAR, KSPACE, MANYBODY, MC, MISC, MOLECULE, MPIIO, OPT, PYTHON, QEQ, REPLICA, RIGID, SRD, USER-CGDNA, USER-CGSDK, USER-COLVARS, USER-DRUDE, USER-FEP, USER-INTEL, USER-MEAMC, USER-MGPT, USER-MISC, USER-MOLFILE, USER-OMP, USER-REAXC, USER-SMTBQ, USER-SPH, USER-TALLY) at the following link:
http://lammps.sandia.gov/doc/Manual.html

Important note: Some of the previous packages need its library to be compiled before compiling LAMMPS itself, and LAMMPS, based on your wishes, may need pre-request packages to be installed on your Ubuntu OS before compiling it, so we advise you to prepare everything it needs before compiling/installing it.

## 5.2 Appendix B: LAMMPS input files

This is the c language code we wrote to generate the input files -based on our models for the dsDNA and the dendrimer- for our simulation systems, after compiling and running it, it will ask you some questions and by answering these questions as you want you will be ready to get and use your input files for running your simulation:

```
/*-------------------------------------------------------------*/
/*   A C lang. script for generating the input files of        */
/*   dsDNA-dendrimer simulation system for LAMMPS program.     */
/*   Written by AL-QUDS University student's Alaa Murrar -     */
/*   for his M.Sc. Thesis (In Biophysics).                     */
/*   Note: this script is written for double-strand DNA c-     */
/*   hain and dendrimer modeled as single-strand bead-spr-     */
/*   ing polymer(chain) and charged sphere respectively.       */
/*   It can be modified to make complex models for ss- an-     */
/*   d ds- DNA and fit other simulation programs.              */
/*-------------------------------------------------------------*/

#include <stdio.h>
#include <stdlib.h>
#include <math.h>

#define NA 6.022e+23 // Define Avogadro's No..
#define PI acos(-1.0) // Define PI.
#define eps0 8.854187817620e-12 // Define vacuum permittivity in
[C^2/N*m^2] unit.
#define kb 1.38064852e-23 // Define Boltzman constant in [m^2*kg/s^2*K]
unit.
#define e 1.60217662e-19 // Define elementry charge in [C] unit.
#define etaw 8.90e-4 // Define water viscosity at 25 ˚C in [kg/s*m] unit.
#define tho 1.0e+3 // Define conversation factor. (special)
#define thoo 1.0e-10 // Define conversation factor # 2. (special)
#define stofs 1.0e+15 // Define conversation factro (from sec to fsec).

int main()
{
    // Enter the # of dsDNA bp, the # of dendrimer types and the # of
dendrimers for each type.
    int bdnabp=0,Dendtnum=0;
    printf("Enter the # of B-dsDNA basepairs [an integer from multiples
of 6]: ");
    scanf("%d",&bdnabp);
    printf("Enter the # of dendrimer types [only integers]: ");
    scanf("%d",&Dendtnum);
    int Dendnum[Dendtnum+1],tDendnum=0;
    for(int i=1; i<=Dendtnum; i++)
    {
        printf("Enter the # of dendrimers of %d type: ",i);
        scanf("%d",&Dendnum[i]);
        tDendnum+=Dendnum[i];
    }

    // Enter the volume of simulation box (x,y and z boundaries).
    double xlo=0.0,xhi=0.0,ylo=0.0,yhi=0.0,zlo=0.0,zhi=0.0;
    printf("Enter the edge length of the simulation box [Cube] [in Ang-
strom]: ");
    scanf("%lf",&xhi);
    yhi=xhi;
    zhi=xhi;
```

```
    // Set the configuration file (.conf) header's variables values.
    int
nAtoms=0,nBonds=0,nAngles=0,nDihedrals=0,nAtypes=0,nBtypes=0,nAntypes=0,n
Dtypes=0,M_ID=0;
    nAtoms=(bdnabp/6)+tDendnum;
    nAtypes=1+Dendtnum; // The # of Atom types (dsDNA bead, dendrimer
types).
    nBonds=(bdnabp/6)-1;
    nBtypes=1; // 1 Bond type.
    nAngles=(bdnabp/6)-2;
    nAntypes=1; // 1 Angle type.
    M_ID=1+Dendtnum; // The # of Molecules (dsDNA molecule, dendrimer
molecules).

    // dsDNA Parameters.
    double DNAq=0.0; // Charge [in e unit].
    DNAq=-12.0;
    double DNAd=0.0; // Diameters d=2r [in Angstrom].
    DNAd=(2*8.0);

    // Initial position of dsDNA beads.
    double x[(bdnabp/6)+1],y[(bdnabp/6)+1],z[(bdnabp/6)+1],Lel=0.0;
    x[1] = (xhi-xlo)/2.0;
    y[1] = ((yhi-ylo)-((bdnabp*3.4)))/2.0;
    z[1] = (zhi-zlo)/2.0;
    Lel=((bdnabp*3.4)-DNAd)/((bdnabp/6)-1);

    for (int i=2; i<=(bdnabp/6); i++)
    {
        x[i] = (xhi-xlo)/2.0;
        y[i] = y[i-1]+Lel;
        z[i] = (zhi-zlo)/2.0;
    }

    // Enter the dendrimer Parameters for each type.
    double Dendq[Dendtnum+1]; // Charge [in e unit].
    for(int i=1; i<=Dendtnum; i++)
    {
        printf("Enter the charge of dendrimers of %d type [in e]: ",i);
        scanf("%lf",&Dendq[i]);
    }
    double Dendr[Dendtnum+1]; // Radii [in Angstrom].
    for(int i=1; i<=Dendtnum; i++)
    {
        printf("Enter the radius of dendrimers of %d type [in Angstrom]:
",i);
        scanf("%lf",&Dendr[i]);
    }

    // Initial position of dendrimers.
    double
xd[Dendtnum+1][tDendnum+1],yd[Dendtnum+1][tDendnum+1],zd[Dendtnum+1][tDen
dnum+1],yds=0.0;

    for (int i=1; i<=Dendtnum; i++)
    {
        for(int j=1; j<=Dendnum[i]; j++)
        {
            xd[i][j] = ((xhi-xlo)/2.0)+DNAd+(2*Dendr[i]);
            yd[i][j] = y[1]+yds;
```

```
            zd[i][j] = ((zhi-zlo)/2.0)+DNAd+(2*Dendr[i]);
            yds+=(4*Dendr[i]);
        }
    }

    // Write the (.conf) file.
    FILE *conf;
    conf = fopen("Init_conf.in","w");

    fprintf(conf,"LAMMPS Description for system of dsDNA modeled as bead-
spring chain and dendrimer modeled as hard charged sphere.\n");

    fprintf(conf,"\n%d atoms\n",nAtoms);
    fprintf(conf,"%d bonds\n",nBonds);
    fprintf(conf,"%d angles\n",nAngles);
    fprintf(conf,"\n%d atom types\n",nAtypes);
    fprintf(conf,"%d bond types\n",nBtypes);
    fprintf(conf,"%d angle types\n",nAntypes);
    fprintf(conf,"\n%lf %lf xlo xhi\n",xlo,xhi);
    fprintf(conf,"%lf %lf ylo yhi\n",ylo,yhi);
    fprintf(conf,"%lf %lf zlo zhi\n",zlo,zhi);

    // Enter the Masses for each dendrimer type in [g/mol].
    double DNAm=0.0,Dendm[Dendtnum+1];
    DNAm=3900.0000;
    fprintf(conf,"\nMasses\n\n");
    fprintf(conf,"1 %lf\n",DNAm);
    for(int i=1; i<=Dendtnum; i++)
    {
        printf("Enter the mass of dendrimers of %d type [in g/mol]: ",i);
        scanf("%lf",&Dendm[i]);
        fprintf(conf,"%d %lf\n",1+i,Dendm[i]);
    }

    fprintf(conf,"\nAtoms\n\n");
    // dsDNA initial configuration part.
    nAtypes=1;
    M_ID=1;
    int i=1;
    fprintf(conf,"%d %d %d -14.000000 %lf %lf
%lf\n",i,M_ID,nAtypes,x[i],y[i],z[i]);
    for(i=2; i<=((bdnabp/6)-1); i++)
    {
       fprintf(conf,"%d %d %d %lf %lf %lf
%lf\n",i,M_ID,nAtypes,DNAq,x[i],y[i],z[i]);
    }
    fprintf(conf,"%d %d %d -14.000000 %lf %lf
%lf\n",i,M_ID,nAtypes,x[i],y[i],z[i]);

    // Dendrimers initial configuration part.
    int Dendcounter=0;
    for(int i=1; i<=Dendtnum; i++)
    {
        nAtypes++;
        M_ID++;
        for(int j=1; j<=Dendnum[i]; j++)
        {
        Dendcounter++;
        fprintf(conf,"%d %d %d %lf %lf %lf
%lf\n",((bdnabp/6)+Dendcounter),M_ID,nAtypes,Dendq[i],xd[i][j],yd[i][j],z
d[i][j]);
```

```
        }
    }

    // Bonds of dsDNA.
    fprintf(conf,"\nBonds\n\n");
    for(int i=1; i<=((bdnabp/6)-1); i++)
    {
        fprintf(conf,"%d %d %d %d\n",i,nBtypes,i,i+1);
    }

    // Angles of dsDNA.
    fprintf(conf,"\nAngles\n\n");
    for(int i=1; i<=((bdnabp/6)-2); i++)
    {
        fprintf(conf,"%d %d %d %d %d\n",i,nAntypes,i,i+1,i+2);
    }

    fclose(conf);

    // Write the (.in) file
    FILE *in;
    in = fopen("Sys_par.in","w");

    fprintf(in,"LAMMPS Description for system of dsDNA modeled as bead-
spring chain and dendrimer modeled as hard charged sphere.\n");
    fprintf(in,"\n# Units and Atoms style.\n");
    fprintf(in,"units\treal\n");
    fprintf(in,"atom_style\tfull\n");
    fprintf(in,"\n# Declare variables.\n");
    // Calculation of relative permittivity of water at T and Sc.
    double T=0.0,Sc=0.0,dieT=0.0,dieSc=0.0,die=0.0;
    printf("Enter the temperature of the Langevin thermostat [in °C]: ");
    scanf("%lf",&T);
    T+=273.15;
    printf("Enter the Salt concentration of the system [e.g. NaBr] [in
mM]: ");
    scanf("%lf",&Sc);
    Sc/=1000.0; // 1000 -> from mM to [M (Molarity)] unit.
    dieT=249.4-(0.788*T)+(7.20*pow(10.0,-4.0)*pow(T,2.0));
    dieSc=1.0-(0.2551*Sc)+(5.151*pow(10.0,-2.0)*pow(Sc,2.0))-
(6.889*pow(10.0,-3.0)*pow(Sc,3.0));
    die=dieT*dieSc;
    fprintf(in,"variable\tT equal %lf # Simulation temperature [Kel-
vin].\n",T);
    fprintf(in,"variable\tMyd equal %lf # Dielectric constant of water
(Depends on T and SaltCon.).\n",die);
    // Calculation of Kappa (Inverse of the Debye length in [A^-1] unit).
    double I=0.0,Ka=0.0;
    I=Sc; // Ionic strength (For 1:1 electrolyte such as NaBr that I used
implicitly it is equal the SaltCon.).
    Ka=(1.0/pow(((eps0*die*kb*T)/(2*NA*pow(e,2.0)*I*tho)),0.5))*thoo; //
tho for [L -> m^3] unit, thoo for [m^-1 -> A^-1] unit.
    fprintf(in,"variable\tKappa equal %lf # Inverse of the Debye length
[A^-1].\n",Ka);
    fprintf(in,"variable\tEtotal equal etotal\n");
    fprintf(in,"\n# Random number seed for Langevin integrator.\n");
    fprintf(in,"variable\tRandom equal 12345\n");
    fprintf(in,"\n# Specify the different interaction styles.\n");
    fprintf(in,"\n# Bond style.\n");
    fprintf(in,"bond_style\tharmonic/omp\n");
    fprintf(in,"special_bonds\tlj/coul 1.0 1.0 1.0\n");
```

```
    fprintf(in,"\n# Angle style.\n");
    fprintf(in,"angle_style\tharmonic/omp\n");
    fprintf(in,"\n# Dielectric constant.\n");
    fprintf(in,"dielectric\t${Myd} # Dielectric constant of water (De-
pends on T and SaltCon.).\n");
    fprintf(in,"\n# Pair styles.\n");
    // Calculation of the Debye-Huckel interaction cutoff radius in [A]
unit.
    double LJcutoff=0.0,DHcutoff=0.0;
    printf("Enter the LJ potential cutoff radius [in Angstrom]: ");
    scanf("%lf",&LJcutoff);
    printf("Enter the Debye-Huckel potential cutoff radius [in Angstrom]:
");
    scanf("%lf",&DHcutoff);
    fprintf(in,"pair_style\tlj/cut/coul/debye/omp ${Kappa} %lf
%lf\n",LJcutoff,DHcutoff);
    fprintf(in,"\n# Boundary conditions.\n");
    fprintf(in,"boundary\tf f f\n");
    fprintf(in,"\n# Turn on Newton's 2nd law.\n");
    fprintf(in,"newton\ton\n");
    fprintf(in,"\n# Read in the configuration data file.\n");
    fprintf(in,"read_data\tInit_conf.in\n");
    fprintf(in,"\n# Bond coeff..\n");
    double LSck=0.0;
    printf("Enter the linear spring constant of dsDNA chain [in
KCal/mol.Angstrom^2] [50.0 is the perfect for dsDNA model used]: ");
    scanf("%lf",&LSck);
    fprintf(in,"bond_coeff\t1 %lf %lf\n",LSck,Lel);
    fprintf(in,"\n# Angle coeff..\n");
    double ASck=0.0,Aea=0.0;
    printf("Enter the angular spring constant of dsDNA chain (for bind-
ing) [in KCal/mol.Rad^2]: ");
    scanf("%lf",&ASck);
    printf("Enter the equilibrium angle of binding of dsDNA chain [in de-
gree]: ");
    scanf("%lf",&Aea);
    fprintf(in,"angle_coeff\t1 %lf %lf\n",ASck,Aea);
    fprintf(in,"\n# Pair coeffs..\n");
    fprintf(in,"# Pair coeff\ttypes-of-atoms eps. sig.\n");
    double eps[nAtypes+1][nAtypes+1],sig[nAtypes+1][nAtypes+1];
    printf("Enter the LJ-epsilon between dsDNA beads [in KCal/mol]: ");
    scanf("%lf",&eps[1][1]);
    fprintf(in,"pair_coeff\t1 1 %lf %lf\n",eps[1][1],DNAd);
    for(int i=2; i<=nAtypes; i++)
    {
        printf("Enter the LJ-epsilon between dsDNA bead and dendrimer of
type %d [in KCal/mol]: ",(i-1));
        scanf("%lf",&eps[1][i]);
        printf("Enter the LJ-sigma between dsDNA bead and dendrimer of
type %d [in Angstrom]: ",(i-1));
        scanf("%lf",&sig[1][i]);
        fprintf(in,"pair_coeff\t1 %d %lf %lf\n",i,eps[1][i],sig[1][i]);
    }
    for(int i=2; i<=nAtypes; i++)
    {
        for(int j=i; j<=nAtypes; j++)
        {
            printf("Enter the LJ-epsilon between dendrimers of types %d
%d [in KCal/mol]: ",(i-1),(j-1));
            scanf("%lf",&eps[i][j]);
            printf("Enter the LJ-sigma between dendrimers of types %d %d
```

```
[in Angstrom]: ",(i-1),(j-1));
            scanf("%lf",&sig[i][j]);
            fprintf(in,"pair_coeff\t%d %d %lf
%lf\n",i,j,eps[i][j],sig[i][j]);
        }
    }
    fprintf(in,"\n# Specify parameters for the neighbor list.\n");
    fprintf(in,"neighbor\t3.0 bin\n");
    fprintf(in,"neigh_modify\tevery 1 delay 0 check yes\n");
    fprintf(in,"\n# Initialize velocities.\n");
    fprintf(in,"velocity\tall create ${T} ${Random}\n");
    fprintf(in,"\n# Group Atom types for a Langevin thermostat damp pa-
rameter.\n");
    // Calculation of LD damp factor.
    double LDDNAd=0.0,LDDendd[nAtypes+1]; // in [fs] unit (real system
units in LAMMPS).
    LDDNAd=((DNAm/(NA*tho))/(3.0*PI*etaw*DNAd*thoo))*stofs; // tho for g
-> kg, thoo for A -> m, stofs for sec -> fmsec.
    fprintf(in,"group\tdsDNA type 1\n");
    for(int i=2; i<=nAtypes; i++)
    {
        LDDendd[i-1]=((Dendm[i-1]/(NA*tho))/(3.0*PI*etaw*(2*Dendr[i-
1])*thoo))*stofs; // tho for g -> kg, thoo for A -> m, stofs for sec ->
fmsec.
        fprintf(in,"group\tDend%d type %d\n",(i-1),i);
    }
    fprintf(in,"\n# Specifying a Langevin integrator to perform a simula-
tion in the NVT ensemble.\n");
    fprintf(in,"fix\t1 dsDNA langevin ${T} ${T} %lf ${Random} gjf
yes\n",LDDNAd);
    int fixscounter=1;
    for(int i=2; i<=nAtypes; i++)
    {
        fixscounter++;
        fprintf(in,"fix\t%d Dend%d langevin ${T} ${T} %lf ${Random} gjf
yes\n",i,(i-1),LDDendd[i-1]);
    }
    fprintf(in,"fix\t%d all nve/omp\n",(fixscounter+1));
    fprintf(in,"\n# Specifying the frequency of thermodynamic out-
put.\n");
    int tcof=0.0;
    printf("Enter the frequency of thermodynamic output [an integer on-
ly]: ");
    scanf("%d",&tcof);
    fprintf(in,"thermo\t%d\n",tcof);
    fprintf(in,"thermo_style\tmulti\n");
    fprintf(in,"\n# Write the new configurations to file.\n");
    fprintf(in,"dump\t1 all xyz %d traj.xyz\n",tcof);
    fprintf(in,"\n# Pair modify.\n");
    fprintf(in,"pair_modify\tshift yes\n");
    fprintf(in,"\n# Minimization.\n");
    fprintf(in,"minimize\t1.0e-7 1.0e-9 100000 100000\n");
    fprintf(in,"\n# Re-Pair modify.\n");
    fprintf(in,"pair_modify\tshift no\n");
    fprintf(in,"\n# A timestep of 25.0 fmsec.\n");
    double Ts=0.0;
    printf("Enter the timestep (dt) of the simulation [in fs] [~ <
sqrt(smallest Mass in your simulation system)]: ");
    scanf("%lf",&Ts);
    fprintf(in,"timestep\t%lf\n",Ts);
    fprintf(in,"\n# Run X number of steps\n");
```

```
    int Xse=0.0,Xs=0.0;
    printf("Enter the number of steps you need to run for equilibrium [an
integer only]: ");
    scanf("%d",&Xse);
    fprintf(in,"run\t%d\n",Xse);
    printf("Enter the number of steps you need to run after equilibrium
[an integer only]: ");
    scanf("%d",&Xs);
    fprintf(in,"\n# New fix\n");
    fprintf(in,"fix\t%d all ave/time 1 1 %d c_thermo_temp file
Temp.txt\n",(fixscounter+2),Xs);
    fprintf(in,"fix\t%d all ave/time 1 1 %d v_Etotal file Eto-
tal.txt\n",(fixscounter+3),tcof);
    fprintf(in,"\n# New dump file (after equilibrium).\n");
    fprintf(in,"dump\t2 all xyz %d ftraj.xyz\n",tcof);
    fprintf(in,"\n# Re-Run X number of steps\n");
    fprintf(in,"run\t%d",Xs);

    fclose(in);

    printf("\n# Your LAMMPS input files (Init_conf.in & Sys_par.in) are
ready for use. Enjoy. #\n");

    return 0;
}
```

## 5.3 Appendix C: The codes we wrote for calculated quantities

### 5.3.1. The translational diffusion coefficient ($D_t$):

We downloaded the “Diffusion Coefficient Tool” from the following link:

https://github.com/tonigi/vmd_diffusion_coefficient

Then un-compress and install it by run VMD program and going to **Extensions menu** > **VMD Preferences** > **Custom**, and add a **new description** with name **D_C** and **code** as in the next snapshot:

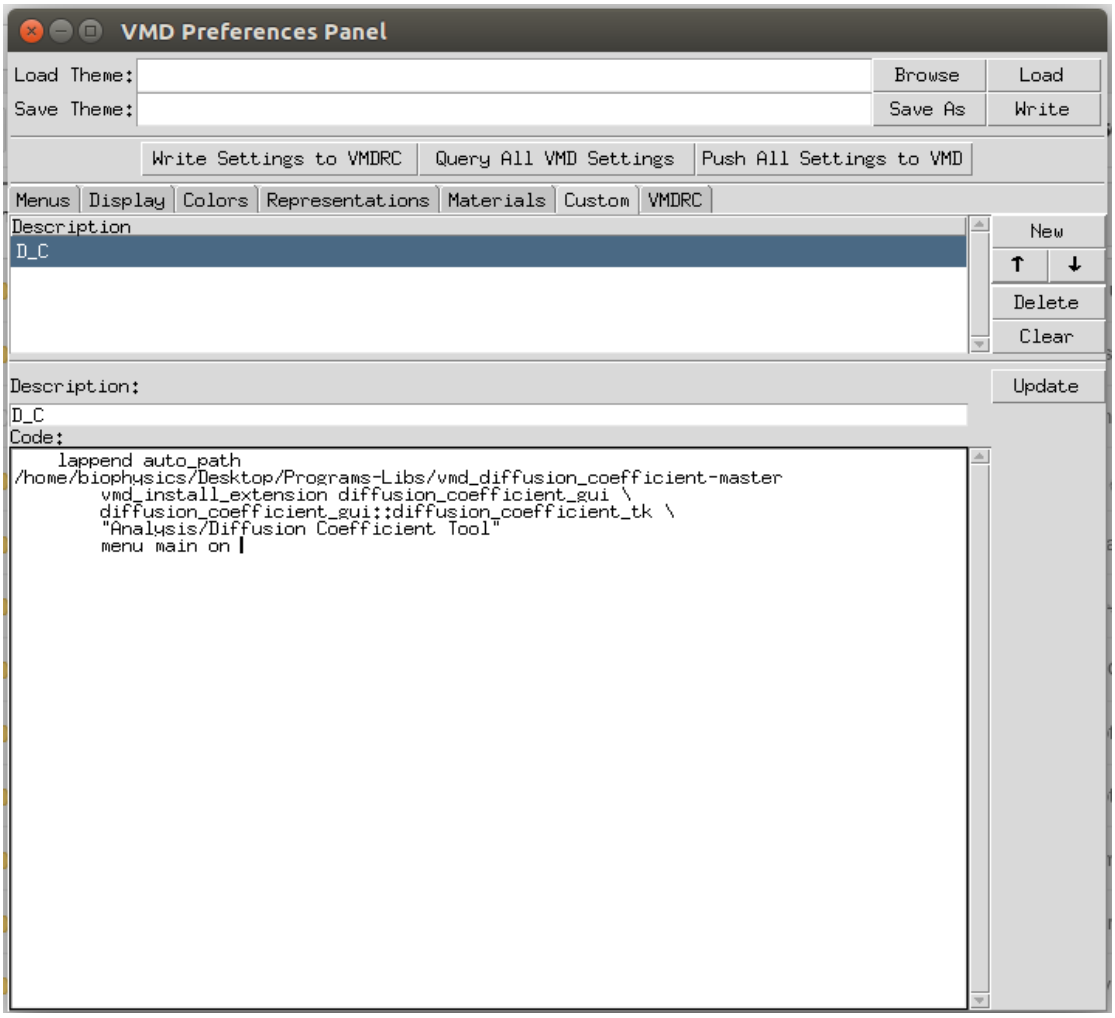


Where "/home/biophysics/Desktop/Programs-Libs/vmd_diffusion_coefficient-master" is my tool folder path which you must replace it with your one.

The following snapshot shows how we used this tool to calculate the $MSD(\tau)$ and $D_t(\tau)$ for a system from the dsDNA systems (after running VMD program, loading the dsDNA chain and entering its bead radius and mass):

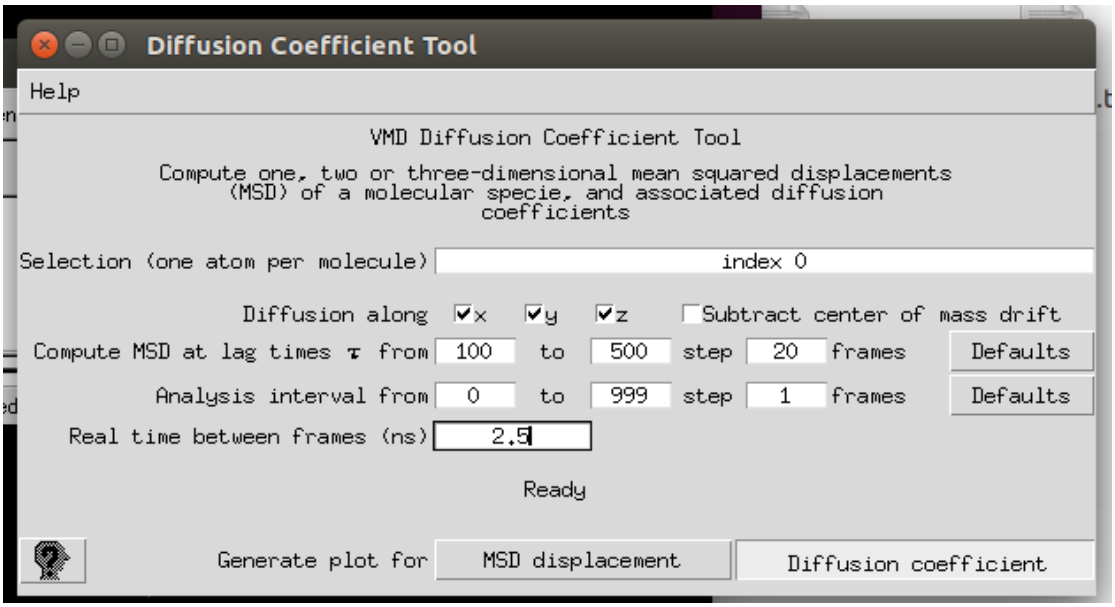


### 5.3.2. The persistence length ($l_p$):

This is the c language code we wrote to calculate $l_p$ of the dsDNA chain, after compiling and running it, it will ask you some questions and by answering these questions you will get output files with names (L_NIp.txt & Ave_Ln(NIp)_L.txt) and by plotting the values of <L> Vs. Ln(<cos(θ)>) that are in (Ave_Ln(NIp)_L.txt) and their linear fit you will be able to obtain $l_p$ from the slope of the linear fit which equals to - $l_p$:

```
/*-------------------------------------------------------------/
/   A C lang. script for calculating the Persistance length    /
/    for double-strand DNA.                                     /
/   Written by AL-QUDS University student's Alaa Murrar for    /
/   his M.Sc. Thesis (In Biophysics).                          /
/   Note: this script is written for double-strand DNA cha-    /
/   in modeled as single-strand bead-spring polymer(chain),    /
/   and it takes the coordinates of beads from xyz formate-    /
/   d file. Also, it uses the same method that de Pablo and    /
/   coworkers used in their paper [Sambriski, E. J., Schwa-    /
/   rtz, D. C., & de Pablo, J. J. (2009). A Mesoscale Mode-    /
/   l of DNA and its Renaturation. Biophys. J., 96(5), 1675    /
/   -1690.]                                                    /
/   It can be modified to fit complex models for ss- and ds    /
/   - DNA and other formats of coordinates file.               /
/-------------------------------------------------------------*/

#include <stdio.h>
#include <stdlib.h>
#include <math.h>

int main()
{
    // Enter the # of dsDNA beads, # of frames in the simulation and the
# of Sampling points for the calculations.
    int bdnabp=0,dnanum=0,nfr=0,NSP=0;
    printf("Enter the # of B-dsDNA basepairs [only integers from multi-
ples of number 6]: ");
    scanf("%d",&bdnabp);
    printf("Enter the # of frames of the simulation [only integers]: ");
```

```
    scanf("%d",&nfr);
    printf("Enter the # of sampling points that you need for your calcu-
lations of the lp [only integers and <= the # of frames]: ");
    scanf("%d",&NSP);
    dnanum=bdnabp/6;

    // Enter the xyz formated file name.
    char filename[1024];
    printf("Enter the name of the xyz coordinates file [with .xyz]: ");
    scanf("%s",filename);
    FILE *xyz_f;
    xyz_f=fopen(filename,"r");

    // Reading the file.
    char ignore[1024]; // Declare a char. matrix for ignored lines and
names of atoms.
    int fcounter=1,nV=0; // fcounter -> frames counter and nV -> the # of
unit distance vectors between dsDNA beads.
    nV=dnanum-1;

    // Declare matrices for coordinates, chain lengths, vectors between
beads, normalized vectors and inner products.
    double
xyz[dnanum+1][3+1],L[nfr+1][nV+1],Vect[nV+1][3+1],NVect[nV+1][3+1],Innp_N
[nfr+1][nV+1];
    while(!feof(xyz_f))
    {
        // Scan lines and store coordinates of dsDNA beads.
        fgets(ignore,sizeof(ignore),xyz_f);
        fgets(ignore,sizeof(ignore),xyz_f);
        for(int i=1; i<=dnanum; i++)
        {

fscanf(xyz_f,"\t%s\t%lf\t%lf\t%lf\n",ignore,&xyz[i][1],&xyz[i][2],&xyz[i]
[3]); // %s is for the name of the atom in the xyz file.
            //printf("%lf\t%lf\t%lf\n",xyz[i][1],xyz[i][2],xyz[i][3]);
for checking.
        }

        // Make vectors between beads.
        int vcounter=1; // Counter for vectors number (used for store the
length of the chain at specific inner product).
        double Vsum=0.0; // Declare matrix for vectors between dsDNA
beads and variable for the sum of these vectors.
        for(int j=2; j<=dnanum; j++)
        {
            for(int k=1; k<=3; k++)
            {
                Vect[j-1][k]=xyz[j][k]-xyz[j-1][k];
            }

            // Calculate the length of the vector and store it.
            Vect[j-1][0]=sqrt(pow(Vect[j-1][1],2.0)+pow(Vect[j-
1][2],2.0)+pow(Vect[j-1][3],2.0));

            // Calculate the sum of the vectors lengths(chain lengths for
each inner products) and store them.
            Vsum=0.0;
            if(vcounter==1)
            {
                L[fcounter][vcounter]=0.0;
```

```
            }
            else
            {
                for(int l=1; l<=vcounter; l++)
                {
                    if(l==1) Vsum+=(Vect[l][0]/2.0);
                    else if(l==vcounter) Vsum+=(Vect[l][0]/2.0);
                    else Vsum+=Vect[l][0];
                }
                L[fcounter][vcounter]=Vsum;
            }

            vcounter++; // Increment the counter of vectors.

            // Normalize the vector.
            NVect[j-1][1]=Vect[j-1][1]/Vect[j-1][0];
            NVect[j-1][2]=Vect[j-1][2]/Vect[j-1][0];
            NVect[j-1][3]=Vect[j-1][3]/Vect[j-1][0];
        }

        // Calculate the inner(dot) product between normalized vec-
tor(bond) #1 and the all normalized vectors(bonds).
        int nIP=0;
        nIP=dnanum-1;
        for(int m=1; m<=nIP; m++)
        {

Innp_N[fcounter][m]=((NVect[1][1]*NVect[m][1])+(NVect[1][2]*NVect[m][2])+
(NVect[1][3]*NVect[m][3]));
        }
        fcounter++; // Increment the counter of frames.
    }
    fcounter--; // To make fcounter=nfr.
    printf("The # of frames in this simulation is %d\n",fcounter);
    fclose(xyz_f);

    // Prints L's & Innp_N's in a file.
    FILE *L_Innp_N_f;
    L_Innp_N_f=fopen("L_NIp.txt","w");
            fprintf(L_Innp_N_f,"# [fc][vc]|\tL[Angstrom]|\tInnp_N\n");
    for(int n=1; n<=nfr; n++)
    {
        for(int o=1; o<=nV; o++)
        {
            fprintf(L_Innp_N_f,"
[%d][%d]|\t%lf|\t%lf\n",n,o,L[n][o],Innp_N[n][o]);
        }
    }
    fclose(L_Innp_N_f);

    // Calculate the sum of the picks "L & Innp_N" from NSP sampling
points after equilibrium and store them in a file.
    int nSP=0;
    double Innp_N_sum[nV+1],L_sum[nV+1];
    for(int p=1; p<=nV; p++)
    {
        Innp_N_sum[p]=0.0;
        L_sum[p]=0.0;
        for(int q=1; q<=nfr; q+=(nfr/NSP))
        {
            nSP++;
```

```
            Innp_N_sum[p]+=Innp_N[q][p];
            L_sum[p]+=L[q][p];
        }
    }
    printf("The # of sampling points = %d\n",(nSP/nV)); // Check the # of
sampling points from the output of for loop.

    // Calculate the average of the sum of the picks "L & Innp_N" from
NSP sampling points and store them in a file.
    FILE *LnI_L_ave_f;
    LnI_L_ave_f=fopen("Ave_Ln(NIp)_L.txt","w");
        fprintf(LnI_L_ave_f,"# Ln(Innp_N_sum_ave)|\tL_sum_ave\n");
    double Innp_N_sum_ave[nV+1],L_sum_ave[nV+1];
    for(int r=1; r<=nV; r++)
    {
        Innp_N_sum_ave[r]=Innp_N_sum[r]/(double)NSP;
        L_sum_ave[r]=L_sum[r]/(double)NSP;

fprintf(LnI_L_ave_f,"%lf\t%lf\n",log(Innp_N_sum_ave[r]),L_sum_ave[r]);
    }
    fclose(LnI_L_ave_f);

    printf("Enjoy!, the results are in the output files (L_NIp.txt &
Ave_Ln(NIp)_L.txt)\n");

    return 0;
}
```

### 5.3.3. The radius of gyration ($R_g$):

This is the Tcl language code we wrote to calculate $R_g$ of the dsDNA chain or the dsDNA-dendrimer complex, as we said in $R_g$ section in chapter two, this code is run by VMD through Tk Console (**Extensions menu** > **Tk Console**) after running VMD program, loading the dsDNA chain or the dsDNA-dendrimer complex and entering the radius and mass for both dsDNA bead and dendrimer sphere.

This is for the dsDNA chain only:

```
#/*-------------------------------------------------------/
#/   A Tcl lang. script used by VMD program for calcul-   /
#/   ating the radius of gyration for the dsDNA chain.    /
#/   Written by AL-QUDS University student's Alaa Murr-   /
#/   ar for his M.Sc. Thesis (In Biophysics).             /
#/-------------------------------------------------------*/

set dsDNA [atomselect top {name dsDNA}] ; # Select the dsDNA chain beads.
$dsDNA set radius value ; # Set the dsDNA bead radius.
$dsDNA set mass value ; # Set the dsDNA bead mass.
$dsDNA delete ; # Delete the dsDNA chain beads selection.
set outfile [open Rg-dsDNA.txt w] ; # Create the output file.
set sel [atomselect top all] ; # Define a Selection for all at-
oms/beads/spheres in the simulated system.
puts $outfile "Time\t|Rg" ; # Insert the titles of columns in the output
file.
set Nf [molinfo top get numframes] ; # Getting the simulation frames num-
ber and store it.
for { set i 0 } { $i <=($Nf-1) } {incr i} { ; # Loop for calculation of
the Rg for each frame.
```

```
  $sel frame $i ; # Turn the selection of atoms to the desired frame.
  set Time [expr ($i+1)*(100000)*(25.0)] ; # Time = (frame #(+1 because
the frames begins with 0 in VMD)) * (# of steps/frame) *
timestep(dt/step) [unit time]
  set Rg [measure rgyr $sel weight mass] ; # Calculate the mass weighted
Rg and store it.
  puts $outfile "$Time\t$Rg" ; # Print the results as "Time Rg" in the
output file.
}
close $outfile ; # close the output file.
$sel delete ; # Delete the atom/s selection.
```

And this is for the dsDNA-dendrimer complex:

```
#/*-------------------------------------------------------/
#/   A Tcl lang. script used by VMD program for calcul-   /
#/   ating the radius of gyration for the dsDNA-Dendri-   /
#/   mer complex.                                         /
#/   Written by AL-QUDS University student's Alaa Murr-   /
#/   ar for his M.Sc. Thesis (In Biophysics).             /
#/-------------------------------------------------------*/

set Dendr [atomselect top {name Dendr}] ; # Select the dendrimer sphere.
$Dendr set radius value ; # Set the dendrimer radius.
$Dendr set mass value ; # Set the dendrimer mass.
$Dendr delete ; # Delete the dendrimer selection.
set dsDNA [atomselect top {name dsDNA}] ; # Select the dsDNA chain beads.
$dsDNA set radius value ; # Set the dsDNA bead radius.
$dsDNA set mass value ; # Set the dsDNA bead mass.
$dsDNA delete ; # Delete the dsDNA chain beads selection.
set outfile [open Rg-Complex.txt w] ; # Create the output file.
set sel [atomselect top all] ; # Define a Selection for all at-
oms/beads/spheres in the simulated system.
puts $outfile "Time\t|Rg" ; # Insert the titles of columns in the output
file.
set Nf [molinfo top get numframes] ; # Getting the simulation frames num-
ber and store it.
for { set i 0 } { $i <=($Nf-1) } {incr i} { ; # Loop for calculation of
the Rg for each frame.
  $sel frame $i ; # Turn the selection of atoms to the desired frame.
  set Time [expr ($i+1)*(100000)*(25.0)] ; # Time = (frame #(+1 because
the frames begins with 0 in VMD)) * (# of steps/frame) *
timestep(dt/step) [unit time]
  set Rg [measure rgyr $sel weight mass] ; # Calculate the mass weighted
Rg and store it.
  puts $outfile "$Time\t$Rg" ; # Print the results as "Time Rg" in the
output file.
}
close $outfile ; # close the output file.
$sel delete ; # Delete the atom/s selection.
```

With replacing the words “value” with its corresponding value according to the simulation system used.

The previous codes produce files contain 1000 values for $R_g$ from 1000 frames, so we wrote a c language code to calculate the average over a certain number of sampling points and it is in the last section in this appendix.

### 5.3.4. The distance between COMs ($D_{coms}$):

This is the Tcl language code we wrote to calculate $D_{coms}$ in the dsDNA-dendrimer complex, it is run by VMD through Tk Console (**Extensions menu** > **Tk Console**) after running VMD program, loading the dsDNA-dendrimer complex and entering the radius and mass for both dsDNA bead and dendrimer sphere.:

```
#/*-----------------------------------------------------------/
#/   A Tcl lang script used by VMD program for calculating   /
#/   the distance between centers of masses of dsDNA and     /
#/   dendrimer in the dsDNA-dendrimer complex.               /
#/   Written by AL-QUDS University student's Alaa Murrar     /
#/   for his M.Sc. Thesis (In Biophysics).                   /
#/-----------------------------------------------------------*/

set Dendr [atomselect top {name Dendr}] ; # Select the dendrimer sphere.
$Dendr set radius value ; # Set the dendrimer radius.
$Dendr set mass value ; # Set the dendrimer mass.
set dsDNA [atomselect top {name dsDNA}] ; # Select the dsDNA chain beads.
$dsDNA set radius value ; # Set the dsDNA bead radius.
$dsDNA set mass value ; # Set the dsDNA bead mass.
set outfile [open Dcoms.txt w] ; # Create the output file.
puts $outfile "Time\t|Dcoms" ; # Insert the titles of columns in the out-
put file.
set Nf [molinfo top get numframes] ; # Getting the simulation frames num-
ber and store it.
for { set i 0 } { $i <=($Nf-1) } {incr i} { ; # Loop for calculation of
the Dcoms for each frame.
  $Dendr frame $i ; # Turn the selection of the dendrimer sphere to the
desired frame.
  $dsDNA frame $i ; # Turn the selection of the dsDNA chain beads to the
desired frame.
  set Time [expr ($i+1)*(100000)*(25.0)] ; # Time = (frame #(+1 because
the frames begins with 0 in VMD)) * (# of steps/frame) *
timestep(dt/step) [unit time]
  set com1 [measure center $Dendr weight mass] ; # Calculate the mass
weighted com for the dendrimer and store it.
  set com2 [measure center $dsDNA weight mass] ; # Calculate the mass
weighted com for the dsDNA chain and store it.
  set Dcoms [veclength [vecsub $com1 $com2]] ; # Calculate the Dcoms be-
tween coms of the dsDNA chain and the dendrimer and store it.
  puts $outfile "$Time\t$Dcoms" ; # Print the results as "Time Dcoms" in
the output file.
}
close $outfile ; # close the output file.
$Dendr delete ; # Delete the dendrimer selection.
$dsDNA delete ; # Delete the dsDNA chain selection.
```

With replacing the words “value” with its corresponding value according to the simulation system used.

Again, the previous code produce file contains 1000 values for $D_{coms}$ from 1000 frames, see the last section in this appendix to know how we calculated the average of this quantity.

### 5.3.5. The fraction of adsorption DNA beads onto dendrimer surface (ω):

This is the c language code we wrote to calculate $\omega$ in the dsDNA-dendrimer complex, after compiling and running it, it will ask you some questions and by answering these questions you will get output files with names (W.txt & W_ave.txt).

```
/*-------------------------------------------------------------/
/   A C lang. script for calculating the Adsorption fraction   /
/  (W) of dsDNA beads onto dendrimer surface for dsDNA-Dend-   /
/   rimer complex.                                            /
/   Written by AL-QUDS University student's Alaa Murrar for   /
/   his M.Sc. Thesis (In Biophysics).                         /
/   Note: this script is written for double-strand DNA chain  /
/   modeled as single-strand bead-spring polymer(chain), and  /
/   dendrimer molecule modeled as charged sphere and it tak-  /
/   es the coordinates of the hole system from an xyz forma-  /
/   ted file with a specific structure. It can be modified -  /
/   to fit some needs and other formats or structures of co-  /
/   ordinates file.                                           /
/-------------------------------------------------------------*/

#include <stdio.h>
#include <stdlib.h>
#include <math.h>

int main()
{
    // Enter the # of dsDNA bp, # of dendrimers, # of frames in the simu-
lation and the # of Sampling points for the calculations.
    int bdnabp=0,dnanum=0,dendnum=0,nfr=0,NSP=0;
    printf("Enter the # of B-dsDNA basepairs in the simulation system
[only integers from multiples of number 6]: ");
    scanf("%d",&bdnabp);
    printf("Enter the # of dendrimers in the simulation system [only in-
tegers]: ");
    scanf("%d",&dendnum);
    printf("Enter the # of frames of the simulation [only integers]: ");
    scanf("%d",&nfr);
    printf("Enter the # of sampling points that you need for your calcu-
lations of the lp [only integers and <= the # of frames]: ");
    scanf("%d",&NSP);
    dnanum=bdnabp/6;
    //printf("Dnanum+Dendnum = %d\n",dnanum+dendnum); for checking.

    // Define the cutoff radius for the adsorption fraction
[=R(Dend.)[A]+R(dsDNA-bead)[A]+lB=(7.1)[A]] Angstrom.
    double R_dsDNA=8.0,R_d=0.0,R_cutoff=0.0;
    printf("Enter the radius of the dendrimer [in Angstrom]: ");
    scanf("%lf",&R_d);
    R_cutoff=R_dsDNA+R_d+7.1; // [in Angstrom].

    int fcounter=1; // fcounter -> frames counter.

    // Enter the xyz formated file name.
    char filename[1024];
    printf("Enter the name of the xyz coordinates file [with .xyz]: ");
    scanf("%s",filename);
    FILE *xyz_f;
    xyz_f=fopen(filename,"r");
```

```
    // Reading the file.
    char ignore[1024]; // Declare a char. matrix for ignored lines and
atom names.

    // Declare coordinates [in Angstrom], vectors between dendrimer and
dsDNA beads, and W-Values matrices.
    double
xyz[dnanum+dendnum+1][3+1],Vect[dnanum+dendnum+1][3+1],W[nfr+1];

    // Scan and store the coordinates of the hole system and perform the
needed calculations.
    while(!feof(xyz_f))
    {
        // Scan lines.
        fgets(ignore,sizeof(ignore),xyz_f);
        fgets(ignore,sizeof(ignore),xyz_f);
        for(int i=1; i<=(dnanum+dendnum); i++)
        {

fscanf(xyz_f,"\t%s\t%lf\t%lf\t%lf\n",ignore,&xyz[i][1],&xyz[i][2],&xyz[i]
[3]);
            //printf("%lf\t%lf\t%lf\n",xyz[i][1],xyz[i][2],xyz[i][3]);
for checking.
        }

        // Make vectors between dendrimer and dsDNA beads.
        int N=0; // The # of adsorbed dsDNA beads.
        for(int j=1; j<=dnanum; j++)
        {
            for(int k=1; k<=3; k++)
            {
                Vect[j][k]=xyz[j][k]-xyz[dnanum+dendnum][k]; //
xyz[dnanum+dendnum][k] means that the dendrimer has the last atom id in
the simulation.
            }
            // Calculate the length of the vector and store it.

Vect[j][0]=sqrt(pow(Vect[j][1],2.0)+pow(Vect[j][2],2.0)+pow(Vect[j][3],2.
0));

            // Check if the dsDNA bead is adsorbed onto dendrimer surface
or not.
            if(Vect[j][0]<R_cutoff) N+=1;
        }

        // Calculate W and store it.
        W[fcounter]=(((double)N)/((double)dnanum));
        fcounter++; // Increment the frames counter.
    }
    fcounter--; // To make fcounter=nfr.
    printf("The # of frames in this simulation is %d\n",fcounter);
    fclose(xyz_f);

    // Print the values of W in a file.
    FILE *W_f;
    W_f=fopen("W.txt","w");
    for(int l=1; l<=nfr; l++)
    {
        fprintf(W_f,"W = %lf\n",W[l]);
    }
    fclose(W_f);
```

```
    // Calculate the average of adsorption fraction and its error from
NSP sampling points after equilibrium and store them.
    int No=0,nSP=0; // A counters for the picks W and the sampling
points.
    double W_Ne[NSP+1],W_sum=0.0,W_ave=0.0;
    for(int m=1; m<=nfr; m+=(nfr/NSP))
    {
        No+=1;
        nSP++;
        W_Ne[No]=W[m];
        W_sum+=W[m];
    }
    printf("The # of sampling points is %d\n",nSP); // Check the # of
sampling points from the output of the for loop.
    W_ave=W_sum/((double)NSP);

    // The error.
    double SD_sum=0.0,SD=0.0,W_err=0.0;
    for(int n=1; n<=NSP; n++)
    {
        SD_sum+=pow((W_Ne[n]-W_ave),2.0);
    }
    SD=sqrt(SD_sum/((double)(NSP-1)));
    W_err=SD/sqrt((double)NSP);

    // Store the W_ave +/- its error in a file.
    FILE *W_ave_f;
    W_ave_f=fopen("W_ave.txt","w");
    fprintf(W_ave_f,"W = %lf +/- %lf",W_ave,W_err);
    fclose(W_ave_f);

    printf("Enjoy!, the results are in the output files (W.txt &
W_ave.txt)\n");

    return 0;
}
```

### 5.3.6. The order (curvature) parameter of DNA-dendrimer complex ($\gamma$):

This is the c language code we wrote to calculate $\gamma$ of the dsDNA-dendrimer complex, after compiling and running it, it will ask you some questions and by answering these questions you will get output files with names (Cur.txt & Cur_ave.txt).

```
/*-----------------------------------------------------------/
/   A C lang. script for calculating the Curvature(order)   /
/   parameter for a double-strand DNA wrapped around Den-   /
/   drimer molecule.                                        /
/   Written by AL-QUDS University student's Alaa Murrar     /
/   for his M.Sc. Thesis (In Biophysics).                   /
```

```
/   Note: this script is written for double-strand DNA      /
/   chain modeled as single-strand bead-spring polymer      /
/   (chain), and dendrimer molecule modeled as charged s-   /
/   phere and it takes the coordinates of beads from xyz-   /
/   formated file with a specific structure. It can be m-   /
/   odified to fit complex models for ss- and ds- DNA an-   /
/   d dendrimer, and other formats or structures of coor-   /
/   dinates file.                                           /
/   The definition of this parameter will be found in Shi   /
/   Yu and Ronald G. Larson article [Yu, S., & Larson, R.   /
/   G. (2014). Monte-Carlo simulations of PAMAM dendrime-   /
/   r-DNA interactions. Soft Matter, 10(29), 5325-5336.],   /
/   but here it will use for my model of dsDNA.             /
/-------------------------------------------------------------*/

#include <stdio.h>
#include <stdlib.h>
#include <math.h>

int main()
{
    // Enter the # of dsDNA bp, # of dendrimers, # of frames in the simu-
lation and the # of Sampling points for the calculations.
    int bdnabp=0,dnanum=0,dendnum=0,nfr=0,NSP=0;
    printf("Enter the # of B-dsDNA basepairs in the simulation system
[only integers from multiples of number 6]: ");
    scanf("%d",&bdnabp);
    printf("Enter the # of dendrimers in the simulation system [only in-
tegers]: ");
    scanf("%d",&dendnum);
    printf("Enter the # of frames of the simulation [only integers]: ");
    scanf("%d",&nfr);
    printf("Enter the # of sampling points that you need for your calcu-
lations of the lp [only integers and <= the # of frames]: ");
    scanf("%d",&NSP);
    dnanum=bdnabp/6;

    // Define the cutoff radius for the adsorption fraction
[=R(Dend.)[A]+R(dsDNA-bead)[A]+lB=(7.1)[A]] Angstrom.
    double R_dsDNA=8.0,R_d=0.0,R_cutoff=0.0;
    printf("Enter the radius of the dendrimer [in Angstrom]: ");
    scanf("%lf",&R_d);
    R_cutoff=R_dsDNA+R_d+7.1; // [in Angstrom].

    int fcounter=1; // fcounter -> frames counter.

    // Enter the xyz formated file name.
    char filename[1024];
    printf("Enter the name of the xyz coordinates file [with .xyz]: ");
    scanf("%s",filename);
    FILE *xyz_f;
    xyz_f=fopen(filename,"r");

    // Reading the file.
    char ignore[1024]; // Declare a char. matrix for ignored lines and
atom names.

    /* Declare coordinates [in Angstrom], vectors between dendrimer and
dsDNA beads, coordinates for adsorbed dsDNA beads
    (onto dendrimer surface), new vectors betweem adsorbed dsDNA beads,
normalized new vectors betweem adsorbed dsDNA beads,
```

```
    cross product between normalized new vectors, and Cur values matri-
ces. */
    double
xyz[dnanum+dendnum+1][3+1],Vect[dnanum+dendnum+1][3+1],xyz_Ne[dnanum+dend
num+1][3+1],Vect_Ne[dnanum+dendnum+1][3+1],nVect_Ne[dnanum+dendnum+1][3+1
],Cp_nVNe[dnanum+dendnum+1][3+1],sCp[1+1][3+1],Cur[nfr+1];

    // Scan and store the coordinates of the hole system and perform the
needed calculations.
    while(!feof(xyz_f))
    {
        // Scan lines.
        fgets(ignore,sizeof(ignore),xyz_f);
        fgets(ignore,sizeof(ignore),xyz_f);
        for(int i=1; i<=(dnanum+dendnum); i++)
        {

fscanf(xyz_f,"\t%s\t%lf\t%lf\t%lf\n",ignore,&xyz[i][1],&xyz[i][2],&xyz[i]
[3]);
            //printf("%lf\t%lf\t%lf\n",xyz[i][1],xyz[i][2],xyz[i][3]);
for checking.
        }

        // Make vectors between dendrimer and dsDNA beads.
        int N=0; // The # of adsorbed dsDNA beads.
        for(int j=1; j<=dnanum; j++)
        {
            for(int k=1; k<=3; k++)
            {
                Vect[j][k]=xyz[j][k]-xyz[dnanum+dendnum][k]; //
xyz[dnanum+dendnum][k] means that the dendrimer has the last atom id in
the simulation.
            }
            // Calculate the length of the vector and store it.

Vect[j][0]=sqrt(pow(Vect[j][1],2.0)+pow(Vect[j][2],2.0)+pow(Vect[j][3],2.
0));

            // Check if the dsDNA bead is adsorbed onto dendrimer surface
and store the coordinates of dsDNA bead.
            if(Vect[j][0]<R_cutoff)
            {
                N+=1;
                for(int l=1; l<=3; l++)
                {
                    xyz_Ne[N][l]=xyz[j][l]; // xyz[j][l] is because the
dendrimer has the last atom id in the simulation.
                }
            }
        }

        // Make vectors between adsorbed dsDNA beads.
        int nV=0; // # of vectors.
        nV=N-1;
        for(int m=1; m<=nV; m++)
        {
            for(int n=1; n<=3; n++)
            {
                Vect_Ne[m][n]=xyz_Ne[m+1][n]-xyz_Ne[m][n];
            }
            // Calculate the length of the vector and store it.
```

```
Vect_Ne[m][0]=sqrt(pow(Vect_Ne[m][1],2.0)+pow(Vect_Ne[m][2],2.0)+pow(Vect
_Ne[m][3],2.0));

            // Normalize the vectors between adsorbed dsDNA beads.
            nVect_Ne[m][1]=Vect_Ne[m][1]/Vect_Ne[m][0];
            nVect_Ne[m][2]=Vect_Ne[m][2]/Vect_Ne[m][0];
            nVect_Ne[m][3]=Vect_Ne[m][3]/Vect_Ne[m][0];
        }

        // Calculate the cross product(determinant) between adjacent vec-
tors that connect adsorbed dsDNA beads.
        int nCp;
        nCp=nV-1;
        // The components of the net vector of the cross products vec-
tors.
        sCp[1][1]=0.0;
        sCp[1][2]=0.0;
        sCp[1][3]=0.0;
        for(int o=1; o<=nCp; o++)
        {
            Cp_nVNe[o][1]=(((nVect_Ne[o][2])*(nVect_Ne[o+1][3]))-
((nVect_Ne[o][3])*(nVect_Ne[o+1][2])));
            Cp_nVNe[o][2]=(-1.0)*(((nVect_Ne[o][1])*(nVect_Ne[o+1][3]))-
((nVect_Ne[o][3])*(nVect_Ne[o+1][1])));
            Cp_nVNe[o][3]=(((nVect_Ne[o][1])*(nVect_Ne[o+1][2]))-
((nVect_Ne[o][2])*(nVect_Ne[o+1][1])));
            sCp[1][1]+=Cp_nVNe[o][1];
            sCp[1][2]+=Cp_nVNe[o][2];
            sCp[1][3]+=Cp_nVNe[o][3];
        }
        // Calculate the Cur. (Order parameter) and store it.

Cur[fcounter]=(sqrt(pow(sCp[1][1],2.0)+pow(sCp[1][2],2.0)+pow(sCp[1][3],2
.0)))/((double)N);
        fcounter+=1; // Increment the frames counter.
    }
    fcounter--; // To make fcounter=nfr.
    printf("The # of frames in this simulation is %d\n",fcounter);
    fclose(xyz_f);

    // Print the values of Cur in a file.
    FILE *Cur_f;
    Cur_f=fopen("Cur.txt","w");
    for(int p=1; p<=nfr; p++)
    {
        fprintf(Cur_f,"Cur. = %lf\n",Cur[p]);
    }
    fclose(Cur_f);

    // Calculate the average of the Curvature(order) parameter and its
error from NSP sampling points after equilibrium and store them.
    int No=0,nSP=0; // A counters for the picks Cur and the sampling
points.
    double Cur_Ne[NSP+1],Cur_sum=0.0,Cur_ave=0.0;
    for(int q=1; q<=nfr; q+=(nfr/NSP))
    {
        nSP++;
        if(isfinite(Cur[q]))
        {
            No+=1;
```

```
            Cur_Ne[No]=Cur[q];
            Cur_sum+=Cur[q];
        }
    }
    printf("The # of finite Cur values in %d sampling points is
%d\n",nSP,No); // Check the # of finite values of Cur in a #(NSP) of sam-
pling points.
    Cur_ave=Cur_sum/((double)No);

    // The error.
    double SD_sum=0.0,SD=0.0,Cur_err=0.0;
    for(int r=1; r<=No; r++)
    {
        SD_sum+=pow((Cur_Ne[r]-Cur_ave),2.0);
    }
    SD=sqrt(SD_sum/((double)(No-1)));
    Cur_err=SD/sqrt((double)No);

    // Store the Cur_ave +/- its error in a file.
    FILE *Cur_ave_f;
    Cur_ave_f=fopen("Cur_ave.txt","w");
    fprintf(Cur_ave_f,"Cur. = %lf +/- %lf",Cur_ave,Cur_err);
    fclose(Cur_ave_f);

    printf("Enjoy!, the results are in the output files (Cur.txt &
Cur_ave.txt)\n");

    return 0;
}
```

### 5.3.7. The not adsorbed DNA beads (it can be in-between adsorbed ones or linker or tail/s) in the DNA-(G4-G6)-dendrimers aggregate:

This is the c language code we wrote to calculate the not adsorbed DNA beads (it can be in-between adsorbed ones or linker or tail/s) in (G4-G6)-dendrimers-DNA aggregate, after compiling and running it, it will ask you some questions and by answering these questions you will get output files with names (Nad_Nnad.txt & Nad_Nnad_ave.txt).

```
/*-------------------------------------------------------------/
/   A C lang. script for calculating the number of Adsorption   /
/   dsDNA beads onto two dendrimer surfaces and the number of   /
/   not adsorbed ones ( it can be Linker between two Dendrim-   /
/   ers (G4 and G6) or tails or in between adsorbed ones ).     /
/   Written by AL-QUDS University student's Alaa Murrar for     /
/   his M.Sc. Thesis (In Biophysics).                           /
```

```
/   Note: this script is written for double-strand DNA chain    /
/   modeled as single-strand bead-spring polymer(chain), and    /
/   dendrimer molecule modeled as charged sphere and it take-   /
/   s the coordinates of the hole system from an xyz formate-   /
/   d file with a specific structure. It can be modified to     /
/   fit some needs and other formats or structures of coordi-   /
/   nates file.                                                 /
/-------------------------------------------------------------*/

#include <stdio.h>
#include <stdlib.h>
#include <math.h>

int main()
{
    // Enter the # of dsDNA bp, # of dendrimers, # of frames in the simu-
lation and the # of Sampling points for the calculations.
    int bdnabp=0,dnanum=0,dendnum=0,nfr=0,NSP=0;
    printf("Enter the # of B-dsDNA basepairs in the simulation system
[only integers from multiples of number 6]: ");
    scanf("%d",&bdnabp);
    printf("Enter the # of dendrimers in the simulation system [only in-
tegers]: ");
    scanf("%d",&dendnum);
    printf("Enter the # of frames of the simulation [only integers]: ");
    scanf("%d",&nfr);
    printf("Enter the # of sampling points that you need for your calcu-
lations of the lp [only integers and <= the # of frames]: ");
    scanf("%d",&NSP);
    dnanum=bdnabp/6;

    // Define the cutoff radius for the adsorption fraction
[=R(Dend.)[A]+R(dsDNA-bead)[A]+lB=(7.1)[A]] Angstrom.
    double R_dsDNA=8.0,R_d[dendnum+1],R_cutoff[dendnum+1];
    for(int aa=1; aa<=dendnum; aa++)
    {
        printf("Enter the radius of the dendrimer number %d [in Ang-
strom]: ",aa);
        scanf("%lf",&R_d[aa]);
        R_cutoff[aa]=R_dsDNA+R_d[aa]+14.2;
    }

    int fcounter=1,Nad[dendnum+1][nfr+1],Nnad[nfr+1]; // Declare a coun-
ter for frames and matrices for the # of adsorbed, id of end dsDNA bead
adsorbed onto the dendrimer and the # of linker dsDNA beads between den-
drimers.
    double
xyz[dnanum+dendnum+1][3+1],Vect[dendnum+1][dnanum+dendnum+1][3+1]; // De-
clare coordinates [in Angstrom], and vectors between dendrimer and dsDNA
beads.

    // Enter the xyz formated file name.
    char filename[1024];
    printf("Enter the name of the xyz coordinates file [with .xyz]: ");
    scanf("%s",filename);
    FILE *xyz_f;
    xyz_f=fopen(filename,"r");

    // Reading the file.
    char ignore[1024]; // Declare a char. matrix for ignored lines and
atom names.
```

```
    // Scan and store the coordinates of the hole system and perform the
needed calculations.
    while(!feof(xyz_f))
    {
        // Scan lines.
        fgets(ignore,sizeof(ignore),xyz_f);
        fgets(ignore,sizeof(ignore),xyz_f);
        for(int i=1; i<=(dnanum+dendnum); i++)
        {

fscanf(xyz_f,"\t%s\t%lf\t%lf\t%lf\n",ignore,&xyz[i][1],&xyz[i][2],&xyz[i]
[3]);
            //printf("%lf\t%lf\t%lf\n",xyz[i][1],xyz[i][2],xyz[i][3]);
for checking.
        }

        // Make vectors between dendrimers and dsDNA beads.
        int nV=0; // The # of vectors.
        nV=dnanum;
        for(int j=1; j<=dendnum; j++)
        {
            Nad[j][fcounter]=0;
            for(int k=1; k<=nV; k++)
            {
                for(int l=1; l<=3; l++)
                {
                    Vect[j][k][l]=xyz[k][l]-xyz[dnanum+j][l]; //
xyz[dnanum+j][l] means that the first dendrimer has [dnanum+j] atom id in
the simulation.
                }
                // Calculate the length of the vector.

Vect[j][k][0]=sqrt(pow(Vect[j][k][1],2.0)+pow(Vect[j][k][2],2.0)+pow(Vect
[j][k][3],2.0));

                // Check if dsDNA bead is adsorbed or not and calculate
the # of adsorbed beads for each dendrimer.
                if(Vect[j][k][0]<R_cutoff[j]) Nad[j][fcounter]+=1;
            }
        }

        // Calculate the # of linker dsDNA beads between dendrimers and
store it.
        Nnad[fcounter]=(dnanum-(Nad[1][fcounter]+Nad[2][fcounter]));

        fcounter+=1; // Increment the frames counter.
    }
    fcounter--; // To make fcounter=nfr.
    printf("The # of frames in this simulation is %d\n",fcounter);
    fclose(xyz_f);

    // Print the Nad and Nnad values in a file.
    FILE *Nad_Nnad_f;
    Nad_Nnad_f=fopen("Nad_Nnad.txt","w");
        fprintf(Nad_Nnad_f,"# Nad[G4]\t|Nad[G6]\t|Nnad[L/T/In]\n");
    for(int m=1; m<=nfr; m++)
    {
        fprintf(Nad_Nnad_f,"
%d\t|%d\t|%d\n",Nad[1][m],Nad[2][m],Nnad[m]);
    }
```

```
    fclose(Nad_Nnad_f);

    // Calculate the average of Nad and Nnad values and their errors from
NSP sampling points after equilibrium and store them.
    int No=0,nSP1=0,nSP2=0; // A counters for the picks "Nad & Nnad" and
the sampling points.
    int
Nad_Ne[dendnum+1][NSP+1],Nad_Sum[dendnum+1],Nnad_Ne[NSP+1],Nnad_sum=0;
    for(int n=1; n<=dendnum; n++)
    {
        No=0;
        nSP1=0;
        Nad_Sum[n]=0;
        for(int o=1; o<=nfr; o+=(nfr/NSP))
        {
            No++;
            nSP1++;
            Nad_Ne[n][No]=Nad[n][o];
            Nad_Sum[n]+=Nad[n][o];
        }
    }
    No=0;
    for(int p=1; p<=nfr; p+=(nfr/NSP))
    {
        No++;
        nSP2++;
        Nnad_Ne[No]=Nnad[p];
        Nnad_sum+=Nnad[p];

    }
    printf("The # of sampling points for Nad is %d and for Nnad is
%d\n",nSP1,nSP2); // Check the # of sampling points from the output of
the for loop.
    double Nad_ave[dendnum+1],Nnad_ave=0.0;

    Nad_ave[1]=((double)Nad_Sum[1])/((double)NSP);
    Nad_ave[2]=((double)Nad_Sum[2])/((double)NSP);

    Nnad_ave=((double)Nnad_sum)/((double)NSP);

    // The errors.
    double
SDNad_sum[dendnum+1],SDNad[dendnum+1],Nad_err[dendnum+1],SDNnad_sum=0.0,S
DNnad=0.0,Nnad_err=0.0;
    for(int q=1; q<=dendnum; q++)
    {
        SDNad_sum[q]=0.0;
        for(int r=1; r<=NSP; r++)
        {
            SDNad_sum[q]+=pow((((double)Nad_Ne[q][r])-Nad_ave[q]),2.0);
        }
    }

    for(int s=1; s<=NSP; s++)
    {
        SDNnad_sum+=pow((((double)Nnad_Ne[s])-Nnad_ave),2.0);
    }

    SDNad[1]=sqrt(SDNad_sum[1]/((double)(NSP-1)));
    SDNad[2]=sqrt(SDNad_sum[2]/((double)(NSP-1)));
    Nad_err[1]=SDNad[1]/sqrt((double)NSP);
```

```
    Nad_err[2]=SDNad[2]/sqrt((double)NSP);

    SDNnad=sqrt(SDNnad_sum/((double)(NSP-1)));
    Nnad_err=SDNnad/sqrt((double)NSP);

    // Store the Nad_ave and Nnad_ave values +/- their errors in a file.
    FILE *Nad_Nnad_ave_f;
    Nad_Nnad_ave_f=fopen("Nad_Nnad_ave.txt","w");

    fprintf(Nad_Nnad_ave_f,"Nad_ave[G4] = %d +/-
%d\n",(int)floor(Nad_ave[1]),(int)floor(Nad_err[1]));
    fprintf(Nad_Nnad_ave_f,"Nad_ave[G6] = %d +/-
%d\n",(int)floor(Nad_ave[2]),(int)floor(Nad_err[2]));

    fprintf(Nad_Nnad_ave_f,"\n");

    if(floor(Nnad_ave)<0) fprintf(Nad_Nnad_ave_f,"Nnad_ave[L/T/In] = 0
+/- 0 -> (The original value < 0, there is/are common adsorbed
bead/s)\n");
    else fprintf(Nad_Nnad_ave_f,"Nnad_ave[L/T/In] = %d +/-
%d\n",(int)floor(Nnad_ave),(int)floor(Nnad_err));

    fclose(Nad_Nnad_ave_f);

    printf("Enjoy!, the results are in the output files (Nad_Nnad.txt &
Nad_Nnad_ave.txt)\n");

    return 0;
}
```

### 5.3.8. The toroidal parameter ($\tau$):

This is the c language code we wrote to calculate $\tau$ of the dsDNA-dendrimer aggregate, after compiling and running it, it will ask you some questions and by answering these questions you will get output files with names (Taw.txt & Taw_ave.txt).

```
/*-------------------------------------------------------------/
/   A C lang. script for calculating the Toroidal parameter   /
/   for a double-strand DNA-dendrimer aggregate.              /
/   Written by AL-QUDS University student's Alaa Murrar for   /
/   his M.Sc. Thesis (In Biophysics).                         /
/   Note: this script is written for double-strand DNA cha-   /
/   in modeled as single-strand bead-spring polymer(chain),   /
/   and dendrimer molecule modeled as charged sphere and it   /
/   takes the coordinates of beads from xyz formated file     /
/   with a specific structure. It can be modified to fit c-   /
/   omplex models for ss- and ds- DNA and dendrimer, and o-   /
/   ther formats or structures of coordinates file.           /
/   The definition of this parameter will be found in Dani-   /
/   el George Angelescu, Robijn Bruinsma and Per Linse art-   /
/   icle [Angelescu, D. G., Bruinsma, R., & Linse, P. (200-   /
```

```
/    6). Monte Carlo simulations of polyelectrolytes inside    /
/    viral capsids. Phys. Rev. E, 73(4), 041921.], but here    /
/    it will be used for the dsDNA-dendrimer aggregate.        /
/--------------------------------------------------------------*/

#include <stdio.h>
#include <stdlib.h>
#include <math.h>

int main()
{
    // Enter the # of dsDNA bp and # of frames in the simulation.
    int bdnabp=0,dnanum=0,dendnum=0,nfr=0,sfr=0;
    printf("Enter the # of B-dsDNA basepairs in the simulation system
[only integers from multiples of number 6]: ");
    scanf("%d",&bdnabp);
    printf("Enter the # of dendrimers in the simulation system [only in-
tegers]: ");
    scanf("%d",&dendnum);
    printf("Enter the # of frames of the simulation [only integers]: ");
    scanf("%d",&nfr);
    printf("Enter the # of frame that you need to stop the calculation at
[integer only]: ");
    scanf("%d",&sfr);
    dnanum=bdnabp/6;
    //printf("Dnanum+Dendnum = %d\n",dnanum+dendnum); for checking.

    int fcounter=1,Vdim=18; // fcounter -> frames counter and Vdim is the
# of vectors between picks dsDNA beads (needed by the dimension of the
vectors matrix and making vectors between the picks dsDNA beads).

    // Declare coordinates [in Angstrom], vectors between picks dsDNA
beads, cross product between previous vectors, first_sum in toroidal pa-
rameter equation and toroidal parameter matrices.
    double
xyz[dnanum+dendnum+1][3+1],Vect[Vdim+1][3+1],Cp[Vdim+1][3+1],Fs_Cp[3+1],T
aw[nfr+1];

    // Enter the xyz formated file name.
    char filename[1024];
    printf("Enter the name of the xyz coordinates file [with .xyz]: ");
    scanf("%s",filename);
    FILE *xyz_f;
    xyz_f=fopen(filename,"r");

    // Reading the file.
    char ignore[1024]; // Declare a char. matrix for ignored lines and
atom names.

    // Scan and store the coordinates of the hole system and perform the
needed calculations.
    while(!feof(xyz_f))
    {
        // Scan lines.
        fgets(ignore,sizeof(ignore),xyz_f);
        fgets(ignore,sizeof(ignore),xyz_f);
        for(int i=1; i<=(dnanum+dendnum); i++)
        {

fscanf(xyz_f,"\t%s\t%lf\t%lf\t%lf\n",ignore,&xyz[i][1],&xyz[i][2],&xyz[i]
[3]);
```

```
            //printf("%lf\t%lf\t%lf\n",xyz[i][1],xyz[i][2],xyz[i][3]);
for checking.
        }

        // Make vectors between the picks dsDNA beads.
        int dsbid=0;
        for(int j=1; j<=Vdim; j++)
        {
            for(int k=1; k<=3; k++)
            {
                if(j==1)
Vect[j][k]=xyz[dsbid+((int)(floor(dnanum/18.0)))][k]-xyz[1][k];
                else
Vect[j][k]=xyz[dsbid+((int)(floor(dnanum/18.0)))][k]-xyz[dsbid][k];
            }
            dsbid+=((int)(floor(dnanum/18.0)));
        }
        //printf("The end bead id of the dsDNA chain is %d\n",dsbid); for
checking.

        // Calculate the cross product(determinant) between adjacent vec-
tors that connect adsorbed dendrimers.
        int nCp=0; // The # of cross products.
        nCp=Vdim-1;
        // The components of the net vector of the cross products vec-
tors.
        Fs_Cp[1]=0.0;
        Fs_Cp[2]=0.0;
        Fs_Cp[3]=0.0;
        for(int l=1; l<=nCp; l++)
        {
            Cp[l][1]=(((Vect[l][2])*(Vect[l+1][3]))-
((Vect[l][3])*(Vect[l+1][2])));
            Cp[l][2]=(-1.0)*(((Vect[l][1])*(Vect[l+1][3]))-
((Vect[l][3])*(Vect[l+1][1])));
            Cp[l][3]=(((Vect[l][1])*(Vect[l+1][2]))-
((Vect[l][2])*(Vect[l+1][1])));

Cp[l][0]=sqrt(pow(Cp[l][1],2.0)+pow(Cp[l][2],2.0)+pow(Cp[l][3],2.0));
            Fs_Cp[1]+=(Cp[l][1]/Cp[l][0]);
            Fs_Cp[2]+=(Cp[l][2]/Cp[l][0]);
            Fs_Cp[3]+=(Cp[l][3]/Cp[l][0]);
        }

        // Calculate the Taw (Toroidal parameter) and store it.
        double Ss_Cp=0.0;
        Ss_Cp=pow(Fs_Cp[1],2.0)+pow(Fs_Cp[2],2.0)+pow(Fs_Cp[3],2.0);
        Taw[fcounter]=(sqrt(Ss_Cp)/((double)(Vdim-1))); // (# of picks
dsDNA beads for Taw)-2=Vdim-1=nCp it is a normalization process :).

        if(fcounter==sfr) break;
        fcounter+=1; // Increment the frames counter.
    }
    printf("The # of frames in this simulation is %d\n",fcounter);
    fclose(xyz_f);

    // Print the values of Taw in a file.
    FILE *Taw_f;
    Taw_f=fopen("Tawt.txt","w");
        fprintf(Taw_f,"Time\t|Taw\n");
    for(int m=1; m<=fcounter; m++)
```

```
    {
        fprintf(Taw_f,"%lf\t%lf\n",(m*100000*25.0e-9),Taw[m]); //
(m*100000*25.0e-9) is for printing the time for each frame in micro-
second.
    }
    fclose(Taw_f);

    // Calculate the average of the Toroidal parameter and its error from
all of the simulation steps and store them.
    int Nf=0;
    double Taw_Ne[nfr+1],Taw_sum=0.0,Taw_ave=0.0;
    for(int n=1; n<=fcounter; n++)
    {
        if(isfinite(Taw[n]))
        {
            Nf++;
            Taw_Ne[Nf]=Taw[n];
            Taw_sum+=Taw[n];
        }
    }
    printf("The # of finite Taw's in %d frames is %d\n",fcounter,Nf);
    Taw_ave=Taw_sum/((double)Nf);

    // The error.
    double SD_sum=0.0,SD=0.0,Taw_err=0.0;
    for(int o=1; o<=Nf; o++)
    {
        SD_sum+=pow((Taw_Ne[o]-Taw_ave),2.0);
    }
    SD=sqrt(SD_sum/((double)(Nf-1)));
    Taw_err=SD/sqrt((double)Nf);

    // Store the Taw_ave +/- its error in a file.
    FILE *Taw_ave_f;
    Taw_ave_f=fopen("Tawt_ave.txt","w");
    fprintf(Taw_ave_f,"Taw = %lf +/- %lf",Taw_ave,Taw_err);
    fclose(Taw_ave_f);

    printf("Enjoy!, the results are in the output files (Taw.txt &
Taw_ave.txt)\n");

    return 0;
}
```

### 5.3.9. Additional codes:

This is the c language code we wrote to calculate the average of any quantity from a certain number of sampling points, after compiling and running it, it will ask you some questions and by answering these questions you will get output file begin with (Ave_).

```
/*-----------------------------------------------------------/
/   A C lang. script for calculating the average of any     /
/   quantity from sampling points.                          /
/   Written by AL-QUDS University student's Alaa Murrar     /
/   for his M.Sc. Thesis (In Biophysics).                   /
/   Note: this script is written for a specific input       /
/   file structure and it can be modified to fit other      /
/   structures.                                             /
/-----------------------------------------------------------*/
```

```c
#include <stdio.h>
#include <stdlib.h>
#include <string.h>
#include <math.h>

int main()
{
    // Enter the total # of points and the # of sampling points for the calculations.
    int ntp=0,NSP=0;
    printf("Enter the total # of points [only integers]: ");
    scanf("%d",&ntp);
    printf("Enter the # of sampling points that you need for your calculations [only integers]: ");
    scanf("%d",&NSP);

    double Qun[ntp+1],Time[ntp+1]; // Declare Qun and Time(will be ignored) matrices.

    // Enter the name of the file of the quantity.
    char ifilename[1024];
    printf("Enter the name of the input file of the quantity [with its extension]: ");
    scanf("%s",ifilename);
    FILE *Qun_f;
    Qun_f=fopen(ifilename,"r");

    // Reading the file.
    char ignore[1024]; // Declare a char. matrix for ignored lines.
    fgets(ignore,sizeof(ignore),Qun_f);
    while(!feof(Qun_f))
    {
        // Scan and store the quantity values.
        for(int i=1; i<=ntp; i++)
        {
            fscanf(Qun_f,"\t%lf\t%lf\n",&Time[i],&Qun[i]);
            //printf("%lf\t%lf\n",Time[i],Qun[i]); for checking.
        }
    }
    fclose(Qun_f);

    // Calculate the average of the picks quantity values and its error from NSP sampling points and store them in a file.
    int N=0,nSP=0; // A counters for the picks quantity values and the sampling points.
    double Qun_Ne[NSP+1],Qun_sum=0.0,Qun_ave=0.0;
    for(int j=1; j<=ntp; j+=(ntp/NSP))
    {
        N+=1;
        nSP++;
        Qun_Ne[N]=Qun[j];
        Qun_sum+=Qun[j];
    }
    printf("The # of sampling points is %d\n",nSP); // Check the # of sampling points from the output of the for loop.
    Qun_ave=Qun_sum/((double)NSP);

    // The error.
    double SD_sum=0.0,SD=0.0,Qun_err=0.0;
    for(int k=1; k<=NSP; k++)
```

```
    {
        SD_sum+=pow((Qun_Ne[k]-Qun_ave),2.0);
    }
    SD=sqrt(SD_sum/((double)(NSP-1)));
    Qun_err=SD/sqrt((double)NSP);

    // Store the Qun_ave +/- its error in a file.
    char ofilename[]="Ave_";
    strcat(ofilename,ifilename);
    FILE *Qun_ave_err_f;
    Qun_ave_err_f=fopen(ofilename,"w");
    fprintf(Qun_ave_err_f,"Qun.      =      %lf      +/-      %lf      Ang-
strom.",Qun_ave,Qun_err);
    fclose(Qun_ave_err_f);

    printf("Enjoy!,    the    results    are    in    the    output    file
(%s)\n",ofilename);

    return 0;
}
```

We wrote the following c language code in order to draw the bonds between the dsDNA beads in the dsDNA chain using VMD or Ovito program, clearly, this code reformats the XYZ trajectory file that we obtained as a result from the simulation by numbering the atoms in the simulation, after compiling and running it, it will ask you some questions and by answering these questions you will get output file with name (Modified_traj_file_(num_for_bond_draw).xyz).

```
/*-------------------------------------------------------------/
/   A C lang. script for reformating the xyz file of complex   /
/   of double-strand DNA and dendrimer in order to draw the    /
/   bonds betweem dsDNA beads using Ovito or VMD program.      /
/
/   Written by AL-QUDS University student's Alaa Murrar for    /
/   his M.Sc. Thesis (In Biophysics).                          /
/   Note: this script is written for double-strand DNA chain   /
/   and dendrimer modeled as single-strand bead-spring poly-   /
/   mer(chain) and charged sphere respectively.                /
/   It takes the coordinates of the hole system from specif-   /
/   ic xyz formated file (i.e, .xyz). It can be modified to    /
/   fit complex models for ss- and ds- DNA and other formats   /
/   and structures of coordinates file.                        /
/-------------------------------------------------------------*/
```

```
#include <stdio.h>
#include <stdlib.h>
#include <string.h>

int main()
{
    // Enter the xyz formated file name.
    char in_xyz[1024];
    printf("Enter the name of the xyz coordinates file [with .xyz]: ");
    scanf("%s",in_xyz);
    FILE *xyz_f_i,*xyz_f_f;
    xyz_f_i=fopen(in_xyz,"r");
    xyz_f_f=fopen("Modified_traj_file_(num_for_bond_draw).xyz","w"); //
Modified .xyz file.

    // Reading the file.
    int fcounter=1,atomnum=0; // fcounter -> frames counter and atomnum
for the total # of atoms in the system.
    printf("Enter the # of particles/atoms in the simulation (it must re-
main constant during the simulation): ");
    scanf("%d",&atomnum);
    // Declare char. matrices for starting lines and atom names(types) in
the frame.
    char slis[2+1][1024],ptypes[atomnum+1][1024];
    // Declare matrix for atom coordinates.
    double xyz[atomnum+1][3+1];

    while(!feof(xyz_f_i))
    {
        // Scan the first two lines.
        fgets(slis[1],sizeof(slis[1]),xyz_f_i);
        fgets(slis[2],sizeof(slis[2]),xyz_f_i);

        // Scan atom names and their coordinates and stores them.
        for(int i=1; i<=atomnum; i++)
        {

fscanf(xyz_f_i,"\t%s\t%lf\t%lf\t%lf\n",ptypes[i],&xyz[i][1],&xyz[i][2],&x
yz[i][3]);
        }

        // Re-write the new xyz file with numberd atom names(types).
        fprintf(xyz_f_f,"%s",slis[1]);
        fprintf(xyz_f_f,"%s",slis[2]);
        for(int i=1; i<=atomnum; i++)
        {
            fprintf(xyz_f_f,"
%s%d\t%lf\t%lf\t%lf\n",ptypes[i],i,xyz[i][1],xyz[i][2],xyz[i][3]);
        }

        fcounter++; // Increment the counter of frames.
    }
    fcounter--; // To make fcounter = # of frames.
    fclose(xyz_f_i);
    fclose(xyz_f_f);

    printf("The # of frames in this simulation system is %d\n",fcounter);
// Print the # of frames in the simulation.

    printf("Enjoy!, the result output file is (Modi-
fied_traj_file_(num_for_bond_draw).xyz)\n");
```

```
    return 0;
}
```

## Bibliography

*Abbreviations and Symbols for Nucleic Acids, Polynucleotides and their Constituents*. (n.d.). Retrieved from IUPAC-IUB Commission on Biochemical Nomenclature (CBN): http://www.sbcs.qmul.ac.uk/iupac/misc/naabb.html

Abdelhady, H. G., Allen, S., Davies, M. C., Roberts, C. J., Tendler, S. J., & Williams, P. M. (2003). Direct real-time molecular scale visualisation of the degradation of condensed DNA complexes exposed to DNase I. *Nucleic Acids Res., 31*(14), 4001–4005.

Ainalem, M.-L., Carnerup, A. M., Janiak, J., Alfredsson, V., Nylander, T., & Schillén, K. (2009). Condensing DNA with poly(amido amine) dendrimers of different generations: means of controlling aggregate morphology. *Soft Matter, 5*(11), 2310-2320. doi:10.1039/B821629K

Alberts, B., Johnson, A., Lewis, J., Morgan, D., Raff, M., Roberts, K., & Walter, P. (2014). Chapter 4: DNA, Chromosomes and Genomes. In B. Alberts, A. Johnson, J. Lewis, D. Morgan, M. Raff, K. Roberts, & P. Walter, *Molecular Biology of the Cell* (6th ed., p. 1464). Garland Science.

Alberts, B., Johnson, A., Lewis, J., Raff, M., Roberts, K., & Walter, P. (2002). *Molecular Biology of the Cell* (4th ed.). New York and London: Garland Science.

Angelescu, D. G., Bruinsma, R., & Linse, P. (2006). Monte Carlo simulations of polyelectrolytes inside viral capsids. *Phys. Rev. E, 73*(4), 041921. doi:10.1103/PhysRevE.73.041921

Arcesi, L., Penna, G. L., & Perico, A. (2007). Generalized electrostatic model of the wrapping of DNA around oppositely charged proteins. *Biopolymers, 86*(2), 127–135. doi:10.1002/bip.20711

Asthana, A., Chauhan, A. S., Diwan, P. V., & Jain, N. K. (2005). Poly(amidoamine) (PAMAM) dendritic nanostructures for controlled sitespecific delivery of acidic anti-inflammatory active ingredient. *AAPS PharmSciTech, 6*(3), E536–E542. doi:10.1208/pt060367

Basu, H. S., Feuerstein, B. G., Zarling, D. A., Shaffer, R. H., & Marton, L. J. (1988). Recognition of Z-RNA and Z-DNA Determinants by Polyamines in Solution: Experimental and Theoretical Studies. *J. Biomol. Struct. Dyn., 6*(2), 299-309. doi:10.1080/07391102.1988.10507714

Baumann, C. G., Smith, S. B., Bloomfield, V. A., & Bustamante, C. (1997). Ionic effects on the elasticity of single DNA molecules. *Proc. Natl. Acad. Sci. U.S.A., 94*(12), 6185-6190. doi:10.1073/pnas.94.12.6185

Berg, J. M., Tymoczko, J. L., & Stryer, L. (2002). *Biochemistry* (5th ed.). W. H. Freeman and Company.

Bhadra, D., Bhadra, S., Jain, P., & Jain, N. K. (2002). Pegnology: a review of PEG-ylated systems. *Pharmazie, 57*(1), 5–29.

Bhadra, D., Bhadra, S., Jain, S., & Jain, N. K. (2003). A PEGylated dendritic nanoparticulate carrier of fluorouracil. *Int. J. Pharm., 257*(1-2), 111-124. doi:10.1016/S0378-5173(03)00132-7

Bielinska, A. U., Chen, C., Johnson, J., & Baker, J. R. (1999). DNA Complexing with Polyamidoamine Dendrimers: Implications for Transfection. *Bioconjugate Chem., 10*(5), 843–850. doi:10.1021/bc990036k

Bloomfield, V. A. (1997). DNA condensation by multivalent cations. *Biopolymers, 44*(3), 269–282. doi:10.1002/(SICI)1097-0282(1997)44:3<269::AID-BIP6>3.0.CO;2-T

# Bibliography


Böhme, U., Klenge, A., Hänel, B., & Scheler, U. (2011). Counterion Condensation and Effective Charge of PAMAM Dendrimers. *Polymers, 3*(2), 812-819. doi:10.3390/polym3020812

Boroudjerdi, H., Naji, A., & Netz, R. R. (2011). Salt-modulated structure of polyelectrolyte-macroion complex fibers. *Eur Phys J E Soft Matter., 34*(7), 72. doi:10.1140/epje/i2011-11072-1

Buhleier, E., Wehner, W., & Vögtle, F. (1978). "Cascade"- and "Nonskid-Chain-like" Syntheses of Molecular Cavity Topologies. *Synthesis, 2*, 155-158. doi:10.1055/s-1978-24702

Cakara, D., Kleimann, J., & Borkovec, M. (2003). Microscopic Protonation Equilibria of Poly(amidoamine) Dendrimers from Macroscopic Titrations. *Macromolecules, 36*(11), 4201–4207. doi:10.1021/ma0300241

Campos, B. B., Algarra, M., & Silva, J. C. (2010). Fluorescent Properties of a Hybrid Cadmium Sulfide-Dendrimer Nanocomposite and its Quenching with Nitromethane. *J. Fluoresc., 20*(1), 143–151. doi:10.1007/s10895-009-0532-5

Cao, Q., Zuo, C., Ma, Y., Li, L., & Zhang, Z. (2011). Interaction of double-stranded DNA with a nanosphere: a coarse-grained molecular dynamics simulation study. *Soft Matter, 7*(2), 506-514. doi:10.1039/C0SM00512F

Carnerup, A. M., Ainalem, M.-L., Alfredssona, V., & Nylander, T. (2011). Condensation of DNA using poly(amido amine) dendrimers: effect of salt concentration on aggregate morphology. *Soft Matter, 7*(2), 760-768. doi:10.1039/C0SM00644K

Carr, S. M. (n.d.). *The Watson-Crick Model of DNA (1953)*. Retrieved from Memorial University of Newfoundland: https://www.mun.ca/biology/scarr/Watson-Crick_Model.html

Chauhan, A. S., Sridevi, S., Chalasani, K. B., Jain, A. K., Jain, S. K., Jain, N., & Diwan, P. V. (2003). Dendrimer-mediated transdermal delivery: enhanced bioavailability of indomethacin. *J. Control. Release, 90*(3), 335-343. doi:10.1016/S0168-3659(03)00200-1

Cheng, Y., Wu, Q., Li, Y., & Xu, T. (2008). External Electrostatic Interaction versus Internal Encapsulation between Cationic Dendrimers and Negatively Charged Drugs: Which Contributes More to Solubility Enhancement of the Drugs? *J. Phys. Chem. B, 112*(30), 8884–8890. doi:10.1021/jp801742t

Cheng, Y., Xu, Z., Ma, M., & Xu, T. (2008). Dendrimers as drug carriers: Applications in different routes of drug administration. *J. Pharm. Sci., 97*(1), 123–143. doi:10.1002/jps.21079

*Chromosomes and Cell Division*. (n.d.). Retrieved from Bio1100 Chapter 6: http://bio1100.nicerweb.com/Locked/src/chap06.html

Dekker, M. (1998). In J. C. Kwak, *Surfactant Science: Polymer-Surfactant Systems* (Vol. 77). New York.

Delong, R., Stephenson, K., Loftus, T., Fisher, M., Alahari, S., Nolting, A., & Juliano, R. L. (1997). Characterization of complexes of oligonucleotides with polyamidoamine starburst dendrimers and effects on intracellular delivery. *J. Pharm. Sci., 86*(6), 762–764. doi:10.1021/js960409f

*Dendrimer technology licensed for herbicide*. (n.d.). Retrieved from Lab+Life SCIENTIST www.labonline.com.au: http://www.labonline.com.au/content/life-scientist/news/dendrimer-technology-licensed-for-herbicide-701112647

*Dendrimers - GlycoFineChem*. (n.d.). Retrieved from GlycoSyn: http://www.glycofinechem.glycosyn.com/collections/dendrimers

# Bibliography


Dendrimers: Design, Synthesis and Chemical Properties. (2006). In U. Boas, J. B. Christensen, & P. M. Heegaard, *Dendrimers in Medicine and Biotechnology: New Molecular Tools* (pp. 1-27). Cambridge: The Royal Society of Chemistry.

Denkewalter, R. G., Kolc, J. F., & Lukasavage, W. J. (1981). *U.S. Patent No. US4410688 A.*

Denkewalter, R. G., Kolc, J., & Lukasavage, W. J. (1979). *U.S. Patent No. US4289872 A.*

Dootz, R., Toma, A. C., & Pfohl, T. (2011). PAMAM6 dendrimers and DNA: PH dependent "beads-on-a-string" behavior revealed by small angle X-ray scattering. *Soft Matter, 7*(18), 8343-8351. doi:10.1039/C1SM05632H

Dunweg, B., & Paul, W. (1991). BROWNIAN DYNAMICS SIMULATIONS WITHOUT GAUSSIAN RANDOM NUMBERS. *Int. J. Mod. Phys. C, 2*(3), 817-827. doi:10.1142/S0129183191001037

Dutta, T., & Jain, N. K. (2007). Targeting potential and anti-HIV activity of lamivudine loaded mannosylated poly (propyleneimine) dendrimer. *Biochim. Biophys. Acta, 1770*(4), 681-686. doi:10.1016/j.bbagen.2006.12.007

Dutta, T., Agashe, H. B., Garg, M., Balasubramanium, P., Kabra, M., & Jain, N. K. (2007). Poly (propyleneimine) dendrimer based nanocontainers for targeting of efavirenz to human monocytes/macrophages in vitro. *J. Drug Target., 15*(1), 84-98. doi:10.1080/10611860600965914

Dutta, T., Garg, M., & Jain, N. K. (2008). Poly(propyleneimine) dendrimer and dendrosome mediated genetic immunization against hepatitis B. *Vaccine, 26*(27-28), 3389-3394. doi:10.1016/j.vaccine.2008.04.058

Dutta, T., Garg, M., & Jain, N. K. (2008). Targeting of efavirenz loaded tuftsin conjugated poly(propyleneimine) dendrimers to HIV infected macrophages in vitro. *Eur. J. Pharm. Sci., 34*(2-3), 181-189. doi:10.1016/j.ejps.2008.04.002

Edelstein, M. L., Abedi, M. R., Wixon, J., & Edelstein, R. M. (2004). Gene therapy clinical trials worldwide 1989-2004-an overview. *J Gene Med, 6*(6), 597-602. doi:10.1002/jgm.619

Ermak, G. (2015). *Emerging Medical Technologies.* World Scientific Publishing Company Pte Limited.

Fant, K., Esbjo□rner, E. K., Jenkins, A., Grossel, M. C., Lincoln, P., & Nordén, B. (2010). Effects of PEGylation and Acetylation of PAMAM Dendrimers on DNA Binding, Cytotoxicity and in Vitro Transfection Efficiency. *Mol Pharm., 7*(5), 1734-46. doi:10.1021/mp1001312

Fant, K., Esbjörner, E. K., Lincoln, P., & Nordén, B. (2008). DNA Condensation by PAMAM Dendrimers: Self-Assembly Characteristics and Effect on Transcription. *Biochem., 47*(6), 1732–1740. doi:10.1021/bi7017199

Fernandes, E. G., Vieira, N. C., Queiroz, A. A., Guimarães, F. E., & Zucolotto, V. (2010). Immobilization of Poly(propylene imine) Dendrimer/Nickel Phtalocyanine as Nanostructured Multilayer Films To Be Used as Gate Membranes for SEGFET pH Sensors. *J. Phys. Chem. C, 114*(14), 6478–6483. doi:10.1021/jp9106052

Frechet, J. M. (1994). Functional polymers and dendrimers: reactivity, molecular architecture, and interfacial energy. *Science, 263*(5154), 1710-1715. doi:10.1126/science.8134834

Fu, H.-L., Cheng, S.-X., Zhang, X.-Z., & Zhuo, R.-X. (2007). Dendrimer/DNA complexes encapsulated in a water soluble polymer and supported on fast degrading star poly(dl-lactide) for localized gene delivery. *J. Control. Release, 124*(3), 181-188. doi:10.1016/j.jconrel.2007.08.031

# Bibliography


Fu, H.-L., Cheng, S.-X., Zhang, X.-Z., & Zhuo, R.-X. (2008). Dendrimer/DNA complexes encapsulated functional biodegradable polymer for substrate-mediated gene delivery. *J. Gene Med., 10*(12), 1334–1342. doi:10.1002/jgm.1258

Gao, C., & Yan, D. (2004). Hyperbranched polymers: from synthesis to applications. *Prog. Polym. Sci., 29*(3), 183-275. doi:10.1016/j.progpolymsci.2003.12.002

Ghosh, A., & Bansal, M. (2003). A glossary of DNA structures from A to Z. *Acta Cryst. D, 59*(Pt 4), 620-626. doi:10.1107/S0907444903003251

Giorgino, T. (2015). *Computing diffusion coefficients in macromolecular simulations: the Diffusion Coefficient Tool for VMD*. Retrieved from GitHub: https://github.com/tonigi/vmd_diffusion_coefficient/

Gitsov, I. (2008). Hybrid linear dendritic macromolecules: From synthesis to applications. *Polym. Sci. Part A: Polym. Chem., 46*(16), 5295–5314. doi:10.1002/pola.22828

Grabchev, I., Staneva, D., & Chovelon, J.-M. (2010). Photophysical investigations on the sensor potential of novel, poly(propylenamine) dendrimers modified with 1,8-naphthalimide units. *Dyes Pigm., 85*(3), 189-193. doi:10.1016/j.dyepig.2009.10.023

Gregory, S. G., Barlow, K. F., McLay, K. E., Kaul, R., Swarbreck, D., Dunham, A., & Scott, C. E. (2006). The DNA sequence and biological annotation of human chromosome 1. *Nature, 441*, 315–321. doi:10.1038/nature04727

Grønbech-Jensen, N., & Farago, O. (2013). A simple and effective Verlet-type algorithm for simulating Langevin dynamics. *Mol. Phys., 111*(8), 983-991. doi:10.1080/00268976.2012.760055

Grønbech-Jensen, N., Hayre, N. R., & Farago, O. (2014). Application of the G-JF discrete-time thermostat for fast and accurate molecular simulations. *Comput. Phys. Commun., 185*(2), 524-527. doi:10.1016/j.cpc.2013.10.006

Gupta, U., Agashe, H. B., Asthana, A., & Jain, N. K. (2006). Dendrimers: Novel Polymeric Nanoarchitectures for Solubility Enhancement. *Biomacromolecules, 7*(3), 649–658. doi:10.1021/bm050802s

Halford, B. (2005). Dendrimers branch out. *Chem. Eng. News, 83*(24), 30-36.

Hardin, J., & Bertoni, G. P. (2015). *Becker's World of the Cell* (9th ed.). Pearson.

Hawker, C. J., & Frechet, J. M. (1990). Preparation of polymers with controlled molecular architecture. A new convergent approach to dendritic macromolecules. *J. Am. Chem. Soc., 112*(21), 7638–7647. doi:10.1021/ja00177a027

Hermanson, G. T. (2008). *Bioconjugate Techniques* (2nd ed.). London, WC1X 8RR, UK: Academic Press.

Holister, P., Vas, C. R., & Harper, T. (2003). Dendrimers: Technology White Papers. Retrieved from https://web.archive.org/web/20110706065720/http://www.sps.aero/Key_ComSpace_Articles/TSA-001_Dendrimers_White%20Paper.pdf

*Home | LibreOffice*. (n.d.). Retrieved from LibreOffice - The Document Foundation: https://www.libreoffice.org/

Humphrey, W., Dalke, A., & Schulten, K. (1996). VMD: Visual molecular dynamics. *J. Mol. Graph., 14*(1), 33-38. doi:10.1016/0263-7855(96)00018-5

Irobalieva, R. N., Fogg, J. M., Jr, D. J., Sutthibutpong, T., Chen, M., Barker, A. K., . . . Zechiedrich, L. (2015). Structural diversity of supercoiled DNA. *Nat. Commun., 6*, 8440. doi:10.1038/ncomms9440

Itaka, K., & Kataoka, K. (2009). Recent development of nonviral gene delivery systems with virus-like structures and mechanisms. *Eur. J. Pharm. Biopharm., 71*(3), 475-483. doi:10.1016/j.ejpb.2008.09.019

Jackson, C. L., Chanzy, H. D., Booy, F. P., Drake, B. J., Tomalia, D. A., Bauer, B. J., & Amis, E. J. (1998). Visualization of Dendrimer Molecules by Transmission

Electron Microscopy (TEM): Staining Methods and Cryo-TEM of Vitrified Solutions. *Macromolecules, 31*(18), 6259–6265. doi:10.1021/ma9806155

Jin, L., Zeng, X., Liu, M., Deng, Y., & He, N. (2014). Current Progress in Gene Delivery Technology Based on Chemical Methods and Nano-carriers. *Theranostics, 4*(3), 240-255. doi:10.7150/thno.6914

Kaanumalle, L. S., Ramesh, R., Maddipatla, V. S., Nithyanandhan, J., Jayaraman, N., & Ramamurthy, V. (2005). Dendrimers as Photochemical Reaction Media. Photochemical Behavior of Unimolecular and Bimolecular Reactions in Water-Soluble Dendrimers. *J. Org. Chem., 70*(13), 5062–5069. doi:10.1021/jo0503254

Kabanov, V. A., Sergeyev, V. G., Pyshkina, O. A., Zinchenko, A. A., Zezin, A. B., Joosten, J. G., . . . Yoshikawa, K. (2000). Interpolyelectrolyte Complexes Formed by DNA and Astramol Poly(propylene imine) Dendrimers. *Macromolecules, 33*(26), 9587–9593. doi:10.1021/ma000674u

Khopade, A. J., Caruso, F., Tripathi, P., Nagaich, S., & Jain, N. K. (2002). Effect of dendrimer on entrapment and release of bioactive from liposomes. *Int. J. Pharm., 232*(1-2), 157-162. doi:10.1016/S0378-5173(01)00901-2

Klajnert, B., & Bryszewska, M. (2001). Dendrimers: properties and applications. *Acta Biochim Pol., 48*(1), 199-208.

Kolb, H. C., Finn, M. G., & Sharpless, K. B. (2001). Click Chemistry: Diverse Chemical Function from a Few Good Reactions. *Angew. Chem. Int. Ed., 40*(11), 2004-2021. doi:10.1002/1521-3773(20010601)40:11<2004::AID-ANIE2004>3.0.CO;2-5

Kukowska-Latallo, J. F., Bielinska, A. U., Johnson, J., Spindler, R., Tomalia, D. A., & Baker, J. R. (1996). Efficient transfer of genetic material into mammalian cells using Starburst polyamidoamine dendrimers. *Proc. Natl. Acad. Sci., 93*(10), 4897-4902.

Kukowska-Latallo, J. F., Candido, K. A., Cao, Z., Nigavekar, S. S., Majoros, I. J., Thomas, T. P., . . . Jr., J. R. (2005). Nanoparticle Targeting of Anticancer Drug Improves Therapeutic Response in Animal Model of Human Epithelial Cancer. *Cancer Res., 65*(12), 5317-24. doi:10.1158/0008-5472.CAN-04-3921

Larin, S. V., Darinskii, A. A., Lyulin, A. V., & Lyulin, S. V. (2010). Linker Formation in an Overcharged Complex of Two Dendrimers and Linear Polyelectrolyte. *J. Phys. Chem. B, 114*(8), 2910–2919. doi:10.1021/jp908196t

Larin, S. V., Lyulin, S. V., Lyulin, A. V., & Darinskii, A. A. (2009). Charge inversion of dendrimers in complexes with linear polyelectrolytes in the solutions with low pH. *Polym. Sci. Ser. A, 51*(4), 459–468. doi:10.1134/S0965545X09040117

Lasic, D. D., Strey, H., Stuart, M. C., Podgornik, R., & Frederik, P. M. (1997). The Structure of DNA−Liposome Complexes. *J. Am. Chem. Soc., 119*(4), 832–833. doi:10.1021/ja962713g

Lee, C. C., MacKay, J. A., Fréchet, J. M., & Szoka, F. C. (2005). Designing dendrimers for biological applications. *Nat Biotechnol., 23*(12), 1517–1526. doi:10.1038/nbt1171

Lee, H., & Larson, R. G. (2009). Multiscale modeling of dendrimers and their interactions with bilayers and polyelectrolytes. *Molecules, 14*(1), 423-438. doi:10.3390/molecules14010423

Lindman, B., & Thalberg, K. (1993). Polymer-Surfactant Interactions-Recent Developments. In E. D. Goddard, & K. P. Ananthapadmanabhan, *Interactions of Surfactants with Polymers and Proteins* (p. 203). Boca Raton, Florida, United States: CRC Press.

Little, R. D., Masjedizadeh, M. R., Wallquist, O., & McLoughlin, J. I. (1995). Chapter2: The Intramolecular Michael Reaction. In L. A. Paquettc, & e. al. (Eds.), *Organic*

*Reactions* (Vol. 47, pp. 315–552). Organic Reactions, Inc. Published by John Wiley and Sons, Inc. doi:10.1002/0471264180.or047.02

Liu, M., Kono, K., & Fréchet, J. M. (2000). Water-soluble dendritic unimolecular micelles:: Their potential as drug delivery agents. *J. Control. Release, 65*(1–2), 121-131. doi:10.1016/S0168-3659(99)00245-X

Lukacs, G. L., Haggie, P., Seksek, O., Lechardeur, D., Freedman, N., & Verkman, A. S. (2000). Size-dependent DNA mobility in cytoplasm and nucleus. *J. Biol. Chem., 275*(3), 1625-1629. doi:10.1074/jbc.275.3.1625

Luo, D., & Saltzman, W. M. (2000). Synthetic DNA delivery systems. *Nat. Biotechnol., 18*(1), 33–37. doi:10.1038/71889

Luo, D., Haverstick, K., Belcheva, N., Han, E., & Saltzman, W. M. (2002). Poly(ethylene glycol)-Conjugated PAMAM Dendrimer for Biocompatible, High-Efficiency DNA Delivery. *Macromolecules, 35*(9), 3456–3462. doi:10.1021/ma0106346

Lyulin, S. V., Darinskii, A. A., & Lyulin, A. V. (2005). Computer Simulation of Complexes of Dendrimers with Linear Polyelectrolytes. *Macromolecules, 38*(9), 3990–3998. doi:10.1021/ma047403u

Lyulin, S. V., Vattulainen, I., & Gurtovenko, A. A. (2008). Complexes Comprised of Charged Dendrimers, Linear Polyelectrolytes, and Counterions: Insight through Coarse-Grained Molecular Dynamics Simulations. *Macromolecules, 41*(13), 4961–4968. doi:10.1021/ma800736p

Maiti, P. K., & Bagchi, B. (2006). Structure and Dynamics of DNA−Dendrimer Complexation: Role of Counterions, Water, and Base Pair Sequence. *Nano Lett., 6*(11), 2478–2485. doi:10.1021/nl061609m

Maiti, P. K., Çağ ın, T., Lin, S.-T., & Goddard, W. A. (2005). Effect of Solvent and pH on the Structure of PAMAM Dendrimers. *Macromolecules, 38*(3), 979-991. doi:10.1021/ma049168l

Mandelkern, M., Elias, J. G., Eden, D., & Crothers, D. M. (1981). The dimensions of DNA in solution. *J. Mol. Biol., 152*(1), 153-161. doi:10.1016/0022-2836(81)90099-1

Martin-Herranz, A., Ahmad, A., Evans, H. M., Ewert, K., Schulze, U., & Safinya, C. R. (2004). Surface Functionalized Cationic Lipid-DNA Complexes for Gene Delivery: PEGylated Lamellar Complexes Exhibit Distinct DNA-DNA Interaction Regimes. *Biophys J., 86*(2), 1160-1168. doi:10.1016/S0006-3495(04)74190-9

Mashaghi, A., & Katan, A. (2013). A physicist's view of DNA. *De Physicus, 24e*(3), 59-61.

Mateescu, E. M., Jeppesen, C., & Pincus, P. (1999). Overcharging of a spherical macroion by an oppositely charged polyelectrolyte. *EPL, 46*(4), 493-498. doi:10.1209/epl/i1999-00290-6

Mishra, I. (2011). Dendrimer: A nivel drug delivery system. *JDDT, 1*(2), 70-74.

Morgan, M. T., Nakanishi, Y., Kroll, D. J., Griset, A. P., Carnahan, M. A., Wathier, M., . . . Grinstaff, M. W. (2006). Dendrimer-Encapsulated Camptothecins: Increased Solubility, Cellular Uptake, and Cellular Retention Affords Enhanced Anticancer Activity In vitro. *Cancer Res., 66*(24), 11913–11921. doi:10.1158/0008-5472.CAN-06-2066

Nandy, B., & Maiti, P. K. (2011). DNA Compaction by a Dendrimer. *J. Phys. Chem. B, 115*(2), 217–230. doi:10.1021/jp106776v

Netz, R. R., & Joanny, J.-F. (1999). Complexation between a Semiflexible Polyelectrolyte and an Oppositely Charged Sphere. *Macromolecules, 32*(26), 9026–9040. doi:10.1021/ma990264+

# Bibliography


Netz, R. R., & Joanny, J.-F. (1999). Complexation between a Semiflexible Polyelectrolyte and an Oppositely Charged Sphere. *Macromolecules, 32*(26), 9026–9040. doi:10.1021/ma990264+

Newkome, G. R., Yao, Z., Baker, G. R., & Gupta, V. K. (1985). Micelles. Part 1. Cascade molecules: a new approach to micelles. A [27]-arborol. *J. Org. Chem., 50*(11), 2003–2004. doi:10.1021/jo00211a052

Newkome, G. R., Yao, Z., Baker, G. R., & Gupta, V. K. (1985). Micelles. Part 1. Cascade molecules: a new approach to micelles. A [27]-arborol. *J. Org. Chem., 50*(11), 2003–2004. doi:10.1021/jo00211a052

Nguyen, T. T., & Shklovskii, B. I. (2001). Overcharging of a macroion by an oppositely charged polyelectrolyte. *Physica A, 293*(3-4), 324-338. doi:10.1016/S0378-4371(01)00020-6

Niu, Y., Sun, L., & Crooks, R. M. (2003). Determination of the Intrinsic Proton Binding Constants for Poly(amidoamine) Dendrimers via Potentiometric pH Titration. *Macromolecules, 36*(15), 5725–5731. doi:10.1021/ma034276d

Örberg, M.-L., Schillén, K., & Nylander, T. (2007). Dynamic Light Scattering and Fluorescence Study of the Interaction between Double-Stranded DNA and Poly(amido amine) Dendrimers. *Biomacromolecules, 8*(5), 1557–1563. doi:10.1021/bm061194z

Park, S. Y., Bruinsma, R. F., & Gelbart, W. M. (1999). Spontaneous overcharging of macro-ion complexes. *EPL, 46*(4), 454-460. doi:10.1209/epl/i1999-00284-x

*Pinta*. (n.d.). Retrieved from PintaProject / Pinta: https://www.pinta-project.com/pintaproject/pinta/

Plimpton, S. (1995). Fast Parallel Algorithms for Short-Range Molecular Dynamics. *J. Comput. Phys., 117*(1), 1-19. doi:10.1006/jcph.1995.1039

Prajapati, R. N., Tekade, R. K., Gupta, U., Gajbhiye, V., & Jain, N. K. (2009). Dendimer-Mediated Solubilization, Formulation Development and in Vitro−in Vivo Assessment of Piroxicam. *Mol. Pharmaceutics, 6*(3), 940–950. doi:10.1021/mp8002489

Purcell, A. (n.d.). *DNA.* Retrieved from Basic Biology: https://basicbiology.net/micro/genetics/dna/

Qamhieh, K., & Abu-Khaleel, A. (2014). Analytical model study of complexation of dendrimer as an ion penetrable sphere with DNA. *Colloids Surf. A, 442*, 191-198. doi:10.1016/j.colsurfa.2013.01.047

Qamhieh, K., Nylander, T., & Ainalem, M.-L. (2009). Analytical Model Study of Dendrimer/DNA Complexes. *Biomacromolecules, 10*(7), 1720–1726. doi:10.1021/bm9000662

Qamhieh, K., Nylander, T., Black, C. F., Attard, G. S., Dias, R. S., & Ainalem, M.-L. (2014). Complexes formed between DNA and poly(amido amine) dendrimers of different generations – modelling DNA wrapping and penetration. *Phys. Chem. Chem. Phys., 16*(26), 13112-13122. doi:10.1039/C4CP01958J

Quintana, A., Raczka, E., Piehler, L., Lee, I., Myc, A., Majoros, I., . . . BakerJr., J. R. (2002). Design and Function of a Dendrimer-Based Therapeutic Nanodevice Targeted to Tumor Cells Through the Folate Receptor. *Pharm. Res., 19*(9), 1310–1316. doi:10.1023/a:1020398624602

Rosenberg, S. A., Aebersold, P., Cornetta, K., Kasid, A., Morgan, R. A., Moen, R., . . . An, W. F. (1990). Gene transfer into humans--immunotherapy of patients with advanced melanoma, using tumor-infiltrating lymphocytes modified by retroviral gene transduction. *N Engl J Med, 323*, 570-578. doi:10.1056/NEJM199008303230904

# Bibliography


Russell, P. J. (2001). *IGenetics.* New York: Benjamin Cummings.

Saenger, W. (1984). *Principles of Nucleic Acid Structure* (4, illustrated ed.). New York: Springer-Verlag.

Sambriski, E. J., Schwartz, D. C., & de Pablo, J. J. (2009). A Mesoscale Model of DNA and Its Renaturation. *Biophys. J., 96*(5), 1675–1690. doi:10.1016/j.bpj.2008.09.061

Schiessel, H. (2003). The physics of chromatin. *J. Phys.: Condens. Matter, 15*(19), R699–R774. doi:10.1088/0953-8984/15/19/203

Schiessel, H., Bruinsma, R. F., & Gelbart, W. M. (2001). Electrostatic complexation of spheres and chains under elastic stress. *J. Chem. Phys., 115*(15), 7245-7252. doi:10.1063/1.1403688

Schneider, T., & Stoll, E. (1978). Molecular-dynamics study of a three-dimensional one-component model for distortive phase transitions. *Phys. Rev. B, 17*(3), 1302-1322. doi:10.1103/PhysRevB.17.1302

*SciDAVis*. (n.d.). Retrieved from SciDAVis: http://www.scidavis.sourceforge.net/index.html

Scott, R. W., Wilson, O. M., & Crooks, R. M. (2005). Synthesis, Characterization, and Applications of Dendrimer-Encapsulated Nanoparticles. *J. Phys. Chem. B, 109*(2), 692–704. doi:10.1021/jp0469665

*Search of: starpharma - List Results - ClinicalTrials.gov*. (n.d.). Retrieved from NIH > U.S. National Library of Medicine ClinicalTrials.gov: https://clinicaltrials.gov/ct2/results?term=starpharma&Search=Search

Smith, S. B., Finzi, L., & Bustamante, C. (1992). Direct mechanical measurements of the elasticity of single DNA molecules by using magnetic beads. *Science, 258*(5085), 1122-1126.

Sowinska, M., & Urbanczyk-Lipkowska, Z. (2014). Advances in the chemistry of dendrimers. *New J. Chem., 38*(6), 2168-2203. doi:10.1039/C3NJ01239E

Stevelmans, S., Hest, J. C., Jansen, J. F., Boxtel, D. A., Berg, E. M.-v., & Meijer, E. W. (1996). Synthesis, Characterization, and Guest−Host Properties of Inverted Unimolecular Dendritic Micelles. *J. Am. Chem. Soc., 118*(31), 7398–7399. doi:10.1021/ja954207h

Stukowski, A. (2010). Visualization and analysis of atomistic simulation data with OVITO–the Open Visualization Tool. *Model. Simul. Mater. Sci. Eng., 18*(1), 015012. doi:10.1088/0965-0393/18/1/015012

Teertstra, S. J., & Gauthier, M. (2004). Dendrigraft polymers: macromolecular engineering on a mesoscopic scale. *Prog. Polym. Sci., 29*(4), 277-327. doi:10.1016/j.progpolymsci.2004.01.001

Tekade, R. K., Dutta, T., Gajbhiye, V., & Jain, N. K. (2009). Exploring dendrimer towards dual drug delivery: pH responsive simultaneous drug-release kinetics. *J. Microencapsul., 26*(4), 287-296. doi:10.1080/02652040802312572

Thomas, T. P., Majoros, I. J., Kotlyar, A., Kukowska-Latallo, J. F., Bielinska, A., Myc, A., & Jr., J. R. (2005). Targeting and Inhibition of Cell Growth by an Engineered Dendritic Nanodevice. *J. Med. Chem., 48*(11), 3729–3735. doi:10.1021/jm040187v

Tian, W.-d., & Ma, Y.-q. (2010). Complexation of a Linear Polyelectrolyte with a Charged Dendrimer: Polyelectrolyte Stiffness Effects. *Macromolecules, 43*(3), 1575–1582. doi:10.1021/ma901988m



Tian, W.-d., & Ma, Y.-q. (2010). Complexation of a Linear Polyelectrolyte with a Charged Dendrimer: Polyelectrolyte Stiffness Effects. *Macromolecules, 43*(3), 1575–1582. doi:10.1021/ma901988m

# Bibliography


Tomalia, D. A. (1994). Starburst/Cascade Dendrimers: Fundamental building blocks for a new nanoscopic chemistry set. *Adv. Mater., 6*(7-8), 529–539. doi:10.1002/adma.19940060703

Tomalia, D. A. (2005). Birth of a new macromolecular architecture: dendrimers as quantized building blocks for nanoscale synthetic polymer chemistry. *Prog. Polym. Sci., 30*(3-4), 294-324. doi:10.1016/j.progpolymsci.2005.01.007

Tomalia, D. A., & Dewald, J. R. (1983). *U.S. Patent No. US4507466 A.*

Tomalia, D. A., Baker, H., Dewald, J., Hall, M., Kallos, G., Martin, S., . . . Smith, P. (1985). A New Class of Polymers: Starburst-Dendritic Macromolecules. *Polymer Journal, 17*, 117–132. doi:10.1295/polymj.17.117

Tomalia, D. A., Christensen, J. B., & Boas, U. (2012). *Dendrimers, Dendrons, and Dendritic Polymers: Discovery, Applications, and the Future.* Cambridge University Press.

Tomalia, D. A., Naylor, A. M., & Goddard(III), W. A. (1990). Starburst Dendrimers: Molecular-Level Control of Size, Shape, Surface Chemistry, Topology, and Flexibility from Atoms to Macroscopic Matter. *Angew. Chem. Int. Ed. Engl., 29*(2), 138–175. doi:10.1002/anie.199001381

Toms, S., Carnachan, S. M., Hermans, I. F., Johnson, K. D., Khan, A. A., O'Hagan, S. E., . . . Rendle, P. M. (2016). Poly Ethoxy Ethyl Glycinamide (PEE-G) Dendrimers: Dendrimers Specifically Designed for Pharmaceutical Applications. *ChemMedChem, 11*(15), 1583–1586. doi:10.1002/cmdc.201600270

*Treelike molecules branch out.* (1996). Retrieved from The Free Library: https://www.thefreelibrary.com/Treelike+molecules+branch+out.-a017817461

Tropp, B. E. (2011). *Molecular Biology.* Jones & Bartlett Publishers (Learning).

Twyman, L. J., & Ge, Y. (2006). Porphyrin cored hyperbranched polymers as heme protein models. *Chem. Commun., 0*(15), 1658-1660. doi:10.1039/B600831N

Twyman, L. J., Ellis, A., & Gittins, P. J. (2012). Pyridine encapsulated hyperbranched polymers as mimetic models of haeme containing proteins, that also provide interesting and unusual porphyrin-ligand geometries. *Chem. Commun., 48*(1), 154-156. doi:10.1039/C1CC14396D

*Ubuntu*. (n.d.). Retrieved from Ubuntu: https://www.ubuntu.com/

Venter, J. C., Adams, M. D., Myers, E. W., Li, P. W., Mural, R. J., Sutton, G. G., & Smith, H. O. (2001). The Sequence of the Human Genome. *Science, 291*(5507), 1304-1351. doi:10.1126/science.1058040

Wang, R., Zhou, L., Zhou, Y., Li, G., Zhu, X., Gu, H., . . . Yan, D. (2010). Synthesis and Gene Delivery of Poly(amido amine)s with Different Branched Architecture. *Biomacromolecules, 11*(2), 489–495. doi:10.1021/bm901215s

Watson, J. D., & Crick, F. H. (1953). Molecular Structure of Nucleic Acids: A Structure for Deoxyribose Nucleic Acid. *Nature, 171*(4356), 737–738. doi:10.1038/171737a0

Welch, P., & Muthukumar, M. (2000). Dendrimer−Polyelectrolyte Complexation: A Model Guest−Host System. *Macromolecules, 33*(16), 6159–6167. doi:10.1021/ma000021d

Wolfert, M. A., Schacht, E. H., Toncheva, V., Ulbrich, K., Nazarova, O., & Seymour, L. W. (1996). Characterization of vectors for gene therapy formed by self-assembly of DNA with synthetic block co-polymers. *Hum Gene Ther., 7*(17), 2123-33. doi:10.1089/hum.1996.7.17-2123

Yakovchuk, P., Protozanova, E., & Frank-Kamenetskii, M. D. (2006). Base-stacking and base-pairing contributions into thermal stability of the DNA double helix. *Nucleic Acids Res., 34*(2), 564–574. doi:10.1093/nar/gkj454

# Bibliography

Yoo, H., Sazani, P., & Juliano, R. L. (1999). PAMAM Dendrimers as Delivery Agents for Antisense Oligonucleotides. *Pharm. Res.*, *16*(12), 1799-804.

Yu, S., & Larson, R. G. (2014). Monte-Carlo simulations of PAMAM dendrimer-DNA interactions. *Soft Matter*, *10*(29), 5325-5336. doi:10.1039/c4sm00452c

Zinchenko, A. A., & Chen, N. (2006). Compaction of DNA on nanoscale three-dimensional templates. *J. Phys.: Condens. Matter*, *18*(28), R453-80. doi:10.1088/0953-8984/18/28/R01

# مجموعة عملياتِ محاكاةٍ ديناميكيةٍ براونيةٍ لمركب سلسلة الحمض النَّوَويْ مزدوجة الشَّريطة (dsDNA) مع جزيء الـ (dendrimer) النَّانَويِّ موجب الشَّحنة

**إعداد: علاء جواد يعقوب مرار**

**إشراف: أ. د. خولة قمحية**

## الملخص

أجرينا مجموعة من عمليات المحاكاة البراونية الديناميكية (BD) لدراسة تأثير تركيز الملح ودرجة الحموضة على تفاعلات سلسلة الحمض النووي مزدوجة الشريطة مع جزيء الـ ( Polyamidoamine (PAMAM) dendrimer)، وتحديد دور كل من تركيز الملح وطول سلسلة الحمض النووي مزدوجة الشريطة (عدد الأزواج القاعدية في السلسلة) في تكوين الرابط بين الـ (dendrimers) والذيل أو الذيول في مجموع (aggregate) سلسلة الحمض النووي مزدوجة الشريطة وجزيئات الـ (dendrimers)، و معرفة ما هي الأشكال التي تظهر عندما تُكوِّن الأجيال المختلفة من الـ (dendrimers) تجمعاً مع سلسلة الحمض النووي مزدوجة الشريطة. لنناسب قدرة الحوسبة التي لدينا ولنحقق سرعة للمحاكاة دون الخوض في بعض التفاصيل المعقدة، استخدمنا نموذج "كرة - نابض" لسلسلة الحمض النووي مزدوجة الشريطة ونموذج الكرة الصلبة المشحونة لجزي الـ (dendrimer).

تتنبأ نماذجنا بأن سلسلة الحمض النووي مزدوجة الشريطة تلتف بقوة حول جزيء الـ (dendrimer) في كل من تركيز الملح المنخفض (10 مللي مولر (mM)) ودرجة حموضة (pH) $\geq 7$ ويتكون مركب سلسلة الحمض النووي مزدوجة الشريطة مع جزيء الـ (dendrimer)، في حين لا يتشكل أي مركب في كل من تركيز الملح العالي ودرجة الحموضة العالية.

في المجموع المتكون من سلسلة الحمض النووي مزدوجة الشريطة وجزيئين الجيل الرابع (G4) والسادس (G6) من الـ (dendrimers)، يظهر الرابط بين الـ (dendrimers) و/أو الذيل أو الذيول بوضوح في تركيز الملح المحصور بين الـ 10 والـ 120 مللي مولر مع طول لسلسلة الحمض النووي مزدوجة الشريطة $\leq 97$ نانومتر (nm) (عدد الأزواج القاعدية في السلسلة $\leq 288$). بالإضافة إلى ذلك، لسلاسل الحمض النووي مزدوجة الشريطة الطويلة لاحظنا وجود ظاهرة الشحنة الزائدة (The overcharge) للـ (dendrimers) في المجموع ووجدنا أنَّ درجتها تعتمد على طول سلسلة الحمض النووي مزدوجة الشريطة (أي عدد الأزواج القاعدية في السلسلة).

عندما تُكوِّن أعداد معينة من الأجيال الدنيا من الـ (dendrimers) مثل الجيل الثاني والرابع (G2 وG4) مع سلسلة الحمض النووي مزدوجة الشريطة مجاميعاً عند تركيز ملحٍ 10 مللي مولر فإن الشكل الخطي "القضيب" يظهر، كما ويظهر الشكل الكروي أيضاً لمجموع الجيل الرابع، في حين أنَّا حصلنا تقريباً على شكلٍ شبه الخطي "القضيب" للأجيال العالية من الـ (dendrimer) كالجيل السادس (G6).


الحمد لله رب العالمين